STUDYING "FITNESS FOR SERVICE" OF THE SEALING ASSEMBLIES AND CEMENT SYSTEM IN SHALLOW WELL DESIGNS BY CONDUCTING SCALED LABORATORY TESTING, LEAKAGE MODELLING AND RISK ASSESSMENT

FINAL REPORT

AUTHORS:

Saeed Salehi (PhD), Principal Investigator

Ramadan Ahmed (PhD), Co-Principal Investigator

Catalin Teodoriu (PhD), Co-Principal Investigator

Chinedum Peter Ezeakacha, Graduate Research Assistant

Harshkumar Patel, Graduate Research Assistant

George Kwatia, Graduate Research Assistant

Shawgi Ahmed, Graduate Research Assistant

Mustafa Al-Ramadan, Graduate Research Assistant

Prepared under BSEE Project NO: E17PC00005

by

THE UNIVERSITY OF OKLAHOMA

October 2018

1 EXECUTIVE SUMMARY

This final report presents the accomplishments of the Bureau of Safety and Environmental Enforcement (BSEE) Project #E17PC00005. The project title is: Studying "Fitness for Service" of the Sealing Assemblies and Cement System in Shallow Well Designs by Conducting Scaled Laboratory Testing, Leakage Modelling and Risk Assessment. In this report, the term "barrier(s)" defines the use of cement sheath and the liner hanger sealing assembly to prevent uncontrolled influx and migration of formation fluid to a shallow formation or surface facilities. This report is divided into four major sections: three laboratory-scaled test setups for three sections and one leakage modelling and risk assessments section. A comprehensive literature review was conducted for all the sections. These reviews provide a road map to address the integrity of sealing assemblies and cement systems in downhole conditions.

Cement Tests (Setup I)

This project section discusses different approaches to evaluate and improve cement sealability. The objectives of this project section are: i) Evaluate annular cement integrity and its ability to seal as a primary barrier, by using different classes of Portland cements and gas migration additives; ii) Verify the reliability of current liner overlap pressure test and investigate the critical liner-casing overlap length; and iii) Characterize and report critical cement properties for different anti-gas migration slurry designs.

The results showed that neat Class H and Class G cements are not capable of preventing gas migration and providing a good seal as a primary barrier. The physical properties of various anti-gas migration slurry designs have provided a holistic characterization of the slurries. A gas-tight cement slurry that was designed with a commercial additive proved to mitigate gas flow through a set cement sheath. Analytical results revealed that the combined annular cement permeability increases as the cement age increases. The leakage scenarios that were evaluated showed an increase in leakage time as the liner-casing overlap increases. Liner-casing overlap lengths that range from 50 ft to 250 ft may not provide sufficient time for detecting and controlling gas influx when the cement sheath is faulty. The leakage time increases as the combined cement sheath permeability decreases. Finally, the current liner-casing pressure test duration of 30 minutes may not be adequate for detecting a faulty cement barrier, should the elastomer in the liner hanger be faulty.

Elastomer Aging Cell Tests (Setup III)

The objectives of this project section are: i) Investigate elastomer integrity as "fit for service" in shallow well construction applications; and ii) Determine elastomer performances under downhole corrosive conditions (temperature, pressure, and corrosive gases). The intrinsic elastomer properties that were investigated include: hardness, volumetric swelling, and compression.

The results showed that elastomer's hardness deteriorates with exposure to the downhole corrosive conditions. The order of corrosive gas effect on elastomer hardness (from high to low) is CO_2 > All gases > H_2S > CH_4. The H_2S used in this study is 500 ppm H_2S in CH_4 carrier. The term "All gases" stands for a combination of 50% CO_2 and 50% H_2S with CH_4 carrier. Elastomers tend to swell when they are exposed to these corrosive conditions. The change in this property is because of the initial chain rupture in the elastomer, followed by chain growth. Chain rupture increases the elastomer size (swelling), while chain growth causes the elastomer to shrink. H_2S and CH_4 had the least effect on volumetric swelling, while a combination of CO_2, H_2S, and CH_4 had the most detrimental swelling effect on the elastomers. Elastomer compression is characterized by how much strain is recorded at various stresses. Compression results revealed that exposing an elastomer to the least aging condition is enough to compromise its sealing integrity to the point where altering the aging parameters becomes redundant. The order of corrosive gas impact on elastomer compression (from high to low) is CO_2 > All gases > H_2S > CH_4.

Sealing Assemblies Tests (Setup II)

The objectives of this project section are: i) Evaluate the performance of common elastomeric seals used in liner hanger sealing systems as independent barrier element, ii) Evaluate the performance of a liner hanger seal assembly and cement sheath to determine which of them acts as a primary barrier; and iii) Evaluate the testing protocols for proper testing of different barriers.

The results from the experiments revealed that the elastomeric seals such as ethylene propylene diene monomer (EPDM) and nitrile butadiene rubber (NBR), did not exhibit any leakage when they were independently subjected to a pressure test of 40 psig under normal conditions. The independent sealing performance of EPDM and NBR after surfactant degradation was not impaired for the test conditions used in this study. However, both elastomers failed the pressure tests when a mechanical defect was intentionally created and after exposure to CO_2. The pressure cycling results showed that elastomers energization plays a critical role in maintaining their seal integrity. The results also showed that prolonged pressure test duration (up to 60 minutes) did not affect the elastomers performance for pressures up to 40 psig. The "wait on cement" time (WOC) improves cement sealability as indicated by the progressively slow pressure decline in the pressure tests after the six WOC intervals. The seal integrity of the commercial gas migration additive cement from setup I was verified in the dual barrier system (setup II). No leaks were observed within the cement sheath or between the cement sheath and inner steel pipe. Therefore, in the case where a dual barrier system has a faulty elastomer and cement designed with the commercial gas migration additive, the cement sheath can act a primary barrier.

Leakage Modeling and Risk Assessments

The goal of this study is to assess "fitness-for-service" of seal assemblies and cement sheath using the approach of leakage modelling, simulations, and risk assessment. This fills-in some of the existing knowledge gaps and helps regulators and operators improve design, selection, and qualification of these barrier elements. To achieve the objectives, a comprehensive finite element

analysis was conducted using three-dimensional computer models consisting of liner, casing, seal assembly, and cement elements. The sealability of the elastomer component in a hanger assembly was evaluated in terms of the contact stress generated at the seal-pipe interface. The performance of cement sheath was assessed by analyzing the radial, hoop, and maximum shear stresses for mechanical failure. An extensive literature review was conducted to identify various parameters that can affect the performance of barrier elements. Parametric analyses were performed to understand the behavior of elastomer seals and cement sheath under various conditions, considering different design parameters such as dimensions and material properties. Various potential failure scenarios were selected and examined to identify the effects on seal performance and cement integrity. Simulation results were normalized, and sensitivity analysis was performed to compare and identify the critical parameters affecting sealability. Operating curves, correlations, and rules of thumbs were generated for quick and easier prediction of performance of both barriers independently.

The results suggest that annular fit, compression ratio, energization quality, elastic modulus, and Poisson's ratio are the most critical factors affecting the sealability of an elastomer element in seal assembly. Important design parameters for cement include: annular fit, wellbore pressure, Young's modulus, and Poisson's ratio. The effect of temperature has been considered in the form of change in material properties. Based on all the simulation results, recommendations for assessing "fitness-for-service" of seal assemblies and cement systems are provided.

TABLE OF CONTENTS

LIST OF FIGURES

LIST OF TABLES

2 CEMENT TESTS USING SET UP I

2.1 INTRODUCTION

2.1.1 Overview

Cement plays a major role in the oil and gas industry, especially during the drilling and completion phase. Cement sealability helps to maintain the integrity of a well and prevent subsurface fluid movement/migration to other formations and surface. The cement's ability to withstand mechanical and chemical deteriorations while maintaining its properties is known as cement durability. Cement durability and sealability strongly depends on the cement properties such as permeability, thickening time, rheology, static gel strength (SGS), and unconfined compressive strength (UCS). While some of these properties are more critical than others during the pumping phase of a cement slurry, others are more crucial during the setting phase. A slurry with excellent thickening time and SGS is desired during cement pumping. An ultra-low permeable cement is usually desired during the setting phase to prevent fluid movement and provide excellent zonal isolation. A cement sheath with high UCS is typically required over time to withstand the thermal and pressure cycling that occurs in the life time of a well.

However, during the pumping and setting phase of cement, especially in gas prone zones, annular gas flow through the cemented annulus can occur and this is known as gas migration. Annular gas flow can lead to catastrophic events such as loss of well control, broaching of the shallow formation or a blowout. Most times, these flows are encountered before the blowout preventer in installed (Murray et al. 1995). In most cases, gas will migrate through a cemented annulus if the cement matrix is permeable and has poor bonding with the casing and rock surface. In addition, the development of microannuli, channels, and induced fractures (even with an ultra-low-permeable cement matrix) allows formation fluid migration through these features rather than the cement matrix itself. Gas migration control additives are usually mixed into cement slurries to increase sealability, bonding, and help prevent the evolution of microannuli. Cement sealability can be evaluated by quantifying the cemented annulus total permeability. Limited laboratory studies have been conducted to evaluate the oil well cement sealability (Christian et al. 1976; Tarco and Asghari 2010; Omosebi 2016; Stormont et al. 2017).

2.1.2 Problem Statement

The concept of gas migration has been of major concern since the 1960's. Various aspects of experimental and field case studies (Cook et al. 1983; Al-Buraik et al. 1998), development of new products and techniques (Watters and Sabins 1980; Siedel and Greene 1985), and technical recommendations (Cheung and Beirute 1985; Dean and Brennen 1992) have been discussed to try to mitigate gas migration. Shallow gas migration through a cement sheath in the early stages of setting endangers the integrity of a well by creating flow paths in the cement sheath such as microannuli and channels. Shallow gas flow can lead to blowouts in the open-hole section, usually below the conductor or surface casing because of gas migration through the cement (Adams and

Kuhlman 1990). Nelson and Guillot (2006) and Talabani et al. (1997) stressed that the root cause of gas migration is the pathways in the annulus through which the gas can migrate.

This is especially relevant today as the oil and gas industry is exploring and producing hydrocarbon from harsh environments. This has made shallow gas incidents much more of a concern in many regions of the world, including the Pacific Rim, the Norwegian Continental Shelf (NCS), UK Continental Shelf, and the Gulf of Mexico (Moore and Hamilton 1993). Lécolier et al. (2010) argued that a substantial amount of the world's remaining gas reserves has over 2% of CO_2 and substantial amounts of H_2S. The presence of these gases has complicated well construction design. Deepwater cementing operations present several challenges all around the world because of shallow flow. Appropriate well design procedures require a cement system that can mitigate gas migration. This section of the project and report evaluates annular cement integrity, critical cement properties with time, and reliability verification of the current liner lap pressure testing.

2.1.3 Objectives

A neat Portland cement is often thought of as the primary barrier to prevent formation fluid influx during the early setting phase of a cement slurry. This is not completely certain considering the loss of well control incidents that have been reported because of gas migration during this phase. The possible failure of a neat cement raises the need to develop a cement slurry capable of mitigating gas influx and migration. The objectives of the tasks in this section include:

- Evaluate annular cement integrity and its ability to seal as a primary barrier, by using different classes of Portland cements and gas migration additives.
- Verify the reliability of current liner overlap pressure test and investigate the critical liner-casing overlap length.
- Characterize and report critical cement properties for different anti-gas migration slurry designs.

2.2 LITERATURE REVIEW

Shallow flows usually occur because of high pore pressures from under-compaction and over-pressurization of sands during rapid depositions. Shallow flows can consist of water, gas, and formation fines. One out of every five potential surface casing hazards were identified to be shallow flows (Bogaerts et al. 2012). Shallow gas is usually encountered at shallow subsurface depths of 300 ft with low fracture gradients. They often result in cratering and blowouts in the open-hole sections. Gas leakage in the annulus has been recorded as a major hazard in drilling and completions operations, and records show that one out of three blowouts occur because of a shallow influx (Adams and Kuhlman 1990; Prince 1990). Danenberger's study in 1993 showed that 58 out of the 83 blowouts that were encountered between the years of 1971 and 1991 on the outer continental shelf (OCS) of the United States had gases associated with them. This was a strong indication of the severity of shallow gas flows and cratering which costed significant expenditure to the operators. To curb some of these problems, steps have been taken by the industry

over the years to improve shallow well casing and cement designs. These include: API RP 65 (2002) and API RP 65–Part 2 (2010).

2.2.1 Gas Migration

Gas migration is defined as gas entry into a cemented annulus with the potential to provide a flow path into the wellbore for gas, water, and hydrocarbons. Gas migration can cause fluid flow through the annulus to the surface. If gas goes undetected, it can lead to severe consequences such as underground blowouts and sustained casing pressure. Gas migration phenomenon can be caused by numerous factors at any given time. The root causes of gas migration have been attributed to i) a decline in annulus hydrostatic pressure and ii) pathways in the annulus through which gas can migrate (Nelson and Guillot 2006). Primary causes of gas migration are related to the cementing process. Gas migration through a cemented annulus can be categorized into three types based on their migration pathways (Talabani et al. 1997). The first type occurs between the casing and the cement; a situation whereby gas molecules migrate through the void created between the casing and cement. A common practice to remedy this problem is adding the appropriate amount of magnetite to the cement slurry. The second type of gas migration occurs through the void created between the cement and the wellbore wall. This void is created when the filter cake that is formed on the wellbore wall adversely affects the bonding process. Anchorage Clay and some other additives can be used to eliminate this problem in drilling. The third gas migration path exists because of hydrostatic pressure changes that appear in the cement during the setting phase. This is also referred to as primary gas migration when gas molecules migrate into the cement because of loss of the hydrostatic head.

On the other hand, secondary gas migration occurs much later after cement placement is complete. This is because of mechanical and thermal stresses which compromises the integrity of the hydraulic bond or the integrity of the cementing material (Rupak 2007). According to the Mineral Management Service (MMS) safety alert (2003), annular flow related to cementing surface casing has been identified as one of the most frequent causes of the loss of well control incidents in the Gulf of Mexico (GoM). When zonal isolation is not achieved, and gas molecules migrate behind the casing, it charges the shallow formations. These shallow formations become a formidable challenge when there is little proximity between the pore pressure and fracture gradients in the operational mud window. In such situations, the gas can broach the casing, leading to a blowout. There are several aspects and literatures on gas migration, additives that are used to prevent gas migration, cement combined permeability, and analytical modelling for gas migration. These have been discussed extensively in sections **2.2.1**, **2.2.2, 2.2.3, and 2.2.4** of the report on laboratory results for sealing assemblies and cement systems.

2.3 RESEARCH METHODOLOGY

To achieve the objectives in this section of the project, theoretical, experimental, and analytical approaches were used. An extensive literature review provided information on cement properties, slurry designs, and additives that can be added to make cement slurries gas tight. The outcomes of

reviews and theoretical analysis provided useful information in comprehending the inadequacy of set cement to prevent migration of formation fluids, mainly gas. Sealability of cement strongly depends on the cement to casing bonds and available pores within the cement.

In this study, different slurry designs have been investigated using additives like latex, microsilica, and bentonite. The key properties of cement with regards to gas migration control, mechanisms for wellbore cement failure, and relationship between cement design and its integrity were examined. A gas-tight slurry was successfully designed. The gas-tight cement slurry was made of Class H and 1.5 liters/100 kg commercial additive. The formulation was rigorously tested to evaluate the slurry's performance.

2.3.1 Scope of Work

Two different oil well cements (Class G and Class H) were compared in their ability to seal during the very early stages of cementing. Cement slurries are sensitive to downhole conditions such as temperature and pressure (Ahmed et al. 2009). Besides cement rheology and thickening time tests, all the experiments with setup I were performed at ambient temperature and the cement sheath surface was exposed to ambient pressure. Shallow reservoirs have relatively low pressure and temperature. It was difficult to mimic these conditions considering the large scale (field size) setup. To accomplish the specific goals in this section of the project and report, setup I was split into different setups: big setup I and small setup I.

In the big setup I, two different "wait on cement" (WOC) times were used to investigate the effect of WOC time on the cement sealability (12 and 24 hours). Nitrogen gas (N_2) was injected at 60 psig to examine and test the integrity of the system. Latex and Bentonite were mixed with oil well cement to evaluate cement integrity and sealability. In each experiment (slurry design), two to three major pressure cycles were performed and each of these cycles contained at least two to three tests. The pressure decline curves were used to generate the combined permeability of the cement system. Three methods were used to measure the combined permeability of the system for each test. These were used to evaluate cement sealability and in developing a model for the critical liner-casing overlap.

The primary goal for developing the small setup I was to test various combinations of slurry additives. In this setup, pressure was kept constant at 60 psig and WOC was 24 hours. Class H cement was used for the investigations in this setup. Experimental investigations were conducted in two phases. In the first phase, neat Class H cement was used while in the second phase, neat Class H cement was mixed with different additives (bentonite, latex, microsilica and nanomaterials). To quantify the level of slurry improvement, leakage time of set cements were measured and compared. In addition, cement physical properties such as compressive strength, rheology, thickening time, density, and gas transit time were evaluated to verify the suitability of the new cement mixtures.

All the test materials, cement mixing and property measuring procedures, components and arrangements of the big and small setup I, test matrices for the big and small setup I, and

experimental test protocols for both setups have been described in detail in the report on laboratory results for sealing assemblies and cement system (**2.3.2** to **2.3.10**). In addition to these, data preparation techniques such as pressure data cleaning and denoising were used in preparing the pressure data for leakage time and combined permeability calculations. In this study, the calculated permeability is not only the cement matrix permeability, but also includes the permeability of induced cracks, channels, and microannuli. Thus, this permeability is referred to as the combined permeability or system permeability. This permeability was calculated using three different methods with the aid of the estimated gas flow rates. These methods are the Darcy's method, Forchheimer's method, and pulse-decay methods. These have all been discussed in section **2.3.11** of the report on laboratory results for sealing assemblies and cement system

2.4 RESULTS

In this subsection, the results from each experiment using the big setup I and small setup I are presented and discussed. Beginning with the big setup I, the results from the four experiments are discussed and compared, followed by four leakage scenarios and modelling results for gas migration through the cement sheath in a liner-casing overlap (**2.4.1** to **2.4.5**). The results from the experiments and tests using small setup I are presented from **2.4.6** to **2.4.12**.

2.4.1 Big Setup I Experiment 1 with Neat Class H and 24 hours WOC

Experiment 1 with big setup I was conducted with neat Class H cement with 38 % water/cement (W/C) ratio and 24 hours WOC. After the WOC time, three gas injection tests were performed at 60 psig. Figure 2.1 shows the leakage time versus the cement age for three cycles, with three tests in cycles 2 and 3 and two preliminary tests in cycle 1. In the first test within cycle 1, the first bubble appeared and was recorded after 11 minutes. However, the leakage time decreased to 5 minutes in the second test when the cement age was 2 days. The leakage time increased again to 11 minutes in the first test of cycle 2 when the cement age was 11 days and then decreased afterwards in the second and third tests within this cycle. This trend was also observed in cycle 3. The reason for an increase in leakage time between the end of the last test in a cycle and the beginning of the first test in the next cycle can be linked to the fallow period between the cycles. This also contributed to the disappearance of some bubbling positions. The phenomenon of disappearing positions is referred to as "self-healing" and has been reported by Carroll et al. (2016), Carey (2013), and Huerta et al. (2012). The authors attributed this phenomenon to the mobilization and precipitation of minerals along the pathways within the cement sheath.

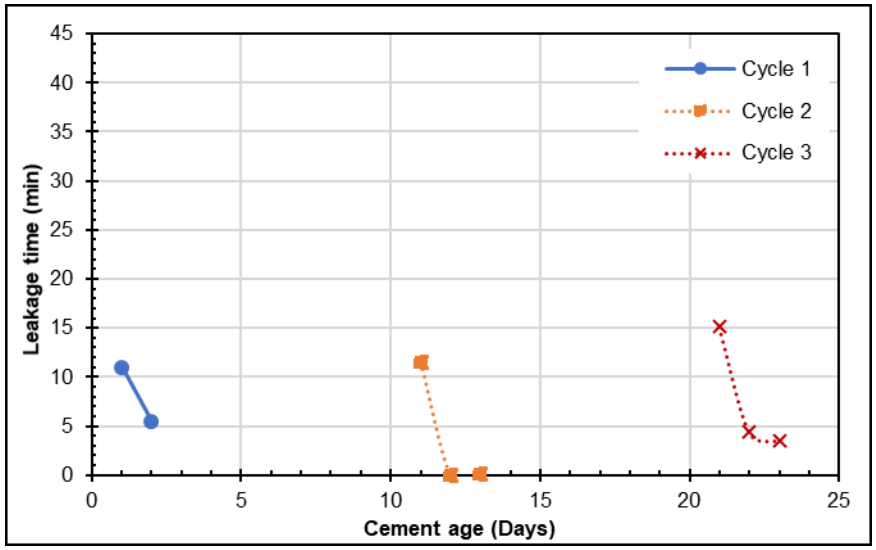

Figure 2.1: Leakage time versus cement age for all the three cycles and tests performed in experiment 1 (neat Class H, WOC: 24 hours)

The combined permeability values for this experiment were estimated using the three different methods discussed in section **2.3.11.4** of the report on laboratory results for sealing assemblies and cement system. The permeability values in cycle 1 were calculated from only the Darcy's method because of lack of continuous pressure measurements required for the other two methods. In addition, the two tests conducted in this cycle were considered preliminary. The Darcy's method was not used in estimating permeability values in cycle 3 because of the difficulty in counting and detecting the bubbles. Figure 2.2 shows the combined permeability calculated from these methods versus cement age. A general observation is that the combined permeability increases as the cement age increase. Parrott (1995) reported such a trend when measuring the air permeability for different cement specimens for approximately 800 days. The calculated permeability values fall under the range of neat Class H cement permeability reported in literatures.

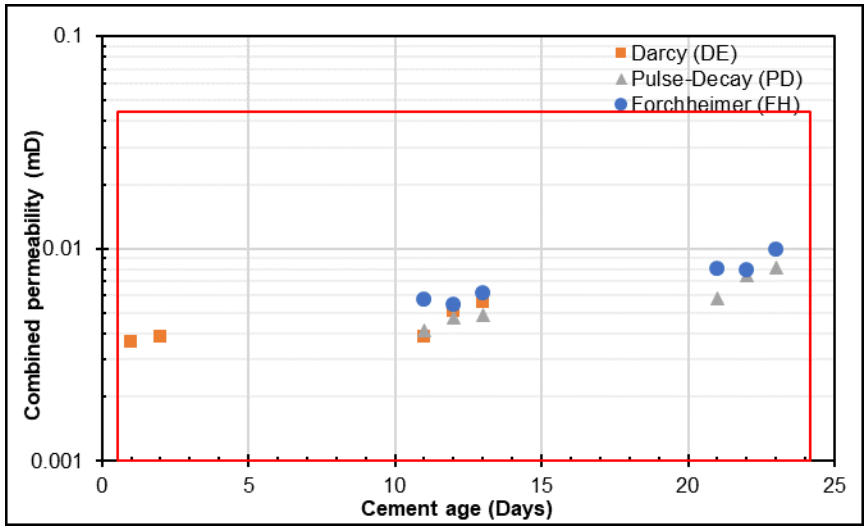

Figure 2.2: Combined permeability versus cement age for experiment 1 (neat Class H, WOC: 24 hours)

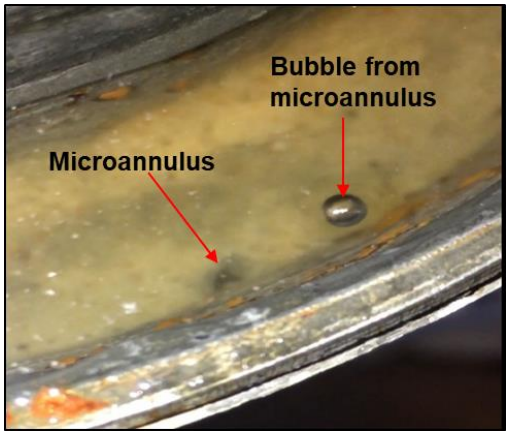

Figure 2.3: A microannulus bubbling from big setup I experiment 1

2.4.2 Big Setup I Experiment 2 with Neat Class H and 12 hours WOC

The major difference between experiment 1 and 2 (using big setup I) was the WOC time. The first test was performed after 12 hours WOC and the first bubble was detected approximately after 5 minutes. Figure 2.4 shows the leakage time versus the cement age for only one cycle. The second test was performed 8 days after the first test and the "self-sealing" phenomenon was observed with an increase in cement age. The combined permeability values were estimated using the three methods. Figure 2.5 shows that all the calculated permeability values fall between 0.001 mD and 0.045 mD, except the value calculated from the Darcy's method in test 1. The values from the Forchheimer and pulse-decay methods were 0.002 mD and 0.003 mD respectively.

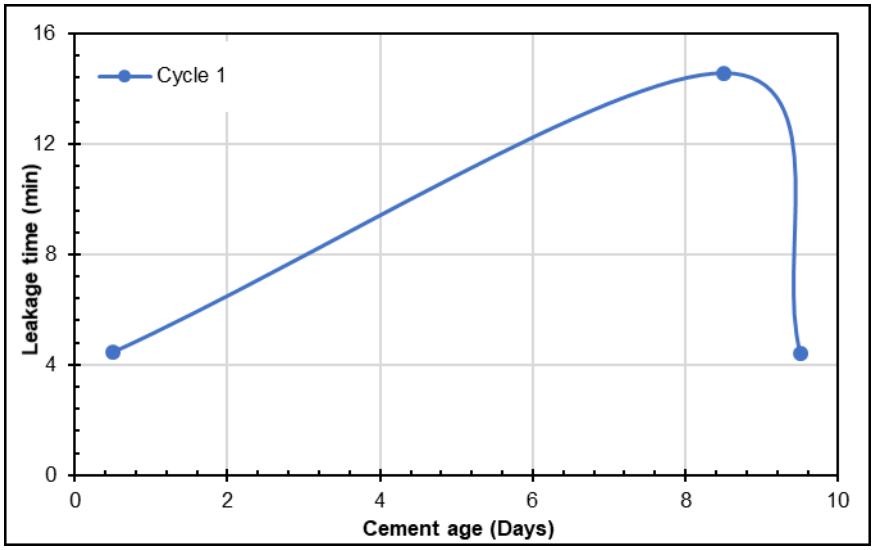

Figure 2.4: Leakage time versus cement age for 60 psig cycle in experiment 2 (neat Class H, WOC: 12 hours)

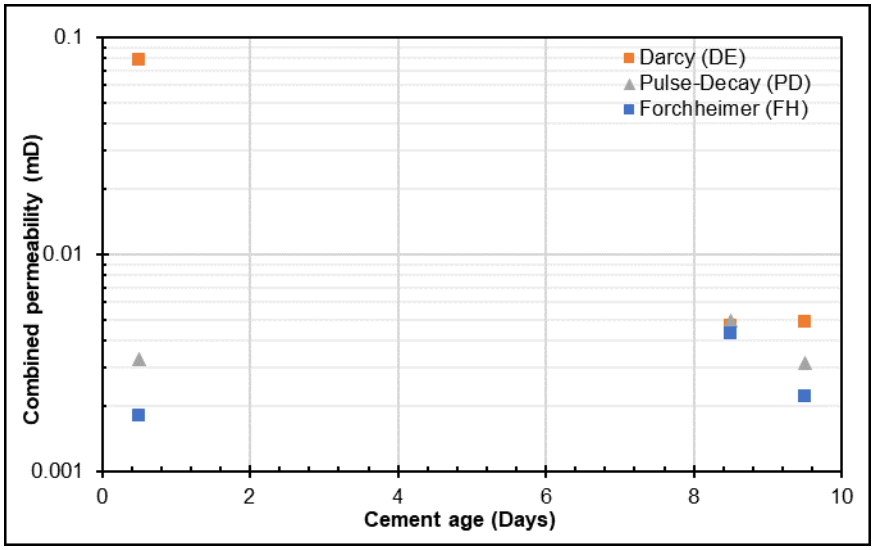

Figure 2.5: Combined permeability versus cement age for experiment 2 (neat Class H, WOC: 12 hours)

Table 2.1 compares the results from the first tests in the cycle 1 of each experiment conducted in the big setup I. The difference between experiments 1 and 2 was their WOC time (24 hours WOC for experiment 1 and 12 hours WOC for experiment 2). Considering the first test in cycle 1, after the WOC time, experiment 2 had a shorter leakage time (less than half of the leakage time for experiment 1) and a higher combined permeability value (0.079 mD). Thus, a cautious conclusion can be drawn that the WOC time affects gas migration rate and cement permeability for neat Class H cement.

Table 2.1: Summary of the results from the first tests in each of the experiments from big setup I

Exp. No.	Cement Grade	WOC (hrs)	Leakage Time (min)	Combined Permeability (mD) Darcy's Method	Combined Permeability (mD) Pulse-Decay Method	Combined Permeability (mD) Forchheimer's Method
1	H	24	11	0.004	N/A	N/A
2	H	12	5	0.079	0.003	0.002
3	H	24	16	0.132	0.070	0.032
4	G	24	0.22	N/A	0.001	0.001

2.4.3 Big Setup I Experiment 3 with Class H, Latex, and 24 hours WOC

Experiment 3 was conducted with Class H cement, 3 gallons/sack Thin Mortar Latex, and 1% by weight of Bentonite. These two additives were added to the cement slurry to prevent gas migration and reduce fluid loss in the cement. The WOC time was 24 hours and other test conditions (60 psig after WOC, for 30 minutes) remained constant. During the first test in cycle 1, the first bubble was detected after 16 minutes as shown in Figure 2.6, while the first bubble was detected after 3 minutes in the second test. Furthermore, the self-healing phenomenon was not observed because of the additives. Latex is a gas migration additive and when mixed with cement forms an

impermeable polymer structure within the cement pores which reduces the cement's permeability. Although, experiment 3 had the longest first bubble appearance time (leakage time) compared to experiments 1 and 2, this slurry was expected to have superior performance by preventing gas migration for at least the 30 minutes testing period. Visual observations also suggested that experiment 3 had a higher bubbling intensity compared to experiments 1 and 2, and that the bubble diameters appeared to be larger as shown in Figure 2.7.

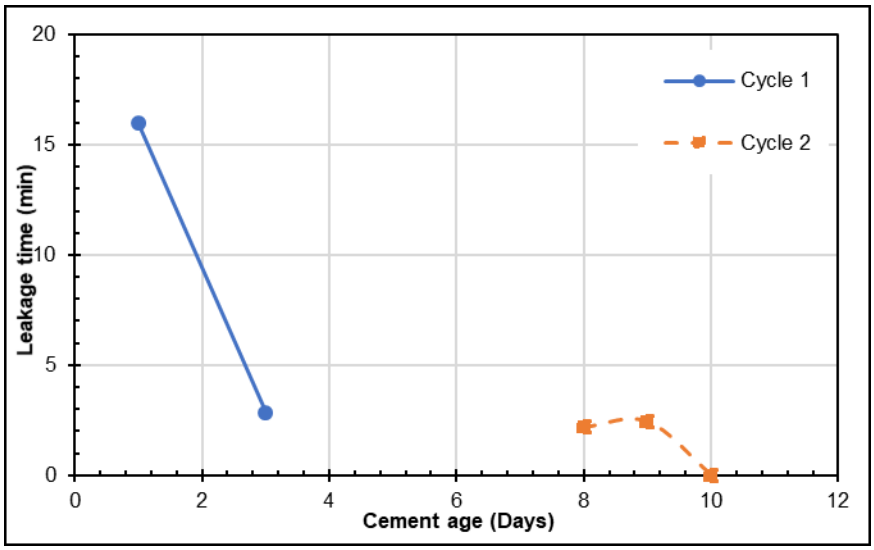

Figure 2.6*:* Leakage time versus cement age for the performed cycles in experiment 3 (Class H with Latex and Bentonite, WOC: 24 hours)

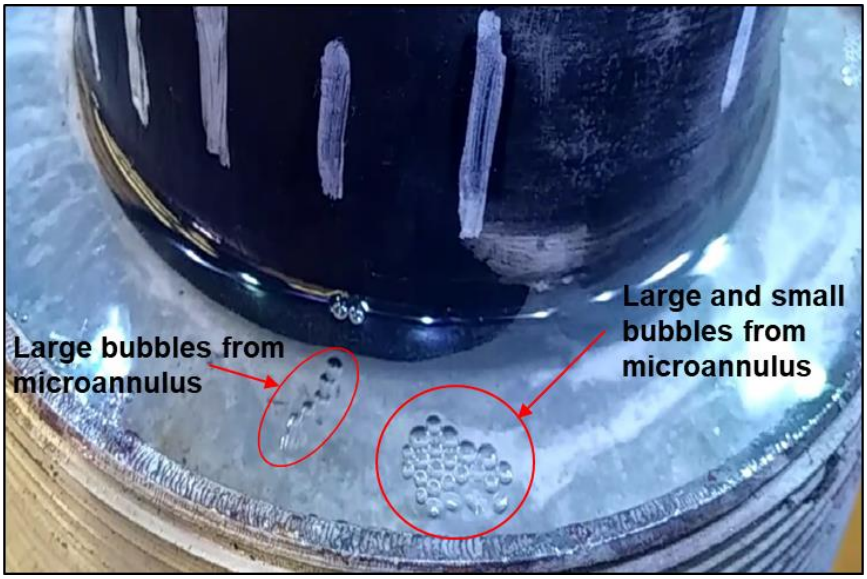

Figure 2.7: Large and small bubbles from microannuli within the set cement from big setup I experiment 3

One possible explanation for the reduced performance of this slurry is that latex, like any other polymer, requires some degree of elevated temperature to activate its polymer chains (Jones and Carpenter 1991; Al-Buraik et al. 1998). It is this temperature activated process that allows the cross

linking of latex polymer chains to form impermeable structures within the cement pores; thus, reducing the pore spaces and impeding the development of potential microannuli. This experiment was performed at ambient temperature because it was difficult to mimic the elevated temperature condition considering the big setup I and the arrangement used. Moreover, the latex used in this experiment was liquid and will most likely act like an additional water requirement (at an ambient temperature).

The reduced performance of this slurry was also evident in the high permeability values that were obtained. These were much higher compared those calculated from experiments 1 and 2 as shown in Figure 2.8. In addition, all the values except one, were higher than the range reported in literature for neat Class H and G. Given that this slurry had additives, its permeability values were expected to be lower than those for neat cement or fall within their range at the very least. The set cement from this slurry had severe microannuli and the combined permeability values shows an increasing trend as the cement age increases.

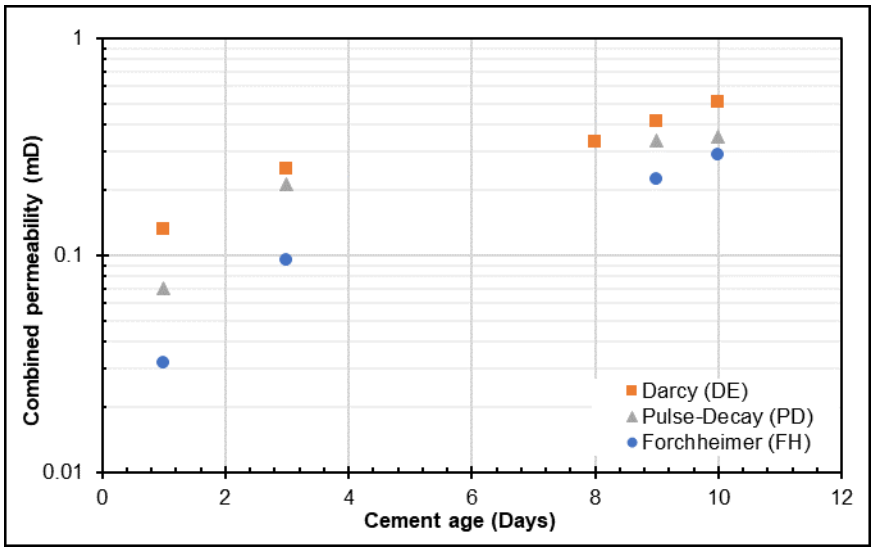

Figure 2.8: Combined permeability versus cement age for experiment 3 (Class H, Latex and Bentonite, WOC: 24 hours)

2.4.4 Big Setup I Experiment 4 with Neat Class G and 24 hours WOC

Neat Class G cement with 44% water to cement ratio was used in this experiment. The WOC time was 24 hours and other test conditions (60 psig after WOC, for 30 minutes) remained constant. Of all the experiments that were conducted using the big setup I, Class G cement showed the shortest leakage time. Figure 2.9 shows the leakage time versus cement age, and the first bubble in the first test was detected after 13 seconds. It was also observed that the leakage time for the set cement sheath was less than one minute for all the tests. The combined permeability values were estimated with only the pulse-decay and Forchheimer's methods. The Darcy's method was not used because the cameras did not detect the bubbles effectively. Figure 2.10 shows an increase in permeability with an increase in cement age. The values are within the range of reported permeability values and the values from both methods were very close.

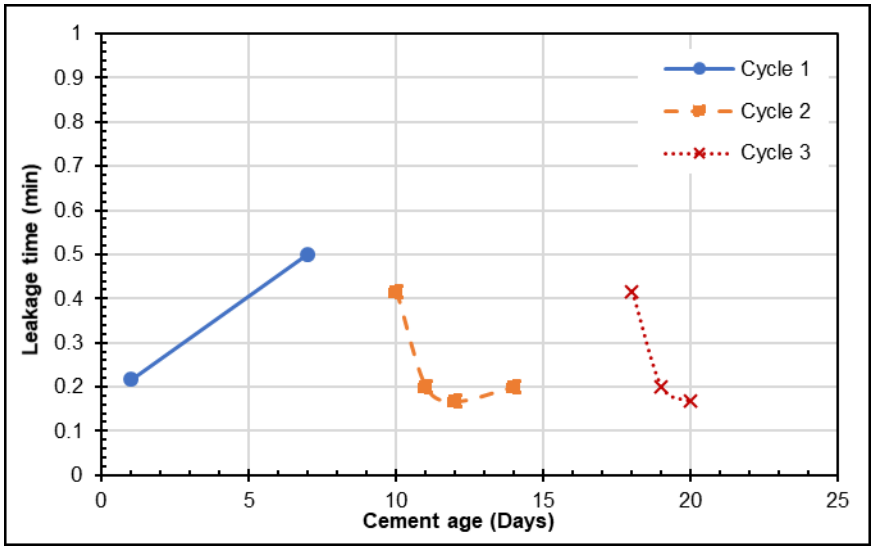

Figure 2.9: Leakage time versus cement age performed for the cycles in experiment 4 (neat Class G, WOC: 24 hours)

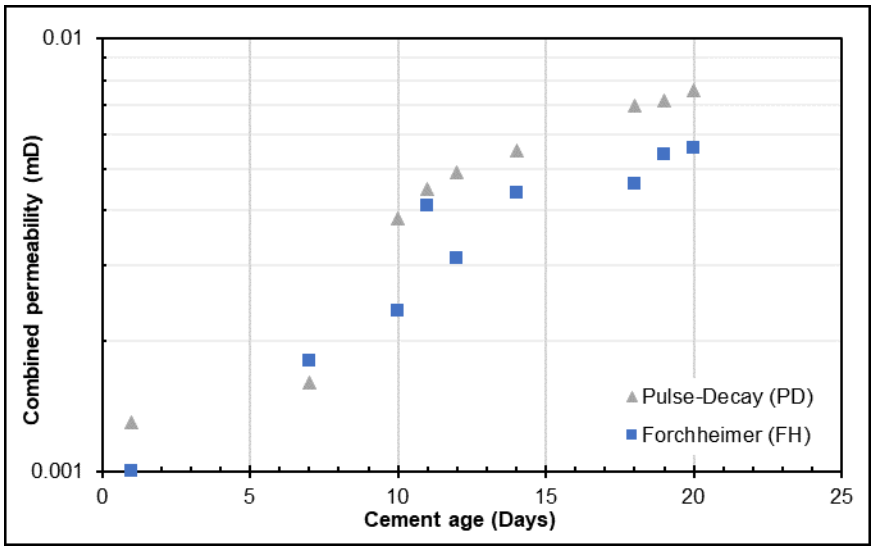

Figure 2.10: Combined permeability versus cement age for experiment 4 (neat Class G, WOC: 24 hours)

2.4.5 Gas Leakage Scenario Investigation

In this section, four scenarios are presented for gas leakage through the cement sheath in a liner-casing overlap. The difference between these scenarios is the differential pressure across the cement behind the liner-casing overlap. The goal of creating these scenarios is to investigate the optimum liner-casing overlap. In each scenario, four permeability values were used to assess the risk associated with each one of them. In addition, the liner-casing overlap was varied to investigate how the overlap length is going to help ensure good well integrity, especially during drilling and completions. The analytical derivations used to investigate these scenarios have been detailed in section **2.4.5** of the report on laboratory results for sealing assemblies and cement

system. Figure 2.11 shows gas flowing through different liner-casing overlaps. The following assumptions have been applied to the scenarios and they are:

- The last casing shoe is set at 1000 ft.
- Casing diameter is 22 inches.
- Liner hanger diameter is 18 inches.
- Temperature is 100^{o}F.
- Four permeability values of 0.01, 0.1, 0.3, and 0.5 mD.
- Faulty elastomers in the liner hanger.

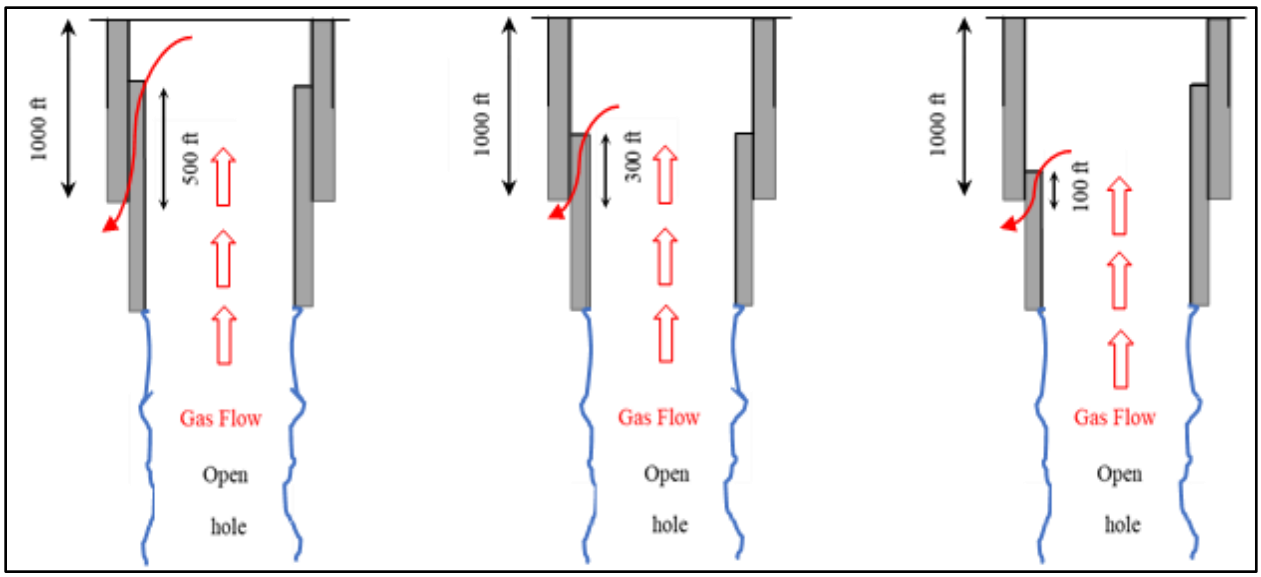

Figure 2.11: Gas leakage scenarios through different liner-casing overlap lengths

In the scenarios that were investigated, the leakage time was considered the primary variable for determining the optimum liner-casing overlap. According to API Bulletin E3 (1993), the liner-casing overlap length can vary from 50 to 500 ft. Therefore, the overlap lengths in the scenarios were varied from 50 to 500 ft with 50 ft increment.

In the first scenario, a differential pressure of 250 psi across the cement column behind the liner-casing overlap was assumed. Figure 2.12 shows the leakage time versus the overlap length for 250 psi differential pressure across the cement column. For 50 ft overlap, the leakage time was approximately 3 hours for a permeability of 0.01 mD, while the leakage time decreased below 30 minutes for the rest of the permeability values. A general trend that was observed is that as the liner-casing overlap length increases, the leakage time increases. For 0.3 mD, the gas takes almost 25 minutes to appear when the overlap length is 100 ft, while it takes 95 minutes for 200 ft overlap.

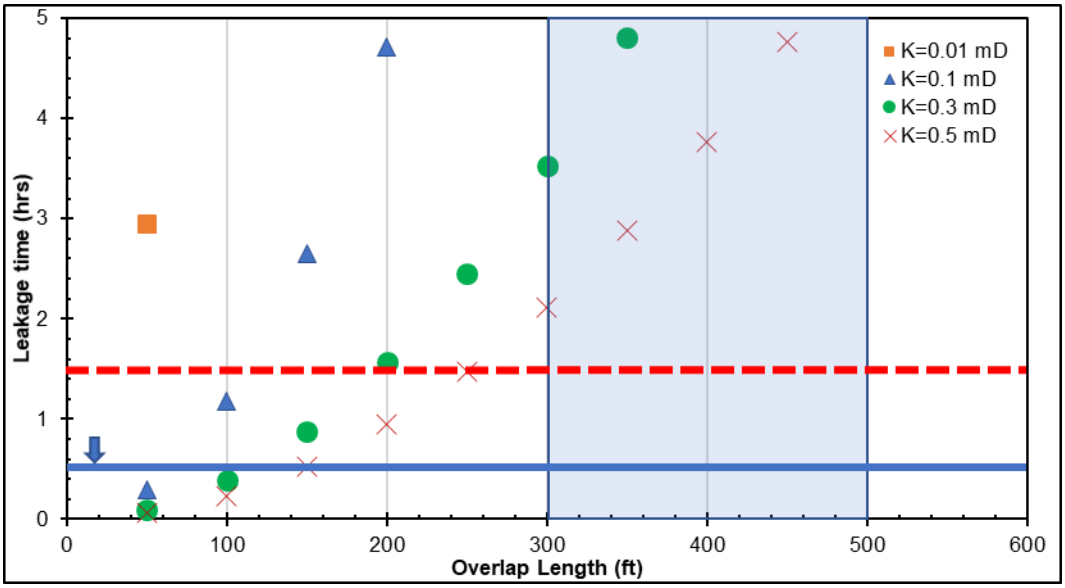

Figure 2.12: Leakage time versus liner-casing overlap for 250 psi pressure differential across the cement.

The second scenario assumes a differential pressure of 500 psi across the cement column behind the liner-casing overlap. Figure 2.13 shows how the leakage time varies with the overlap length for 500 psi differential pressure across the cement column. For 50 ft of overlap, the leakage time was approximately 1 ½ hours (with a permeability of 0.01 mD), while it was less than 30 minutes for the rest of the permeability values. The leakage time increases as the liner-casing overlap increases. For a permeability of 0.3 mD, the leakage time is 15 minutes when the overlap is 100 ft, while it is 55 minutes for 200 ft of overlap. It can be observed that as the differential pressure across the cement (within the overlap) increases, the leakage time decreases.

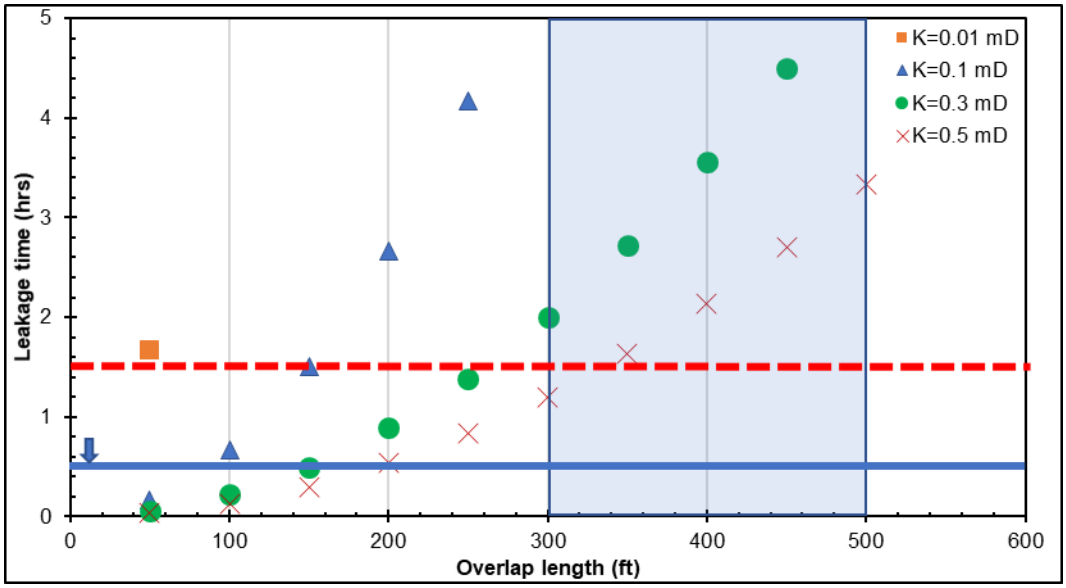

Figure 2.13: Leakage time versus liner-casing overlap for 500 psi pressure differential across the cement.

The third and fourth leakage scenarios assumed differential pressures of 1000 psi and 1500 psi respectively across the cement column behind the liner-casing overlap. Figure 2.14 and Figure 2.15 show the leakage time versus the overlap length for 1000 psi and 1500 psi differential pressures respectively. It can be observed that the 50 ft overlap has the shortest leakage time especially for permeability values ranging from 0.1 to 0.5 mD.

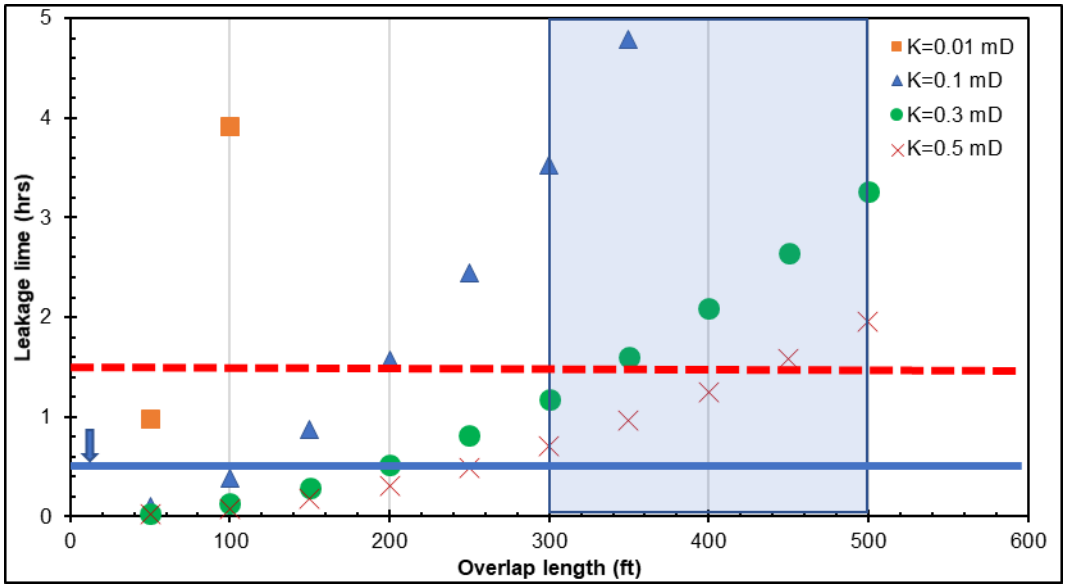

Figure 2.14: Leakage time versus liner-casing overlap for 1000 psi pressure differential across the cement.

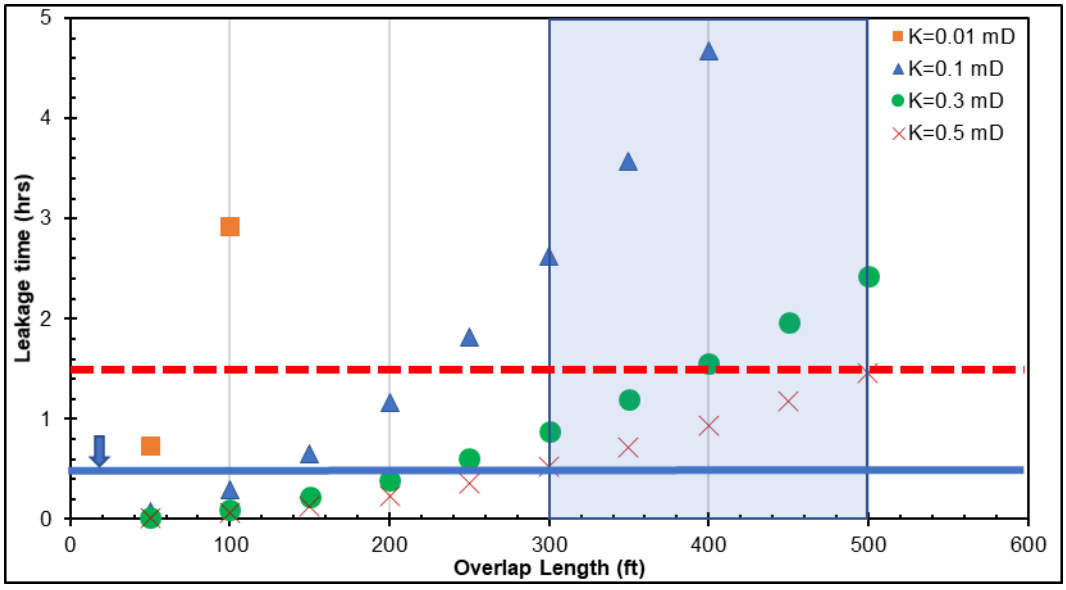

Figure 2.15: Leakage time versus liner-casing overlap for 1500 psi pressure differential across the cement.

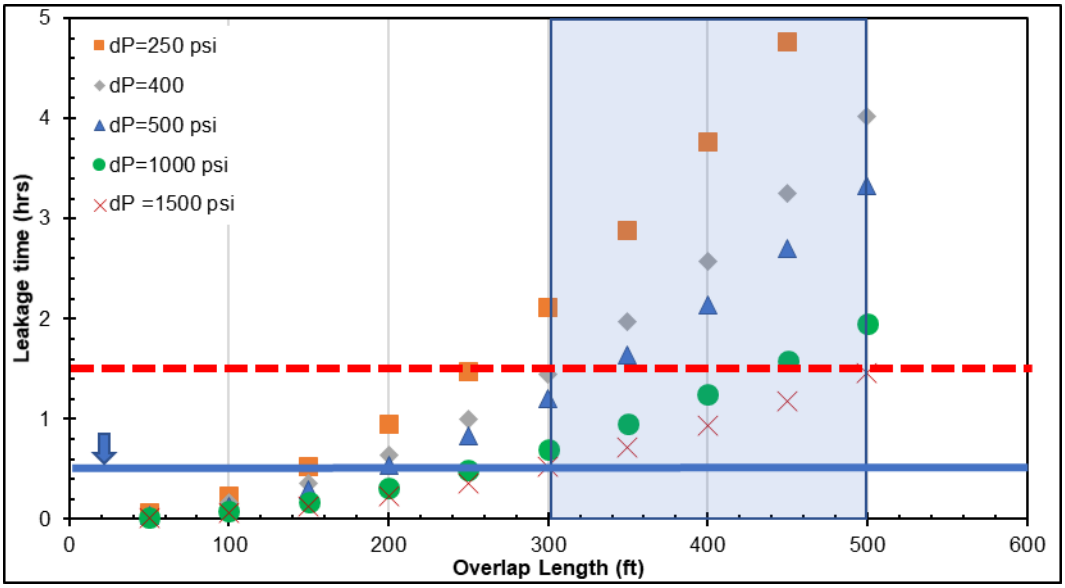

Figure 2.16: Leakage time versus liner-casing overlap for 0.5 mD combined permeability for several differential pressures.

Figure 2.16 shows how the leakage time will vary with the overlap length for various differential pressures at 0.5 mD combined permeability. It can be observed that as the differential pressure across the overlap increases, the leakage time decreases. For 150 ft overlap and 250 psi differential, the leakage time is 30 minutes, while for 1000 psi it is 10 minutes. However, as the overlap length increases, the difference in leakage time increases. For 300 ft overlap and 250 psi differential the leakage time is approximately 2 hours 7 minutes, while for 1000 psi differential it is 42 minutes. Some recommendations have been made from these scenarios. Please review the draft recommendation report for the details.

2.4.6 Small Setup I with Neat Class H Cement Sample

In all the small setups, a maximum of two 60 psig cycles were performed before discarding them. The mixing, curing, and testing procedures for all tests with the small setups are the same. One of the major observations that was documented during tests was that the leakage time decreased within a cycle as time elapsed. Another observation was that some bubble positions disappeared, and some appeared as time elapsed. Figure 2.17 shows the leak positions on small setup I experiment 1 (a) and experiment 2 (b). In experiment 1, the positions that disappeared in cycle 1 were positions 2, 3, 4, and 5. In cycle 2, position 6 disappeared. In small setup I experiment 2, positions 3 and 4 disappeared in cycle 1.

One of the objectives of small setup I was to investigate the effect of pipe size. Looking at Table 2.2 and comparing the leakage times of small setup I experiment 1 and 2 to big setup I experiment 1, a significant deviation in leak times were observed. The small setups had faster leak times than the big setup. An explanation for this could be the total volume to be filled with 60 psig of the inlet gas. Big setup I had a volume of 8303 ml to be filled while the small setup I had a

volume of 463.33 ml (1-inch) and 1853.3 ml (2-inch) to be filled with N_2 gas. The volume difference allows the gas to migrate faster in the small setups; thus, the shorter leak time recorded. In Table 2.2, a shorter leak time is observed for the small setup I experiment 1 compared to experiment 2. The volume difference – small setup I experiment 1 (463.33 ml) and small setup I experiment 2 (1853.3 ml) – accounts for the change in time, since the pressure was kept constant at 60 psig throughout the experiments.

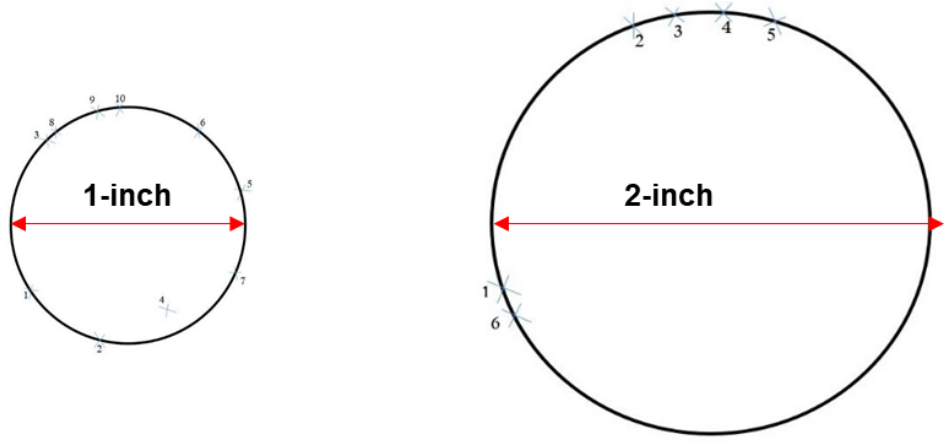

a **b**

Figure 2.17: Small setup I showing experiment 1 (a) and experiment 2 (b)

Table 2.2: Leakage time for big setup I experiment 1 and small setup I experiments 1 and 2.

Experimental Setup	Leakage Time (minutes)
Big setup I experiment 1	11
Small setup I experiment 1	1
Small setup I experiment 2	5

2.4.7 Small Setup 1 with Class H, Latex, and Bentonite Cement Sample

Using this setup, experiment 3 was performed with neat Class H cement, 1 gal/sack Thin Mortar Latex, and 0.5% bentonite. The first test was performed after 24 hours WOC. Before the test, water was poured on the cement surface to help track the bubbling. Prior to flowing the gas into the system, just after pouring water on top of the set cement, there were bubbles already emanating from the surface of the cement. This observation was deemed to be normal since a similar experience was encountered in big setup I experiment 3 (with the same formulation and additives).

The cement surface bubbled for over 45 minutes; thus, delaying the commencement of the test. After most bubbles disappeared, the setup was connected, and the first test was performed. 21 minutes after beginning the test, the first bubble and position were observed. Position 2 started bubbling 1 hour 32 minutes after the test began. However, the bubbles from this position were not consistent and were coming out intermittently. The second test was performed the following day, and there was one bubble from positions 2 and 3. There were also 3 random bubbles observed from various positions on the cement surface, but these were not classified as leaks. In this study, the appearance of gas bubbles is classified as a leak only when there is a continuous bubbling of

the gas. After 9 minutes 53 seconds, position 2 experienced its first gush of bubbles. After 1 hour, there were random bubbles that appeared from time to time but no consistent bubbles were observed.

A third test (72 hours WOC) was conducted on small setup I experiment 3. After 9 minutes 31 seconds of starting the test, the first random bubble was observed followed by other random bubbles with one of them coming from position 3. None of these were recorded as the leak time because no constant bubbling was observed. The leak time was recorded as 20 minutes 9 seconds because position 3's bubbling became more pronounced and consistent at this time. In this study, the consistency and pronouncement of a leak is defined when there is a 7 to 20 seconds delay between one bubble and the next coming from the same leak position. Since the bubbling in small setup I experiment 3 was inconsistent, an extended experiment was carried on the setup. The valve was opened at 3:42 pm on September 26, 2017 (8 days WOC). The first leak occurred after 8 hours of testing and after 20 hours of testing, two constant leak positions were observed.

2.4.8 Small Setup I with Class H and Fly Ash Cement Sample

Fly ash cement slurry was one of the recipes that was tested. The composition of fly ash has been discussed under section **2.3.2** of the report on laboratory results for sealing assemblies and cement system. Figure 2.18 shows that fly ash particles are generally spherical (Federal Highway Administration, 2017). In small setup I experiment 4, 30% fly ash BWOC and 1 gal/sack latex was used. A water requirement of 3.6 gal/74 lbm was used for the fly ash. The first test was performed on November 10, 2017 (24 hours WOC), using the standard testing procedure. During the first test, a rise in the water level was visually observed and shortly after, there was a leak. The leak was recorded at position 1, 21 minutes 26 seconds after commencing the test. After bubbling continuously for about an hour, the bubbling seized but continued almost immediately. This was approximately 1 hour 18 minutes from the test commencement. Two other tests were conducted on this sample, one on November 11, 2017 (48 hours WOC) and the last on November 14, 2017. Their leak times were recorded as 14 minutes 25 seconds and 20 minutes 48 seconds respectively. Visual observation suggests that the bubbling intensity in the last experiment was lower compared to the 48 hours WOC test. This indicates an improvement in the cement compressive strength and a potential decrease in cement permeability with hydration. The shorter leak time is attributed to residual gas in the cement sheath from the test performed the day before. The 2-day fallow period allows all the gas to escape the setup and an increase in the leakage time was observed once again. This observation directly corresponds to the self-healing effect discussed in big setup I experiment 1. It is to be noted that all through the tests with this slurry, only one leak position was observed (as shown in Figure 2.19).

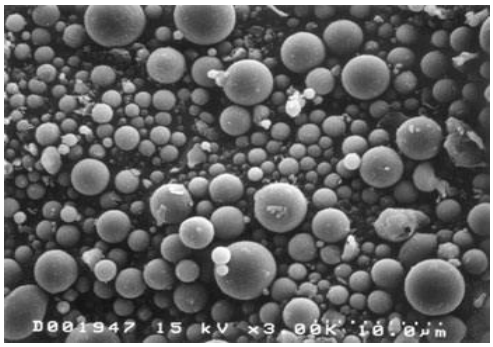

Figure 2.18: Fly ash particles at 2000x magnification (Federal Highway Administration, 2017).

(a) **(b)**

Figure 2.19: Fly ash cement showing gas bubbles during test (a) and leak position after test (b) for small setup I experiment 4.

2.4.9 Small Setup I with Microsilica Cement Sample

Microsilica cement slurry was investigated with small setup I experiment 5. The cement slurry was formulated with Class H cement, 38% water requirement, 5.5% microsilica (Silica Fume White) BWOC, and a 5% water requirement for the microsilica. A 5% water requirement was selected because no water reducers were used during the mixing. Prior to this selection, a range of (5% to 12%) water requirement could have been used for the experiment. Both low and high ranges were prepared, but the sample with 5% water requirement was used so that the slurry density (16.05 ppg) is kept close to that of neat Class H slurry (16.65 ppg). The resulting density from the 12% water requirement sample was 15.5 ppg.

The first test was performed after 24 hours WOC and the first leak was observed 15 seconds into the test. This indicates poor bonding between the microsilica cement and the casing since the leak occurred at the wall (position 1). The test continued for 30 minutes, and no subsequent leaks were recorded. The second test was conducted the following day and two new leak positions were recorded, making a total of 3 leak positions. The second and third leaks occurred 57 seconds and 2 minutes 11 seconds respectively, after starting the test. After 72 hours WOC, test 3 was performed and the first leak occurred 11 seconds after beginning the test. The leak in position 2 was recorded 35 seconds into the test. Figure 2.20 (b) shows the three leak positions in small setup

I experiment 5. Position 3 was identified within the cement sheath and this can translate to a faulty cement slurry. Images of the cement sheath were obtained with a Dino-Lite Digital Microscope. Figure 2.20 (a) shows the surface of the slurry before the first test while Figure 2.20 (c) shows leak position 1 observed during the test. The leak came from beneath the cement crack and steel pipe wall as shown by the red circle and arrow.

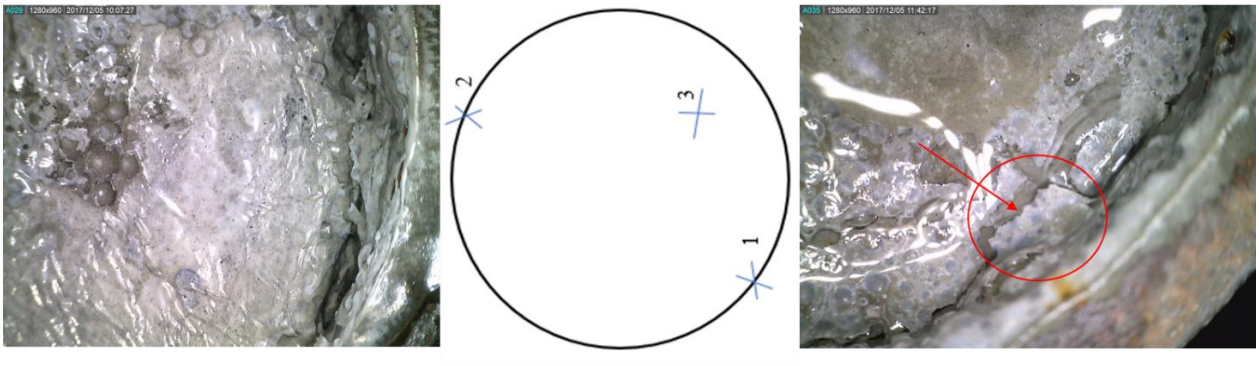

(a) **(b)** **(c)**

Figure 2.20: Microsilica cement before the first test (a), leak positions (b), and leak position 1 during a test (c) for small setup I experiment 5

To verify the inadequacy of Silica Fume White, the slurry for small setup I experiment 6 was designed. This was similar to the slurry design for small setup I experiment 5, except that 12% of microsilica was used instead of 5.5% used in experiment 5. The microsilica concentration was increased in a bid to create an improved cement slurry. No additional water was needed for this experiment. After 24 hours WOC, the first test was conducted, and a leak was observed within the first 7 to 10 seconds. The second test (48 hours WOC) that was conducted on this setup had the first leak within 10 seconds of commencing the test. Both tests had the gas leaking through the same position (between the cement and the steel wall) like experiment 5. The leak times which were almost instantaneous indicated poor bonding through the entire length of the cement column.

One plausible mechanism for the poor slurry performance is slurry densification. It was highlighted in literature that microsilica has a particle size ranging from 0.02 to 0.5 μm, with an average of 0.15 μm. Cement on the other hand has a particle size ranging from 1 μm to 90 μm, with 10 wt% of the cement being made of particles larger than 50 μm and only a few wt% consisting of particles larger than 90 μm. On the fine end, less than 10% of the cement particles were smaller than 2 μm. From the particle size distribution (PSD) of cement, undensified, and densified microsilica, it can be observed that the fine particle size of microsilica allows packing between the cement grains, resulting to an improved microstructure within the cement matrix. Undensified microsilica has a typical bulk density between 200 kg/m^3 and 350 kg/m^3, while densified microsilica has a typical bulk density between 500 kg/m^3 and 700 kg/m^3. The microsilica used in this study had an approximate density of 400 kg/m^3. Per Daou and Piot (2009), "only microsilica with a bulk density of approximately 300 kg/m^3 is the adequate compromise between proper handling characteristics and good slurry performance".

2.4.10 Small Setup I with Nanomaterial Cement Sample

Nanomaterial was used as an additive in small setup I experiment 7. A 0.5% BWOC concentration of nanomaterial was used in combination with Class H cement. As a result of the fine nature of the nanomaterial, the mixing procedure was slightly modified to effectively homogenize the slurry. After completing the standard API mixing procedure, an additional 15 seconds of shearing at 4000 rpm was allowed, followed by another 15 seconds of shearing at 12000 rpm. This modification allowed for complete dispersion of the nanomaterial within the new slurry. The normal curing and testing procedures were followed. The first leak was detected after 9 minutes 54 seconds into the first test and the bubbles that were observed were extremely tiny. Position 2 was recorded 11 minutes after position 1 was marked. The bubbles at position 2 were also miniscule and had an average of 1 minute 28 seconds delay between one bubble and the next. This delay was determined by an average of the time between 4 consecutive bubbles. Two other tests were conducted after 48 hours and 72 hours WOC. No bubbles were recorded on the second day of testing. On the third day of testing, continuous bubbling was recorded after 2 hours 4 minutes and 35 seconds of beginning the test. This leak was small and was spotted on a different surface location of the set cement which was marked position 3. Figure 2.21 (a) shows the surface of the set cement before the test and Figure 2.21 (b) shows position 1 where the first leak was detected.

(a) **(b)**

Figure 2.21: Nanomaterial cement sample before test without leaks (a) and during the test showing position 1 within the cement

After allowing the nanomaterial cement to fallow for 5 days, another test was conducted on the sample. The first leak was detected at position 3 after 1 minute and 11 seconds into the test. Five new positions were spotted after the first leak, some being at the center of the set cement while others were between the cement and casing. Figure 2.22 shows all the leak positions on small setup I experiment 7 during the test conducted after the fallow period.

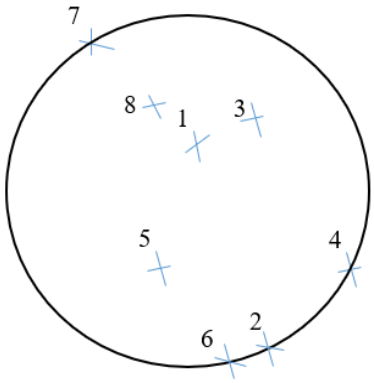

Figure 2.22: Leak positions in small setup 1 experiment 7 during the test conducted after the fallow period

2.4.11 Small Setup I with Class H, Flyash, Latex, and Nanomaterial Cement Sample

To improve on the previous slurry designs, a combination of additives was tried. In small setup I experiment 8, a cement slurry with Class H cement, 30% fly ash, 1 gal/sack Latex, and 0.5% nanomaterial was formulated. The water requirement for fly ash was kept at 3.6 gal/74 lbm. The first leak during the test was recorded at 1 minute 14 seconds, while the second leak was recorded at 1 minute 20 seconds. The bubbling intensity observed on the first day of the test was high and the bubbles were coming from multiple positions as shown in Figure 2.23 (a and b). Three tests were performed for 3 consecutive days on the sample and the bubbling intensity appeared to have decreased as the number of days increased. By the end of the 3-day testing period, a total of eight bubbling positions were identified. Five of these were within the set cement while the other 3 were located at the interface between the set cement and the steel pipe. Figure 2.23 (c) shows the identified leak positions in small setup I experiment 8 after all the tests.

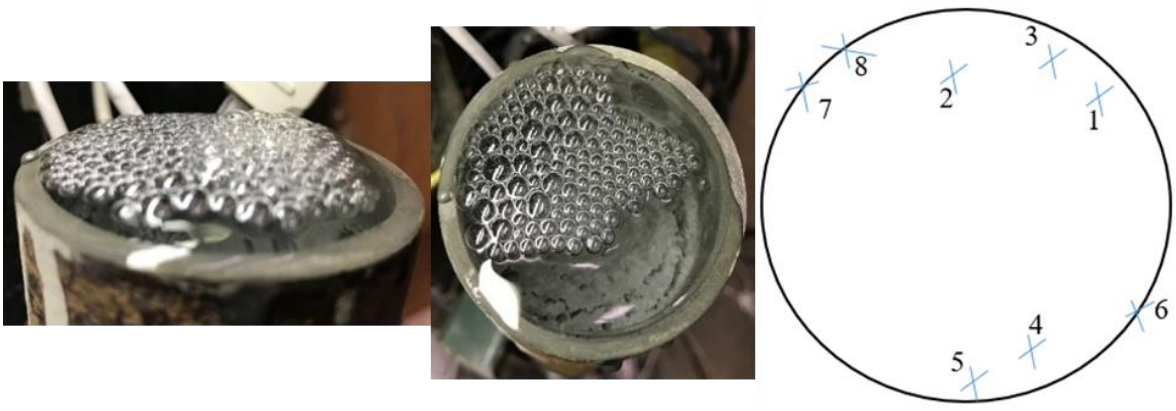

(a) **(b)** **(c)**

Figure 2.23: Side and top view of gas bubbles (a and b) and bubble positions (c) in small setup I experiment 8

2.4.12 Small Setup I with Class H, 1.5 liters/100 kg Commercial Additive Cement Sample

A commercial additive from a service company was used to design a new slurry for small setup I experiment 9. The recommended range was from 4.5 liters to 9 liters per 100 kg of cement. 6 and 3 liters/100 kg were tried but both concentrations made the cement slurry too viscous to be used in the lab. A concentration of 1.5 liters/100 kg was finally used. The new slurry revealed a high

static gel strength (SGS) but regular thickening time. These results are discussed in detail in section **2.5**. No leaks were observed during the first test which was after 24 hours WOC. After 48 hours WOC, the set cement was pressurized for 6 hours – 4 hours followed by a 2-hour session. No leaks were noticed as the system remained gas tight. The last test was conducted for 2 hours after 72 hours WOC and the system still proved to be gas tight.

Figure 2.24: Small setup I experiment 9 showing no bubbles after two tests.

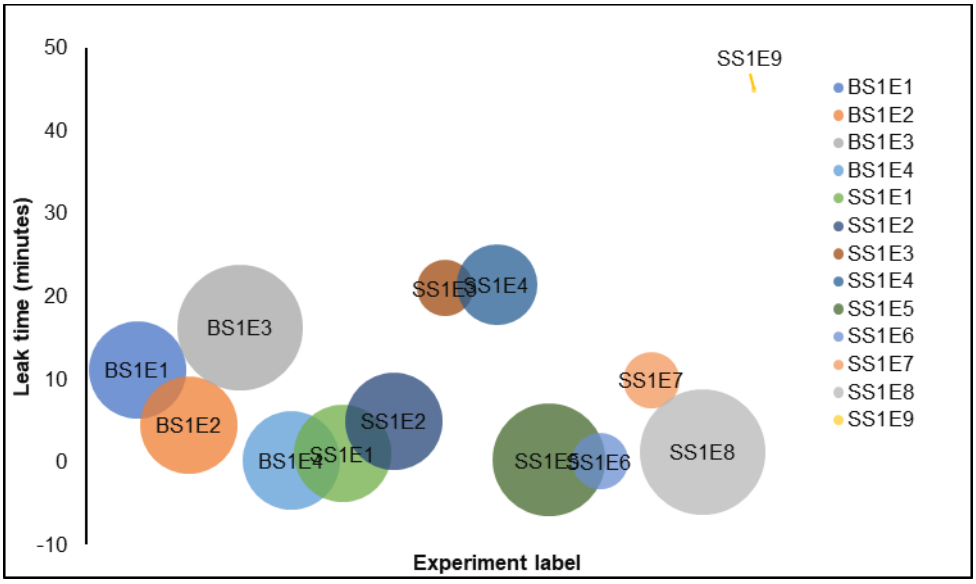

Figure 2.25: Bubble graph showing the leak times for all the tests using setup I

Table 2.3: Summary of results for all the tests using setup 1

Big setup I					
Setup/Experiment	**WOC (hrs.)**	**Density (ppg)**	**Composition**	**Leak time (mins:secs)**	**Bubbling description**
S1E1	24	16.65	Neat Class H	11 mins 08 secs	3
S1E2	12	16.65	Neat Class H	4 mins 28 secs	3
S1E3	24	12.5	3 gals/sack latex, 1% bentonite	16 mins 17 secs	5
S1E4	24	16.65	Neat Class G	13 secs	3
Small setup I					
Setup Experiment	**WOC (hrs.)**	**Density (ppg)**	**Composition**	**Leak time (mins:secs)**	**Bubbling description**
SS1E1	24	16.65	Neat Class H	1 min	3
SS1E2	24	16.65	Neat Class H	5 mins	3
SS1E3	24	16.65	1 gal/sack latex, 0.5% bentonite	21 mins	1
SS1E4	24	14	1 gal/sack latex, 30% flyash	21 mins 26 secs	2
SS1E5	24	16.05	5.5% microsilica	15 secs	4
SS1E6	24		12% microsilica	7 secs	1
SS1E7	24	16.55	0.5% nanomaterial	9 mins 54 secs	1
SS1E8	24	14.5	1 gal/sack latex, 30% fly ash, 0.5% nanomaterial	1 min 14 secs	5
SS1E9	24	16.4	1.5 liters/ 100 kg commercial additive from a service company	N/A	0

1 - Tiny inconsistent bubbling, 2 - Tiny consistent bubbling, 3 - Regular bubbling, 4 - Intense bubbling, 5 - Intense bubbling with multiple locations.

Figure 2.25 depicts the bubble graph for **Error! Reference source not found.**. The level at which the center of each bubble stands, represents the leak time of that experiment. It is worthy to mention that none of the centers of the bubbles are below zero leak time. The bubbles whose circumferences extend to the negative leak time axis are because of the sizes of the bubbles, which indicates the degree of bubbling, and not because they have negative leak times. The bubbling degree is on a scale of 1 to 5. '1' indicates tiny and consistent bubbling, whereas '5' indicates intense bubbling with multiple locations. The bubble graph provides a pictorial view of the tests conducted with the big setup I and small setup I. For the big setup I, the nomenclature "BS1E1" represents big setup I experiment 1, while for the small setup I, "SS1E1" represents small setup I experiment 1.

2.5 PHYSICAL PROPERTIES OF CEMENT SAMPLES

2.5.1 Rheology

Rheology is the science and study of the deformation and flow of matter, especially the flow of non-Newtonian fluids. All cement slurries are considered non-Newtonian and they can be shear thinning or shear thickening. The addition of some additives like fly ash and nanomaterial can make the formulated slurries develop higher viscosity. A combination of nanomaterial and fly ash in the same slurry increases the viscosity of the slurry. Although cement slurries with additives tend to be more viscous, they also prove to be much more shear thinning than the base slurry. This is indicated by the reduction in the flow behavior index (n) for the slurries with additives. The addition of 0.5% nanomaterial to the base slurry made the slurry design more shear thinning. The addition of 30% fly ash and 1 gal/sack of latex also made the cement slurry more shear thinning. However, adding 0.5% nanomaterial to the slurry design with 30% fly ash and 1 gal/sack of latex increased the 'n' value, drawing it closer to a Newtonian fluid. Table 2.4 shows the rheological properties of all the slurry designs that were tested. The shear stress values were obtained after ramping the slurry temperature from ambient to 102^{o}F.

Table 2.4: Cement slurry rheological properties

Table 2.9. Shear stress values at corresponding shear rates of tested cement slurries						
	Neat Class H	Class H cement, 30% Fly ash and 1% latex	Class H, 0.5% nanomaterial	Neat Class G	Class H, 30% fly ash, 1 gal/sack latex 0.5% nanomaterial	Class H, 1.5 liters/100 kg commercial additive
Shear Rate (1/s)	**Shear Stress (Pa)**					
1021.3809	161.32	107.60	131.58	58.32	120.34	105.66
510.9969	82.32	71.44	76.38	40.40	70.28	70.56
340.6986	53.64	57.50	58.14	34.24	53.74	55.84
170.2982	38.64	44.58	44.22	27.10	38.90	42.32
10.2138	7.98	14.26	9.840	8.68	13.36	12.98
5.1069	6.14	10.94	6.90	4.14	10.30	7.64

2.5.2 Gas Transit time

Gas transit time is the period during which the cement slurry changes from a true hydraulic fluid capable of providing hydrostatic pressure to a highly viscous material showing solid characteristics. The gas transit time starts when the cement slurry develops enough static gel strength (SGS) to restrict transmission of full hydrostatic pressure and ends when the cement is solid enough to prevent gas flow. SGS is measured using a cement consistometer. It is calculated by the geometry and slow motion of the consistometer paddle (10°). This slow movement allows SGS to be measured but does not inhibit gel strength development. Sabins et al. (1982) estimated that transition time ends when the cement slurry has developed an SGS exceeding 250 Pa (522 lbf/100ft^2). Generally, gas transit time is the time it takes for the SGS of a cement slurry to rise from 100 lbf/100ft^2 to 500 lbf/100ft^2.

The gas transit time of the slurry designs are displayed in Figure 2.26. The shorter gas transit times in the new slurry mixtures show higher potential for mitigating gas flow through the cement slurry. With the addition of 30% flyash and 1 gal/sack latex, the gas transit time was reduced by almost 1 hour, making the new slurry design desirable. The new slurry design with 30% flyash and 1 gal/sack latex proved to be a better substitute to neat Class H. It had a leak time of 21 minutes and 26 seconds in a 2-inch pipe, while neat Class H proved to prevent gas flow for only 5 minutes.

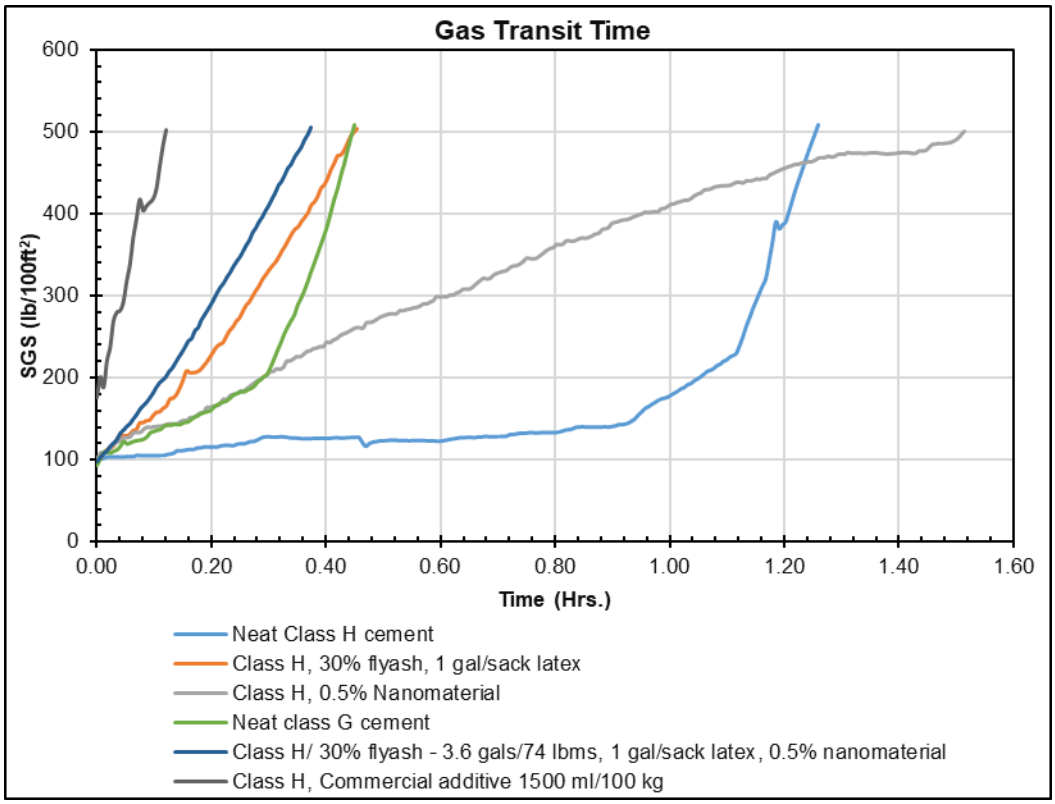

Figure 2.26: Gas transit time for various cement slurry samples.

Class H with 0.5% nanomaterial had a better gas transit time compared to neat Class H. This slurry design showed better performance with an improved leak time of 9 minutes and 54 secs. A cautious inference can be made that a slurry with a shorter gas transit time has a good potential to mitigate gas migration. However, this may not always hold for all slurry designs, especially when different additives are mixed. For instance, the slurry design with neat Class H, 30% BWOC flyash, 1 gal/sack latex, and 0.5% BWOC nanomaterial took 12.5 minutes (0.2089 hrs.) to attain 100 lbf/100 ft^2 and 35 minutes to attain 500 lbf/100 ft^2. The gas transit time was 22 minutes and 30 seconds. Although this slurry design had a short gas transit time, the leak time when it was used in small setup I experiment 8 was within 1 minutes and 14 seconds after 24 hours WOC. This is attributed to the properties of some of the additives which tends to impede early UCS development. This will be discussed in the next subsection. With the addition of 1.5 liters/100 kg of commercial additive, the gas transit time reduced to 7 minutes 19 seconds, this was the least recorded time. This slurry had no leaks occur throughout the testing period proving to be completely gas tight.

2.5.3 Unconfined Compressive Strength and Ultrasonic Testing

Unconfined compressive strength (UCS) is the maximum axial compressive stress that a right-cylindrical or cubic material can withstand under unconfined conditions (zero confining stress). The materials used for UCS test were set cement samples. UCS is also known as the uniaxial compressive strength of a material (cement cubes) because the application of compressive stress is only along one axis — the longitudinal axis — of the sample. In an ultrasonic compressive-

strength test, a high-frequency sound pulses through a set cement sample and measures the time required for the sound wave to travel completely across the lateral dimension of the sample. This generates an ultrasonic pulse velocity (UPV). As the cement sets with time, the sound wave travels faster; thus, taking a shorter time to reach the other end of the sample.

In this study, both the ultrasonic cement test and unconfined compressive strength tests were carried out on the slurry designs which were cured for 1 and 3 days, and have been used in the big and small setups I. This was done to provide a holistic picture of the performance of cement slurries used for testing. Using the API RP 10B-2 (2013) procedures, cubical cement samples were prepared for both UPV and UCS testing. The preparation of the cement samples are as follows: i) the molds were put together and greased, ii) the right slurry was selected, and iii) the appropriate mixing procedure was used for each cement slurry. The cement slurries were then poured into the molds, each cube in a mold was filled to half of its capacity, followed by the next cube, and finally the third cube. After filling the third cube to half of its capacity, the first cube was topped up to the brim, followed by the second cube, and finally the third cube to complete one mold.

After curing the samples in a water bath for the appropriate number of days (1 or 3 days) at atmospheric temperature and pressure, the samples were taken out of the water bath and dried shortly. For each test, three samples were prepared to provide more accurate data. Before each test, the dimensions of the samples were recorded (Figure 2.27 a). Three values for length and width were taken and averaged out to provide the final length and width of the sample. This was done for each of the three samples to be used for the test. The ultrasonic test was conducted first since it is a nondestructive test. The probes were placed on both ends of the cubic cement sample and high frequency sounds were propagated through the cement sample. The time it takes for the sound frequencies to propagate through the sample was recorded. Figure 2.27 (b) shows an ultrasonic test being conducted on a cement sample. The same procedure was followed for each slurry design and Table 2.5 shows the ultrasonic pulse velocity (UPV) readings.

(a) **(b)**

Figure 2.27: Dimensions of cement samples (Class H and G) measured (a) and ultrasonic cement test being carried out (b).

Table 2.5: Ultrasonic pulse velocity (UPV) and unconfined compressive strength (UCS) test results.

Cement slurry type	Day	UPV (m/s)	UCS (MPa)
Neat Class H	1	2191.69	4.00
	3	2972.17	15.36
Neat Class G	1	2915.39	15.34
	3	3406.41	28.36
Class H, Nanomaterial	1	2369.56	6.09
	3	3123.44	19.66
Class H, Flyash, latex Nanomaterial	1	1888.46	1.69
	3	2686.24	6.41

For the unconfined compressive strength (UCS) tests, a Test Mark Compressive Strength machine was used. A uniaxial force was applied to the cement matrix till it failed by shearing. The value at which the maximum stress is applied on the body is termed as the UCS of the sample. UCS tests were performed on all the samples with the same curing day(s) and the average of the values was considered the strength of the set cement. Figure 2.28 shows an unconfined compressive strength test being conducted and the shear failure of the cement sample. The 1-day and 3-days compressive strengths of various samples are reported in Table 2.5. From this table, an increase in UCS for neat Class H cement sample was observed. This increase was in the range of 220% and 285% for a period of 1 day to 3 days. The addition of additives like nanomaterial and fly ash impaired compressive strength development in the samples.

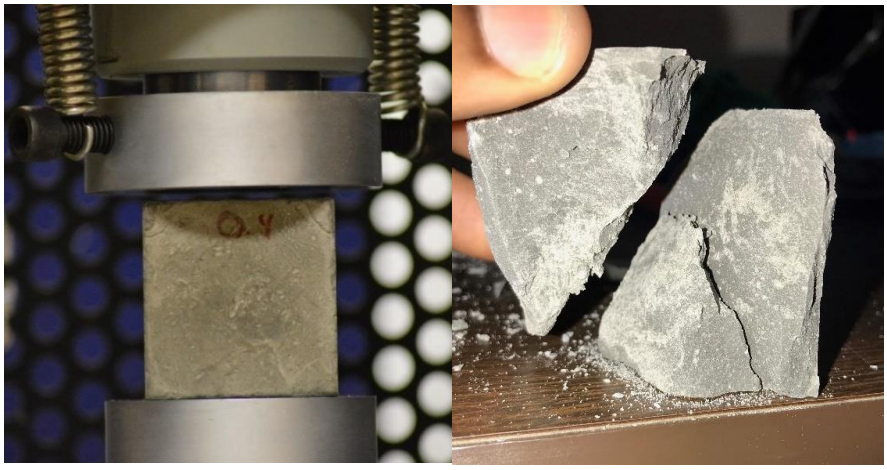

(a) **(b)**

Figure 2.28: Unconfined Compressive Strength conducted

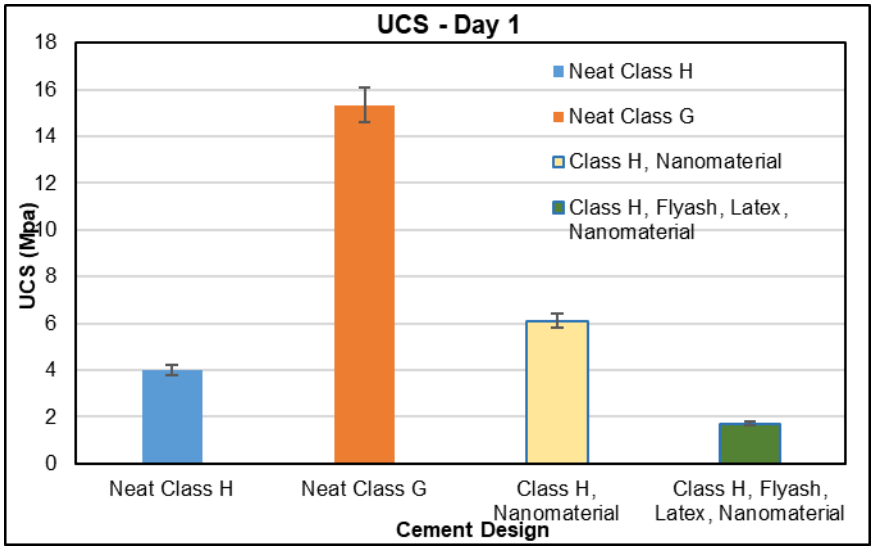

Figure 2.29: Day 1 results for unconfined compressive strength (UCS) tests.

From Figure 2.29, it can be observed that adding 0.5% nanomaterial to the slurry design improved the initial compressive strength of the new slurry. A 52.3% increase in compressive strength after 1 day was recorded. However, Figure 2.30 shows that the late time effect of nanomaterial is not as significant as the early time improvement. A 28% increase in UCS was recorded for the nanomaterial cement slurry design after 3 days. This increase is related to the neat Class H cement slurry after the third day of UCS test. The combination of latex, nanomaterial, and fly ash did not improve the UCS test values. The light weight of fly ash and latex are plausible factors that impeded compressive strength development. Apart from the recorded decrease in density, this slurry design showed a decrease in compressive strength by 57.75% on the first day and 58.27% on the third day of testing. Comparing Class H and Class G cement samples, Class G revealed better compressive strength development in both the first and third day of UCS test. A 283.5% increase in UCS was recorded in the first day.

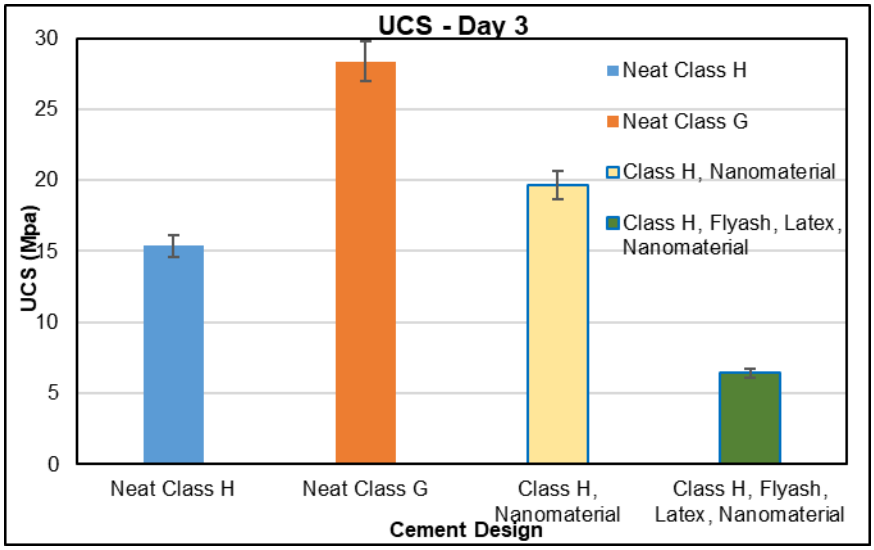

Figure 2.30: Day 3 results for unconfined compressive strength (UCS) tests.

2.6 SUMMARY AND CONCLUSIONS

In this section of the report, the findings from the cement tests (big setup I and small setup I) are summarized. The conclusions drawn from the theoretical, experimental, and analytical studies are as follows:

- Neat Class H and Class G cement slurry (without gas migration additives) are inadequate to serve as a primary well barrier.
- The combined permeability of annular cement increases as cement age increases.
- The leakage time of gas increases as the combined annular cement permeability decreases.
- The leakage scenario results reveal that 62% of the total leakage time falls under the liner-casing overlap range between 50 and 250 ft. This overlap range may not permit longer duration for detecting and controlling gas influx, when the cement sheath is faulty.
- The leakage scenario results suggest that 35% of the leakage times are between 1 and 30 minutes. The current casing pressure test duration of 30 minutes may not be enough to verify the integrity of the cement sheath in the liner-casing overlap.
- Partially densified and densified microsilica both behave as inert materials in a cement slurry. They do not exhibit superior performance for adequate zonal isolation.
- Besides the commercial additive cement slurry, the slurry designs with the longest leakage times (21 minutes and 21 minutes 7 seconds) both had latex in their formulation. Cement formulation with latex may have superior performance at temperatures above the ambient temperature.
- Nanomaterial in low concentrations of 0.5% BWOC improved 1-day compressive strength of the sample.

- A slurry design with short gas transit time shows a good potential for mitigating gas migration. This depends on the additives added. Other tests such as the UCS and pressure tests can be used to confirm their gas migration mitigation ability.
- The inclusion of nanomaterial improves the property of set cement which mitigates gas migration.
- 1.5 liters/100 kg of the commercial additive used in this study is enough to mitigate gas migration in the cement column completely.

3 ELASTOMER AGING CELL TESTS USING SET UP III

3.1 INTRODUCTION

3.1.1 Overview

There are many elastomers used in the oil and gas industry. Some of these include but are not limited to: acrylonitrile butadiene rubber (NBR), ethylene propylene diene rubbers (EPDM), hydrogenated nitrile-butadiene (HNBR), fluoroelastomers (FKM), perfluoro-elastomers (FFKM), and tetrafluoro ethylene/propylene rubber (FEPM). The deterioration or degradation of any elastomer during use would render the elastomer not "fit for service". Elastomer degradation can occur because of physical, chemical, or both physical and chemical processes. Physical degradation can occur when an elastomer is exposed to extreme stress loading conditions for a prolonged period. In downhole conditions, elastomers are often in a compressed state, especially when used in liner hanger systems, BOPs, gaskets, and seals. These conditions tend to alter the physical structure of the elastomer. Pressure, temperature, ultra-violet rays, atmospheric ozone, and moisture are factors that can alter the physical structure of an elastomer. In addition, surrounding downhole gas molecules tend to permeate the pores of the compressed elastomer. A sudden release of the surrounding gases causes the gas molecules within the pores to escape in what is known as rapid gas decompression (RGD) or explosive decompression. These conditions could cause the elastomer to lose its physical sealing abilities. Although, most physical changes of an elastomer are reversible, there are few exceptions. Extreme physical and non-physical compression of elastomers can break the London dispersion forces (instantaneously induced dipole forces) existing in an elastomer. This causes an irreversible physical change in the elastomer.

Elastomers are also susceptible to chemical attacks. A good elastomer for oil and gas application is one that exhibits both chemical and heat resistance, while maintaining properties of resilience and rebound in aggressive chemical media, including H_2S, hydrocarbon, and polar solvents (Parker Hannifin 2002). Elastomer sealing properties vary with time as it interacts with the surrounding fluid under downhole conditions. Depending on the nature and abundance of the fluid interacting with the elastomer, severe degradation can occur, accompanied with significant changes in tensile strength, swelling, ultimate elongation, and hardness of the elastomer. Limited laboratory studies (Cong et al. 2013; Fernández et al. 2016; Tynan 2016; Dajiang et al. 2017) have been conducted to access the degradation behavior of elastomers under acidic wellbore environments.

3.1.2 Statement of the Problem

Exploration and production of oil and gas wells has witnessed a progressive change over the years. From producing conventional sands to exploring unconventional shale plays in harsh environments, shallow gas kicks and blowouts still pose a wellbore drilling challenge to the industry. The substantial presence of CO_2, H_2S, and methane gas has complicated the art and design of well construction. Typically, these gases are first encountered during drilling. Therefore, it is imperative that a wellbore design procedure incorporates careful selection of suitable

elastomers that would not degrade when exposed to these gases, combined with other downhole conditions.

Oil field elastomers are vulnerable to acid attacks and harsh downhole environments. Different physical and chemical mechanisms are involved in deteriorating the properties of an elastomer. There are limited available studies that have been conducted to study the effects of H_2S, CO_2, and other harsh downhole conditions on elastomers. Published research on elastomer degradation mechanisms when exposed to these conditions are scarce (Cong et al. 2013). Thus, more studies are needed to ensure that elastomers are "fit for service" in the environments they are used.

3.1.3 Objectives

This section of the project and report focuses on the aging of the following elastomers which are frequently used in the oil and gas industry: Nitrile butadiene rubber (NBR), Ethylene propylene diene monomer (EPDM), Fluoroelastomers (FKM), and Polytetrafluoroethylene (PTFE). The investigations are focused on examining the effects of acidic and corrosive fluids on the physical properties (hardness, volumetric swelling, and compression) of the elastomers. The possible failure of elastomers in a wellbore makes it imperative to understand the various elastomer degradation mechanisms and develop methods to reduce the degradation. Hence, the objectives of this section of the project and report are:

- To investigate if elastomers are "fit for service" in shallow well construction applications.
- Determine elastomer performances under downhole corrosive conditions (temperature, pressure, and corrosive gases).

3.2 LITERATURE REVIEW ON ELASTOMER DEGRADATION

Elastomers require a comprehensive standard set of tests before obtaining approval. These tests are necessary to determine the seal performance at high pressures, wide temperature fluctuations, loading conditions, and exposure to corrosive environments. In harsh and acidic environments, elastomers can quickly lose their performance because of thermal degradation and chemical attacks. Selecting a suitable elastomer for an onshore or offshore operation requires evaluation of many inter-dependent elastomer characteristics. It is often a challenge to predict the life of an elastomer seal under a harsh borehole environment, because of the physical and chemical changes that occur in the elastomer. Table 3.1 lists some of the acclaimed properties of typical elastomers used in the oil and gas industry. The ability of an elastomer to seal effectively depends on its physical and mechanical properties in downhole conditions. In most cases, elastomers are required to exhibit excellent performance while retaining their physical properties at high and low temperature conditions respectively. A good description would be the Joule-Thompson effect, which occurs when there is a sudden pressure release in a subsea wellhead and blow out preventer (BOP); thus, leading to rapid changes in temperature (Chen et al. 2016).

Table 3.1: Some of the properties of typical elastomers used in the oil and gas industry.

Property \ Elastomer	NBR	HNBR	Viton® (FKM)	Aflas® (FEPM)	Kalrez® (FFKM)
Max. Temperature (°F)	250	300	400	400	620
Tensile Strength (psi)	200-3500	1500-3500	500-2000	1900	2000
Steam Compatibility	Poor	Fair to Good	Poor	Excellent	Excellent
Brine High Density (Na/CaBR)	Poor	Fair to Good	Excellent	Excellent	Excellent
Brine Low Density (Ca/NaCl)	Excellent	Excellent	Excellent	Excellent	Excellent
Crude Oil. Sour (< 2000 ppm H_2S)	Poor	Excellent	Fair to Good	Excellent	Excellent
Drilling Mud (Diesel Based)	Fair to Good	Excellent	Fair to Good	Fair to Good	Excellent
Hydraulic Fluid, Oil/Water (HFA)	Fair to Good	Excellent	Poor	Excellent	Excellent

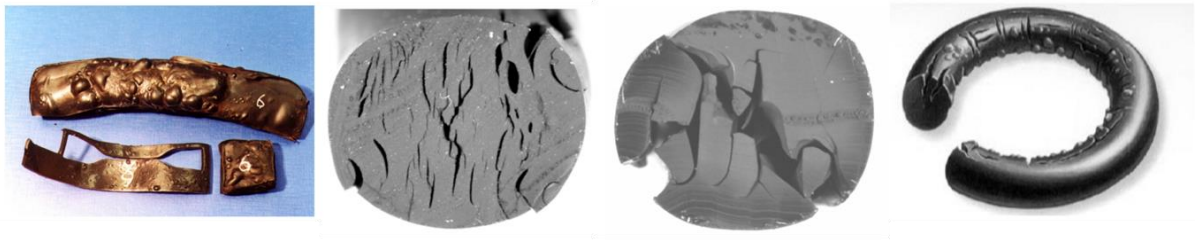

Figure 3.1: Examples of elastomer failure caused by RGD and overload pressure.

In downhole conditions, elastomers are often in a compressed state especially when they are used in liner hanger systems, BOPs, gaskets, and seals. Under these conditions, surrounding gas molecules tend to penetrate the pores of the compressed elastomer. For instance, elastomers like HNBR are known for absorbing a high level of hydrogen sulfide under pressure, which limits its applicability in the oil and gas industry (Cong et al. 2013). A sudden release of the surrounding gases causes the gas molecules within the elastomer pores to expend and escape in what is known as rapid gas decompression (RGD) or explosive decompression. RGD occurs because of trapped-gas expansion when the shear modulus of an elastomer is low. As shown in Figure 3.1, this phenomenon reduces the seal integrity of elastomers because they experience harsh blistering and cracking when the expanding surrounding gas energy exceeds the physical strength of the elastomer. Elastomers with high temperature sealing performance and excellent rapid-gas-decompression (RGD) resistance tend to have limited low temperature sealing performance because of their high modulus characteristics (Chen et al. 2016). It is often difficult to identify elastomers that have excellent rapid-gas-decompression resistance and are suitable for both high and low temperatures.

Over the years, aging experiments have gained recognition as one of the commonly used methods for evaluating the behavior and performance of elastomers. These tests are conducted in special autoclaves by exposing test samples to corrosive gases and liquid contaminants. Per Schweitzer (2000), the properties of an elastomer can be destroyed only by chain growth or chain rupture. Some of the contributing agents to elastomer aging are atmospheric ozone and moisture,

heat, sunlight, CO_2, H_2S, CH_4, drilling fluids, and brine. These agents are used to evaluate the seal integrity of elastomers.

3.2.1 Experimental Studies of Elastomer Degradation in H_2S Environment

Exposing an elastomer to sour fluid conditions such as H_2S, at elevated temperatures, will accelerate aging and degradation. Thus, it is imperative to have adequate insight on elastomer degradation when exposed to H_2S. Tynan (2016) conducted a study to investigate temperature and corrosive fluid effects on elastomers by comparing the reactivity of various elastomers to H_2S with their glass transition temperature (T_g) and high temperature performance (as shown in Table 3.2). It was suggested that low temperature and H_2S resistance are two properties that can exist for the same elastomer type. This was like one of the author's previous observations in which an elastomer seal was selected with the combined qualities of high performance at low temperatures, excellent resistance to sour gas (H_2S), and a good amine corrosion inhibitor. Low temperature FFKM elastomer was chosen against FKM because the design allowed for a life of 20+ years, while maintaining a good low temperature resistance. Furthermore, the study recommended FFKM as the most viable option for low temperature and H_2S conditions.

Table 3.2: H_2S resistance of various elastomers, at their respective glass transition and high temperature performance (Tynan 2016).

Elastomer Type	Resistant to H_2S	Glass Transition (T_g) °F	Upper Service Temp. °F
NBR	Most reactive	-22	248
Low Temp. HNBR	Most reactive	-40	320
HNBR	Less reactive	-22	356
FEPM (TFE/P)	Non-reactive	41	482
Low Temp. FKM	Less reactive	-40	437
FKM	Most reactive	1.4	437
Low Temp. FFKM	Non-reactive	-22	464
FFKM	Non-reactive	32	500

Cong et al. (2013) published the experimental results of an aging cell study for HNBR samples in aqueous solutions of H_2S and HCl. The authors used nuclear magnetic resonance (NMR), infrared spectroscopy, and X-ray photoelectron to analyze the samples. The H_2S experiment was carried out at 1000±100 psi and 212°F, while the HCl experiment was carried out at 284°F. They observed that exposing HNBR to HCl solution resulted in a slight reduction of tensile strength and ultimate elongation because of the hydrolysis of the C≡N group to —OH or O=C—NH_2. Once exposed to the H_2S solution, all the three parameters (tensile strength, ultimate elongation, and hardness) deteriorated significantly. Given the high reaction activity of H_2S, homolysis and heterolysis are two reactions of H_2S that may take place during elastomer degradation. Heterolysis coverts H_2S into H^+ and HS^-. H^+ causes the acidic hydrolysis of the C≡N group, while HS^- attacks C=O because of its strong nucleophilicity, giving rise to C=S and C—C=S groups (Figure 3.2). During homolysis, H_2S can alter into mercapto radicals of $H^\cdot$ and $HS^\cdot$. $HS^\cdot$ reacts with the macromolecule radicals of the elastomer that forms at high temperatures. It then forms mercapto compounds.

These compounds undergo further pyrolysis to form macromolecule radicals which reacts with the mercapto radicals ($HS^{\cdot}$) in a continuous reaction cycle. This chain of reactions increases the C—S—C bonds. The breakdown of the triple bond in the CN group to double and single bonds, as shown by these reactions, is responsible for the deteriorating properties of the HNBR elastomer. Studies have shown that when exposed to H_2S solution, the structure of HNBR would change because of formation of new chemical compounds.

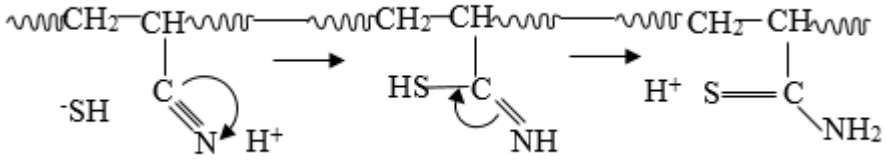

Figure 3.2: Nucleophilic reaction mechanism showing the breakdown of the acrylonitrile group in HNBR (redrawn after Cong et al. 2013).

Fernández and Castaño (2016) studied the elastomeric properties of two NBR's (high and low acriylonitrile-ACN) using two separate autoclave tests in liquid and gas contaminants respectively. They varied the concentrations of crude oil compositions to obtain three liquid contaminants, while using H_2S and CO_2 as the gas contaminants. In their experiments, the H_2S concentration was increased from 714 ppm to 5000 ppm. A reduction in the elastic properties was observed, causing the elastomers to be less retractable. Tensile strength and elongation at break properties decreased significantly with an increase in H_2S concentration. The SEM images in Figure 3.3 show an increase in the brittle fracture surface with an increase in H_2S concentration. The authors concluded that permanent deformation of the elastomer is a function of the H_2S concentration.

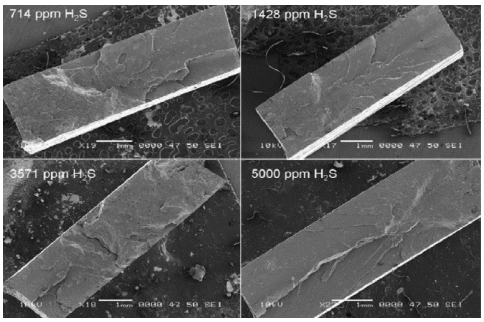

Figure 3.3: SEM images of NBR aged with H_2S (203°F, 168 hrs.) (Fernández and Castaño 2016).

3.2.2 Experimental Studies on Elastomer Degradation in CO_2 Environment

In studying the elastomeric properties of two NBRs (high and low ACN), Fernández and Castaño (2016) recorded an increase in the volumetric swelling and permanent deformation of the elastomers, with an increase in CO_2 concentration. The increase in permanent deformation was finite and plateaued at very high concentrations of CO_2. An increase in hardness was recorded for low CO_2 concentration. The SEM image in Figure 3.4 shows a decrease in the brittle fracture surface of the NBR with an increase in CO_2 concentration.

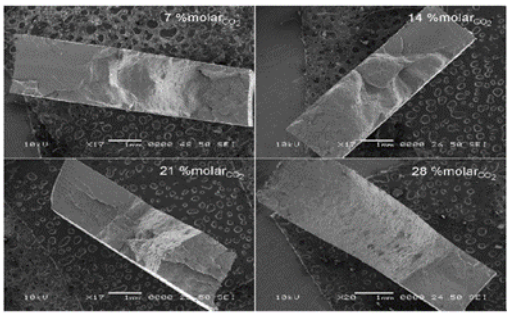

Figure 3.4: SEM images of NBR aged with CO_2 (203°F, 168 hrs.) (Fernández et al. 2016).

Dajiang et al. (2017) characterized NBR and HBNR samples by aging the elastomers in the presence of liquid and gaseous CO_2, under mechanical compression. Their control group samples were compressed in laboratory ambient temperature and pressure. Two separate groups of elastomers were aged in liquid and gaseous CO_2 respectively for 168 hours, at 230°F, and CO_2 partial pressure of 145 psi. Compared to the control samples, an increase in elastomer weight was recorded for the aged elastomers. The increase in weight was more pronounced for the elastomers that were aged in liquid CO_2. They also observed that the reduction in elastomer hardness was more severe in the gaseous contaminant, compared to the liquid contaminant. The samples were compressed up to 25% of their original height for 24 hours at ambient temperature and left to recover for 30 minutes. The authors recorded compression set results in the range of 9.94% to 17% and 10.33% to 26.02% for NBRs aged in liquid and gaseous CO_2 respectively. They also reported similar values for the HNBR samples, suggesting that mechanical loading would increase the elastomer's damage in the presence of CO_2.

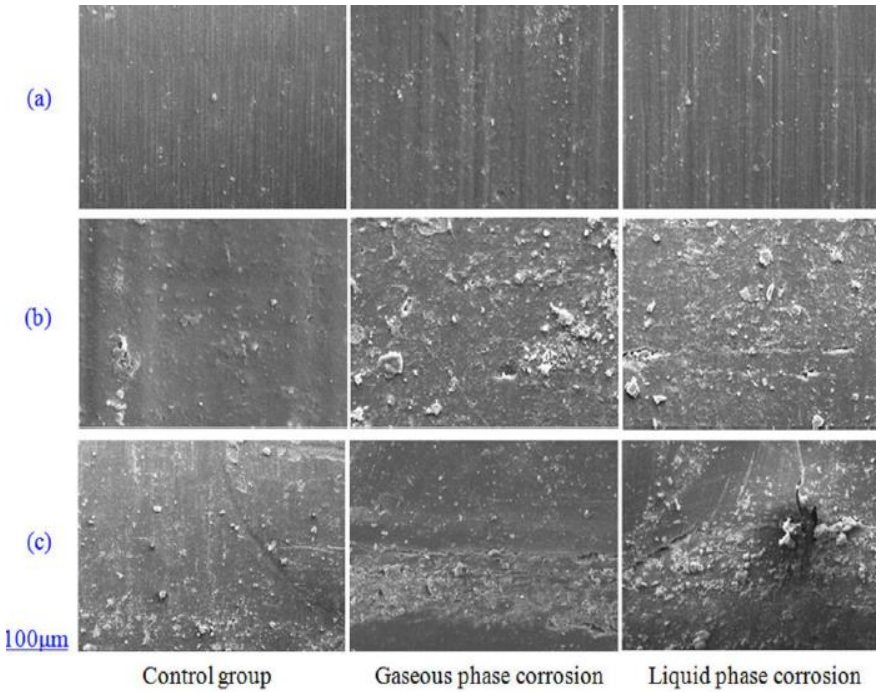

Figure 3.5: SEM image of HNBR after aging at 0 lbf (a), 1349 lbf (b), and 2698 lbf (c) (Dajiang et al. 2017).

In addition, Dajiang et al. (2017) observed slight deformation in the HNBR control group, compared to an obvious swelling and deformation revealed by the aged samples. Figure 3.5 shows HNBR SEM images at various compressional loads. The authors observed holes, fractures, and more damage in the aged HNBR samples. Furthermore, their energy dispersive spectroscopy (EDS) results for the 2698 lbf compressed samples showed a decrease in the weight percent of the main constituent elements (C, O, Si, and Ca). They concluded that the swelling and damage of an elastomer tends to increase with an increase in compressional load in liquid CO_2 corrosion. This appears to be more severe than gaseous CO_2 corrosion. Elastomer degradation can also occur when they are exposed to other corrosive fluids such as crude oil and brine. These have been discussed in section ***3.2.1.3*** of the report on laboratory results for seal assemblies and cement system.

3.3 RESEARCH METHODOLOGY

To achieve the objectives in this section of the project and report, both theoretical and experimental investigations were conducted. Elastomer degradation strongly depends on the elastomer's chemical structure as well as the composition and abundance of the liquid and gaseous phases they are in contact with. In this section of the project, the relationship between elastomer degradation and downhole conditions such as temperature, exposure time, and acid gas variations were studied. The outcome of the theoretical analyses provided useful information in understanding the mechanisms that are involved in the elastomer degradation process. The degree of degradation after experimental studies was measured from the changes in intrinsic properties of the elastomer such as hardness, volumetric swelling, and compression. These investigations were used to determine whether the elastomers are "fit for service" for a given set of downhole conditions.

3.3.1 Scope of Work

Elastomers are sensitive to downhole conditions (temperature, pressure, acid gas variations, and acid gas concentration). To perform the tests under simulated wellbore conditions, elastomer-aging experiments were carried out at varying temperatures of 120°F and 180°F. Pressure was kept constant at 1000 psi, with two fluid phases - a vapor and brine phase. For each experiment, the same types of elastomers were used. Half of them were immersed in the brine phase and the other half exposed to the vapor from the brine (vapor phase). The gas variations include: methane (CH_4), hydrogen sulfide (H_2S), and carbon dioxide (CO_2). Some experiments were conducted with 100% CH_4, 100% H_2S (500 ppm) with methane carrier, and 100% CO_2. Subsequent experiments were conducted with a mixture of the three gases (50% CO_2 and 50% 500 ppm H_2S with methane carrier). The aging duration which was used to quantify the effects of time on elastomer degradation was 1 and 7 days. Some experiments were also conducted with an aging duration of 3 days to study the patterns in the changing properties. Four different elastomers (NBR, EPDM, FKM, and PTFE) were considered in the investigation.

To quantify the level of degradation, elastomer properties (hardness, volumetric swelling, and compression) were measured and compared before and after aging. In addition, a Dino-Lite Digital Microscope was used in observing the morphology and blistering of severely damaged

elastomers. Two types of elastomer sizes were prepared to carry out the experiments. Cylindrical samples of thickness (height) 0.33-inch and 1-inch were selected based on preliminary tests and results. The 0.33-inch thick elastomer was prepared for compression measurements based on ASTM D575-91, while the 1-inch thick elastomer was prepared for volumetric swelling and hardness measurements. All the elastomers had a constant diameter of 0.75-inch. A detailed description of all the research methods used in this section of the project can be found in the report on laboratory results for sealing assemblies and cement system (**3.3.2** to **3.3.6**). These include: test materials description, test matrix and description, elastomer properties testing equipment's and protocols, elastomer sample preparation procedure, and aging experiments test protocol.

3.4 RESULTS

This section summarizes the results from the experiments conducted in this part of the project. The results comprise of all the useful data collected during the elastomer aging studies. It shows elastomer degradation in terms of change in the performance of three properties: hardness, compression, and volumetric swelling. The parameters that were varied include: aging period (1, 3, and 7 days), temperature (120 °F and 180 °F), and corrosive gases (CO_2, H_2S, and CH_4). Before discussing the results, it is important to discuss the theoretical findings from the chemical and physical changes that occur during elastomer degradation. These findings provide the bases for understanding the results from the aging tests.

3.4.1 Chemical Changes

When elastomers are exposed to harsh chemical conditions, they can fail because of changes in their molecular structure. These changes can occur in a continuous reaction cycle depending on the chemical structure of the elastomer. Chemical reactions in elastomers are irreversible because of the alteration in their molecular structure and the formation of new chemical compounds. The performance of elastomers is not only impacted by their molecular structure, but also by the type and degree of the corrosive conditions. To explain the chemical changes that occur in elastomers, three famous elastomer chemical structures were studied - Acrylonitrile butadiene rubber (NBR), Ethylene propylenediene monomer (EPDM), and Fluoroelastomer (FKM).

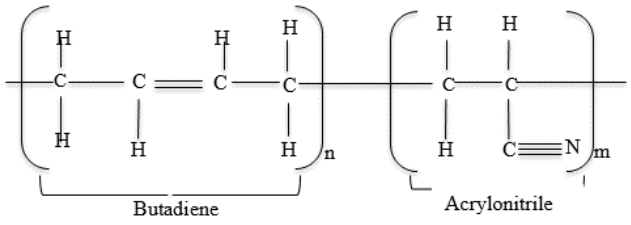

(a)

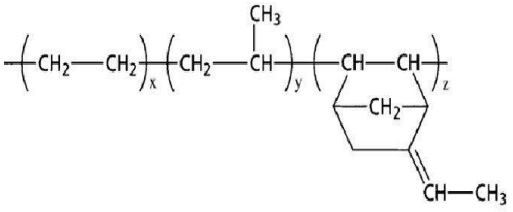

(b)

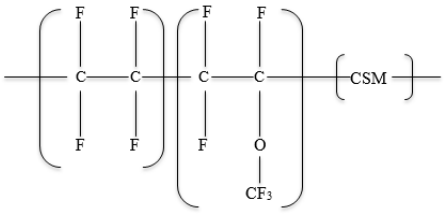

(c)

Figure 3.6: Chemical structures of: (a) acrylonitrile butadiene rubber (NBR); (b) ethylene propylenediene monomer (EPDM); (c) fluoroelastomer (FKM).

Figure 3.6 shows the repeating terms of the chemical structures (used to explain their chemical degradation) of these elastomers. The NBR structure is made of two parts - Acrylonitrile and Butadiene. The carbon triple bond nitrogen (C≡N) group is what distinguishes NBR from other elastomers. The acrylonitrile content is used to categorize NBR into low, medium, and high. To understand the reaction of elastomers with H_2S, CO_2, and other corrosive media, the concepts of electronegativity and bond dissociation energy should be highlighted. Electronegativity is simply a measure of the tendency of an atom to attract a bonding pair of electrons. Bond dissociation energy is a measure of the strength of an existing chemical bond. It can be defined as the standard enthalpy change when a bond is cleaved by homolysis, with reactants and products of the homolysis reaction at absolute zero (-459.67 °F). Elastomer degradation under H_2S exposure has been discussed under **3.2.1** of this report.

3.4.1.1 Elastomer Degradation (Chemical Changes) under CO_2 Exposure

CO_2 is a very stable inert gas made up of two carbon-oxygen double bonds (O=C=O). Each of these carbon-oxygen double bonds are very stable; having a bond dissociation energy of 732 kJ/mol. Based on the stability of these bonds, CO_2 has little to no reason to react with any of the elastomers investigated. However, in the presence of brine, CO_2 reacts with water to form a weak carbonic acid (H_2CO_3). In large quantities, this weak carbonic acid becomes corrosive, and reacts as an acid.

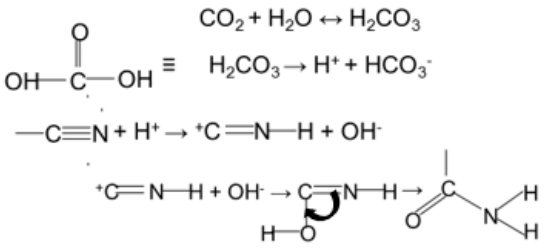

Figure 3.7: Chemical reaction of NBR with CO_2.

Figure 3.7 shows the chemical reaction of CO_2 with brine to form a weak carbonic acid. It also gives detailed reactions of the H^+ with the C≡N group of the NBR elastomer. The C≡N group is made up of two weak pi bonds and one strong sigma bond. The two weak pi bonds contribute to the low bond dissociation energy in C≡N. In addition, carbon and nitrogen are farther from each

other on the electronegativity table, making them more susceptible to a chemical reaction compared to the C─H bond that exists in the butadiene section of the NBR. The product of this reaction is an amine group. After this reaction has occurred, the chemical structure of the elastomer has been altered, as such, this change is irreversible. In the ethylene propylene diene monomer, the carbon to carbon double bond has a bond dissociation energy of 611 kJ/mol. They are also made up of solely hydrogen and carbon elements, which are two elements close to each other in the electronegativity series. High bond dissociation energy and close electronegativity create a high stability in the EPDM structure. With the FKM, despite the large electronegativity difference between carbon and fluorine, the C─F has a bond dissociation energy of 450 kJ/mol because fluorine is a highly stable halogen. Of all the carbon single bonds to hydrogen, nitrogen, oxygen, and florin, C─F has the largest bond dissociation energy; thus, the high stability of FKM.

3.4.1.2 Elastomer Degradation (Chemical Changes) under CH_4 Exposure

The chemical structure of methane in Figure 3.8 shows that it has four single (sigma) carbon-hydrogen bonds. These bonds have a bond dissociation energy of 410 kJ/mol each. Carbon and hydrogen are close elements in the electronegativity series, meaning that they are more stable and less likely to react with any substance until they are burnt in the presence of light or oxygen. This stability causes methane not to react chemically with any of the elastomers investigated.

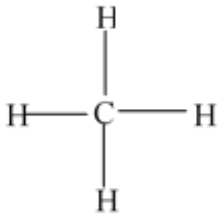

Figure 3.8: Chemical structure of methane.

3.4.2 Physical Changes

Unlike regular metals that have Young's modulus property, the viscoelastic properties of elastomers cause them to have a "modulus", which is the stress at any given strain. Per Schweitzer (2000), the modulus of elastomers is generally measured at a specific elongation (such as at 300% or lower). The stress, strain, and compression changes that occur within an elastomer can change its physical properties. Pressure, temperature, ultra-violet rays, weathering, oxygen, and ozone, amongst others are all factors that can affect the physical structure of an elastomer (Schweitzer 2000). The author claimed that when an elastomer is subjected to such unfavorable conditions, a physical change could occur. The elastomers may shrink or swell, then change size again depending on the conditions. Jin et al. (2008) explained that mobility and crosslinking of the elastomer molecular chains (chain growth) causes the elastomer hardness to increase with an increase in temperature (Figure 3.9). Schweitzer (2000) also suggested that during elastomer aging, chain growth will usually decrease elongation, and increase the hardness and tensile strength. The author further explained that chain breakage or chain rupture will have the reverse effect on these

properties. It should be noted that most physical changes are reversible, except for a few. London dispersion forces are temporary attractive forces that arise when the electrons in two adjacent atoms occupy positions that make the atoms form temporary dipoles. They are the weakest intermolecular forces of attraction that exist in long chain polymers or compounds with similar electronegativity. When an elastomer is subjected to physical or non-physical compression after a certain threshold, the London dispersion forces become weak and tend to break. In some cases, when these compression forces are expelled, the elastomer never regains its original shape and size.

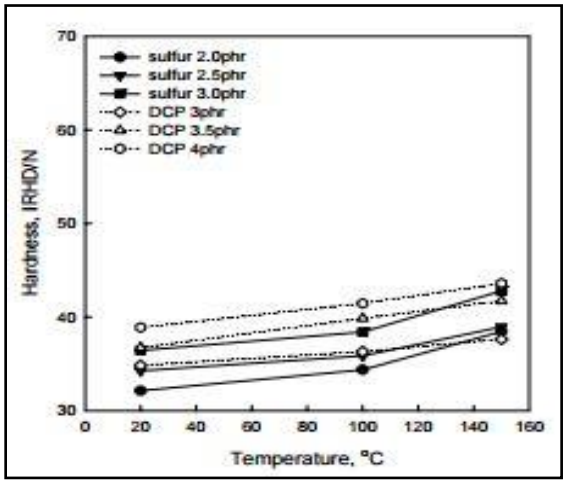

Figure 3.9: Hardness vs. temperature (Jin et al. 2008).

3.4.3 Performance of Elastomers

An elastomer's performance in oil and gas wells is determined by its seal integrity. Elastomer seals are essential for zonal isolation in both vertical and deviated wells. The ability of an elastomer to perform this function is determined by its hardness, volumetric swelling, and compression.

3.4.3.1 Hardness

Effects of Aging Period

Elastomer hardness is defined as the resistance of an elastomer surface to indentation by a Shore A durometer. A general observation is that after one, three, and seven days, elastomer hardness tends to drop from its original value. This observation was consistent for the two temperatures (120^{o}F and 180^{o}F). This is because of exposure to temperature, pressure, and corrosive gas conditions. However, from one to three days and from three to seven days, there is a general increase in hardness irrespective of the temperature. This happens because of chain growth or cross-linkage. Jin et al. (2008) showed that elastomer hardness tends to increase with temperature. However, from the experiments performed in this part of the project, it was discovered that if the temperature is kept constant, but the time of exposure is increased, this could compensate for a slow but steady increase in temperature within the elastomer. Thus, resulting to more cross linking and chain growth. This conclusion was drawn because an increase in the exposure time of an

elastomer to high temperatures, leads to more chain growth within the elastomer. With an increase in chain growth, there is an increase in elastomer hardness and tensile strength. At 120°F (Figure 3.10 a), the decrease in elastomer hardness is greater than 5% and up to 15% from the original hardness. This behavior was not observed in all the PTFE's (both brine and vapor phase) and all Viton (FKM) in the brine phase. At 180°F (Figure 3.10 b), there was a 5% to 10% decrease from original hardness, excluding PTFE (brine and vapor phase). In addition, the 7-day samples of NBR, EPDM, and Viton aged in brine did not follow this general observation.

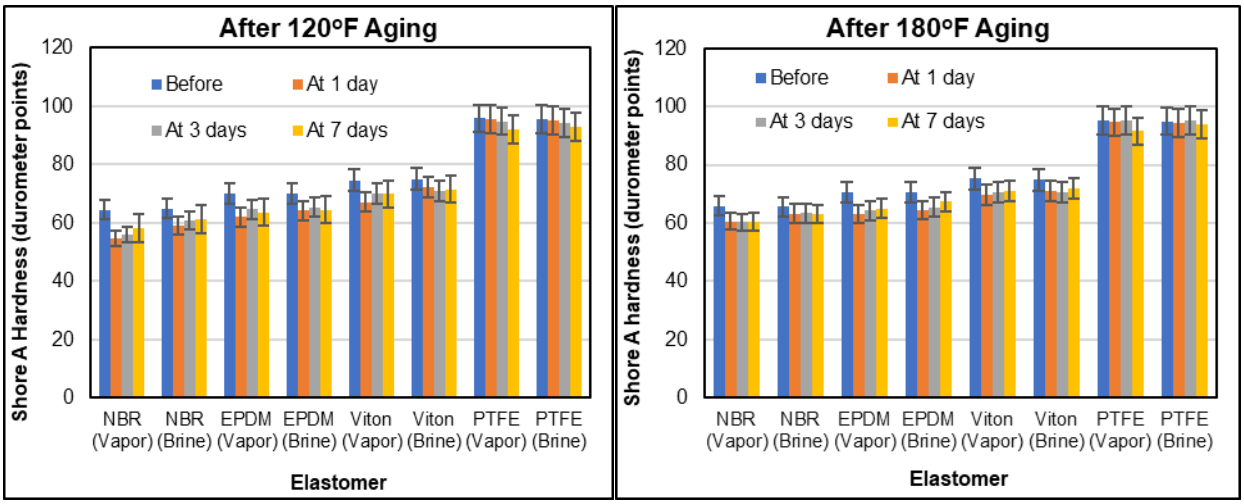

(a) **(b)**

Figure 3.10: Effects of aging period on the hardness of elastomers at 1000 psi and at (a) 120°F, (b) 180°F.

Effects of Temperature

An increase in temperature concurrently increases an elastomer's hardness. The initial exposure of the elastomer to aging conditions (temperature, pressure, and corrosive gas conditions) causes it to soften. Keeping all other conditions in the aging test (1 day or 7 days) constant and altering the temperature from 120°F to 180°F, results in an increase in hardness. This is because of chain growth or cross-linking of the polymer chains within the elastomer. Figure 3.11 (a) shows 1-day aging for 50% CO_2 and 50% H_2S with a CH_4 carrier. A decrease in hardness (more than 5% and up to 15%) from the original hardness is observed. This excludes all the PTFE's (vapor and brine phase) and Viton's in the brine phase. A slight increase in hardness is observed when shifting from 120°F to 180°F. After a 7-day test at the same aging conditions (Figure 3.11 b), a decrease in hardness (more than 5% and up to 10%) from the original hardness was recorded. In addition, a slight increase in hardness was observed with an increase in temperature. In the 3-day test (Figure 3.12), the results were like those from the 1 and 7-day tests. Both Figure 3.11 and Figure 3.12 show that the reduction in elastomer hardness was more severe in the vapor phase (gaseous contaminant) compared to the brine phase (liquid contaminant). This observation is supported by the study carried out by Dajiang et al. (2017). One way to quantity the significance of the variables is by performing hypothesis tests using analysis of variance (ANOVA).

ANOVA is a statistical tool that is used in analyzing experimental data. It is a collection of statistical models (developed by Ronald Fisher) that is used to analyze the variances among group means and their associated procedures (Fisher 1966). This is done to compare the means between groups and determine whether any of these means are significantly different from others. Using a 95% confidence interval ANOVA, age, temperature, and fluid medium variation (vapor or brine phase) significantly affect elastomer aging.

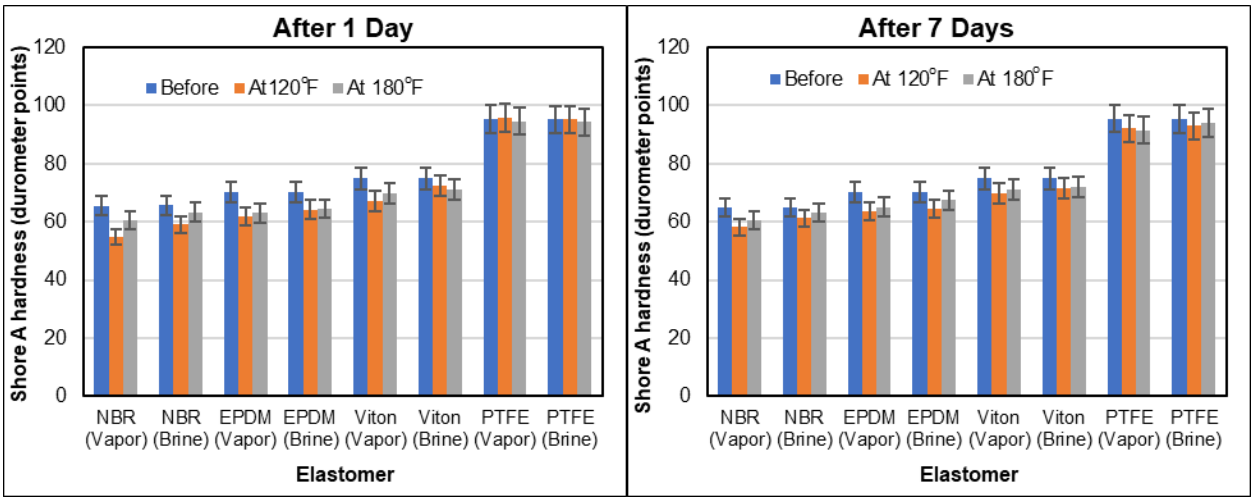

(a) **(b)**

Figure 3.11: Effects of temperature on hardness of elastomers aged at 1000 psi, and after (a) 1 day, (b) 7 days.

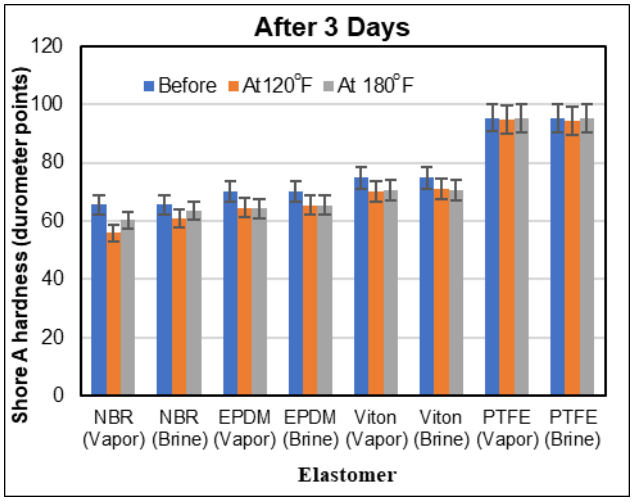

Figure 3.12: Effects of temperature on hardness of elastomers aged at 1000 psi, and after 3 days.

In actual downhole conditions, it is impractical to keep all factors that affect elastomer aging constant while varying one at a time. Each of these factors are constantly varying. Thus, the interaction effect is used to investigate the effect of varying one factor while keeping others constant. In practice, an interaction effect exists when the effect of one factor on the response varies across the levels of another factor. For example, when the effect of aging period (days) on hardness varies across the various levels of temperature. From the ANOVA, a combination of the

effect of aging period and fluid medium variation presented an insignificant variation for NBR and EPDM. However, there is a significant change in hardness between the Viton in the vapor phase and brine phase, from one to seven days. When fluid medium variation and temperature are combined, the effect was also insignificant for NBR and EPDM. Viton showed a significant change in hardness with fluid contaminant and temperature interaction. The results showed that the Viton samples (immersed in brine) had an average drop in hardness of about 3.2 durometer points, while those in the vapor phase dropped by 6.2 durometer points. This implies that the 3.0 durometer points difference is statistically significant. However, Viton does not exhibit a significant change in hardness with aging period and temperature interaction. This is because of its toughness and resistance to temperature. A combination of all the three parameters (aging period, fluid medium variation, and temperature) did not have any significant effect on elastomer aging. It can be inferred that with respect to the hardness of elastomers under corrosive downhole conditions, the time of exposure and downhole temperature would affect the seal integrity of the elastomer significantly.

Effects of Gas Variation

For the CO_2 and CH_4 tests, 100% of each of the gases were exposed to the elastomers. For the H_2S test, 0.05% H_2S in CH_4 carrier was exposed to the elastomers. High bond dissociation energy (410 kJ/mol) and close electronegativity values of carbon and hydrogen in the electronegativity series causes CH_4 to have little to no effect on the aging of elastomers. From Figure 3.13, CH_4 causes less than 5% decrease in hardness from the original hardness in all the elastomers. This decrease is attributed to physical changes in the elastomer under exposed corrosive conditions. More than 5% and up to 15.6% decrease from the original hardness was observed when the elastomers were exposed to CO_2. Figure 3.13 also shows approximately 5% decrease from the original hardness in NBR and EPDM when exposed to H_2S. However, it is to be noted that a conspicuous change was not observed in the subsequent elastomer samples. This is because of the low H_2S concentration (500 ppm or 0.05%) compared to previous studies, with little to no reactivity of the CH_4 carrier gas on the elastomers. A combined effect of CO_2, H_2S, and CH_4 showed more than 5% and up to 9.6% reduction from the original hardness. In conclusion, gas degradation on elastomers hardness is in the order of CO_2 > All gases > H_2S > CH_4.

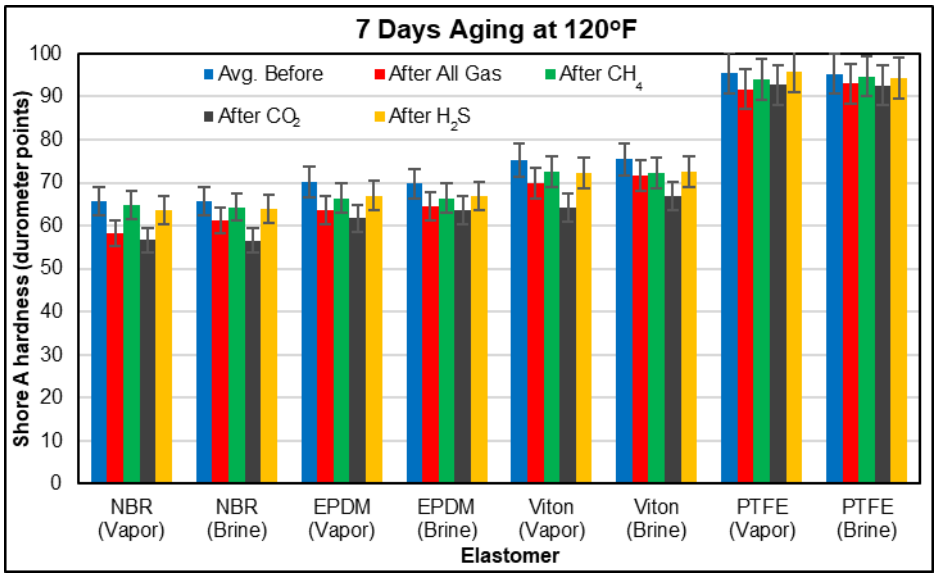

Figure 3.13: Effects of gas variation on the hardness of elastomers aged at 1000 psi after 7 days.

3.4.3.2 Compression at Maximum Stress of 53.2 psi

The compression tests (compressive stress-strain) were conducted to measure the strain of the elastomers after aging at a given compressive stress (psi). According to Schweitzer (2000), an elastomer chain rupture reverses the effects of cross-linkage or polymer chain growth. This implies that when an elastomer chain ruptures, the elastomer decreases in hardness and tensile strength. Chain rupture also increases elastomer elongation. A detailed explanation (with graphs) of elastomer strain response to individual stress values after aging is documented in the report on laboratory results for seal assemblies and cement system (section ***3.4.1.2***). To understand the overall effect of aging on the compression of elastomers, the maximum stress (53.2 psi) from the compression machine was selected, and its behavior on each elastomer was investigated.

Effects of Aging Period

At 120°F (1 and 7-day tests), there was an increase in strain at 53.2 psi applied stress. This increase was more than 5% and up to 39% from the original strain (Figure 3.14) (b)). This observation does not include all PTFE's (vapor and brine phases). The initial rise in strain, irrespective of the aging period, is because of the increase in elastomer elongation. Moving from 1 to 7 days, extended exposure of the elastomer samples to corrosive conditions causes chain growth, thereby increasing the hardness of the elastomer and decreasing its strain deviation.

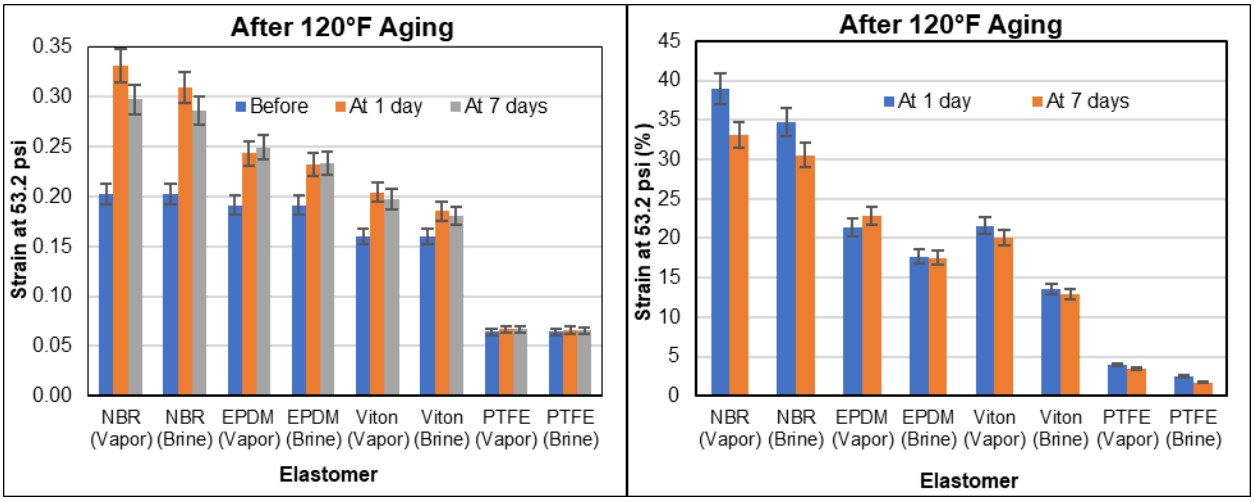

(a) **(b)**

Figure 3.14: Effects of aging period on compression of elastomers at 1000 psi and 120 °F. Actual strain values (a) and percentage increase in strain values (b).

After aging at 180°F, for both 1 and 7-day tests (Figure 3.15), there was an increase in strain at 53.2 psi. This increase was more than 5% and up to 30% from the original strain, except all PTFEs (vapor and brine phases). The initial rise in compression is because of the increase in elastomer elongation. An increase in the number of days causes chain growth, which increases the hardness of the elastomer and decreases its strain deviation. The maximum increase in strain at 120°F was 39%, while the maximum increase in strain at 180°F was recorded as 30%. This observation is explained further in the succeeding section.

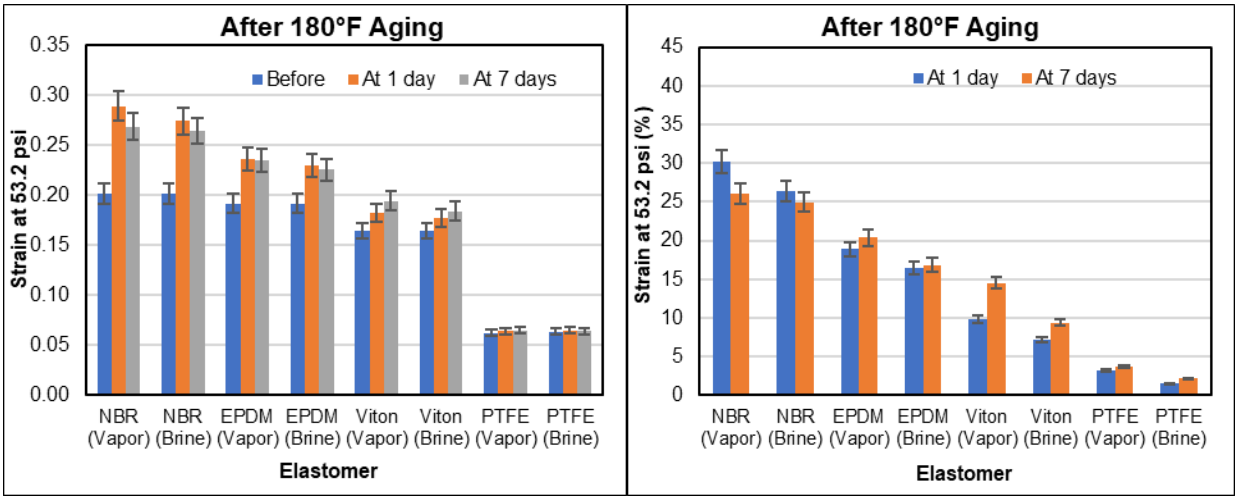

(a) **(b)**

Figure 3.15: Effects of aging period on compression (percentage strain) of elastomers at 1000 psi and 180°F. Actual strain values and percentage increase in strain values (b).

Effects of Temperature

A constant aging period is selected (1 or 7 days) and the temperature is altered. After 1 day of aging, all the elastomers displayed more than 5% and up to 39% increase from the original strain,

besides PTFE in the vapor and brine phases (Figure 3.16 b). After 7 days of elastomer aging, all the samples except the PTFE's demonstrated more than 5% and up to 33% increase from the original strain at 53.2 psi (Figure 3.17 b). From the graphs, it is observed that for both 1 and 7 days, all the elastomer samples exposed to 180°F had lower strain increase compared to those exposed to 120°F. The decrease in percentage strain at higher temperatures is once again linked to the chain growth that occurs in the elastomers. Irrespective of the aging period, exposing the elastomer to higher temperatures diminishes its sealing abilities.

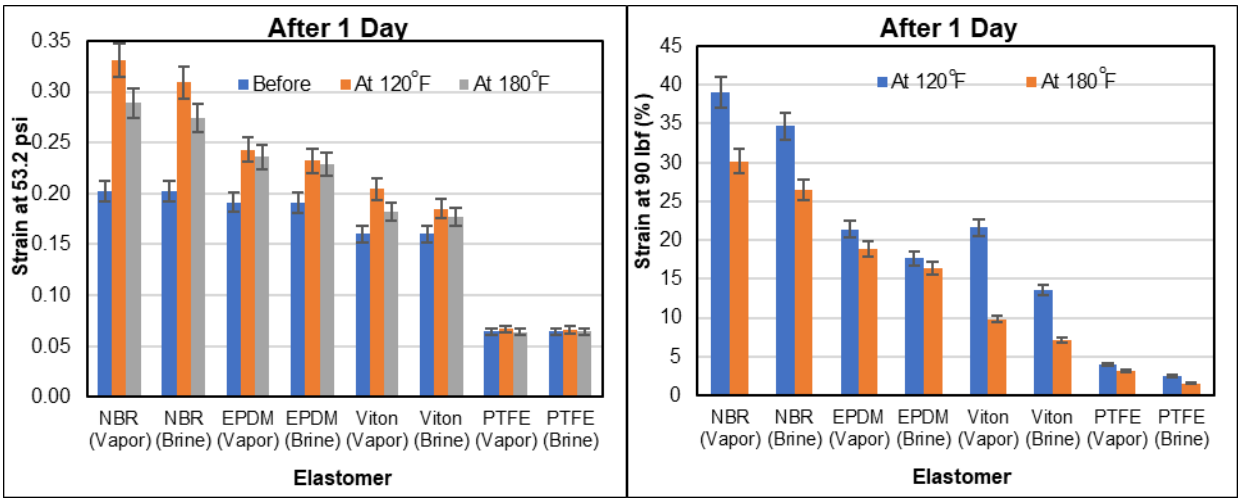

(a) **(b)**

Figure 3.16: Effects of temperature on the compression of elastomers aged for 1 day at 1000 psi (a) actual strain values, (b) percentage increase in strain values.

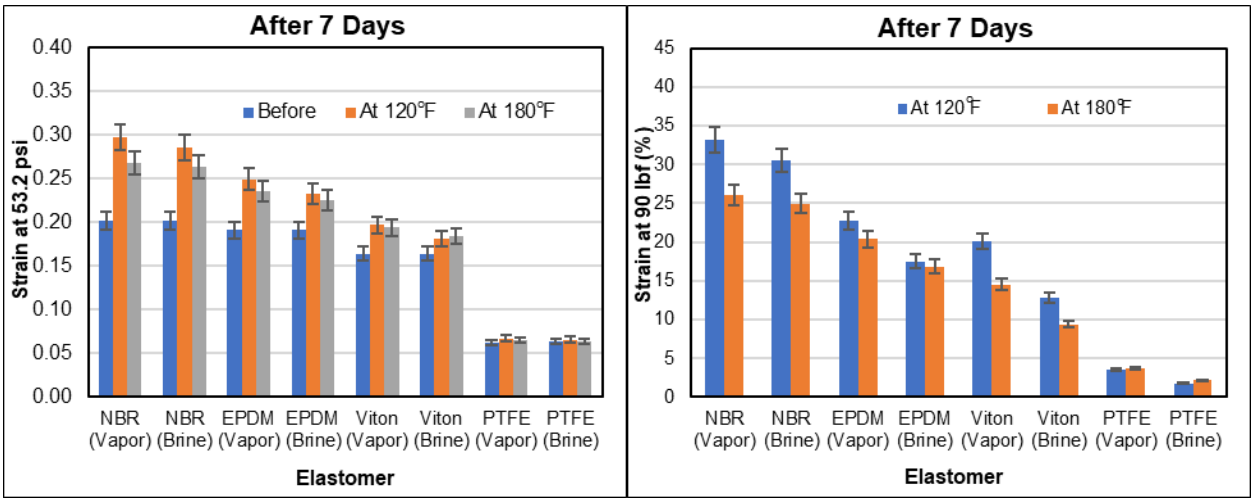

(a) **(b)**

Figure 3.17: Effects of temperature on the compression of elastomers aged for 7 days at 1000 psi. Actual strain values and percentage increase in strain values (b).

After performing ANOVA with a 95% confidence interval, none of the elastomer samples showed significant changes in compression, shifting from one temperature to another or from one aging medium to another. Considering the three parameters (aging period, fluid medium, and

temperature) individually, the changes in the compression of elastomers was insignificant with a change in any of these parameters. This implies that there is no significant change in compression between an elastomer aged for 1 day and 7 days. Neither does a change in temperature (from 120°F to 180°F) nor a shift from the vapor to the brine phase significantly affect the compression of an elastomer. The ANOVA results also provides evidence that the combined effect of the parameters does not affect elastomer compression significantly. Thus, exposing an elastomer to the least corrosive condition (1 day in vapor phase at 120°F) is enough to compromise its seal integrity appreciably. Changing the aging conditions is redundant since the elastomer has already been damaged.

Effects of Gas Variation

The changes in the elastomer that are caused from gas attack are shown in Figure 3.18. Figure 3.18 (a) shows the actual increase in strain values for each elastomer after aging with a particular gas, while Figure 3.18 (b) shows the percentage increase in strain for each elastomer after aging with a particular gas. For CH_4, more than 5% and up to 13.8% increase in strain from the original value was recorded at 53.2 psi, except for PTFE (vapor and brine). For CO_2, more than 5% and up to 36.3% increase in strain from the original value was recorded at 53.2 psi, while an increase from 5% to 17.7% was recorded for H_2S. A combination of the all gases revealed more than 5% increase but no more than 33.1% increase from the original strain at 53.2 psi. These observations exclude all the PTFE's. The order of elastomer degradation from compression, with respect to corrosive gases is in order of CO_2 > All gases > H_2S > CH_4. This order is similar to the order for hardness degradation.

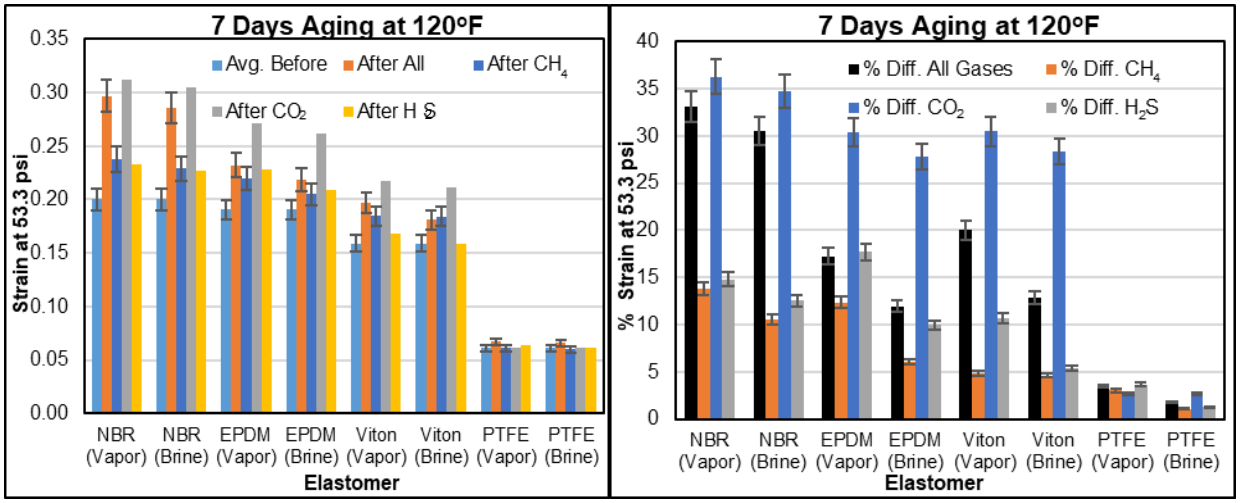

(a) **(b)**

Figure 3.18: Effects of gas variations on compression of elastomers aged at 1000 psi and 120 °F. Compression measurement (a) and percentage difference in compression measurements (b).

3.4.3.3 Volumetric Swelling

Effects of Aging Period

Volumetric swelling is the volume increase of an elastomer. Figure 3.19 (a) and (b) shows the volumetric swelling after aging at 120°F. Figure 3.20 (a) and (b) also show the volumetric swelling after aging at 180°F. These two graphs show a general increase in the elastomer volumes after 1 day, a peak in swelling after 3 days, and a gradual decline in swelling after a week. According to Schweitzer (2000), "some elastomers will continue to harden, and some soften, and some will show an initial hardening followed by softening." In the volumetric tests (except for the PTFE's), the elastomer samples reached a maximum point of softening, then began to harden. Figure 3.19 (b) show more than 5% and up to 59% increase from the original volume except the PTFE's and 1-day Viton (brine phase). After aging at 180°F, more than 5% and up to 43% increase from the original volume was recorded except for the PTFEs and all Viton (Brine). These changes in elastomeric properties are linked to the initial chain rupture in the elastomer followed by chain growth within the elastomer. Chain rupture increases the elastomers size (swelling) while chain growth causes the elastomer to shrink.

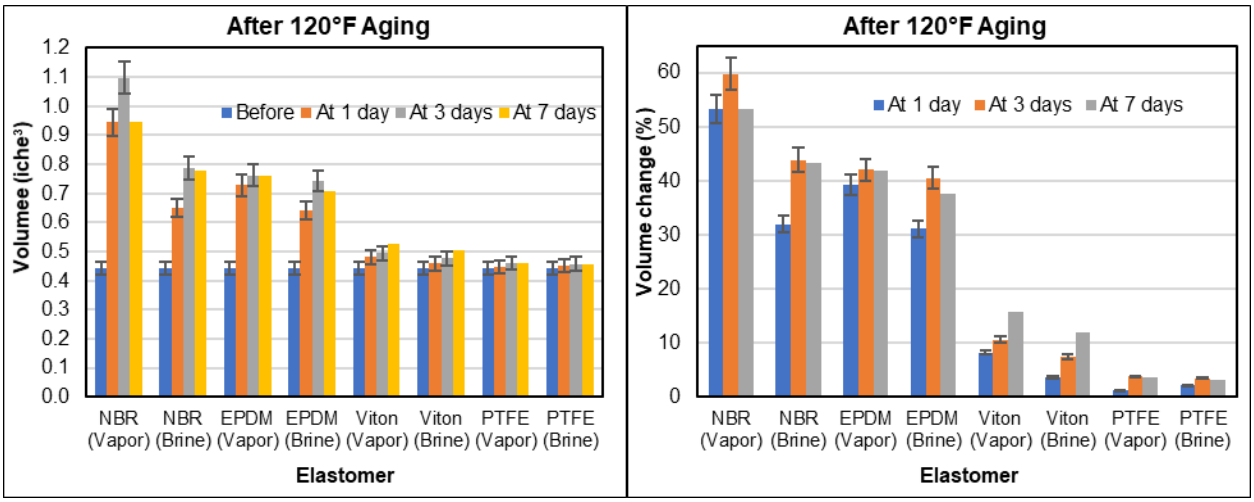

(a) **(b)**

Figure 3.19: Effects of aging period on volumetric swelling of elastomers at 120°F and 1000 psi. Compression measurement (a) and percentage difference in compression measurements (b).

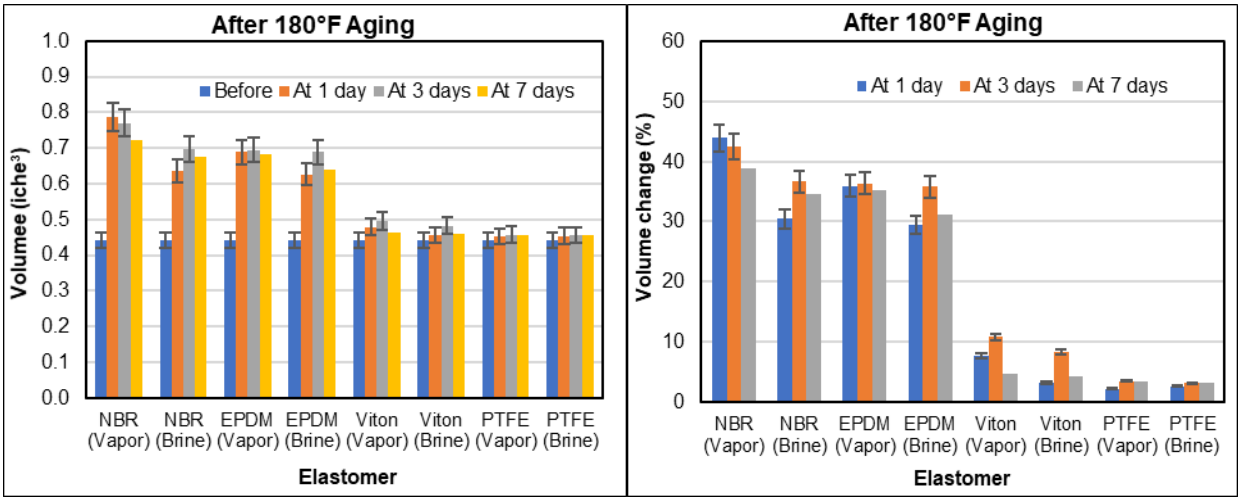

(a) **(b)**

Figure 3.20: Effects of aging period on volumetric swelling of elastomers at 180°F and 1000 psi. Compression measurement (a) and percentage difference in compression measurements (b).

Effects of Temperature

Based on visual observations and measurements shown in Figure 3.21 (a) and (b), NBR in the vapor phase appears to have shown maximum swelling amongst its counterparts (EPDM and Viton). This observation was consistent after aging at 120°F and 180°F. For all the elastomers, the swelling was more predominant in the samples exposed to the vapor phase compared to those exposed to the brine phase. For example, the NBR samples in Figure 3.21 (a) clearly shows more swelling in the vapor phase (particularly at the ends of the elastomer), compared to NBR samples exposed to the brine. An increase in temperature results to a decrease in swelling. All the three samples showed a decrease in swelling when temperature is increases from 120°F and 180°F. Viton, however, at higher temperatures does not only experience swelling but also blistering.

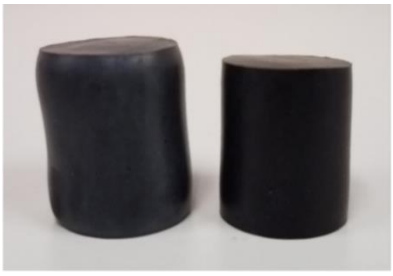

NBR @120°F: Vapor (left), Brine (right)

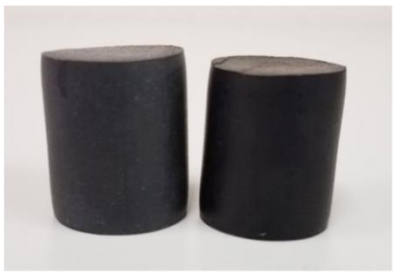

EPDM @120°F: Vapor (left), Brine (right)

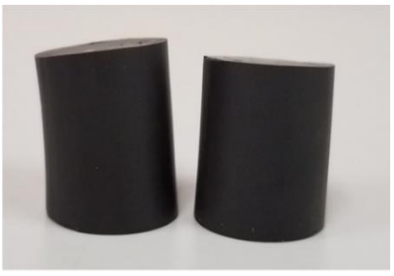

Viton @120°F: Vapor (left), Brine (right)

(a)

NBR @180°F: Vapor (left), Brine (right)

EPDM @180°F: Vapor (left), Brine (right)

Viton @180°F: Vapor (left), Brine (right)

(b)

Figure 3.21: After 1-day aging in CO_2 and H_2S with CH_4 carrier at 1000 psi. (a) 120°F and (b) 180°F.

Blisters refer to bubbles or raised defects that appears on the surface of an elastomer. They are caused by the high energy with which the trapped gases (within the elastomer pores) tend to escape after decompression. It should be noted that the decompression performed after each test was rather gradual, not rapid. Blistering causes delamination and breakage of the elastomer-lining layer, resulting in a loss of its corrosive protection (Van Dinh and Kubouchi 2012). Viton's poor decompression resistance causes this blistering at high temperatures. The test samples showed that blistering occurred in 1, 3, and 7-day tests and was consistent for the aging tests performed at 180°F. Figure 3.22 shows the blistering on the FKM elastomer surface. All the images were taken with the Dino-Lite Digital Microscope. Keeping the aging period constant and varying temperature from 120°F to 180°F, a decrease in volumetric swelling for all the elastomers was recorded. This is because elastomers tend to undergo cross-linkage at elevated temperatures; thus, decreasing their elongation.

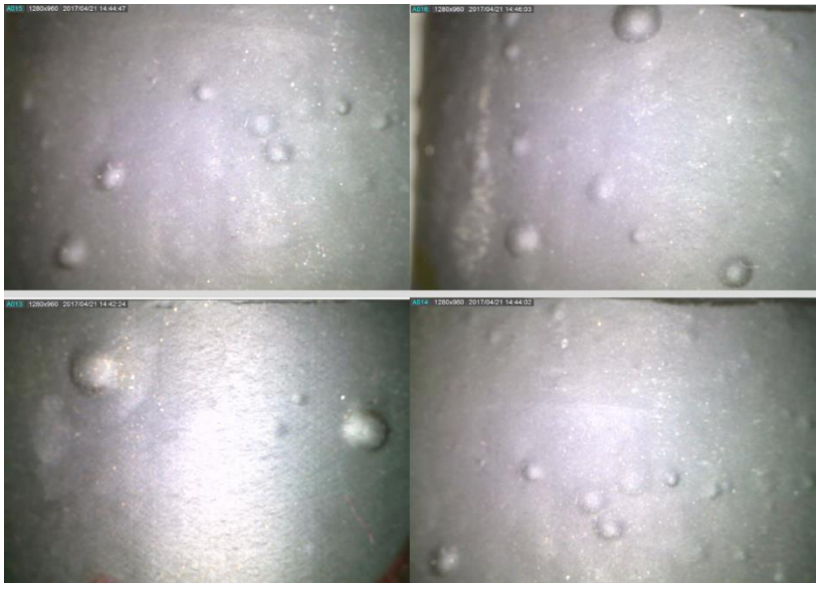

Figure 3.22: Viton blistering image taken with a Dino-Lite Digital Microscope.

Figure 3.23 shows the plots of volumetric increase (percent) after 1, 3, and 7 days of aging. These aging tests were conducted at 1000 psi and at two temperatures (120°F and 180°F). All the tests were conducted with 50% CO_2 and 50% 500 ppm H_2S with CH_4 carrier. After 1-day, volumetric swelling (more than 5% and up to 53%) from the original values was recorded. After 7 days, the volumetric swelling was also between 5% and 53% from the original volume. These observations exclude the PTFE's in both vapor and brine phases. The 3-day aging tests showed the highest recorded volumetric swelling readings - more than 5% and up to 59.7%. Using these numbers, Figure 3.23 suggests that irrespective of the aging period and elastomer type (except PTFE), an increase in temperature tends to decrease volumetric swelling.

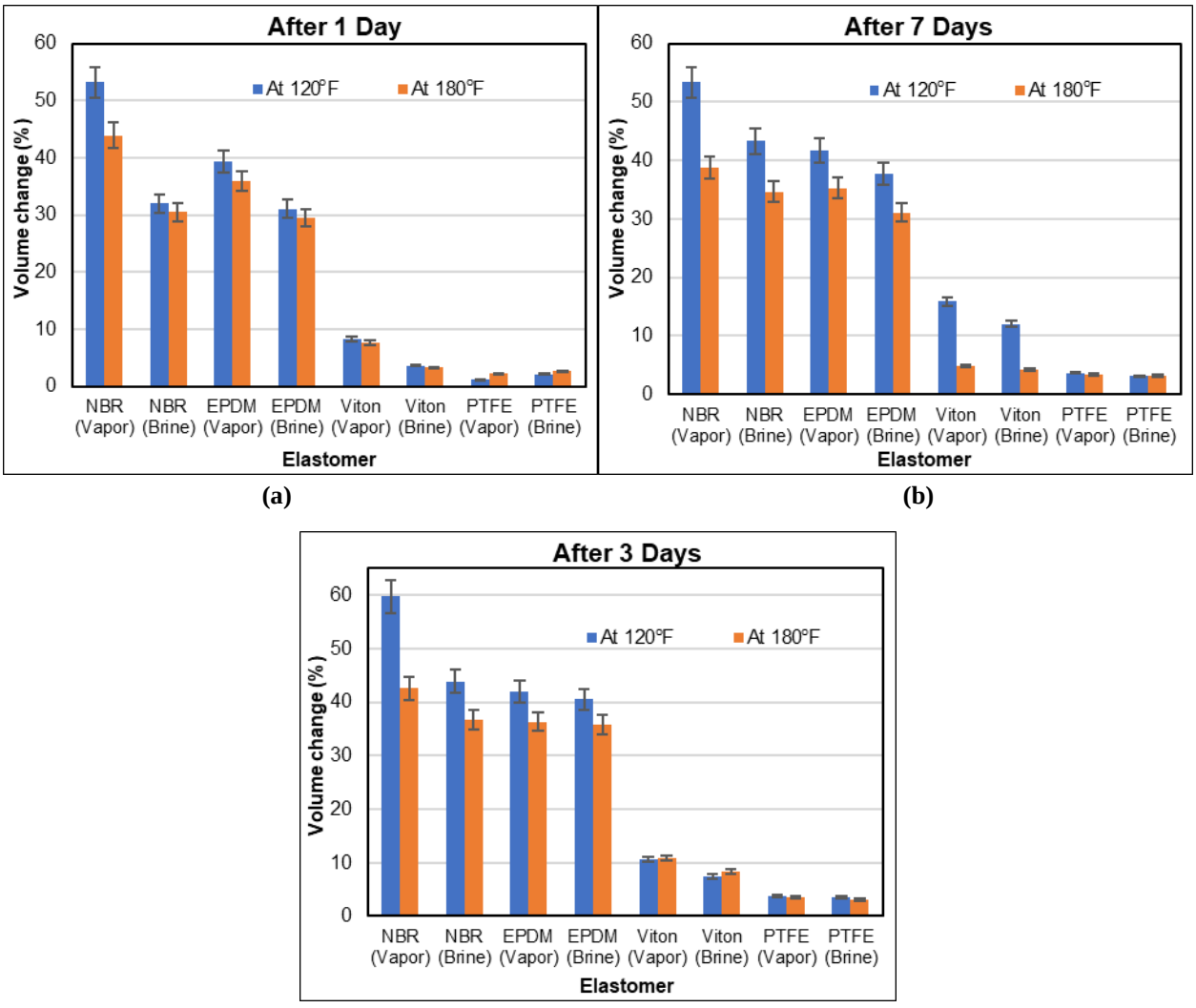

Figure 3.23: Effects of temperature on percentage volumetric change in elastomers aged at 1000 psi after 1 day (a), 7 days (b), and 3 days (c).

The ANOVA results suggest that the volumetric swelling of elastomer samples is not significant with changes in temperature, aging period, and the aging fluid medium. Varying one parameter in the aging test while keeping all others constant, does not show any significant effect. However,

this is impractical given that multiple aging parameters can change simultaneously in actual downhole conditions. The interaction effects for volumetric swelling was also insignificant. Thus, it can be cautiously concluded that exposing an elastomer to the least corrosive condition (1 day in the vapor phase at 120°F) is enough to cause its seal integrity to be compromised. A change in aging conditions after this is considered redundant since the elastomer has already been compromised appreciably.

Effects of Gas Variation

Figure 3.24 (a) compares the effects of gas variation on the volumetric swelling of the elastomers. The least effect of volumetric swelling was experienced with CH_4. The chemistry of methane (high bond dissociation energies and close electronegativity of constituent elements) explains its stability and low reactivity. Thus, it is less likely to react with any elastomer sample. Aging in the presence of 100% methane shows volumetric swelling that is more than 5% and up to 32.6% from the original values. This swelling is mainly because of the physical changes in the elastomer rather than a chemical reaction. H_2S caused a 5% to 34.2% increase in volume after aging the elastomers. From Figure 3.24 (b), aging in 100% CO_2 shows more than 5% and up to 53.2% volumetric increase in all the elastomers except for some PTFE. PTFE aged in 100% CO_2 had an average swelling of 5.3%. For combined gases, the elastomers experienced more than 5% and up to 53.3% increase from the original volume. It is difficult to determine the order of gas degradation for volumetric swelling. This is because 100% CO_2 showed a more detrimental effect on EPDM compared to NBR, while a combination of CO_2, H_2S, and CH_4 had a more detrimental effect on NBR compared to EPDM. However, CH_4 had the least effect on elastomer volumetric swelling.

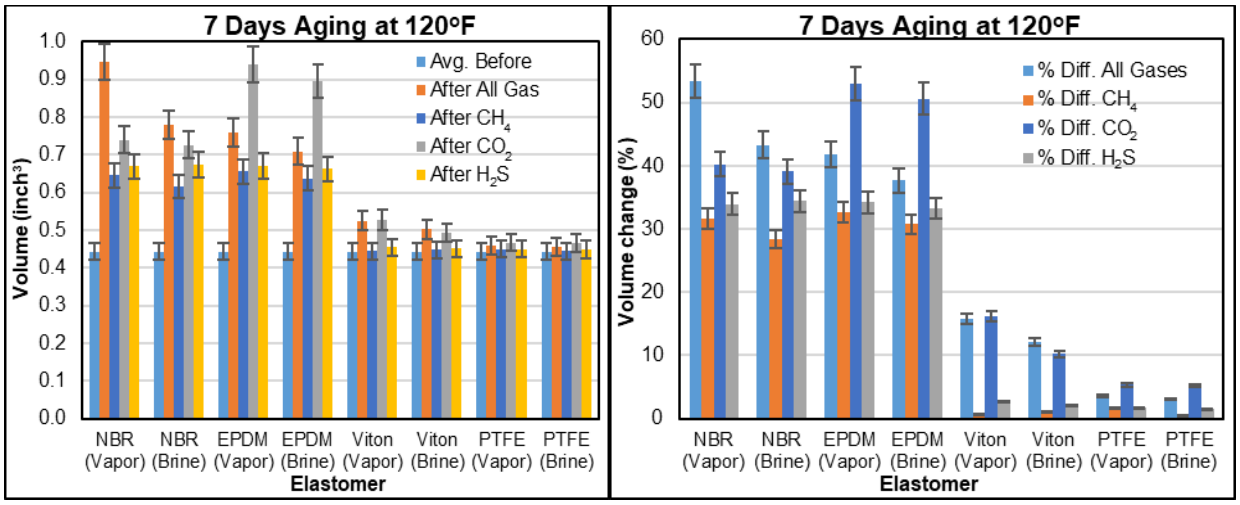

(a) **(b)**

Figure 3.24: Effects of gas variation on percentage volume measurements of elastomers aged at 1000 psi and after 7 days. Volume measurements (a) and percentage volumetric change (b).

3.5 SUMMARY AND CONCLUSIONS

The following conclusions and summaries have been drawn from the theoretical and experimental investigations, results, and analyses conducted in this section of the project and report:

- Physical and chemical degradation of elastomers occur when they are exposed to testing conditions.
- The degree of chain growth and chain rupture depends on the temperature and degree of chemical exposure.
- NBR exhibited the most significant deterioration.
- Viton showed the least amount of degradation but has poor decompression resistance.
- CO_2 showed the most damaging effect of all the corrosive gases used in this study.
- Elastomer hardness is inversely proportional to the volumetric swelling and compression.
- For all the elastomer samples studied in this part of the project, the general order of corrosive gas effect on elastomer degradation is CO_2 > All gases > H_2S > CH_4.
- Statistical analyses indicate that exposing an elastomer to the least corrosive condition (1 day in vapor phase at 120°F) is enough to cause its seal integrity to be compromised appreciably. However, this cannot be extended to higher temperature conditions (greater than 180°F) because of unavailability of experimental data.

4 SEALING ASSEMBLIES TESTS USING SET UP II

4.1 INTRODUCTION

4.1.1 Overview

Drilling operations, particularly in an offshore environment, require special tools and equipment. Liners and liner hangers are commonly used in offshore drilling applications instead of full string casings. They are cost effective, require shorter time for running into the hole, improve cement job, and provide more space to accommodate completion equipment's above the liner (Mohamed and Al-Zuraigi 2013). When a well section is drilled, liner hanger and cement are used to engage and seal off the liner, connecting it to the previous casing. After this, a formation strength test such as leak-off test (LOT), extended leak-off test (XLOT), and formation integrity test (FIT) is performed. Typically, the liner hanger seal assembly is placed up-stream to the cement column. This arrangement prevents the evaluation of both the cement and liner hanger seal assembly independently, since the sealing element isolates the cement sheath and there is no direct or indirect way of assessing its integrity. Moreover, Pleasants et al. (2012) highlighted that it is difficult to evaluate the performance of liner hanger seals and cement independently through the pressure test when both cement and mechanical barriers (seal) are used in series. This concern was also outlined in BSEE internal QC-FIT report #2014-02.

Statistical records have shown that a majority of the incidents associated with drilling operations in offshore shallow sections are attributed to gas migration and failure of liner hanger and cement sheath (Moore et al. 2002; Walvekar and Jackson 2006). This has jeopardized the integrity of many wells and there are no direct methods or standards that may be used to identify which of them (cement sheath or liner hanger sealing element) failed. When uncontrolled gas migrates through the wellbore, the liner hanger and cement acts as a barrier system to prevent the gas from flowing through. The liner hanger sealing system consists of an elastomeric material and its performance depends on the elastomer type, design specifications, and compatibility with the wellbore environment. Elastomers are commonly used rubber materials in oilfield operations because of the unique set of properties they possess, particularly in high-temperature/high-pressure environments (Dolog et al. 2017). They are used to provide the sealing and hanging mechanisms in the liner hangers (Williford and Smith 2007; Wardak et al. 2010). In addition to the elastomeric material, the cement sheath also acts as a barrier. Slurries used in gas migration prone zone are typical mixed with gas migration additives. This has been discussed in detail in section 1 of this report (cement tests using setup I).

4.1.2 Statement of Problem

Well integrity can be compromised when a barrier or multiple barriers fail to prevent formation fluid influx and migration. Failure in seals can be identified by excessive fluid leakage that is caused by a loss of seal interference (seal contact stress) or a loss of seal integrity, which is generally referred to as physical damage (James 2017). In this section of the project, elastomers are investigated as barrier elements that are expected to fulfil specific performance requirements.

Barrier acceptance criteria needs to be evaluated to ensure that the barrier performance requirements are met, and their integrity verified. Barrier verification can be performed directly by conducting a pressure test or through other observations (API RP 96 2013). When liner hangers are deployed in the field, they are sealed off by cement and elastomers. Some of the key questions that may be raised in this situation include: i) Which of these materials (elastomer seal or cement) is considered to be the primary barrier? ii) Should both barriers be tested independently? iii) If this is possible, how can these tests be conducted in the field? iv) Is it necessary to increase the pressure test duration for conductor casing, surface casing, and liners from 30 minutes with less than 10 % pressure decline (30 CFR 250.425) to 60 minutes?

To address these questions, two stages of experiments were conducted to evaluate the sealing capacity of elastomers and cement recipes using setup II. In the first stage, pressure tests were conducted on elastomer samples that are commonly used in liner hanger application. In this case, the elastomer seals were considered a single barrier system and the pressure tests were conducted considering three different experimental scenarios. In the second stage, experiments were conducted to test both elastomer seals and cement as a dual barrier considering two different scenarios. The details of all the experiments are discussed in the methodology. In addition, pressure cycling tests were also performed on elastomer seals because the sealing assembly can be influenced by the pressure cycling that usually occur over the life cycle of a well. During these cycles, an elastomer can damage from explosive decompression because of gas expansion when there is a sudden pressure decline (AP1 RP 96 2013).

4.1.3 Objectives

The specific objectives in this section of the project and report include:

- Identify the primary barrier when a liner hanger seal assembly and cement are used as a dual barrier system to seal off a liner.
- Evaluate the sealing performance of elastomers, particularly EPDM and NBR in preventing uncontrolled gas migration when used as barrier element.
- Evaluate the performance of elastomers under mechanical failure mode (because of improper setting and/or manufacturing defect).
- Evaluate the performance of elastomers when they are exposed to chemical degradation (degradation with surfactant and CO_2).
- Assess the effect of pressure cycling on the elastomer's performance.
- Assess the effect of the pressure cycling when elastomer and cement sheath are used as a dual barrier system.
- Assess the effect of prolonging the pressure test duration from 30 minutes to 60 minutes on the elastomer seals and cement performance.

4.2 LITERATURE REVIEW

Maintaining a well under control is a primary and essential safety requirement during drilling operations. Well control is defined as activities implemented to prevent or mitigate unintentional release of formation fluids and gases from the well to its surroundings (API RP 96 2013). There are many principles for well control set by regulatory agencies and industrial standards. Most of them agreed on a common rule for well control barriers which is: "at least, two tested independent barriers should be in place between the hydrocarbons in the reservoir and the environment at all times" (NORSOK D-010 2014; API RP 96 2013; ISO/TS 16530-2 2013). This rule is also recognized by the Bureau of Safety and Environmental Enforcement (BSEE) and Norwegian Petroleum Safety Authority (PSA) regulations. Oil and gas operators and service providers are expected to adhere to the concept of two well barriers during all well operation activities. However, investigations from many well control related accidents have revealed that most of the two well barriers were inadvertently maintained by the crew during the incidents (Strand 2017).

Barrier analysis and management have received more attention over the years from operating and services companies, contractors, and regulators to ensure that they are properly identified, in place, and functional. The focus on barrier performance requirement verification increased after the significant blowouts in Montara and Macondo (Aggelen 2016), as well as the shallow gas migration event in the Main Pass Block 295. A barrier must meet certain performance requirements such as functionality, availability, reliability, capacity, effectiveness, integrity, ability to withstand loads, robustness, accessibility, and response time (ISO/TS 16530-2 2013; PSA 2013; Hauge and Øien 2016). In addition to these, the following should be considered as part of the performance standards according to ISO/TS 16530-2 2013: failure mechanisms, failure consequences, operating conditions, and interactions with other systems.

There are different failure modes by which a wellbore barrier can fail. The study conducted by Davies et al. (2014) showed that the percentage of wells that have had issues on well barrier or integrity failure is highly variable (1.9%-75%). According to King and King (2013), well barrier failure occurs when individual or multiple well barriers fail to perform their function; however, the well is kept under control. The main causes of barrier failure associated with drilling are: inadequate cementing, leaking tubular, corrosion, degradation, cyclic loads, thermal extremes, earth stresses, wear/abrasion, seals that isolate the top of tubulars, seals between the hangers, and valves amongst others (King and King 2013; Aggelen 2016). One of the well failure mechanisms is pressure cycling which can lead to barrier degradation. The hydraulic fracturing process is a typical example where fluid migration pathways can be created because of the cyclic pressures associated with the stimulation process (Wu et al. 2016).

There are several measures that can be taken to prevent the incidents that arise from barrier failures. The barrier systems must be thoroughly analyzed by conducting hazard and operability (HAZOP) review to ensure that barriers are "fit for service" for all the expected conditions of operation (Thorogood 2017). A detailed literature review on leak mechanisms, well control and barrier failures, types of elastomer materials used in liner hangers, and failure modes of a liner

hanger system have all been documented in the report on laboratory results of sealing assemblies and cement system (**4.2.1 to 4.2.5**).

4.3 RESEARCH METHODOLOGY

4.3.1 Scope of Work

Sealing assembly and cement sheath are used to seal off the liner hanger. It is difficult to differentiate which of the barriers passes the pressure test because of the presence of elastomeric material ahead of the cement column. The scope of this study is to identify a test method that allows for evaluating the performance of seals and cement independently. Furthermore, to identify whether the seals or cement sheath is the primary barrier.

The scope also covers evaluating the impact of manufacturing defects, chemical degradation, and pressure cycling upon seal performance. EPDM and NBR were selected for the tests because they are commonly used in downhole sealing systems. The pressure tests were conducted at 40 psig for safety precautions because the setup was fabricated from an acrylic material and cannot withstand higher pressures. The tests were performed at room temperature similar to the tests in setup I (cement tests). For the details about the experimental setup description and test description, please refer to sections **4.3.2** and **4.3.3** in the report on laboratory results of sealing assemblies and cement system

4.4 RESULTS

This section of the project discusses the test results from all the experiments. They are divided into two main parts: 1) independent pressure tests and pressure cycling tests on elastomers as a single barrier and 2) cement and elastomer pressure tests as a dual barrier.

4.4.1 Elastomer Tests

4.4.1.1 Pressure Tests Under Normal Condition

Normal conditions in this case implies that the elastomers have not been exposed to any form of chemical degradation or mechanical damage such as manufacturing defect, cracks, setting, and installation problems.

EPDM Pressure Tests for 30 Minutes Holding Times

EPDM samples were tested at 40 psig for 30 minutes at 180 in-Ibf and no leak (pressure drop) was observed. The test was repeated after the torque was reduced to 120 in-lbf and 0 in-lbf to evaluate the effect of energization on the elastomers' performance. The test was repeated after the elastomers were allowed to relax for one week and no torque was applied. The goal of the one-week relaxation was to assess the friction force between the pipes and elastomers upon their energization. Figure 4.1 shows that for all the energization conditions and under normal condition, no leaks were recorded within 30 minutes of pressure test. The elastomers exhibited good sealing capacity up to 40 psig.

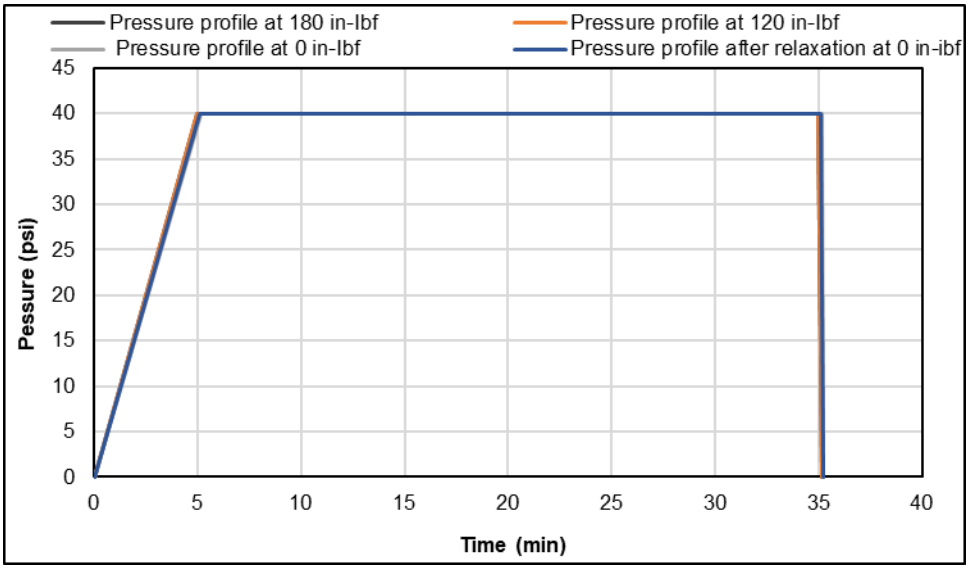

Figure 4.1: EPDM pressure test at different torques and 30 minutes

The same tests (using similar procedure) were conducted for 60 minutes for all the energization conditions and under normal condition. No leak was recorded within 60 minutes of pressure test. Similar results were obtained for all the 60 minutes tests performed in this study (please refer to section ***4.4.1.1*** of the report on laboratory results for sealing assemblies and cement system). The results that were obtained confirmed the claim made by Hopkins (2016). The author suggested that overall, expanding the test holding time to 60 minutes does not improve leak detection and safety because in field operations, pressure test failures can be detected very quickly. While this may be true, the analytical results from setup I supports an increase in pressure test time as the liner-casing overlap length increases. This has been discussed in the draft recommendation report.

EPDM Pressure Cycling Test

The objective of exposing the elastomers to a pressure cycling test was to assess their sealing capacity and failure modes when they encounter high pressure shifts and cycles in field applications. Dusseault et al. (2014) claimed that production, injection, stimulation, and other operations may result in cyclic pressure and/or thermal stresses. Four pressure cycling tests were conducted after the following torque/energization: 180 in-lbf, 120 in-lbf, 0 in-lbf, and one-week relaxation with 0 in-lbf. In each test, the cycle was repeated 10 times and the pressure profiles are shown in Figure 4.2. No leak was observed during these tests as shown from the stability of the pressure profiles over the holding periods (10 minutes), which implies proper sealing.

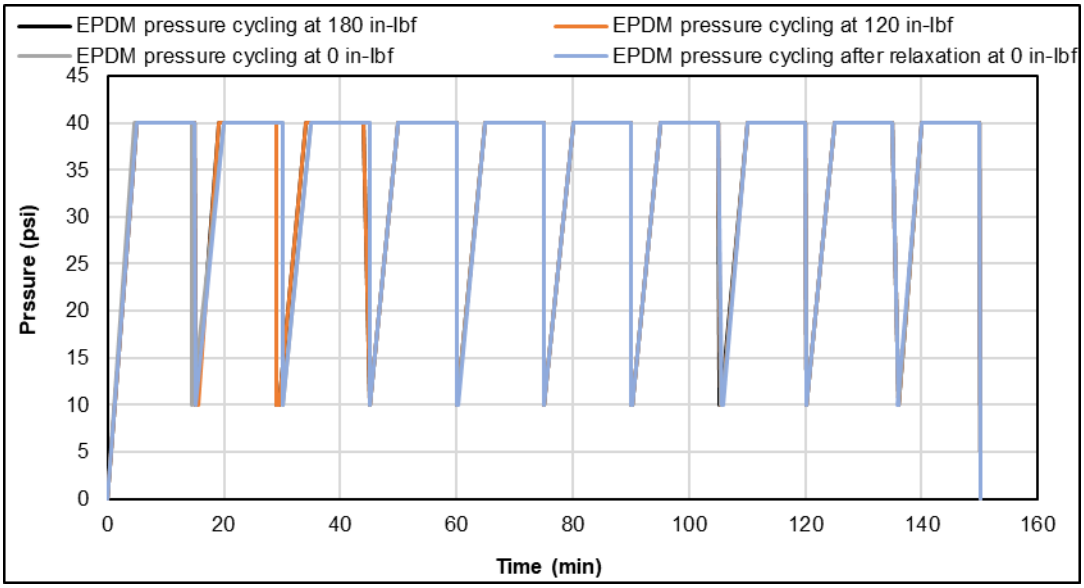

Figure 4.2: EPDM pressure cycling test at different torques.

NBR Pressure Tests for 30 Minutes Holding Times

NBR samples were subjected to 30 minutes pressure test using the same energization from the EPDM tests. Figure 4.3 shows that from 5 minutes to 35 minutes, there was no pressure fluctuation nor decline. This result holds for all the energization conditions. No leak was recorded which confirmed that the NBR samples provided good sealing up to 40 psig.

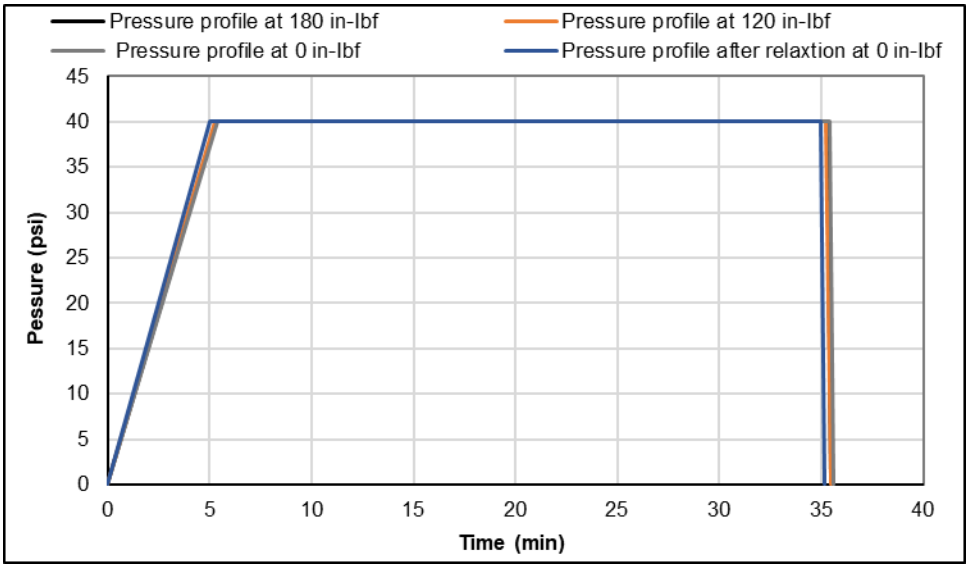

Figure 4.3: NBR pressure test at different torques and 30 minutes

NBR Pressure Cycling Test

NBR samples were subjected to pressure cycling tests. Figure 4.4 shows no leak was recorded during the first and second tests (180 in-lbf and 120 in-lbf). The minor deviations in the 8th and 9th

cycles were from pressuring up and pressure release, which had no effect on the elastomers sealing performance. However, a leak appeared in the form of a blowout during the zero-torque test condition. This is shown in Figure 4.5 (b). The seal integrity was first compromised at the end of the 3rd cycle (first leak) as shown in Figure 4.6. Although the last three cycles in this figure showed a stable pressure profile, the four subsequent cycles before these last three cycles further compromised the elastomers sealing performance, with 4.5 minutes as the minimum holding time.

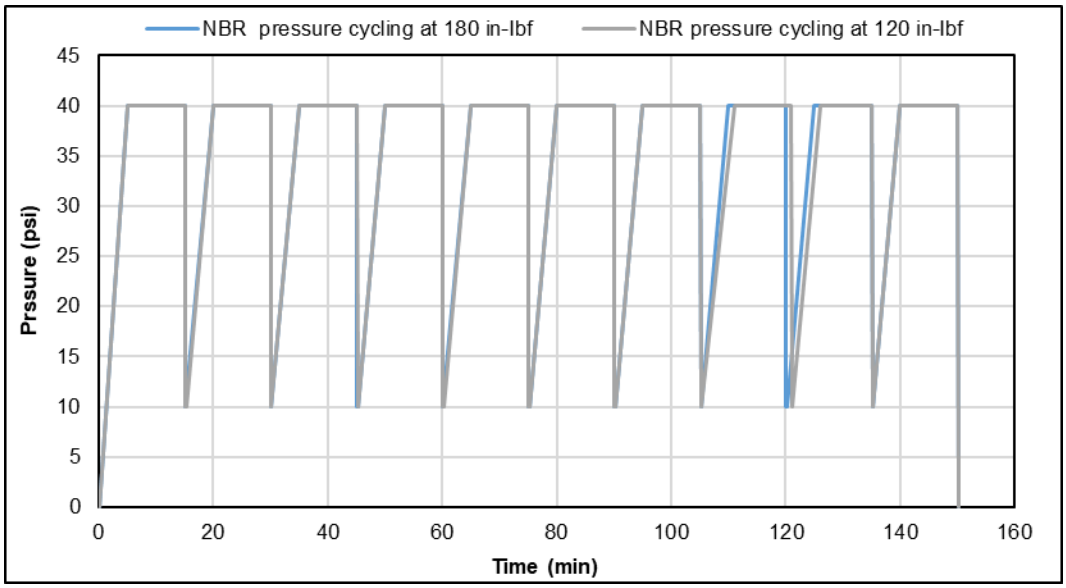

Figure 4.4: NBR pressure cycling test at 180 in-lbf and 120 in-lbf (successful tests).

(a) **(b)**

Figure 4.5: NBR before (a) and after (b) failure during pressure cycling

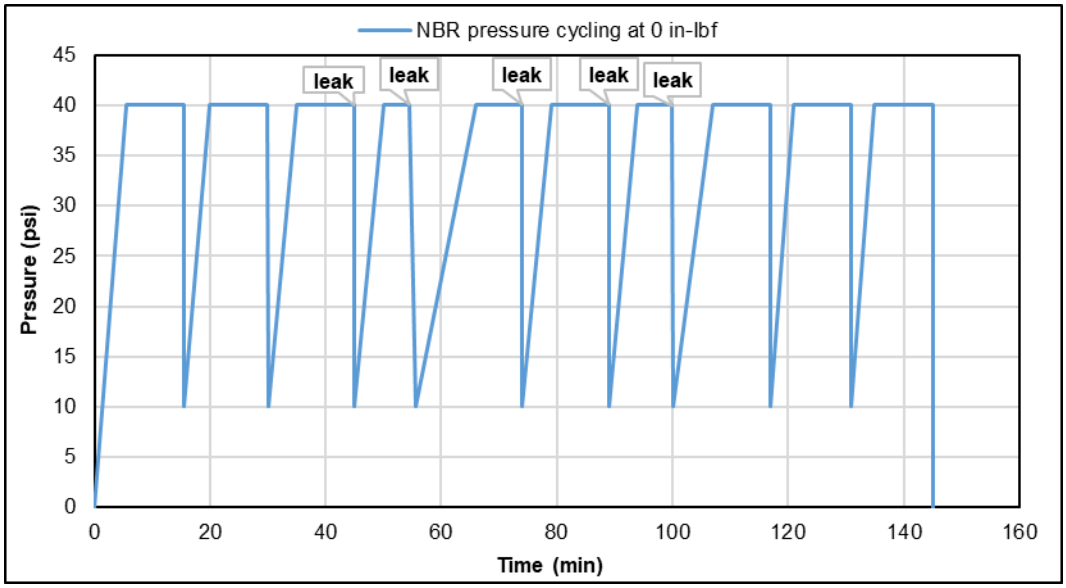

Figure 4.6: NBR pressure cycling test at zero torque (failed test).

After one week of relaxation, pressure cycling tests were performed without torque and as expected, NBR's sealing performance was much inferior. Figure 4.7 shows that the elastomers failed within 2.5 minutes of the second cycle. Other subsequent cycles were incomplete because leaks kept appearing. The sealing integrity worsened towards the end of the pressure cycling test. The practical implication of this result is that at low or no energization, elastomer seals can lose their contact pressure with the casing/liner during pressure cycling activities. This can allow formation fluid influx. To verify this, the torque was increased to 60 in-lbf and the number of failed cycles reduced. The leak completely stopped after the torque was increased to 120 in-lbf. Overall, the EPDM samples exhibited better sealing properties than the NBR samples and the influence of energization was more evident in the NBR performance.

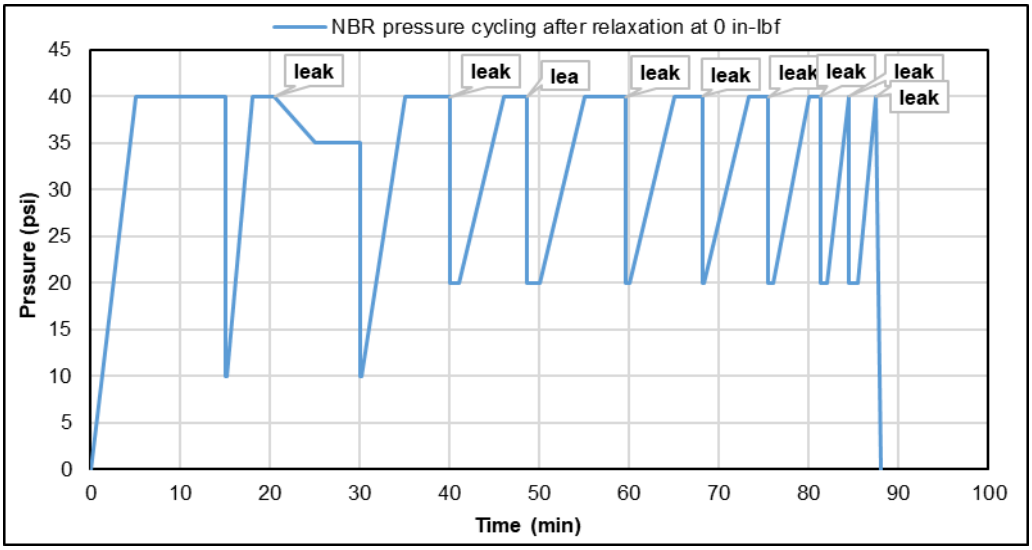

Figure 4.7: NBR pressure cycling test after one-week relaxation (failed test).

4.4.1.2 Pressure Tests After Chemical Degradation

The objective of performing the tests was to evaluate the effect of chemical degradation on the elastomers sealing performance. Both elastomers were exposed to a surfactant that is typically used in non-aqueous drilling fluid (NAF) for one week at atmospheric temperature and pressure. No torque was applied during elastomer installation because of their significant swelling after it was removed from the surfactant. The elastomers swelling added to the difficulty experienced during the installation and increased the contact pressure because of the high friction force between them and the pipes walls. In addition, EPDM samples were also degraded with CO_2.

EPDM Pressure Tests for 30 Minutes Holding Time After Surfactant Degradation

EPDM elastomers were tested at 40 psig and 30 minutes holding time after surfactant exposure. The test was repeated for two consecutive days and the pressure profiles shown in Figure 4.8 revealed no leak or pressure drop. Although, a decrease in hardness (from 75 durometer points to 63.75 durometer points) was recorded, the elastomers diameters increased from 8.74 inches to 8.82 inches and thickness increased from 0.75 inches to 0.78 inches. One plausible explanation for their good sealing performance is the increase in contact pressure between the sealing interfaces (elastomer and pipe walls) because of the volumetric swelling.

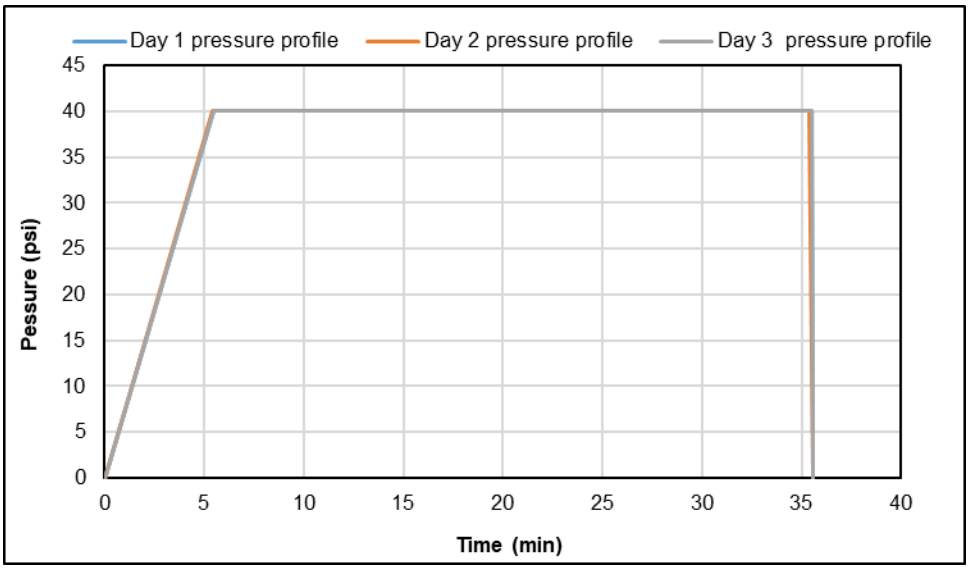

Figure 4.8: EPDM pressure test at Day 1, Day 2, and Day 3 after exposure to a surfactant (30 minutes).

EPDM Pressure Cycling Test After Surfactant Degradation

Pressure cycling tests were performed at day 1, day 2, and day 3 to assess its impact on EPDM performance. The results shown in Figure 4.9 reveals the stability and sealing performance of EPDM for the 10 cycles.

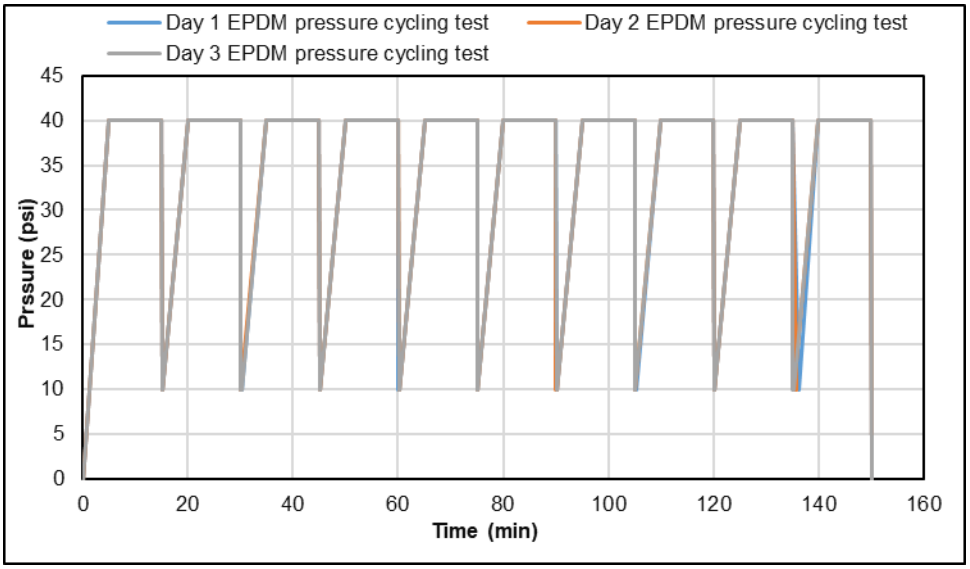

Figure 4.9: EPDM pressure cycling test at Day 1, Day 2, and Day 3 after exposure to surfactant.

NBR Pressure Tests for 30 Minutes Holding Time After Surfactant Degradation

Pressure tests were conducted on NBR samples for 30 minutes using the same procedure and consecutive intervals (days) for EPDM. No torque was applied because of the volumetric swelling of NBR which was more significant than EPDM. The NBR samples diameters increased from 8.74 inches to 8.94 inches and thickness increased from 0.75 inches to 0.87 inches. Figure 4.10 shows the pressure profiles for 30 minutes pressure tests. No leaks were recorded and the increase in duration did not have any effect on NBR's sealing performance.

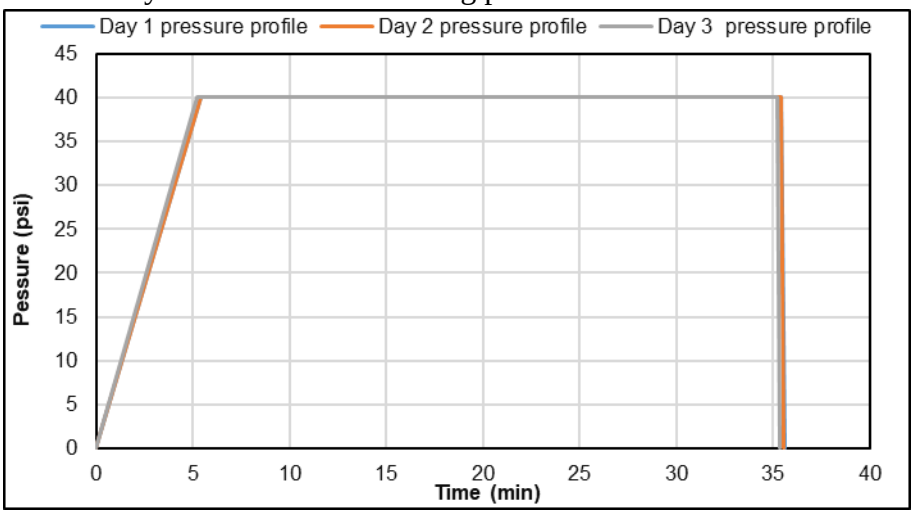

Figure 4.10: NBR pressure test at Day 1, Day 2, and Day 3 exposure to a surfactant (30 minutes).

NBR Pressure Cycling Test After Surfactant Degradation

NBR Pressure cycling tests were performed to evaluate its performance on day 1, day 2, and day 3 after exposure to a surfactant. The surfactant decreased NBR's hardness from 66 durometer

points to 44 durometer points; however, their sealability was improved because of the volumetric swelling of the elastomers. As a result of the volumetric swelling, the elastomer energization was improved from the high friction force between elastomers and pipe while installing. Figure 4.11 shows that no leak was recorded during the pressure cycling test.

It should be noted that the elastomers were exposed to the surfactant at room temperature and pressure. Chemical attacks on elastomers and alteration of molecular structure can be exacerbated at elevated temperatures; thus, reducing the elastomers sealing performance. Other downhole corrosive gases such as H_2S can have more detrimental impact. These have been discussed in the elastomer aging tests section (3) of the report.

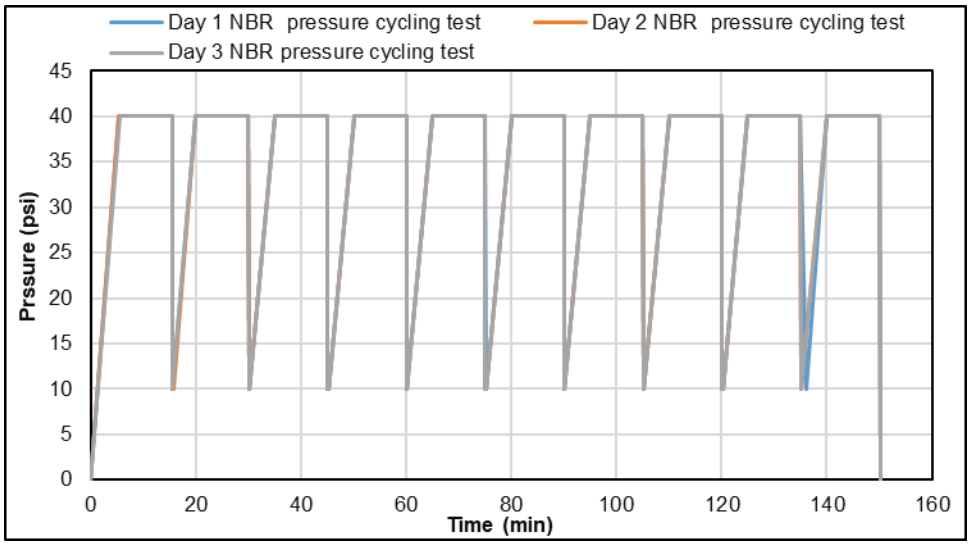

Figure 4.11: NBR pressure cycling test at Day 1, Day 2, and Day 3 after exposure to a surfactant.

EPDM Pressure Tests After CO_2 Degradation

To evaluate the sealing performance of elastomers when they are exposed to other forms of chemical degradation besides a surfactant, EPDM samples were aged for three days with CO_2 at room temperature and 600 psig. After aging, blisters and cracks were created on the elastomers surface. Two pressure tests were conducted: without torque and at 180 in-lbf. In both tests, the elastomers lost their seal integrity and leaks were observed within few seconds of commencing each test. Figure 4.12 (a) and Figure 4.12 (b) illustrates the EPDM failed pressure tests (no torque) after CO_2 exposure and degradation. After 5 minutes of pressuring up, Figure 4.12 (a) shows an instantaneous pressure decline (within 5 to 6 seconds), which becomes more evident as pressure increases. This is supported by Figure 4.12 (b) which shows that as pressure increase, the first bubble leak time decreases. Figure 4.13 (a) and (b) indicates that increasing the torque had little to no effect in preventing the leaks. Similar instantaneous pressure decline was recorded at 180 in-lbf. The effect of torque may have been slightly observed as the first bubble time (for 10 psig test) in Figure 4.13 (b) was later than the first bubble time (for 10 psig test) in Figure 4.12 (b). However, this time difference (0.017 seconds) is quite small, in addition to the small pressure at which this

difference was recorded. Overall, the results from these pressure tests validates the detrimental effect of CO_2 degradation compared to surfactant degradation. While both chemical degradations revealed an increase in volumetric swelling because of elastomer chain rupture, CO_2 degradation created visible cracks and blisters. CO_2's molecular structure allows it to penetrate the elastomer chains more (compared to the surfactant used) such that during decompression (normal or explosive), it results in physical damages shown on the elastomers surface. This explains EPDM's inferior performance during the pressure tests performed under this section.

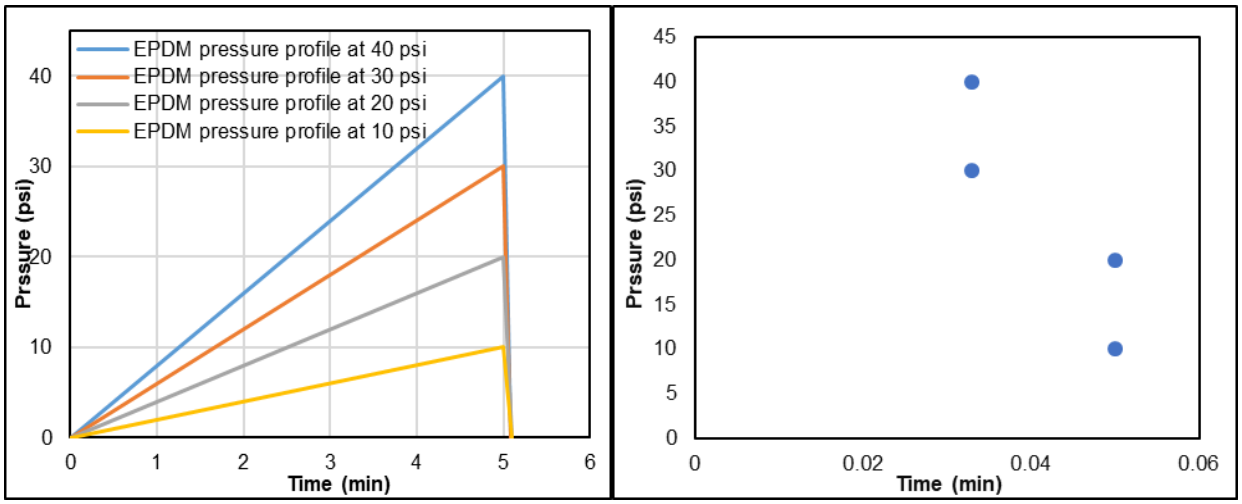

(a) **(b)**

Figure 4.12: EPDM pressure tests (a) and first bubble times (b) after CO_2 degradation with no torque.

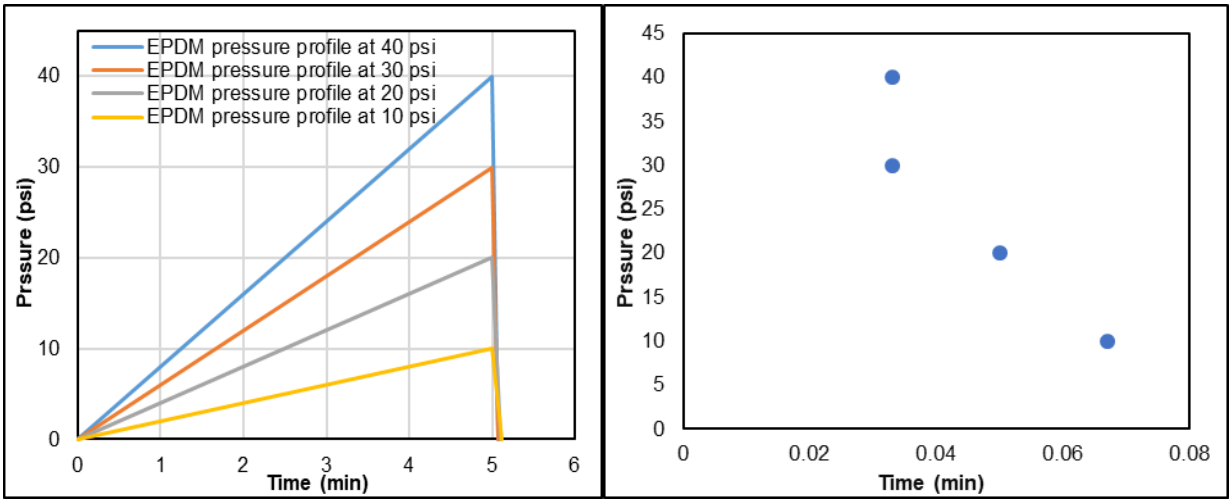

(a) **(b)**

Figure 4.13: EPDM pressure tests (a) and first bubble times (b) after CO_2 degradation with 180 in-lbf.

4.4.1.3 Pressure Tests After Physical (Mechanical) Defect

In this study, seams were intentionally created on the elastomers surface to assess the influence of defects or imperfections that may arise from manufacturing, handling, and/or installation. For both the EPDM and NBR samples, the seams were created similarly in terms of size and area. The

elastomers were torqued up to 180 in-lbf and the pressure tests were performed at 10, 20, 30, and 40 psig.

EPDM Pressure Tests for 30 Minutes

To improve the leak surveillance, the tests were conducted at different pressures beginning with 10 psig (considered as low pressure). Besides, the results from the pressure tests after CO_2 degradation also informed the decision to test at different pressures and only for 30 minutes. Figure 4.14 (a) is the pressure profile for the 30 minutes test. It reveals pressure decline because the physical defects on the EPDM samples compromised their seal integrity. The figure also shows that this pressure decline is more evident as pressure increases. Figure 4.14 (b) shows the time of the first bubble leak which was approximately 12 seconds into the 40-psig test. This figure also validates the evident pressure decline with an increase in pressure (Figure 4.14 a), because the first bubble leak time (Figure 4.14 b) increases as pressure decreases.

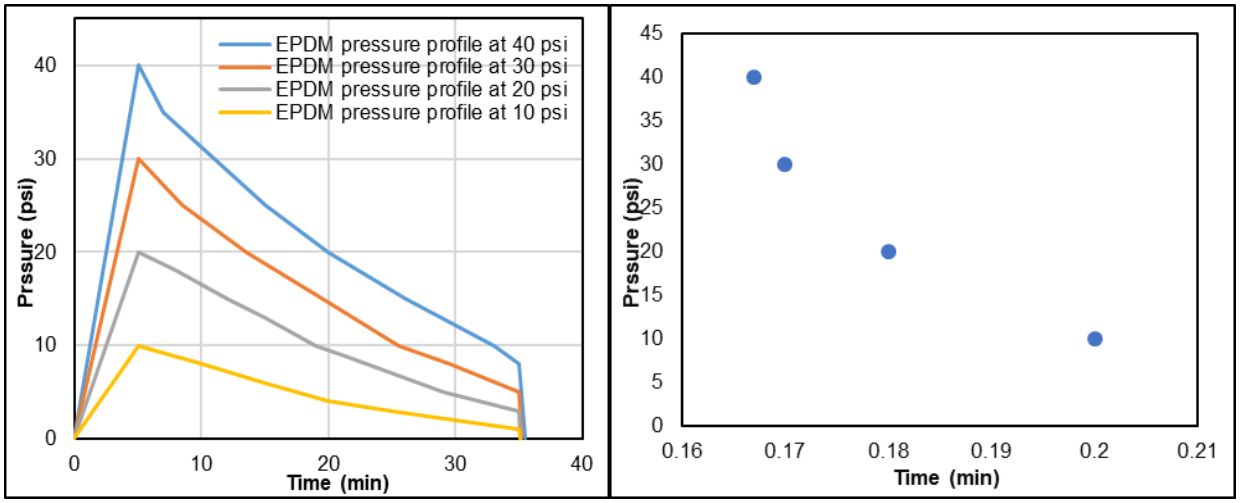

(a) **(b)**

Figure 4.14: EPDM pressure tests (a) and first bubble leak times (b) after physical defects.

NBR Pressure Tests for 30 Minutes

The NBR samples were subjected to the same pressure tests and methods used for the EPDM samples. Figure 4.15 (a) shows that the elastomers did not hold pressure and that pressure declines become obvious with an increase in pressure. Figure 4.15 (b) shows that the first leaks for 20, 30, and 40 psig tests appeared approximately after 5 seconds.

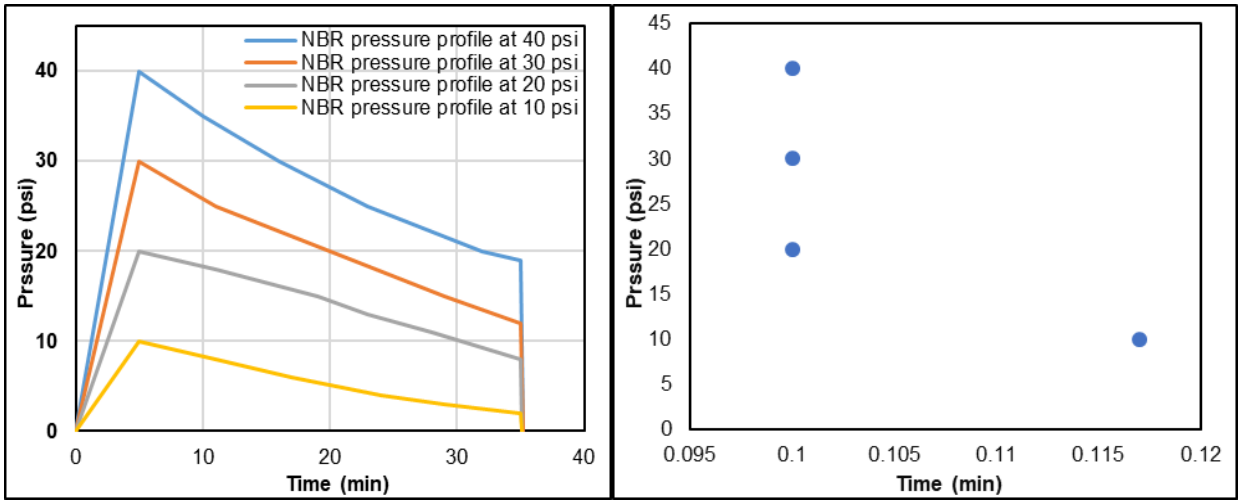

(a) **(b)**

Figure 4.15: NBR pressure tests (a) and first bubble leak times (b) after physical defects.

Comparing the pressure test performances of both elastomers after physical defects, it can be inferred that NBR showed better performance than EPDM. Although, it is possible to argue that the first bubble leak times at 40 psig for EPDM and NBR were 12 and 6 seconds respectively. In addition, the first bubble leak times from the NBR tests were generally shorter (first bubble appear faster) that those from the EPDM test. While the first bubble leak times are important for leak identification, the pressure decline appears to be of better use. Figure 4.16 compares the 40-psig pressure tests of both samples under similar conditions (identical seams, heights, and diameters). The pressure decline from the EPDM test was steeper compared to the decline from the NBR test. This is attributed to its improved energization with an approximate displacement of 0.1 inch compared to 0.06 inch for EPDM under the same torque. The practical implication of this is that gas migration rate may be faster through a mechanically defaced EPDM barrier compared to NBR.

Figure 4.16 compares all the 30-minutes and 40-psig tests for all the conditions (normal, surfactant degradation, physical degradation) at 180 in-lbf. The elastomer samples performed well under normal conditions and after surfactant degradation. However, the EPDM test after CO_2 degradation showed instantaneous failure of the elastomer; thus, it was not included in this figure. Both elastomers' performances were compromised from the physical defect. Practically, all sealing elements used in liner hangers should be tested for the anticipated wellbore conditions before they are deployed.

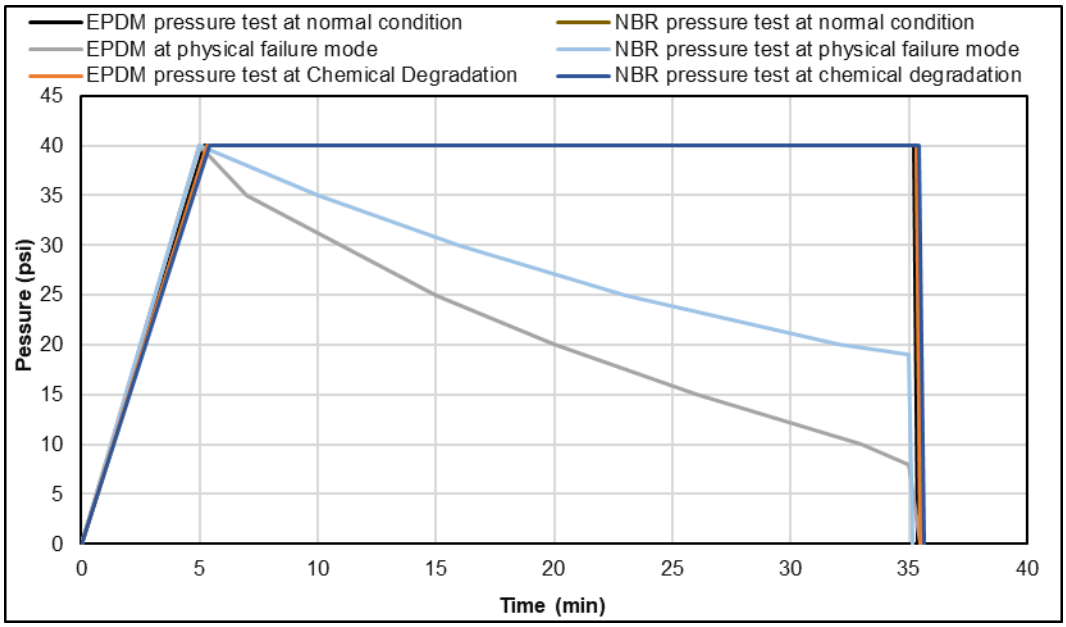

Figure 4.16: Comparison of EPDM and NBR 40 psig pressure test performances at different conditions (normal, surfactant degradation, and physical defect) at 180 in-lbf.

4.4.2 Elastomer and Cement Tests

Three experimental scenarios were considered with EPDM elastomer and Class H cement as a dual barrier system. The tests were conducted at different pressures (10, 20, 30, and 40 psi) and the WOC intervals were 12 hours, 24 hours, 48 hours, 72 hours, 5 days, and 7 days. The goal was to determine which of the materials (EPDM elastomer or cement sheath) may act as a primary barrier to prevent uncontrolled fluid migration during the early stages of cement setting.

4.4.2.1 Faulty Elastomer and Neat Class H Cement

Faulty elastomers were placed at the bottom of the annulus in the setup. Neat Class H cement (16.5 ppg) was placed above the elastomers. The purpose of the faulty elastomers in this scenario is to allow the N_2 to flow across them into the cement column, to examine the effect of WOC periods on gas migration and pressure decline.

Pressure Tests After 12 hours WOC

After 12 hours from the cement displacement (WOC), 10 psi pressure test was performed. The test indicated that the bonding between the cement and the acrylic pipe walls (inner and outer) was insufficient. Leaks were observed from several points between the bonded interfaces. At least two leak points were identified within the cement sheath (micro-channels). A net pressure loss of 5 psi was recorded at the end of the 30-minutes holding period. This test was repeated for 20, 30, and 40 psi. The tests confirmed that the more the pressure was increased, the more pressure declines were recorded as shown in Figure 4.18. A notable observation was that during the 40-psi test, the cement sheath appeared to have moved slightly upwards from the base (Figure 4.17). This occurred during the first 5 minutes of the test. The movement of the cement column confirms the severity

of the debonding issue. A similar observation was also made in the second scenario which will be explained in section ***4.4.2.2***. The pressure declines at 30 and 40 psi were almost instantaneous with approximately 100 % pressure reduction within 5 to 6 minutes.

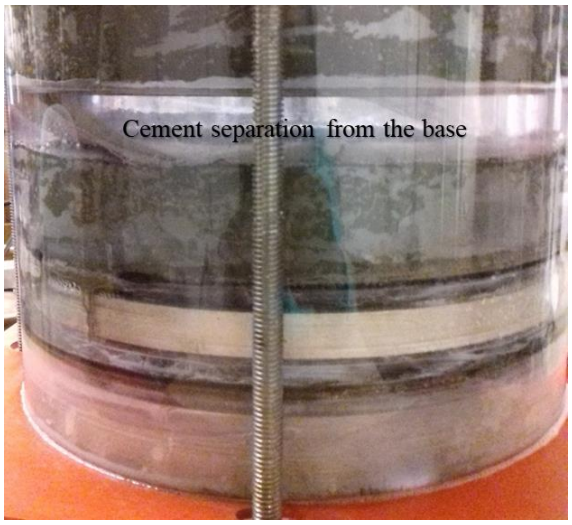

Figure 4.17: Cement separation during the 40-psi pressure test.

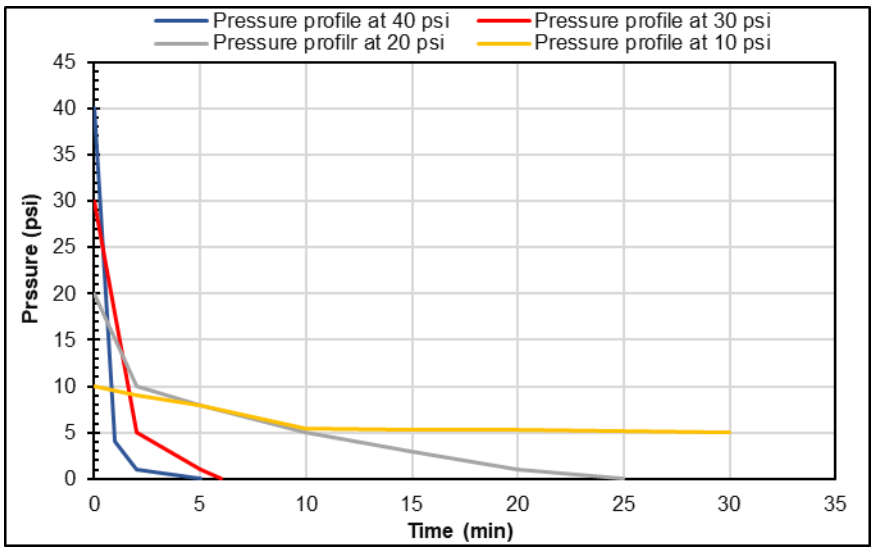

Figure 4.18: Faulty EPDM and neat Class H cement pressure decline after 12 hours WOC.

Pressure Tests After 24 hours WOC

The next tests were run after 24 hours WOC. Figure 4.19 shows the pressure decline curves. At 10 psi, the cement and elastomer prevented gas migration and there was no leak recorded. A leak was slightly recorded for the 20-psi test. Two stages of 1-psi decline each, was recorded at 2 minutes and 18 minutes respectively. The dual barrier held 18 psi to the end of the test. The pressure decline at 30 and 40 psi were obvious, revealing the reduced performance of the dual barrier system. Over the test duration, the 30-psi test showed 53.3% pressure reduction while the 40-psi test showed

67.5% pressure reduction. It is important to note that an increase in the WOC time played a key role in improving cement sealability in the dual barrier system.

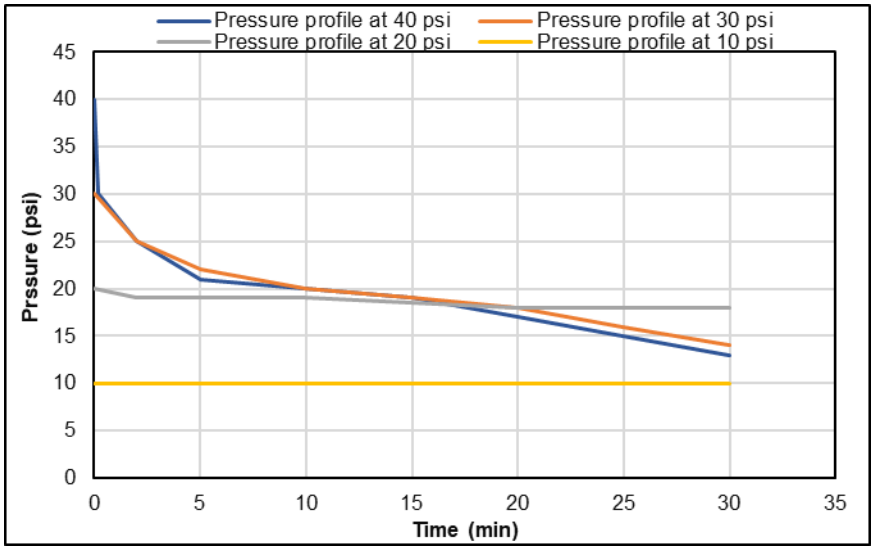

Figure 4.19: Faulty EPDM and neat Class H cement pressure decline after 24 hours WOC.

Pressure Tests After 48 hours and 72 hours WOC

Pressure tests were repeated after 48 and 72 hours WOC. Figure 4.20 shows pressure curves after 48 hours WOC. The 10-psi test had no leaks, while the 20-psi test had 1 psi pressure decline over the test duration. For the 30 and 40 psi tests, a significant pressure drop was recorded within the first five minutes. After which, a transient pressure decline was observed to the end of the experimental duration. Cement sealability improvement was further validated from the 30 and 40 psi pressure tests. The 30-psi test had 36.7% pressure decline while the 40-psi test had 52.5% pressure decline over 30 minutes.

The 72 hours WOC tests are shown in Figure 4.21. The 10 and 20 psi tests showed no leaks, which confirms the sealability of the system at these pressures. A sharp decline within 5 minutes, transient decline between 5 and 20 minutes, and no pressure drop between 20 and 30 minutes were observed for the 30 and 40 psi tests. The overall percent reductions in pressure were 33.3% and 50% for the 30 and 40 psi tests respectively. The pressure decline, which is an indication of the dual barrier sealability (cement in particular) was improved as the WOC time increased. However, it cannot be considered a primary barrier because of the leaks and pressure declines at higher pressures (30 and 40 psi).

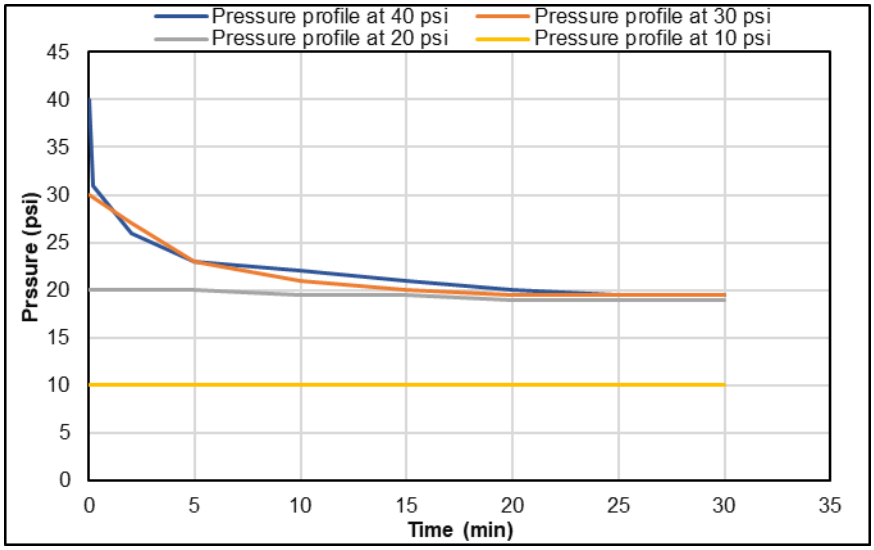

Figure 4.20: Faulty EPDM and neat Class H cement pressure decline after 48 hours WOC.

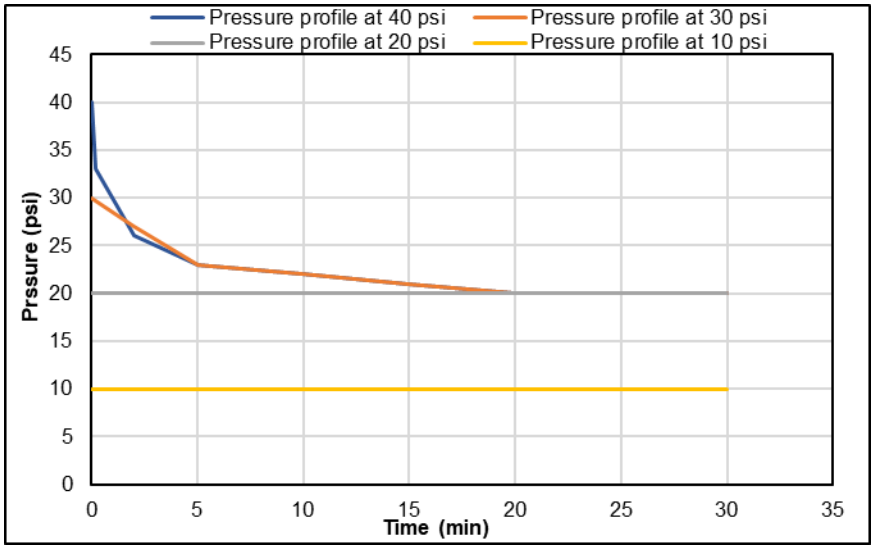

Figure 4.21: Faulty EPDM and neat Class H cement pressure decline after 72 hours WOC.

Pressure Tests After 5 and 7 Days WOC

Further pressure tests were conducted after 5 and 7 days WOC. After 5 days, the cement sheath sealed very well for the 10 and 20 psi tests and no leaks were recoded. However, gas bubbles were seen within 5 minutes and a gradual pressure reduction after this time was observed for the 30 and 40 psi tests shown in Figure 4.22. The last set of tests were performed after 7 days WOC. The test results presented in Figure 4.23 had no pressure decline for the 10 and 20 psi tests. The pressure reduction for the 30 and 40 psi tests were 25 psi (16.67 %) and 24 psi (40 %) respectively. Overall, the WOC time improves cement sealability as a barrier. Neat Class cement cannot act as a primary barrier in the case where the elastomeric elements of the liner hanger are faulty.

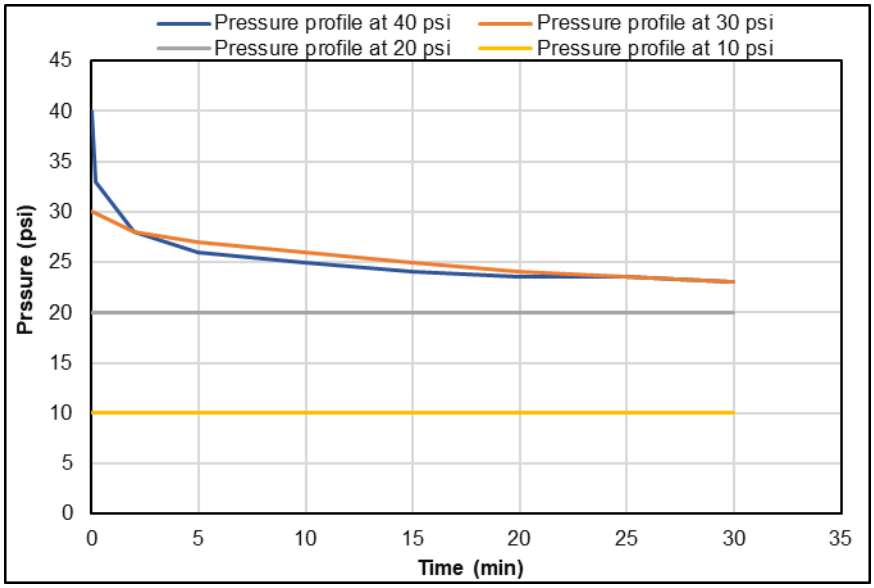

Figure 4.22: Faulty EPDM and neat Class H cement pressure decline after 5 days WOC.

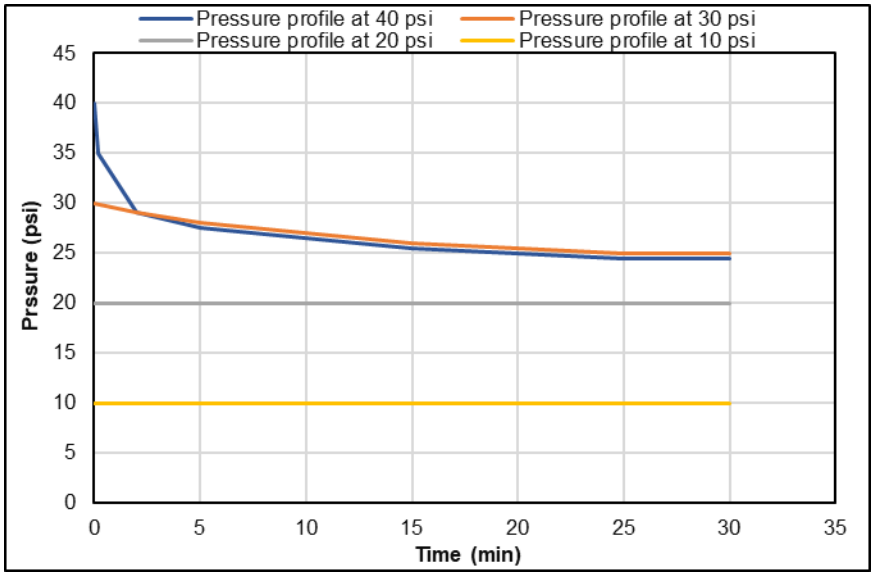

Figure 4.23: Faulty EPDM and neat Class H cement pressure decline after 7 days WOC.

Pressure Tests at 40 psi after 12, 24, 48, 72 hours, 5 and 7 Days WOC

The pressure test results of faulty elastomers and neat Class H cement at 40 psi after 12 hours, 24 hours, 48 hours, 72 hours, 5 days, and 7 days WOC were combined in Figure 4.24. Figure 4.24 shows that after 12 hours WOC, the pressure declined rapidly during the first minute of the holding time because an intensive leak occurred between the pipe walls and cement sheath. Moreover, three leak positions were found on top of the annular cement sheath. Remarkable improvement in cement sealability was observed after 24 WOC. Although there was a sharp pressure drop within the first five minutes during the holding time, the pressure continued to decline gradually over the last 25 minutes. After 48 and 72 hours WOC, progressive improvement in cement sealability was

noticed and 50 % pressure reduction was recorded at the end of both tests. An increase in cement sealability was observed after 5 days WOC, and after 15 minutes of the holding time, the pressure plateaued at 23 psi till the end of test. The cement sealability increased slightly after 7 days and after 15 minutes of the holding time, the pressure decline curve showed a constant profile (approximately 25 psi) till the end of the test. One general inference that can be made from these observations is that the cement sealing performance is improved as the WOC time increases.

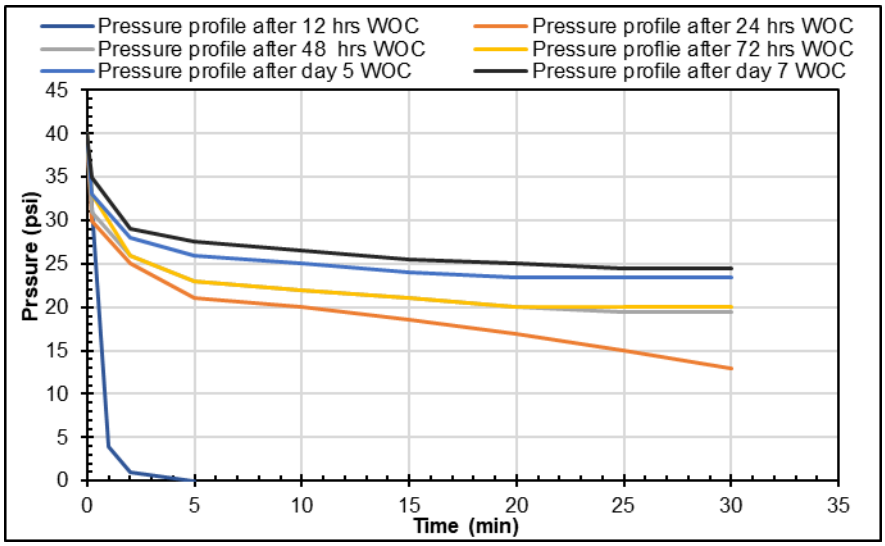

Figure 4.24: Faulty EPDM and neat Class H cement pressure decline at 40 psi and different WOC.

4.4.2.2 Faulty Elastomer and Cement with Commercial Gas Migration Additive

In this experiment, faulty EPDM elastomers and Class H cement blended with the commercial gas migration additive (16.6 ppg) were tested as a dual barrier using inner and outer acrylic pipes. The experiment objective is to examine whether the cement sheath can be a primary when the elastomer seal is exposed to a failure mode. The faulty elastomers were inserted at the bottom section of the setup to bypass the test gas into the cement sheath and evaluate its sealing capacity. A water column was placed on top of the cement to monitor the gas bubbles in case there is a leak from the cement sheath. A series of pressure tests were performed after 12 hours, 24 hours, 48 hours, 72 hours, 5 Day, and 7 Day WOC to investigate the cement performance while transitioning from slurry to early gelation and to a set cement. Specifically, to evaluate its sealability when invaded by gas during the transition phases.

Pressure Tests After 12 hours WOC

A pressure test at 10 psi was performed after 12 hours (WOC). After 55 seconds from the beginning of the test, a leak with high intensity was observed between the cement sheath and acrylic pipe walls (inner and outer). However, no leaks were observed within the cement sheath. From these observations, it can be inferred that there was severe debonding between the cement and the pipe walls, particularly between the inner pipe and cement sheath. The debonding is attributed to the smooth surface of the acrylic pipe walls. After 30 minutes, the nitrogen gas was closed, and a

gradual pressure drop was recorded over the holding time (30 minutes). The test was repeated for 20 psi and after about 5 minutes, the cement sheath separated as shown in Figure 4.25. After the cement sheath separation, the leak rate increased remarkably. Recall that the cement sheath separation was also observed in the first scenario (neat cement sheath in Figure 4.17). The difference between the separation in the first (neat Class H cement) and second (cement with commercial gas migration additive) scenarios is that in the first scenario, the separation was observed during the 40-psi test while the separation in the second scenario was observed during the 20-psi test. This difference can be explained from the slurry design and performance. During the neat cement pressure test (first scenario), leaks were also observed to be coming from within the cement sheath and at the pipe-cement interfaces. Thus, it would require more pressure to cause a separation of the cement column from the base. However, during the pressure test in the second scenario (cement with commercial gas migration additive), the leaks were only coming from the pipe-cement interfaces and not within the cement sheath. Thus, the pressure required to cause the separation would not be as much as that required in scenario 1.

The 30 and 40 psi tests were performed, and the leak intensity increased, especially around the inner pipe circumference and cement column. During these two tests, the pressures declined dramatically over the holding period as shown in Figure 4.26. The pressures dropped to 5 psi within the first 5 minutes of the holding times, confirming the severity of cement and pipe debonding. Cement issues such as microcannulas, cracks, and fractures were not observed and leaks within the cement sheath was not recorded.

Figure 4.25: Cement separation during the 20-psi pressure test.

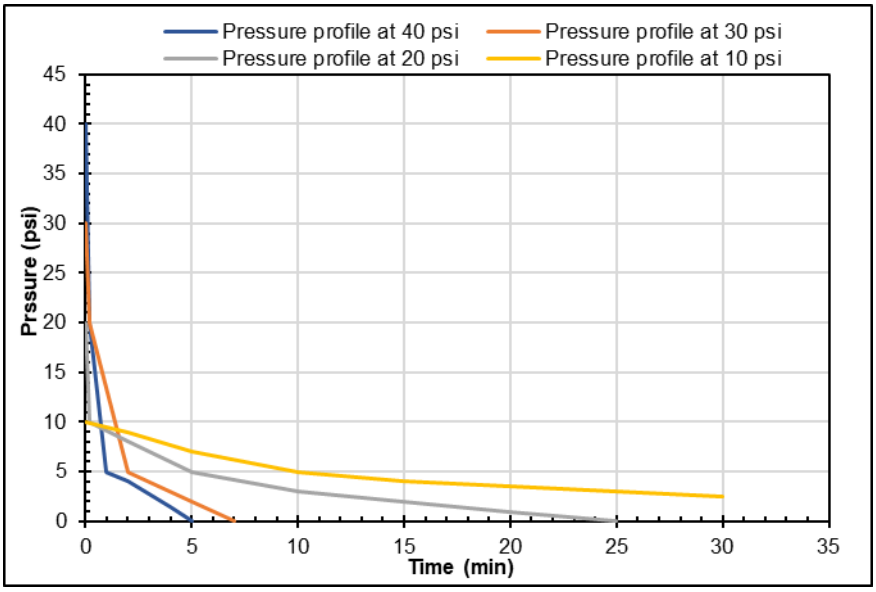

Figure 4.26: Faulty EPDM and Class H cement with gas migration additive pressure decline after 12 hours WOC.

Pressure Tests After 24 hours WOC

After 24 hours WOC, the pressure tests at 10, 20, 30, and 40 psi were performed. The leak intensity was increased because of the cement sheath separation and movement that occurred during the 20-psi test after 12 hours WOC. The separation and movement worsened the bonding issue between the cement sheath and the pipes walls. The inner pipe appeared to have been affected more by the separation than the outer pipe. This observation was supported by many leak positions that were located between the inner pipe and cement sheath and fewer leak positions between the outer pipe and cement sheath (Figure 4.27). In addition, the bubble sizes became bigger than the sizes observed during the tests after 12 hours WOC.

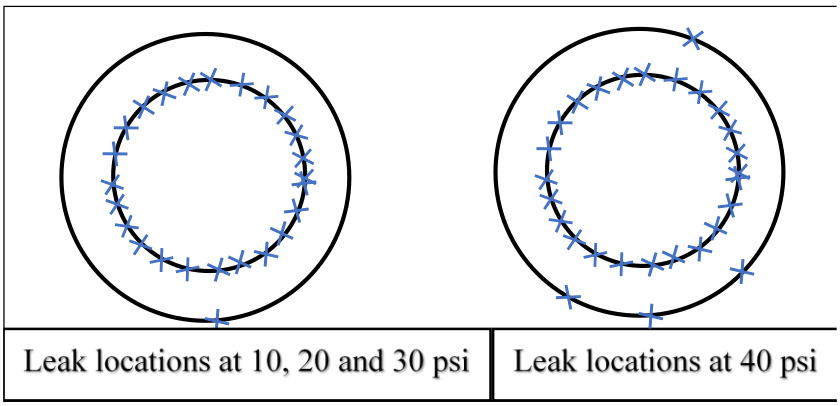

Figure 4.27: Leak locations during pressure tests after 24 hours WOC.

In all the tests, the pressures declined abruptly within the first minute of holding times by 50%, 80%, 94%, and 95% for 10, 20, 30 and 40 psi respective pressure tests (Figure 4.28). It is important

to note that increasing the WOC time improved the bonding between the outer pipe and the cement sheath, particularly for the 10 and 20 psi tests. However, it had no positive effect on the bonding of the inner pipe and cement sheath.

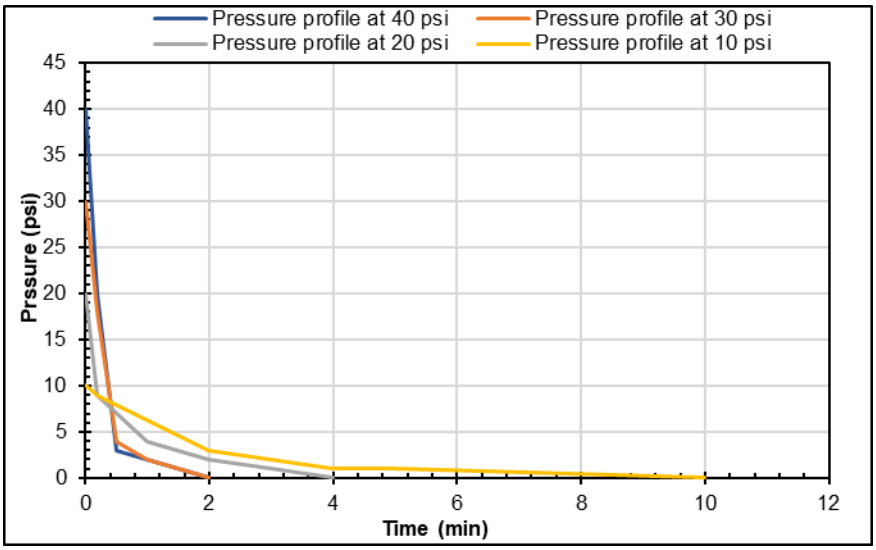

Figure 4.28: Faulty EPDM and Class H cement with the commercial gas migration additive pressure decline after 24 hours WOC.

Pressure Tests After 48 hours and 72 hours WOC

The pressure tests were performed after 48 and 72 hours WOC. The leak intensity between the inner pipe and cement sheath was almost the same at the pressure tests after 24 hours WOC, except for an increase in the bubbles size. No leak between the outer pipe and cement was observed during the 10 and 20 psi tests. However, one leak position was seen during the 30-psi test and four positions appeared during the 40-psi test (same position during the test after 24 hours WOC). After 48 hours WOC, the pressure dropped sharply after one minute of holding time by 50%, 85%, 90%, and 97.5% for the pressure tests of 10, 20, 30, and 40 psi respectively (Figure 4.29). The decline rate was observed to be more compared to the rates after 24 hours WOC. This can translate to more debonding between the inner pipe and cement sheath as WOC increased.

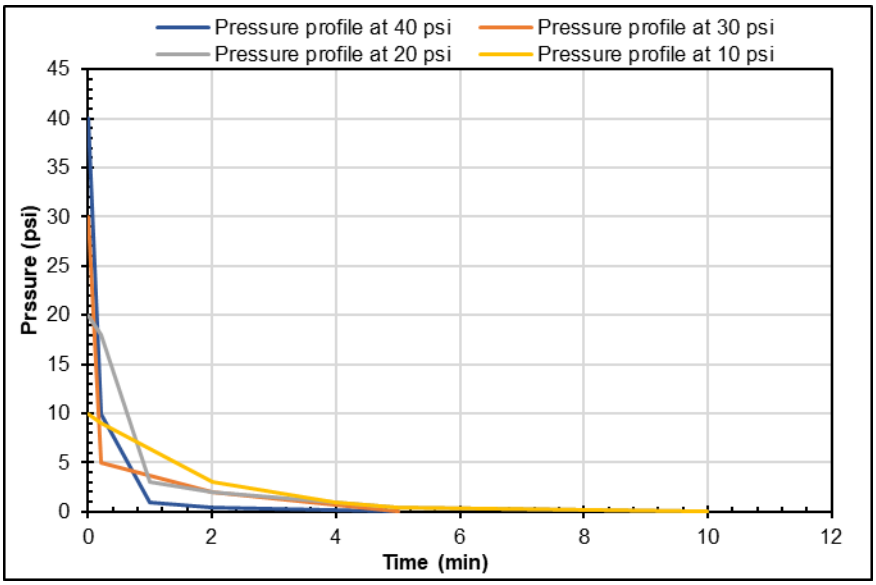

Figure 4.29: Faulty EPDM and Class H cement with the commercial gas migration additive pressure decline after 48 hours WOC.

After 72 hours WOC, the tests were repeated, and pressure drop trends were similar to those after 48 hours WOC as shown in Figure 4.30. In all the tests, majority of the leak paths were found to be between the inner pipe and cement sheath. The leak positions between the outer pipe and cement sheath were not recorded during the 10 and 20 psi tests. However, new positions were seen during the 30 and 40 psi tests as shown in Figure 4.31.

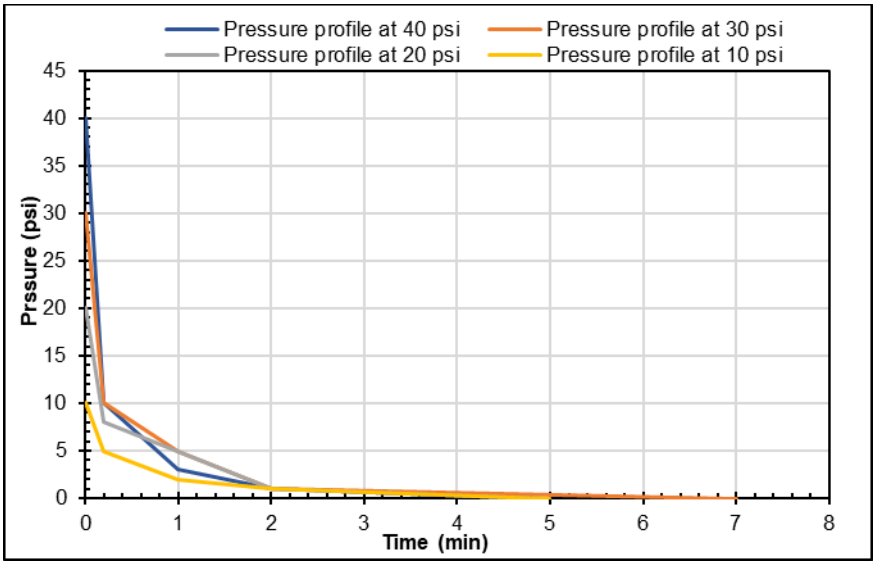

Figure 4.30: Faulty EPDM and Class H cement with the commercial gas migration additive pressure decline after 72 hours WOC.

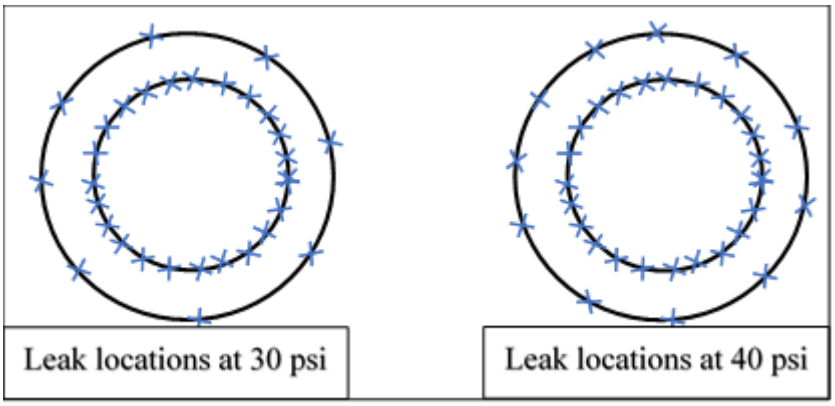

Figure 4.31: Leak locations during pressure tests after 72 hours WOC.

Pressure Tests After 5 and 7 Days WOC

After 5 and 7 days WOC, pressure tests were conducted to evaluate the cement sheath sealability. During the tests (after both WOC period), the leak intensities between the inner pipe and cement sheath appeared to have increased slightly compared to 72 hours WOC. However, during the 30 and 40 psi tests, the leak intensity between the outer pipe and cement decreased slightly compared to the tests after 72 WOC. No leaks were observed at 10 and 20 psi. After 5 and 7 days WOC, the pressure-decline curves were obtained and are shown in Figure 4.32 and Figure 4.33. For the two WOC intervals, the pressure declines were sudden, almost within the first minute of the holding time. The pressure declines were 85%, 92.5 %, 94%, and 95% for the respective pressure tests of 10, 20, 30, and 40 psi.

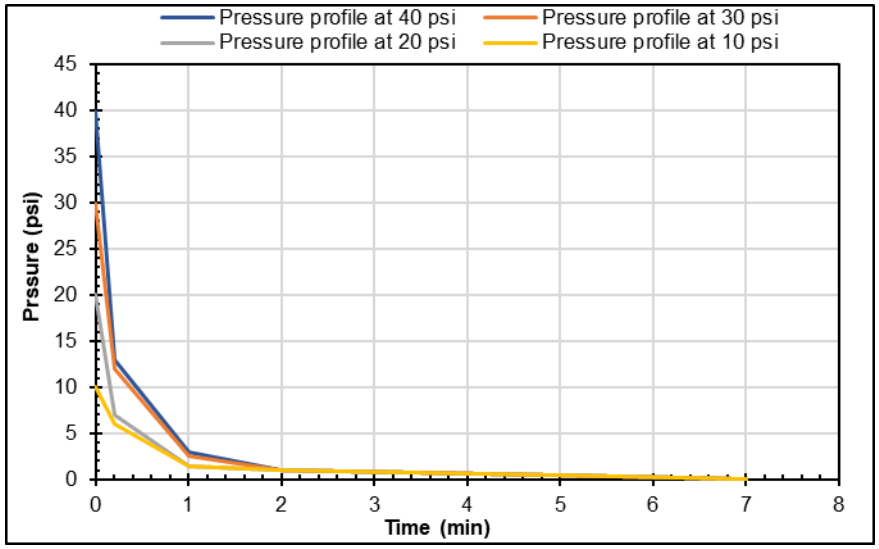

Figure 4.32: Faulty EPDM and Class H cement with gas migration additive pressure decline after 5 days WOC.

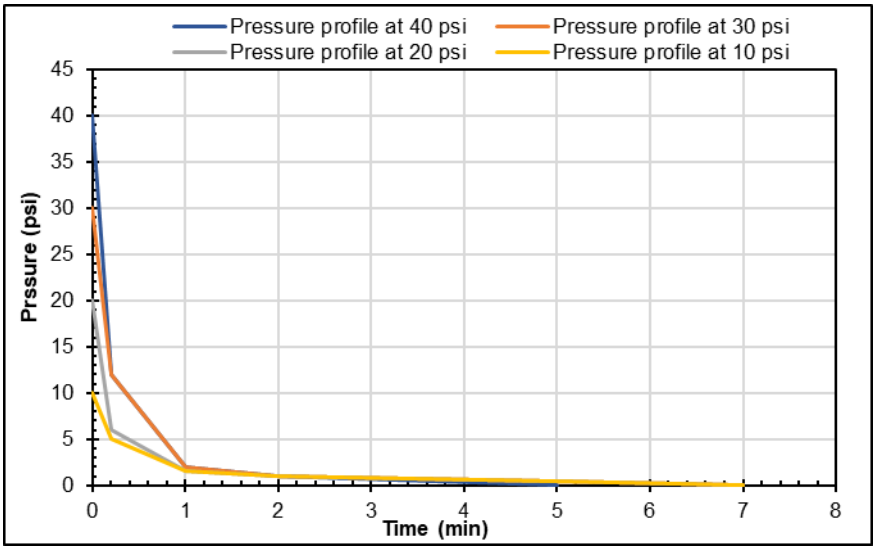

Figure 4.33: Faulty EPDM and Class H cement with gas migration additive pressure decline after 7 days WOC.

Pressure Tests at 40 psi after 12 hours, 24 hours, 48 hours, 72 hours, 5 days and 7 days WOC

All the 40-psi pressure tests were combined in Figure 4.34. This figure shows that after 12 hours WOC, the pressure declined very quickly to 5 psi during the first minute of the holding time. A leak with high intensity was observed between the wall of both pipes and cement sheath, indicating poor bonding between cement sheath and acrylic pipes. Leak positions were not seen within the cement sheath. After 24 WOC, the leak intensity increased slightly, particularly between the inner pipe wall and cement. A sharp pressure-decline up to 95% was also recorded within the first minute of the holding time. After 48 and 72 hours WOC, the leak intensity increased a little bit compared to the pressure test after 24 hours WOC. The pressure decline increased up to 97.5% within the first minute of the holding time. The last pressure tests were conducted after 5 days and 7 days WOC. The pressure continued to decline with almost the same intensity as in 72 hours WOC and it reduced by 95 % within the first minute of the holding time.

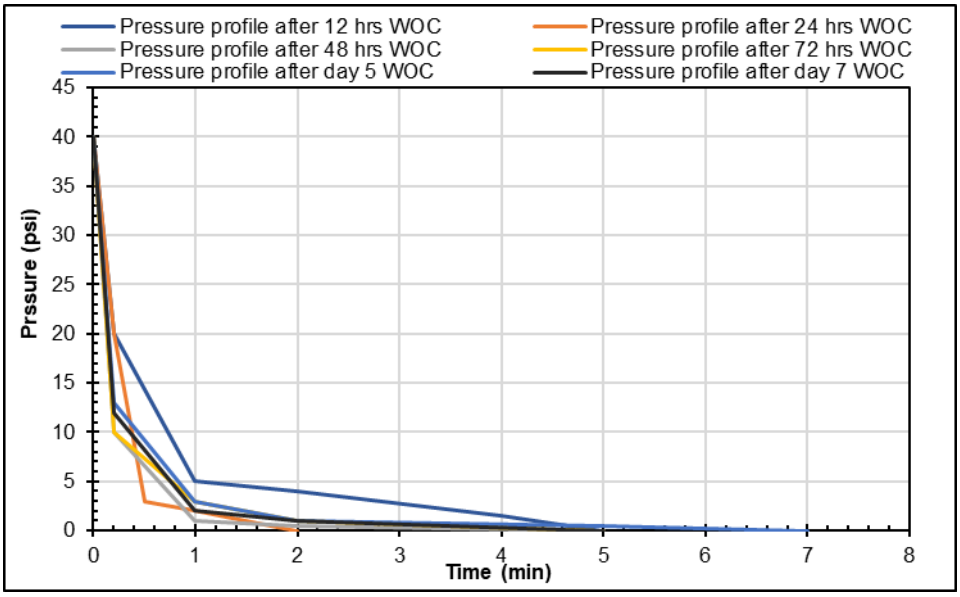

Figure 4.34: Faulty EPDM and Class H cement with gas migration additive pressure decline at 40.

In all the tests in this scenario, the pressure drops were abrupt (within the first minute of the holding time) and were between the range of 50 % and 97.5 %. The high decline percentages suggest weak bonding between the acrylic pipes and cement sheath, specifically between the inner pipe and the cement sheath. The cement sheath movement that occurred during the 20-psi test after 12 hours WOC was also an indication of poor bonding which intensified the leak. Although, high leak intensity and pressure drops were observed and recorded because of debonding, no leak positions were located within the cement sheath itself during all the tests after all the WOC times. This implies that the slurry design can prevent gas migration within the cement sheath.

4.4.2.3 Faulty Elastomer and Cement with Commercial Gas Migration Additive (Setup with Inner Steel Pipe and Outer Acrylic Pipe)

Pressure Tests After 12 hours WOC

A 10-psi pressure test was performed after 12 hours. Within the first 15 seconds of the test, a leak with high intensity was observed between the cement sheath and outer acrylic pipe walls. Interestingly, no leaks were observed within the cement sheath and between the interface of the inner steel pipe wall and cement sheath. In addition, the cement column separations that was attributed to debonding (observed in the first and second scenarios) were not observed in this scenario. It can be inferred that there was severe debonding between the cement sheath and outer acrylic pipe walls. The debonding has been attributed to the smooth surface of the acrylic pipe walls. Although, the outer pipe was tightened with four band clamps to prevent the pipe expansion during the cement placement, the bonding was still weak. The test was repeated for 20 psi and no leaks were observed between the inner steel pipe wall and cement sheath. This was also observed for the 30 and 40 psi pressure tests which confirms the cement sheath's sealability with the inner steel pipe wall. The leaks were from the debonding between the cement sheath and inner diameter

of the outer acrylic pipe. During the four tests, the pressures declined dramatically over the holding period as shown in Figure 4.35. During the 30 and 40 psi tests, the pressures dropped to around 5 psi within the first five minutes of the holding times (89% drop at 40 psi). This decline confirms the severity of cement sheath and acrylic pipe debonding. Cement issues such as microcannulas and fractures were not observed during all the tests.

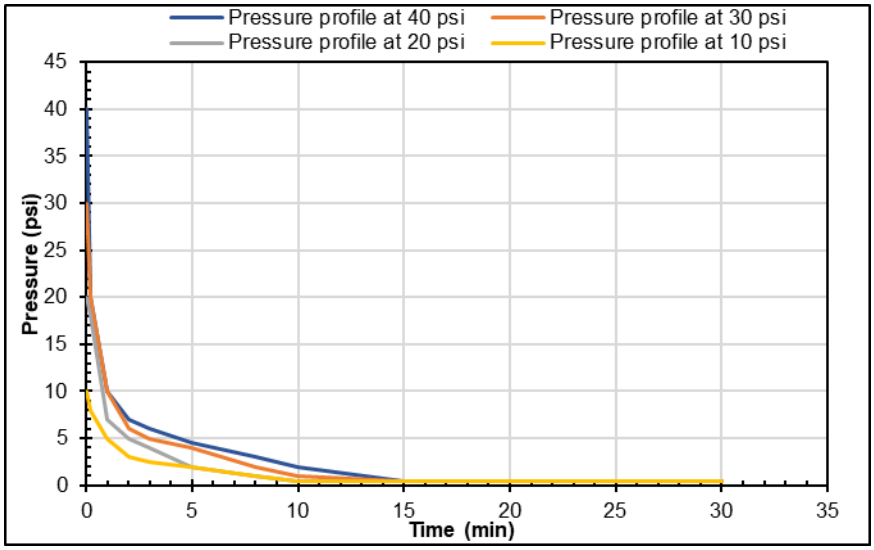

Figure 4.35: Faulty EPDM and Class H cement with the commercial gas migration additive pressure decline after 12 hours WOC (setup with inner steel pipe and outer acrylic pipe).

Pressure Tests After 24 hours WOC

After 24 hours WOC, pressure tests at 10, 20, 30, and 40 psi were performed. The leak intensity slightly decreased compared to the intensity after 12 hours WOC. This observation was supported by the slight improvement of the pressure declines during the holding periods. In all the tests, the pressures showed an abrupt decline within the first minute of the holding time by 40%, 70%, 76%, and 82% for 10, 20, 30, and 40 psi pressure tests respectively. Then the pressures continued to decline gradually until the end of the tests as shown in Figure 4.36.

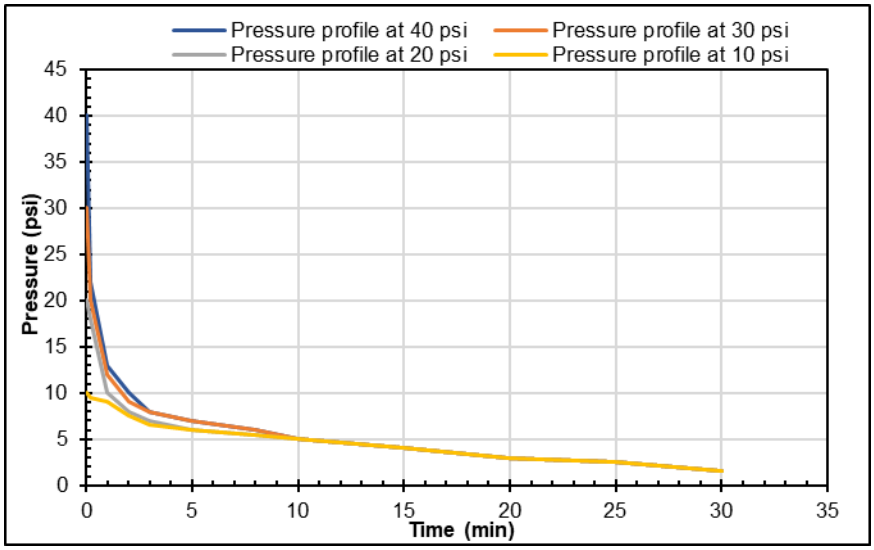

Figure 4.36: Faulty EPDM and Class H cement with the commercial gas migration additive pressure decline after 24 hours WOC (setup with inner steel pipe and outer acrylic pipe).

Pressure Tests After 48 hours and 72 hours WOC

The pressure tests were performed after 48 and 72 hours WOC. The leak intensity between the outer pipe and the cement sheath was almost same as in the pressure tests after 24 hours WOC. No leak between the inner steel pipe and cement sheath was observed for all the tests after both WOC times. Figure 4.37 shows that after 48 hours WOC, the pressure dropped sharply after five minutes by 40%, 70%, 76%, and 82% for the pressure tests of 10, 20, 30, and 40 psi respectively. The decline after five minutes holding time was lower, compared to the decline after 24 hours WOC. This can translate to an increase in the bonding between the pipes and cement sheath as the WOC time increases.

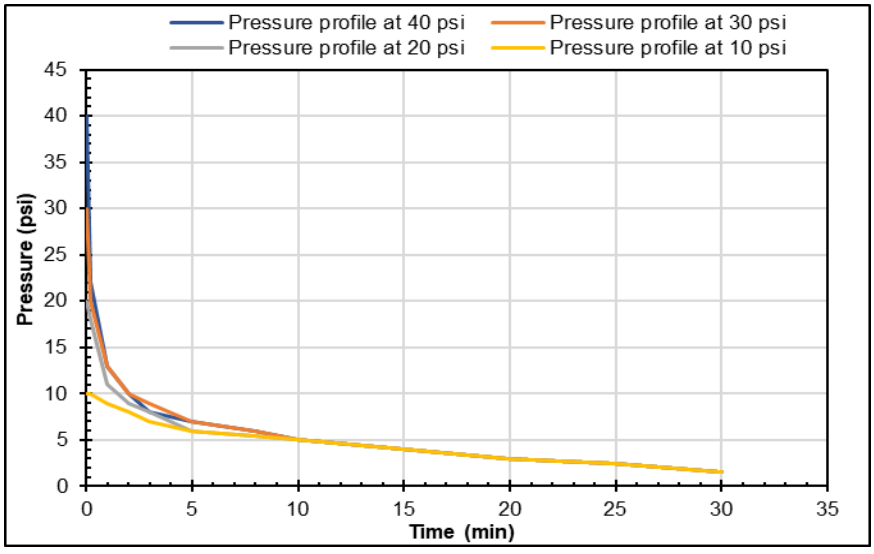

Figure 4.37: Faulty EPDM and Class H cement with the commercial gas migration additive pressure decline after 48 hours WOC (setup with inner steel pipe and outer acrylic pipe).

After 72 hours WOC, the tests were repeated, and the pressure drop trends were similar to those obtained from the tests after 48 hours WOC (see Figure 4.38). In all the tests, all the leak paths and positions were found to be between the outer acrylic pipe and cement sheath.

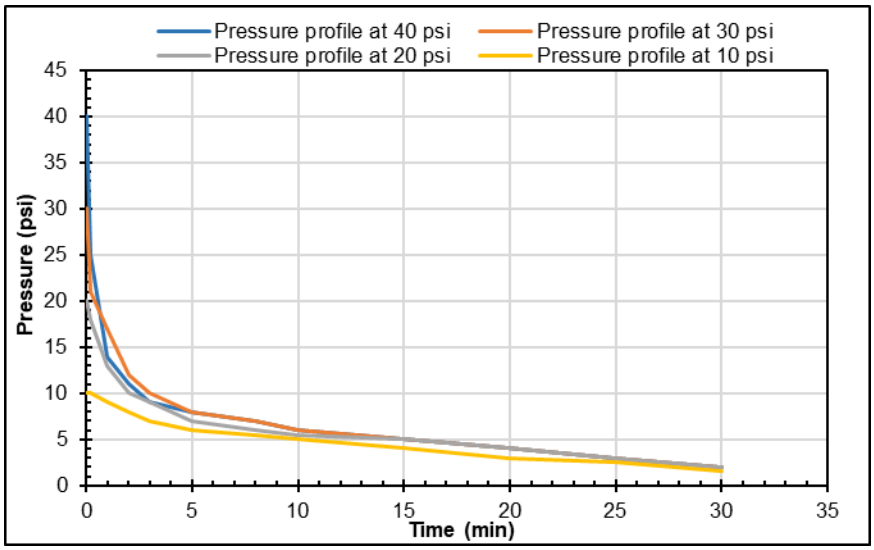

Figure 4.38: Faulty EPDM and Class H cement with gas migration additive pressure decline after 72 hours WOC (setup with inner steel pipe and outer acrylic pipe).

Pressure Tests After 5 and 7 Days WOC

After 5 and 7 days WOC, pressure tests were conducted. During the tests, the leak intensity between the outer acrylic pipe and the cement appeared to have reduced slightly, compared to the test after 72 hours WOC. No leaks were observed within the cement sheath or between the inner steel pipe and cement sheath. During the tests, the pressure declines were sudden (within the first five minutes of the holding time). After 5 days WOC, a 30%, 65%, 73%, and 80% decline for the respective pressure tests of 10, 20, 30 and 40 psi were recorded (Figure 4.39). After 7 days WOC, a 25%, 60%, 70%, and 77.5% decline for the respective pressure tests were recorded (Figure 4.40). The pressure declines after 7 days WOC were slightly lower than the declines after 5 days WOC.

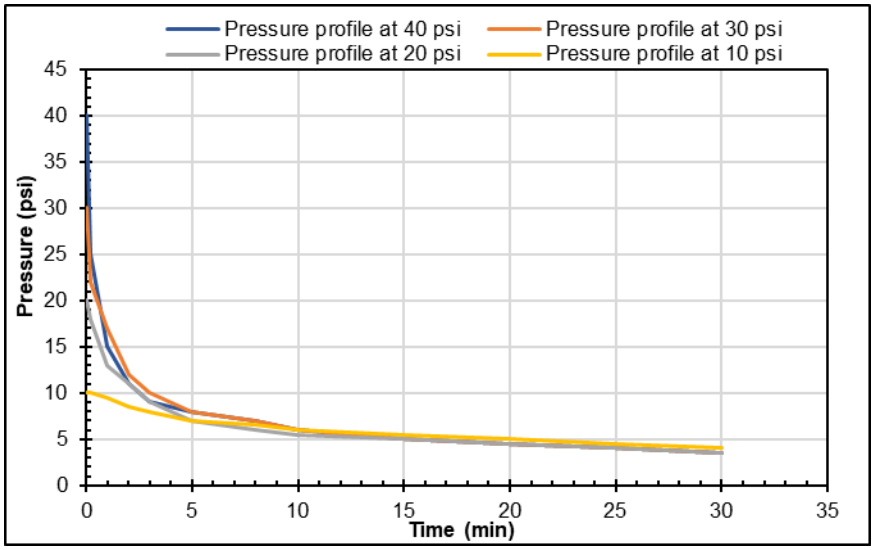

Figure 4.39: Faulty EPDM and Class H cement with gas migration additive pressure decline after 5 days WOC (setup with inner steel pipe and outer acrylic pipe).

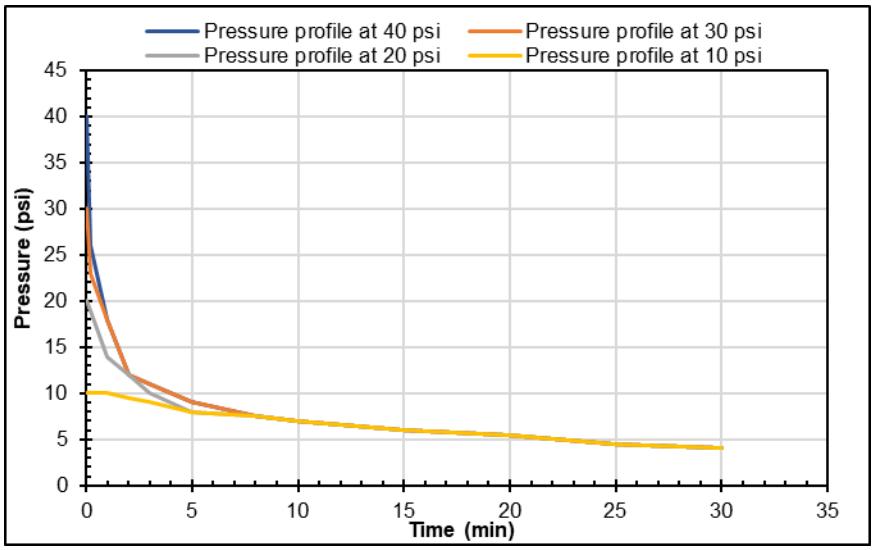

Figure 4.40: Faulty EPDM and Class H cement with gas migration additive pressure decline after 7 days WOC (setup with inner steel pipe and outer acrylic pipe).

Pressure Tests at 40 psi after 12 hours, 24 hours, 48 hours, 72 hours, 5 days and 7 days WOC

All the 40-psi pressure tests were combined in Figure 4.41 for this scenario. The figure shows that after 12 hours WOC, the pressure declined very quickly to 5 psi (89% decline) during the first minute of the holding time. After 24 hours WOC, the pressure declined slightly (82%) compared to the leaks after 12 hours WOC. The pressure decline was up to 80% within the first five minute of the holding time during the tests after 48 and 72 hours WOC. The pressure declines during the tests after 5 and 7 days WOC were 80 % and 77.5% respectively. All the leaks during this pressure test were recorded at high intensity and were observed between the outer pipe wall and cement

sheath, indicating poor bonding between cement sheath and acrylic pipes. Leak positions were not seen within the cement sheath or inner steel pipe and cement sheath.

In all the pressure tests performed after all the WOC intervals, the pressure drops were abrupt (within first five minutes of the holding time) and were between the range of 25% and 89%. The leaks and pressure decline curves were from the debonding between the outer acrylic pipe and cement sheath. No leaks were observed between the inner steel pipe and cement sheath. This observation proves that the pipe material and roughness play a vital role in the cement slurry bonding process.

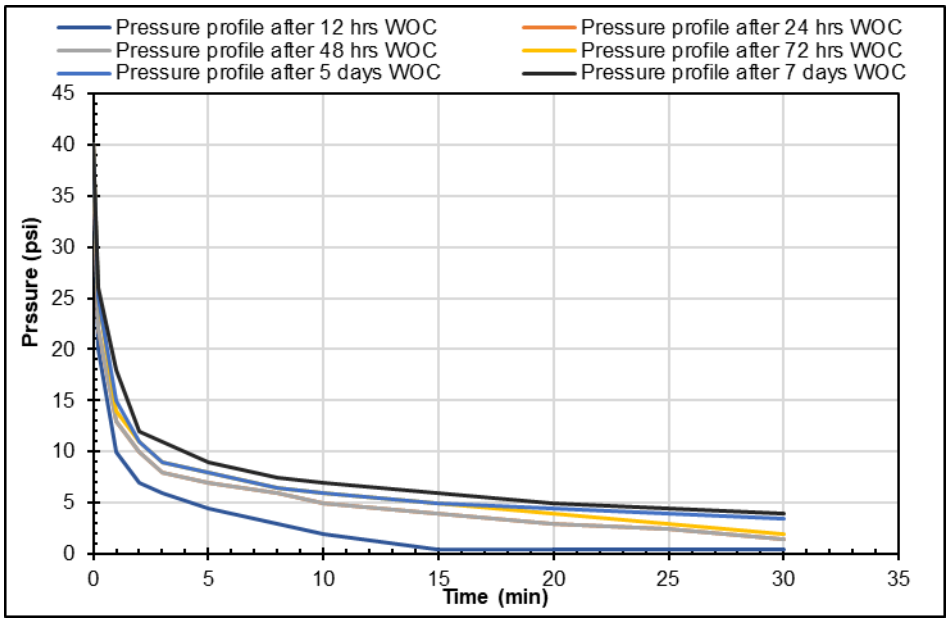

Figure 4.41: Faulty EPDM and Class H cement with gas migration additive pressure decline at 40 psi and different WOC (setup with inner steel pipe and outer acrylic pipe)

4.5 SUMMARY AND CONCLUSIONS

The following conclusions and summaries have been drawn from the theoretical and experimental investigations, results, and analyses conducted in this section of the project and report:

- Pressure test is an effective tool to evaluate and compare the performance of the seals. Under normal condition, both EPDM and NBR elastomers exhibited good sealing capacity for 30 minutes holding time.
- Prolonging the pressure test duration from 30 minutes to 60 minutes may not assist in better evaluation of elastomers as an independent barrier.
- The independent sealing performance of EPDM and NBR after surfactant chemical degradation was not impaired for the test conditions used in this study.
- The independent sealing performance of EPDM was completely compromised after CO_2 chemical degradation. The pressure tests showed instantaneous decline with no sealing effect.

- Physical damage from the manufacturing, handling or installation process influences elastomers sealing performance. EPDM and NBR failed the pressure test after intentionally creating physical defects.
- Elastomer energization plays a critical role in maintaining seal integrity. EPDM and NBR showed good performance at 180 in-lbf and 120 in-lbf during the pressure cycling test. EPDM performed better than NBR without torque. Pressure cycling showed that pre-compression of EPDM was enough to maintain the elastomers seal performance compared to NBR.
- Neat Class H cement cannot act as a primary barrier and prevent gas migration in the case where the elastomeric elements of the liner hanger are faulty.
- The WOC time improves cement sealability as indicated by the progressive slower pressure decline in the pressure tests after WOC time of 12 hours, 24 hours, 48 hours, 72 hours, 5days and 7 days.
- In scenario two, (faulty elastomers and cement with commercial gas migration additive in the acrylic pipes setup), no leaks were observed within the cement sheath. However, more micro-channels with leaks were observed at the pipe interfaces. This was more severe at the inner pipe interface. Thus, cement sheath is more prone to failure by debonding from the OD of the inner pipe (i.e. liner) compared to the ID of outer pipe. The results from the leakage modelling and risk assessment study corroborates this inference.
- The leaks between the inner pipe and cement sheath interface disappeared when the inner acrylic pipe was replaced with a steel pipe (scenario 3). Higher leak intensity was observed at the cement sheath-outer acrylic pipe interface. This observation proves that the pipe material and roughness play a vital role in the bonding process of a cement slurry.
- The cement with the commercial gas migration additive can act as a primary barrier in the case where the elastomeric element of the liner hanger is faulty.

5 LEAKAGE MODELLING AND RISK ASSESSMENT

5.1 INTRODUCTION

In a conventional liner placement, the liner hanger system usually relies only on the cement sheath to provide sealing between liner/casing overlap and maintain the well's integrity. The challenges associated with obtaining a good quality primary cementing, and financial incentive in not running the cement throughout the overlap up to the liner hanger necessitated a backup sealing mechanism or a barrier (Smith and Williford 2006). This led to innovative designs such as liner-top packer or liner hanger with integrated seal assembly.

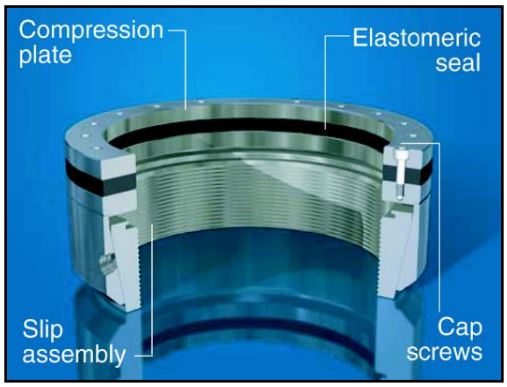

Figure 5.1:Illustration of a mechanical-set slip-and-seal assembly in sub-mudline liner hanger assembly (Speer 2006)

The seal assembly is typically set mechanically by applying weight down or by combined action of weight and rotation. As the weight is applied, the slips travel down and engages the pipe. A load is placed on the elastomer element which expands radially by compression and seals the annulus between the liner and casing (see Figure 5.1). Some of the major factors leading to failure of a seal assembly are: inability to apply the required weight for energization, wear/tear of seal element, material failure attributed to temperature and chemical/gas exposure etc. (Wang et al. 2017; Williford and Smith 2007; Smith and Williford 2006).

Unlike seal assembly, the cement sheath does not have moving elements and it is not an energized barrier. It provides sealability via adhesion or bonding at the pipe interface after it has been set. Cement sheath can fail to provide sealability or zonal isolation because of several design, operational, or mechanical factors such as: high inherent permeability, insufficient hydrostatic head or static gel strength, lack of gas migration additive, fluid loss during cementing, presence of micro-annulus because of lack of bonding or volume shrinkage, structural failure in the form of debonding, radial cracking, shear failure, etc. (Lavrov and Torsæter 2016; Khandka 2007).

5.1.1 Overview

Currently, the industry lacks adequate standards and guidelines for assessing seal assembly in a conventional liner hanger or sub-mudline hanger (BSEE 2014). The industry relies on standards developed for packer equipment (ISO 14310:2008E or API Specification 11D1 and 17D).

Currently, it is unclear whether the new standard for liner hanger equipment 'API 19LH' - being drafted by API, will encompass sufficient guidelines for testing or designing seal assembly. Even though conventional liner-hanger assemblies have had frequent sealability failure issues, no study is available in the public domain that is focused on assessing the sealability of the elastomer element in hanger seal assemblies under various conditions.

The current industry standards, recommended practices, and technical reports for cement, are primarily focused on cement slurries, their material properties, laboratory testing, consideration during field operation, etc. All the documents have helped advance the safety of wells, yet there can still be improvement and expansions in several issues, such as: designing cement for shallow depth wells with potential for gas migration, adequacy of pressure test, and guidelines for evaluating cement system "fitness for service". Furthermore, they lack sufficient discussions on - the selection of appropriate mechanical properties for different conditions, performance curves, responses for set cement under various loading conditions, risk assessment of various failure scenarios, etc.

5.1.2 Statement of the Problem

The goal of this study is to assess "fitness-for-service" of seal assemblies and cement sheath under various conditions. This will fill-in some of the existing knowledge gaps and help regulators and operators alike in improving design, selection, and qualification of these barrier elements. It aims to answer following research questions:

Elastomer Seal:

- What is the relationship between the sealability of an elastomer and the load applied during setting? What type of elastomer material would yield the highest sealability for a given seal energization load?
- What is the effect of temperature and gas exposure on the elastomer sealability?
- What are the optimum seal dimensions for achieving high and robust sealability for long term service?
- In certain conditions such as shallow liner installation or deviated wells, it may not be possible to apply the required force for seal compression. Under such low seal energization conditions, what would be the expected loss in sealability?
- How critical is it to exert uniform weight on the seal element for energization?
- What is the effect of improper seal energization on sealability? In other words, during weight application, how does a faulty equipment such as compression plate or a radial slip affect sealability?

Cement:

- What is the likelihood of structural failure of cement under typical pressure loads in shallow depth wells?

- How does set cement respond to changes in Young's modulus and Poisson's ratio? This can help not only in designing better a cement system, but also in estimating the changes in cement performance upon material degradation.
- How does cement sheath height in a liner overlap and cement radial width affect cement performance?
- What is the effect of micro-annulus presence on cement performance? Can a positive pressure test cause sufficient ballooning of the pipe to temporarily mask the gap?
- How does the performance of a pre-stressed cement system compare against conventional systems?
- Which factors affect cement performance the most? This will inform the decision to select what factors require higher priority while designing.

5.1.3 Objectives

The specific objectives of this section of the project and report are:

- Identify critical material properties, design parameters, and operational factors that affect the performance of elastomer seal and cement sheath.
- Develop and examine various failure scenarios and evaluate the change in the performance of elastomer seal and cement sheath.
- Generate operating curves, correlations, and rules of thumbs that can predict the performance of elastomer seal and cement sheath.
- Develop guidelines for evaluating the "fitness for service" of seal assembly and cement system

5.1.4 Research Methodology

To achieve the objectives, a comprehensive finite element analysis was conducted using three-dimensional computer models consisting of surface liner, previous casing, and seal assembly or cement as barrier elements. The sealability of an elastomer component in a hanger assembly was evaluated in terms of the contact stress generated at the seal-pipe interface. The performance of cement sheath was assessed by analyzing the radial, hoop, and maximum shear stresses for mechanical failure.

Parametric analyses were performed to understand the behavior of elastomer seal and cement sheath under various conditions, considering different design parameters such as dimensions and material properties. Various potential failure scenarios were selected and examined to identify the effects on seal performance and cement sheath integrity. Simulation results were normalized, and sensitivity analysis was performed to compare and identify the critical parameters affecting sealability. Operating curves, correlations, and rules of thumbs were generated for quick and easier prediction of the performance of both barriers independently. A complete detail of the research methodology has been documented in section **1.4** of the leakage modelling and risk assessment report.

5.1.5 Scope of Work

The scope of work for the seal assembly and cement models are as follows:

Seal Assembly Model:

The seal energization process has been modelled to mimic the setting of the conventional sub-mudline liner hanger. The components such as slips or compression plates have been modelled as boundary conditions. Dimensions and material properties of liner and casing components were kept constant throughout the study.

Since the focus is on offshore shallow well designs, the effect of thermal stresses on sealability is not important and has not been examined. The effect of temperature was considered in form of change in material properties. Four types of elastomer material were investigated – NBR (Nitrile Butadiene Rubber), EPDM (Ethylene Propylene Diene Monomer), VITON (a synthetic Flouropolymer elastomer), and PTFE (Polytetrafluoroethylen). The elastic modulus of each material was measured and used in the simulation. Poisson's ratio of each elastomer was not measured since all elastomer materials typically have a value of 0.49. Besides material properties and material failure, the effect of seal dimensions was also examined. Additionally, several operational failure scenarios like insufficient setting load for seal energization, improper centralization, failure in compression plate or slips, wear or erosion of seal element etc. were evaluated for potential effect on sealability.

Cement Model:

The effect of temperature variation i.e. thermal stresses on cement has not been examined since the focus is on shallow well designs. The only loads considered are change in wellbore pressure and change in annulus pressure acting on top of the cement. Effect of temperature has been incorporated in form of changes in Young's modulus and Poisson's ratio. Dimensions and material properties of liner and casing components were kept constant throughout the study. The focus is on liner overlap therefore, the liner-cement-casing system has been modelled. Rock formation was not included in the scope of this study. The radial expansion of shallow casing because of wellbore pressure or annulus pressure was observed not be of significant nature. Besides, the rock formation at shallow depth from sea floor is not highly consolidated to induce significant stresses on the casing so as to notably change the performance of cement. Inclusion of shallow rock formation would introduce another element in the system which is likely prone to failure. Hence, rock formation was not included in the scope of modelling.

In the parametric analysis, the effect of seven parameters have been examined – Young's modulus, Poisson's ratio, wellbore pressure, annulus pressure, cement sheath height, cement radial width, and annular fit. The resulting parameters from the simulation are – radial stress, hoop stress, and maximum shear stress developed in the cement sheath. The sensitivity of these stresses to various parameters was examined for three types of cement systems – ductile cement, brittle cement, and cement with moderate Young's modulus and Poisson's ratio. The same three cement systems were also used as the base case material properties for sensitivity analysis.

5.2 LITERATURE REVIEW

A comprehensive literature review has been conducted and documented in section **2.0** of the leakage modelling and risk assessment report. The following sections highlight the important theory and literature review outcomes.

5.2.1 Seal Assembly

The most common modes of failure in liner hanger sealing assembly are - failure to set or energize the sealing element, centralization issues that cause non-uniform energization, faulty equipment or hanger components such as slips or cones, abrasive wear of the seal element, shearing of elastomer seal across an extrusion gap, temperature and chemical degradation, dynamic fatigue under pressure cycles, compression load catastrophic failures, and explosive decompression/gasification.

Even though conventional liner-hanger assemblies have had frequent sealability failure issues, no dedicated study is available in the public domain that is focused on assessing the sealability of elastomer element in conventional liner hangers. However, there are few modelling studies available in the literature that are focused on expandable liner hanger and packer applications. Some of the information from these studies can be extrapolated and applied to elastomer seal assembly in conventional liner hanger. Considering the various challenges associated with seal assemblies, there is still a need for comprehensive modelling as well as experimental studies (like the ones presented in this project), that is focused on conventional seal assemblies.

5.2.2 Cement

The liner-cement-casing can be considered as a composite hollow cylindrical system. When the set cement is subjected to internal and/or external pressures, it is in the state of tri-axial stresses. As shown in Figure 5.2, the three mutually perpendicular stresses are – radial (σ_r), axial or longitudinal (σ_z), and circumferential or hoop stresses (σ_θ). The radial stress always acts away from or toward the axis of cylinder while the hoop stress acts along the circumference of the cylinder. The axial stress is parallel to the axis of cylinder.

Using Lamé's theory for thick cylinders, equations for radial and hoop stress for the liner-cement-casing system can be easily derived. The details of the mathematical derivation are provided in the leakage modelling and risk assessment report (**Appendix A**). For the system shown in Figure 5.3**,** the radial and hoop stresses at a particular radius (r) within the cement can be calculated using the following equations:

$$\sigma_{r-cement} = \frac{b^2 P_{c1} - c^2 P_{c2}}{(c^2 - b^2)} - \frac{(P_{c1} - P_{c2}) b^2 c^2}{(c^2 - b^2) r^2} \quad \text{(1)}$$

$$\sigma_{\theta-cement} = \frac{b^2 P_{c1} - c^2 P_{c2}}{(c^2 - b^2)} + \frac{(P_{c1} - P_{c2}) b^2 c^2}{(c^2 - b^2) r^2} \quad \text{(2)}$$

Where P_{c1} and P_{c2} are contact pressures at the liner-cement and cement-casing interfaces respectively as shown in Figure 5.3; and b and c are the inner and outer radius of cement sheath respectively. Similar equations can be written for the liner and casing components of the system. The radial and hoop stress calculations require contact pressure values. The calculation of P_{c1} and P_{c2} using material properties and boundary conditions is discussed in the **Appendix A** of the leakage modelling and risk assessment report. The equations will be used later in this work to validate the results from the FEA model.

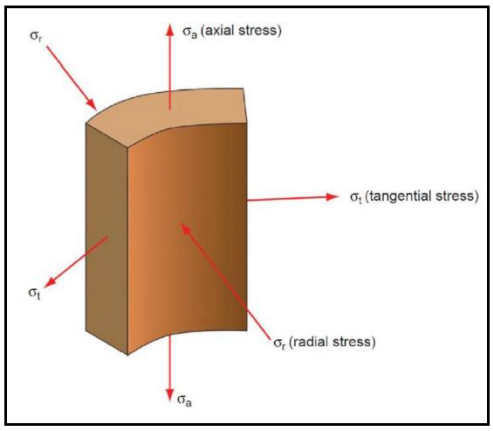

Figure 5.2: Graphical illustration of three principle stresses in set cement – radial, hoop, and axial stresses (Bellarby 2009)

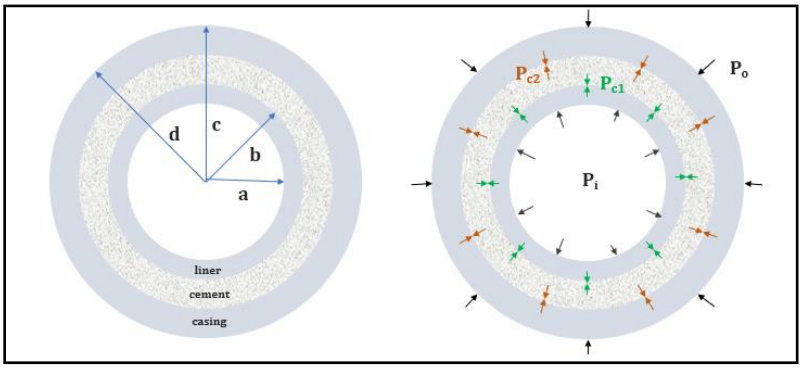

Figure 5.3: Schematic of liner-cement-casing system for analytical equations

There are three primary modes of failure in a cement sheath – radial debonding, radial cracking, and shear failure (Bustgaard and Nesheim 2016). These failure modes are graphically illustrated in Figure 5.4.

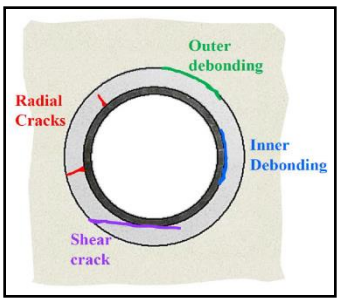

Figure 5.4: Primary modes of failure in a cement sheath (De Andrade and Sangesland 2016)

Debonding depends on the magnitude and direction of the radial stress at the interface between the cement and formation or cement and casing. The primary reason for radial stress development is the change in internal or wellbore pressure. For example, events such as casing pressure tests, formation integrity tests, increased mud weight for drilling subsequent depths, perforation or stimulation operation, etc. can lead to an increase in wellbore pressure. On the other hand, fluid loss or gas kick while drilling or completing a reservoir section can reduce the wellbore pressure. Debonding occurs when the magnitude of radial stress exceeds the limiting strength of the cement (Teodoriu et al. 2008).

$$\sigma_r \geq T_0 \quad \text{(Tension)} \quad \ldots\ldots (3)$$

$$|\sigma_r| \geq C_0 \quad \text{(Compression)} \quad \ldots\ldots (4)$$

where T_0 and C_0 are uniaxial tensile and compressive strengths of the cement sheath respectively. In the case of compressional radial stress, the failure is more like stress crushing than debonding (Khandka 2007). The compressive strength of cement sheaths is typically higher than the tensile strength, often 10 times more (De Andrade and Sangesland 2016). Therefore, a cement sheath is more likely to fail by radial debonding than stress crushing.

The second mode of failure is radial cracking which can occur when the hoop stress exceeds the tensile strength of cement:

$$\sigma_\theta \geq T_0 \quad \text{(Tension)} \quad \ldots\ldots (5)$$

The hoop stress can either be tensile or compressive in nature depending on material properties and loading conditions. However, since tensile strength is usually lower than compressive strength, radial cracking is the most likely mode of failure.

Shear failure is another mode of failure in a cement sheath. When the cement sheath undergoes shear failure, it typically results in a complete failure of the sheath (Bustgaard and Nesheim 2016). The shear failure is primarily dependent on the difference in magnitude between the principle stresses. According to Nelson and Guillot (2006), these effective stresses can rise because of various reasons such as rock subsidence, depletion of the reservoir, vibration from downhole pumps, or ongoing gas lift operations etc. There are several failure criteria for predicting shear failure. The simplest one (which requires minimum information) is the Tresca criterion. It is

based on a special case of Mohr's stress circle with internal friction angle being zero (Rahimi 2014). According to this criterion, shear failure occurs when the maximum shear stress value exceeds the cohesion of rock. Mathematically it is expressed as:

$$\tau_{max} \geq \varsigma \quad \text{..... (6)}$$

$$\tau_{max} = \frac{\sigma_1 - \sigma_3}{2} \quad \text{..... (7)}$$

$$\varsigma \approx \frac{C_0}{2} \quad \text{..... (8)}$$

where τ_{max} is maximum shear stress, σ_1 is maximum principle stress, σ_3 is minimum principle stress, ς is cohesion or intrinsic shear strength of cement, and C_0 is uniaxial compressive strength of cement.

5.3 MODEL DESCRIPTION

This section discusses the process of setting up FEA models of seal assembly and cement. This includes descriptions of models' dimensions, material properties, boundary conditions, meshing, contact formulation, and model verification.

5.3.1 Seal Assembly Model

The schematic of the model is provided in Figure 5.5. This simplified geometry consists of an 18 in. surface liner, an elastomeric packer seal, and a 22 in. conductor casing. The diameter of each component is based on an actual well design of one of the wells with a well control incident (BSEE, 2014). To avoid end-effects, the overall length of the model was kept 8 times greater than the inner diameter. Considering the symmetrical nature of the model, only $^1/_8{}^{th}$ segment of the wellbore cross section has been modelled. This helped to minimize computational requirement without losing accuracy.

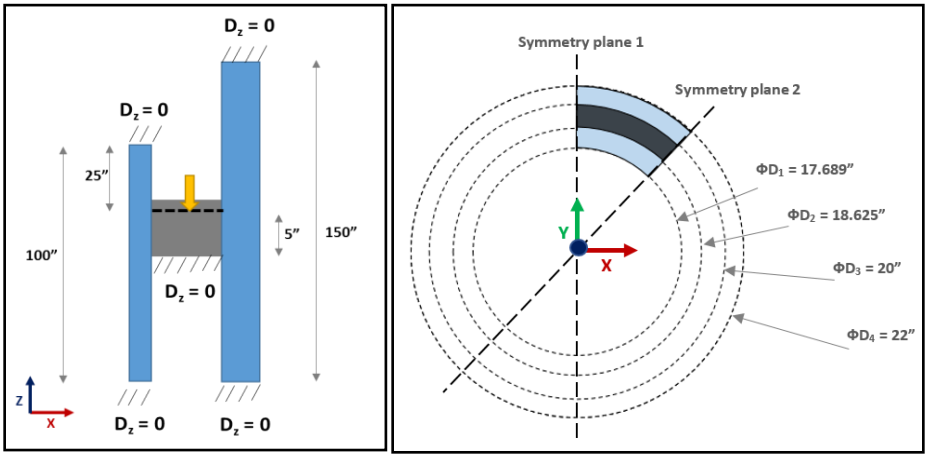

(a) **(b)**

Figure 5.5: Schematic of elastomer seal model (a) 2-D schematic in XZ plane. (b) top view of the model in XY plane

5.3.1.1 Material Properties

The liner and casing components were modelled as isotropic linear elastic material and their material properties are provided in Table 5.1**.** The elastomer seals were also assumed to exhibit isotropic linear elastic behavior with low Elastic modulus and Poisson's ratio of 0.49 (Table 5.2). This assumption is valid for low strains as exhibited by the linear stress vs strain behavior observed during the uni-axial compression tests performed on four different types of elastomer materials. Moreover, the elastomer material used in packers or plug applications are often very stiff and do not exhibit high non-linear behavior. It is not uncommon to model them as linear elastic material (Bosma et al. 2000). Besides, linear elastic behavior is a conservative approach and is often used in design work. Modelling elastomer seal as hyper-elastic material would require model calibration with experimental data from few material properties tests such as uniaxial tension, uniaxial compression, biaxial tension etc. which would be beyond the scope of the study.

Table 5.1: Material properties used for casing and liner in the model

Property	P110 Liner	X80 Casing
Young's Modulus, psi	29 x 10^6 psi	29 x 10^6 psi
Poisson's ratio	0.3	0.3
Yield Strength, psi	110,000 psi	80,000 psi
Tensile Strength, psi	125,000 psi	90,000 psi

5.3.1.2 Boundary Conditions

The top and bottom ends of liner and casing were restrained from any movement in the z direction by assigning a zero-displacement boundary condition. As shown in Figure 5.5, the bottom of the seal is fixed in the z (vertical) direction. To energize the seal, the top boundary of the seal is displaced in the negative z direction by a specified amount. Elastomer will be compressed and exert contact pressure on both the liner and casing interfaces (see Figure 5.6**)**. This process is similar to how a sub-mudline liner hanger seal assembly is set.

Table 5.2:Material properties used for seal element in the model

Elastomer	Elastic Modulus (E), psi	Poisson's Ratio (ν)
NBR	268	0.49
EPDM	277	0.49
VITON	321	0.49
PTFE	797	0.49

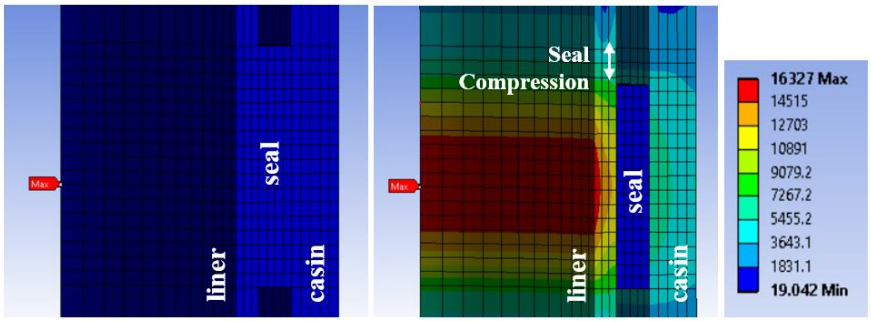

Figure 5.6: Equivalent (von-Mises) stress before (a) and after (b) the seal energization by displacement

There are two reasons for selecting a displacement boundary condition instead of specifying a compressive load condition to energize the seal. First, displacement boundary conditions tend to provide faster and more controlled numerical convergence. The second reason is that it is less susceptible to convergence failure than the load type boundary conditions. The model setup including meshing, contact formulation, mesh sensitivity analysis, model verification, and reliability are discussed in the leakage modelling and risk assessment report (section **3.1**).

5.3.2 Cement Model

The 2-D schematic of the FEA model of cement sheath is provided in Figure 5.7**.** This is similar to the seal assembly model with the replacement of seal by cement. The liner and casing dimensions and their material properties are the same as the seal assembly model. The symmetry planes are also the same, and only $^{1}/_{8}^{th}$ segment of the wellbore cross section was modelled to minimize computational requirement.

5.3.2.1 Material Properties

The material model and properties for liner and casing components are the same as the seal assembly model (see Table 5.1). The cement sheath has been modeled as isotropic linear elastic behavior. Three types of cement systems were selected for simulations – (i) a ductile cement system with low Young's modulus and high Poisson's ratio (Sample A), (ii) a cement system with moderate Young's modulus and moderate Poisson's ratio (Sample B), and (iii) a brittle cement system with high Young's modulus and low Poisson's ratio (Sample C). The material properties for the cement systems Table 5.3 were selected based on typical values found in the literature (Teodoriu et al. 2008).

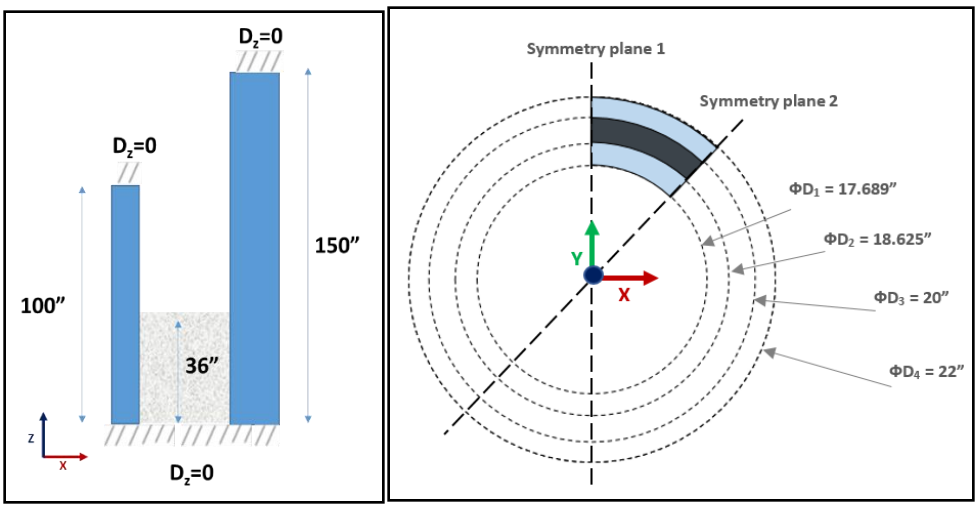

(a) (b)

Figure 5.7: Schematic of cement sheath model (a) 2-D schematic in XZ plane. (b) top view of the model in XY plane

Table 5.3: Material properties of the cement systems selected

Property	Sample A	Sample B	Sample C
Young's Modulus, psi	6.9 x 105 psi	1.0 x 10^6 psi	2.4 x 10^6 psi
Poisson's ratio	0.4	0.25	0.1
Tensile Strength, psi	1000 psi	1500 psi	3000 psi
Compressive Strength, psi	3000 psi	4500 psi	9500 psi
Cohesive Strength, psi	1500 psi	2250 psi	4750 psi

5.3.2.2 Boundary Conditions

The top and bottom ends of the liner and casing were restrained from any movement in the z direction by assigning zero displacement boundary condition. As shown in Figure 5.7, the bottom of the cement sheath was also constrained from any movement in the axial z direction. The model setup including meshing, contact formulation, mesh sensitivity analysis, model verification, and reliability are discussed in the leakage modelling and risk assessment report (section **3.2**).

5.4 SIMULATION RESULTS

5.4.1 Seal Assembly Model

Using the verified model, a parametric analysis was performed. This will provide insight on the behavior of elastomer seal by examining the contact pressure as various parameters are systematically varied. In addition to design parameters such as material properties and seal

dimensions, few important seal failure scenarios have also been examined. Unless otherwise mentioned, the base case parameter values are listed in Table 5.4.

Table 5.4: Base simulation case for parametric analysis of seal assembly

Parameter	Value
Seal elastic modulus	321 psi (VITON)
Seal Poisson's Ratio	0.49
Seal length	5 in.
Seal radial thickness	0.6875 in.
Annular gap between liner and casing	0.6875 in.
Compression Ratio	1%
Seal energization process	No fault in compression and support
Simulated average contact pressure for the base case	51 psi

This model behavior analysis will facilitate identification of the most critical parameters affecting sealability of the liner hanger. Additionally, the simulation results have been used to develop correlations and guidelines for estimating contact pressure in any condition.

5.4.1.1 Compression Ratio and Elastic Modulus

The first in the series of simulation studies was to examine the effect of the elastic modulus of seal material on contact pressure. Contact pressures were simulated at various amounts of seal energization for four types of elastomer materials – NBR, EPDM, VITON, and PTFE. The seal energization has been quantified by a term defined as the compression ratio (δ) which is calculated as:

$$\text{compression ratio } (\delta) = \frac{\text{change in seal height because of compression}}{\text{original seal height}} \times 100\% \quad \text{.....} \quad (9)$$

Two parameters - elastic modulus (E) and compression ratio (δ) were varied. The remaining parameters were the same as the base case described in Table 5.4. The model predictions of contact pressure are graphically presented as a function of E and δ in Figure 5.8. Each data point represents one simulation run. The contact pressure variation on both the casing-seal interface and liner-seal interface were minor; hence, their values were averaged to obtain a single representative value.

It is clear from the results that the contact pressure is linearly correlated with both the elastic modulus and compression ratio. This behavior was anticipated because of the assumption of linear elastic material properties. A linear regression was performed to obtain the following correlation for estimating contact pressure,

$$\text{Contact Pressure } (P_c, \text{psi}) = 15.78\ E\ \delta \qquad (\text{for } \nu = 0.49) \quad \text{.....} \quad (10)$$

The liner hanger should be able to provide hydraulic sealing up to the value of contact pressure generated at the casing-seal interface.

5.4.1.2 Poisson's Ratio

For elastomer materials, a Poisson's ratio of 0.49 is common. However, considering the possibility that in oil field applications, stiffer elastomer materials may be used, it was decided to examine the effects of lower Poisson's ratio on sealability. Contact pressure as a function of Poisson's ratio for different elastomer materials at a 2% compression ratio is plotted in Figure 5.10. Each data point represents the averaged contact pressure value from an independent simulation run.

At the lower end, metallic elements typically have Poisson's ratio of about 0.3 to 0.35. The theoretical upper limit for Poisson's ratio is 0.5. As shown in Figure 5.10, contact pressure increases gradually for less than 0.425 Poisson's ratio, beyond which it increases exponentially and even faster. Considering contact pressure at $\nu = 0.35$ as reference value, the incremental contact pressure or contact pressure multiplier remains approximately the same for all the elastomers and compression ratios (See Figure 5.11). In other words, the contact pressure value as predicated by equation (10**)** can be downscaled or upscaled as shown in Figure 5.11 to adjust for a change in Poisson's ratio.

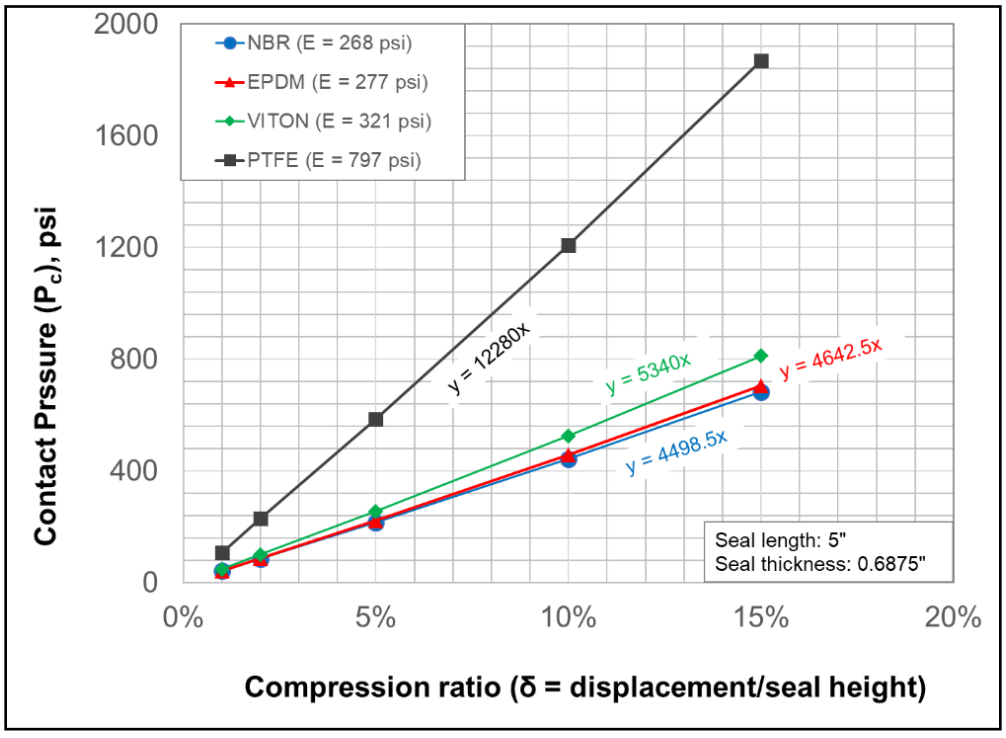

Figure 5.8: Sensitivity of contact pressure to compression ratio at different elastic modulus

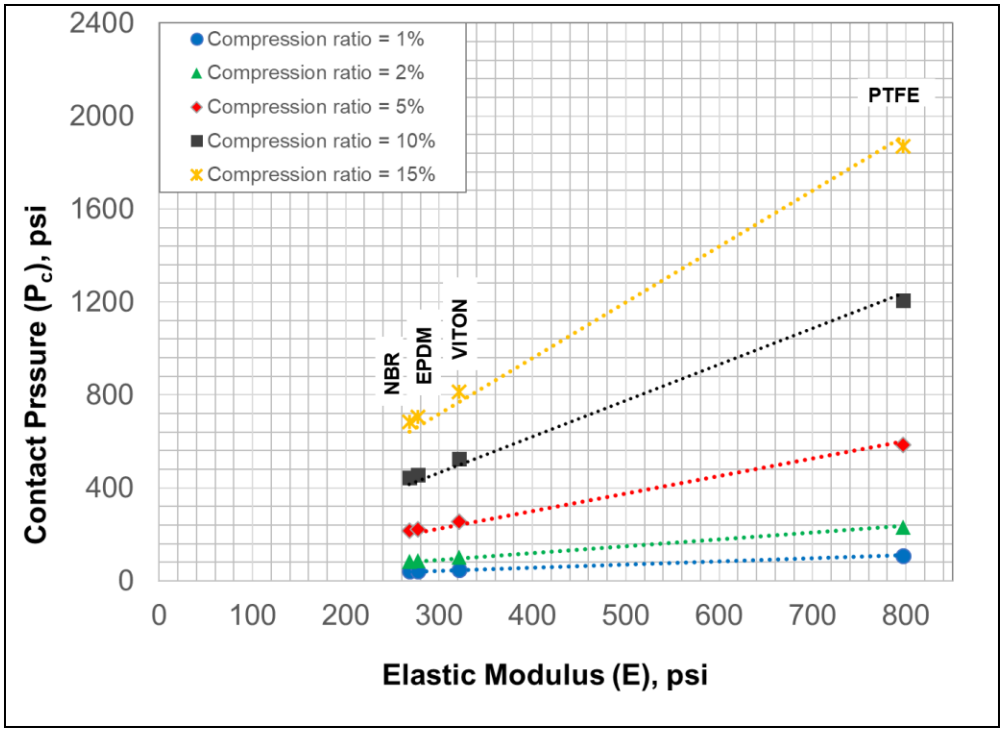

Figure 5.9: Pressure required to achieve certain compression ratio at various elastic modulus

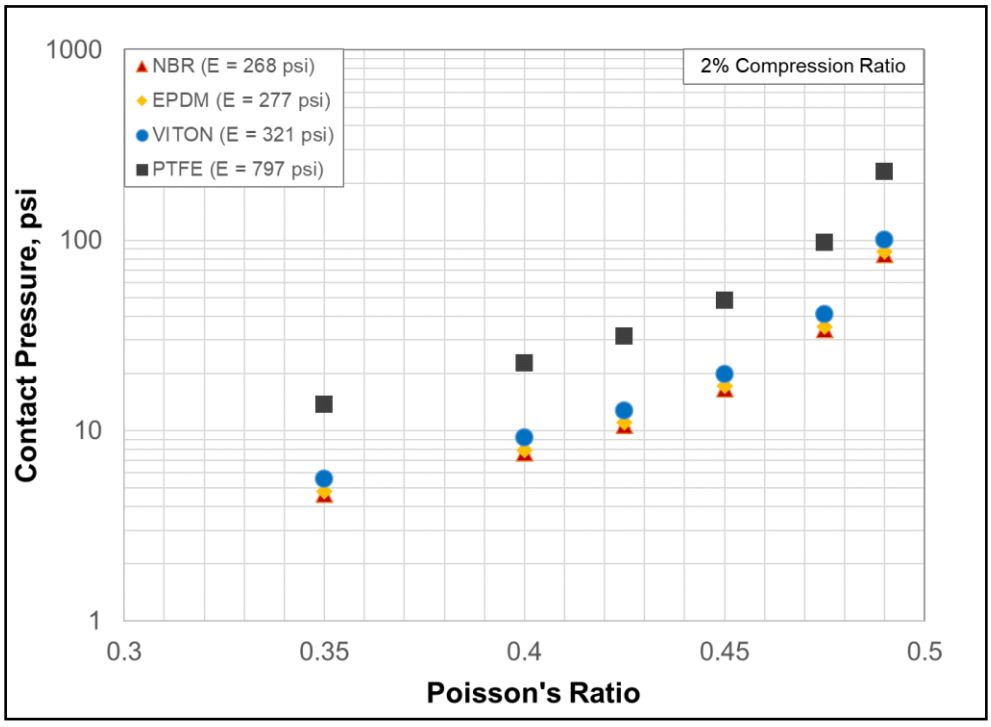

Figure 5.10: Sensitivity of contact pressure to Poisson's ratio of elastomer seal

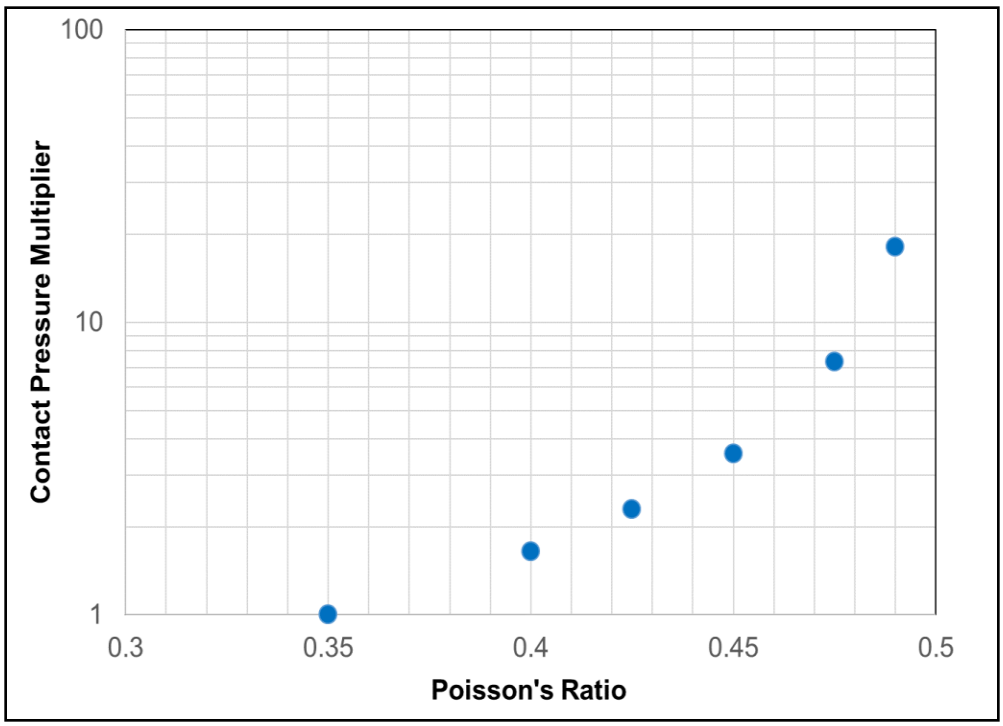

Figure 5.11: Incremental contact pressure with increase in Poisson's ratio remains approximately the same for all the elastomers and compression ratios

5.4.1.3 Seal length

For the same elastomer and compression ratio, seal length does not have a significant effect on contact pressure. Three seal lengths – 0.75-, 2.5-, and 5- in. were examined, and it was observed that contact pressure slightly decreased with increase in seal length (see Figure 5.12) but the reduction is only about 2-3%. So, for practical purposes, it can be considered insignificant.

5.4.1.4 Seal Thickness

Seal thickness in the radial direction depends on the annular gap between the liner and previous casing. The seal thickness was varied from 0.25 to 1 in. This amounts to approximately -60% to +50% change, considering 0.6875 in. thickness as the base case. The liner and casing thicknesses were kept constant. As shown in Figure 5.13, increasing the seal thickness results in higher contact pressures for the same seal length and compression ratio. The effect was more prominent in the case of a longer seal (5 in. seal length) compared to a shorter seal (0.75 in. length). Overall, a change in contact pressure was not significant (mostly < 2%) even for larger changes (±40%) in thickness.

5.4.1.5 Annular fit/gap

Typically, the seal element in a liner hanger assembly would have a drift diameter smaller than the casing internal diameter so that the seal does not get damaged while running in. This analysis was performed to investigate the effect of sealability in scenarios where seal thickness is not equal to

the annular gap between the liner hanger and casing. Understanding the sensitivity of contact pressure to thickness tolerance would help to optimize the dimensions in the design and manufacturing of seal elements.

Figure 5.14 presents the contact pressure for 5 in. and 0.75 in. long VITON seal for various annular fits. The annular gap was fixed at 0.6875 in. and seal thickness was varied from 98% to 102% of annular clearance. 100% being the perfect seal fit. In each case, 2% compression ratio was used to energize the seal.

It can be observed from Figure 5.14 that contact pressure is highly sensitive to the seal's annular fit tolerance. As expected, if the seal is 1% and 2% thicker than the annulus, the contact pressures would be almost 50% and 100% higher respectively than the base case. If the seal is 1% and 2% thinner than the annular space (which is a more likely happen in an actual field scenario), then the contact pressure reduces from the base case by approximately 50% and 100% respectively. This is because some portion of the compression that is applied will be wasted in achieving a contact between the seal and casing. Overall, from various simulation runs, it was observed that if the seal is thinner than the annulus by -x%, then it would require +x% more compression ratio to compensate for the gap and vice versa to achieve the same contact pressure as a 100% fit seal.

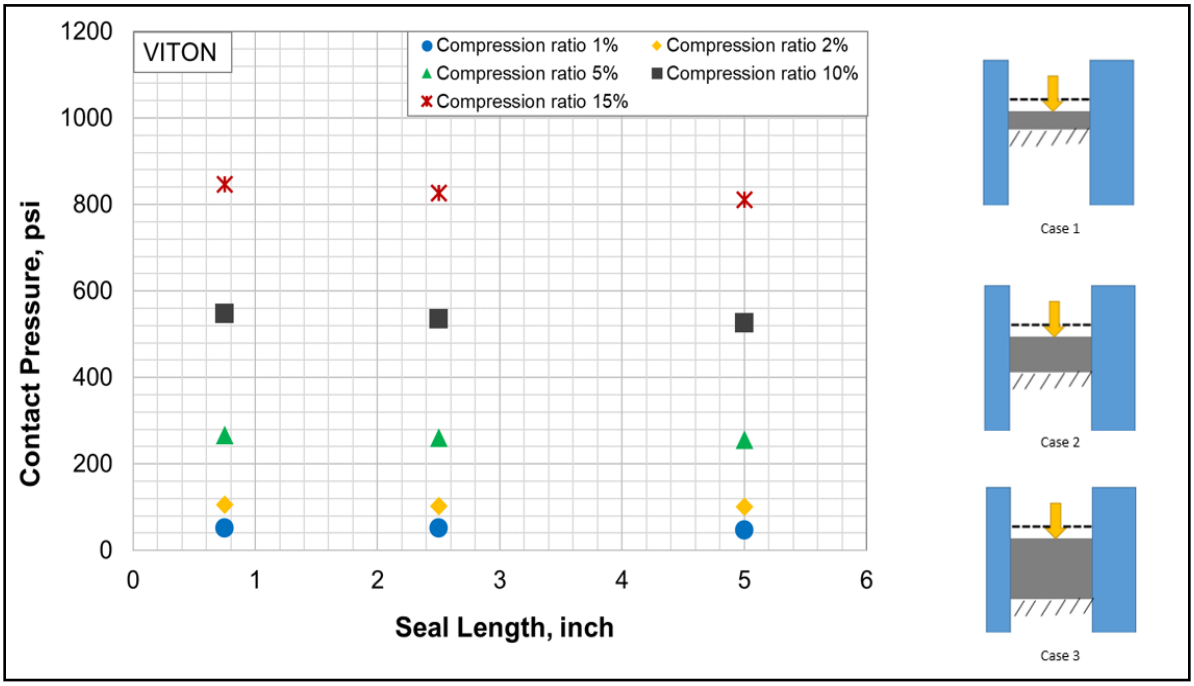

Figure 5.12: Effect of seal length on contact pressure

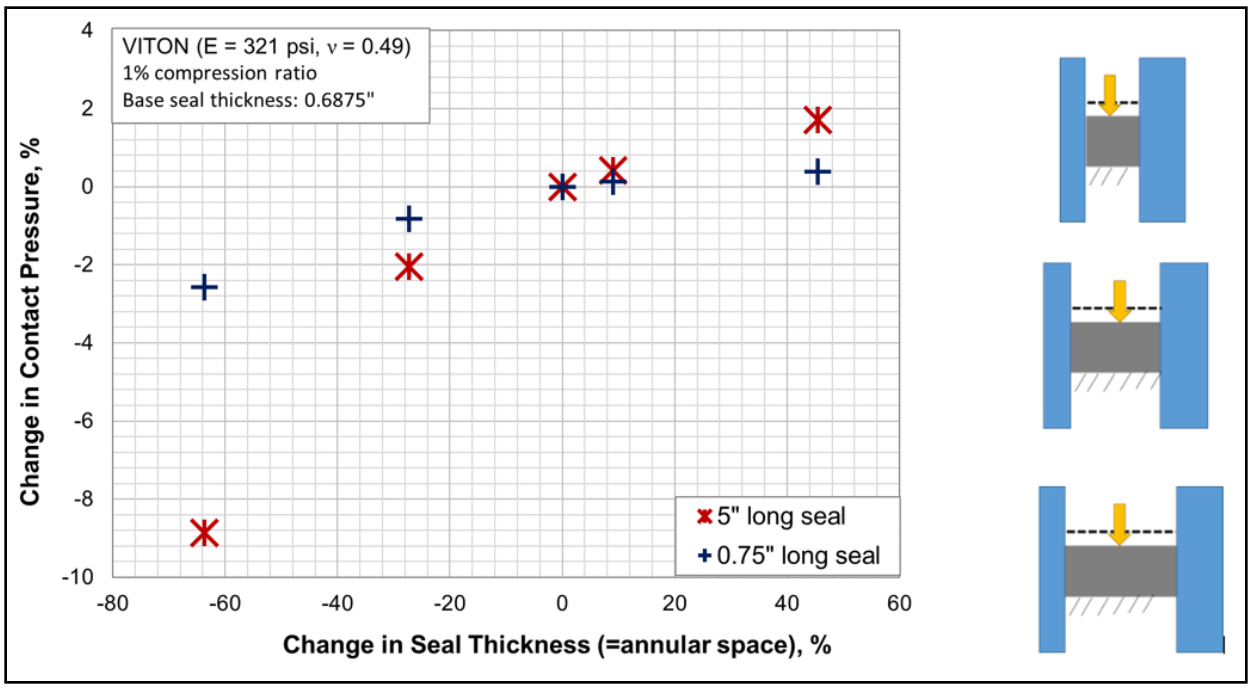

Figure 5.13: Effect of seal thickness on contact pressure

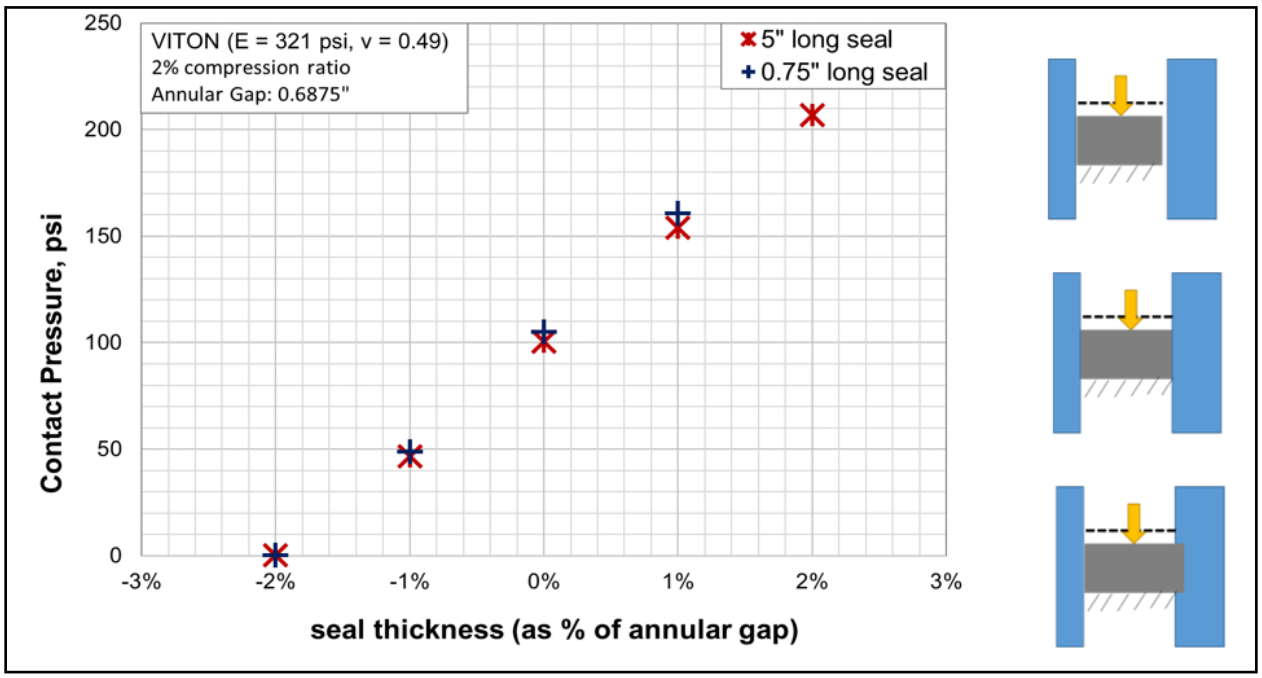

Figure 5.14: Effect of annular fit of seal on contact pressure

Table 5.5: Average reduction in contact pressure (as predicted by eq. 1) after exposure to various gas

Elastomer Type	All gases (50% CH_4 with 500 ppm H_2S + 50% CO_2)								CH_4 (100%)		CO_2 (998,000 ppm)		H_2S (500 ppm in methane carrier)	
	1 day, 120°F		7 days, 120°F		1 day, 180°F		7 days, 180°F		7 days, 180°F		7 days, 180°F		7 days, 180°F	
	Vapor phase	Brine phase	Vapor phase	Brine phase	Vapor phase	Brine phase	Vapor phase	Brine phase	Vapor phase	Brine phase	Vapor phase	Brine phase	Vapor phase	Brine phase
NBR	-41	-38	-36	-35	-36	-31	-30	-29	-16	-13	-40	-38	-14	-11
EPDM	-26	-21	-24	-21	-19	-17	-25	-22	-10	-4	-29	-27	-16	-8
VITON	-22	-14	-20	-13	-14	-7	-17	-11	-4	-6	-31	-28	-9	-6
PTFE	-5	-4	-6	-3	-10	-3	-5	-1	-3	-2	-2	-5	-6	-1

5.4.1.6 Material Failure by Gas Exposure

To examine seal material failure, four types of elastomer samples were exposed to CH_4, CO_2, H_2S, and a mixture of all gases for 1 and 7 days at 120°F and 180°F. After aging, the uniaxial compression data was acquired for each elastomer sample. The stress-strain data in the measured range was still practically linear; hence, new elastic moduli were calculated. Using these new elastic modulus values, contact pressures were simulated at various compression ratio.

The contact pressures were observed to be linearly dependent on the compression ratio. The average % reduction in contact pressures and the slope of energization plot after CO_2 exposure was approximately the same as the reduction in the elastic modulus. Reduction in the elastic modulus of elastomer samples after exposure to various gases are listed in Table 5.5. The worst case is 7 days exposure to CO_2 at 180°F. It resulted in sealability reduction of NBR (40%), EPDM (29%), VITON (9%), and theoretical PTFE elastomer (2%).

5.4.1.7 Faulty Support

The liner hanger assembly typically relies on compression plates and slips for providing the support while the seal element is being compressed by the application of weight. If this support is not uniform in the radial and/or circumferential direction, then the operating contact pressure will be less than the designed one. Such low contact pressure points along the seal may serve as an initiation point for hydraulic penetration. To investigate the effect of partial support on contact pressure, this study was conducted. A total of six simulation cases were run, depending on the location of the support failure and amount of areal support provided (Figure 5.15).

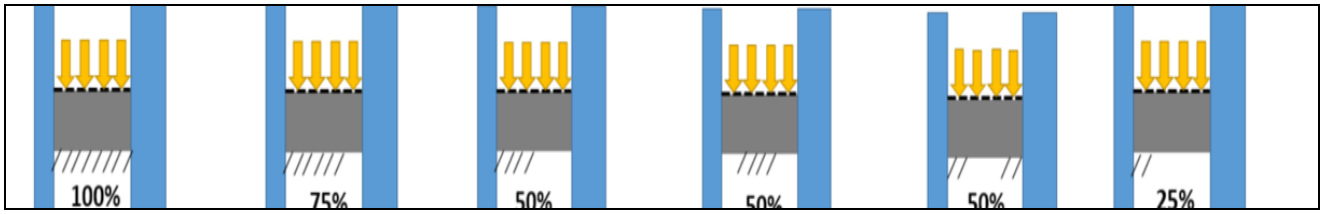

Figure 5.15: Simulation cases of full and various faulty support

The details of the simulation plots are provided in section **4.1.7** of the leakage modelling and risk assessment report. For a 5 in. long seal (Figure 5.17), the average reduction in contact pressure because of partial support ranged from **13% to 68%** for 75% to 25% support respectively. For shorter seal, on the other hand, the loss in sealability was **51% to 95%** for 75% to 25% support respectively. This indicates that the effect of faulty support becomes more detrimental in the case of a shorter seal.

5.4.1.8 Non-uniform Seal Energization

To achieve good sealability, setting forces up to 100,000 lbf are often required. In certain conditions such as shallow liner installation or deviated wells, it is often not possible to apply the required force. Moreover, the weight applied may not be uniformly distributed over the seal in the radial and circumferential direction. This can lead to the operating contact pressure being less than the designed one. To examine the effect of non-uniform compression, seven cases were simulated (Figure 5.16). The seal was supported from the bottom and the displacement boundary condition at the top of seal was varied in terms of location and area coverage.

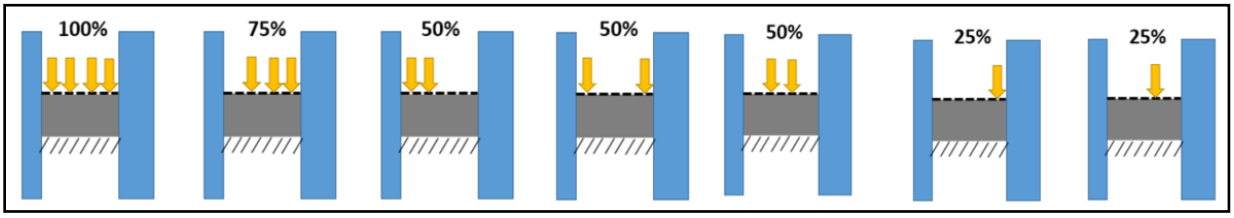

Figure 5.16: Simulation cases of full and different faulty seal energizations

The details of the simulation plots are provided in section **4.1.8** of the leakage modelling and risk assessment report. For a 5 in. long seal (Figure 5.18), the average reduction in contact pressure because of non-uniform compression ranged from **13% to 80%** for 75% to 25% compression area respectively. For shorter seal on the other hand, the loss in sealability was **53% to 95%** for 75% to 25% support respectively. Similar to the faulty support case, the effect of faulty compression becomes more detrimental for a shorter seal. Overall, the faulty support and faulty compression case results are similar in percentage reduction of contact pressure. However, it should be noted that improper compression is a more likely scenario in the field.

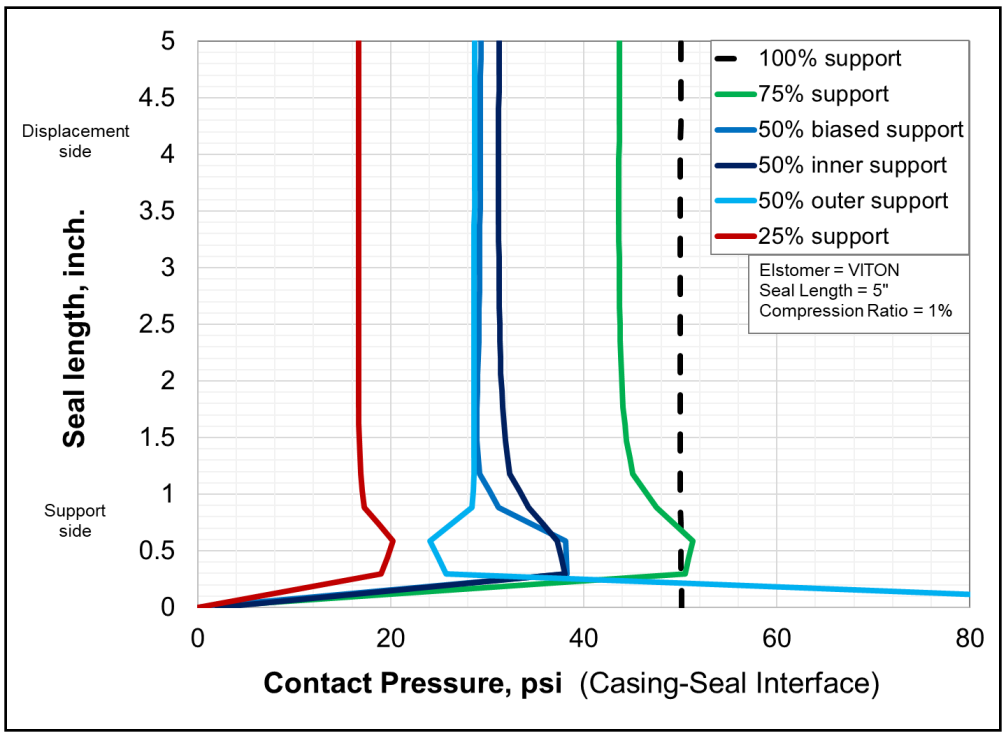

Figure 5.17: 5 in. long VITON seal with partial support: contact pressure profile along the seal length in the z direction at casing-seal interface

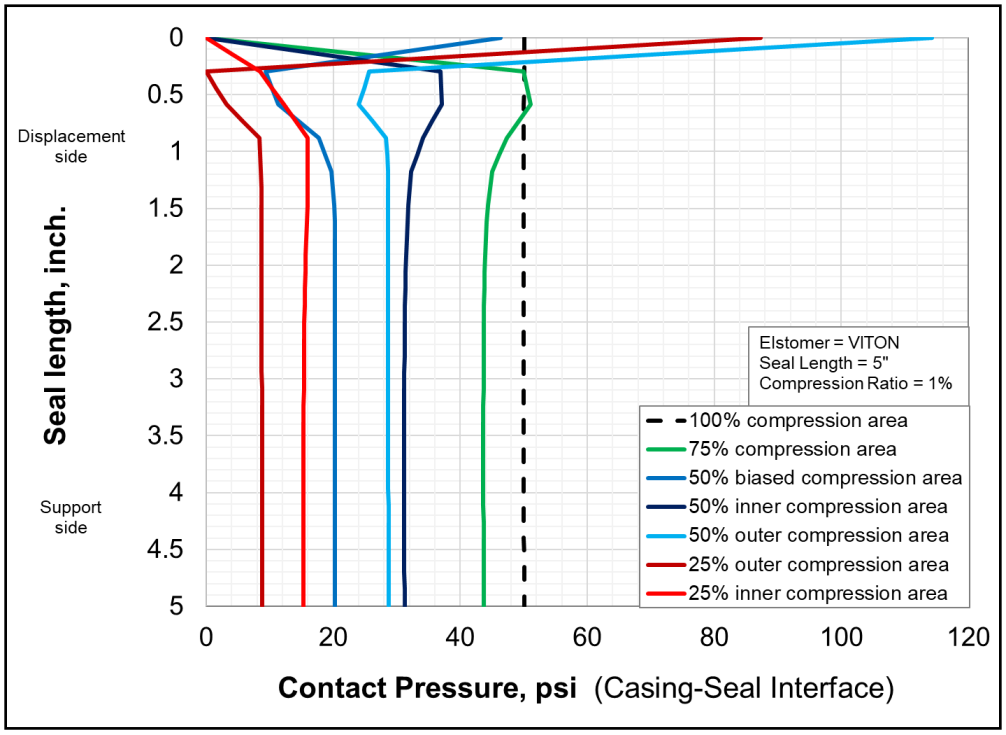

Figure 5.18: 5 in. long VITON seal with partial compression: contact pressure profile along the seal length in the z direction at casing-seal interface

5.4.1.9 Effect of Temperature

As stated earlier, the effect of temperature has been included in the form of change in material properties. The temperature effect can be indirectly predicted by observing and understanding the effect of variation in Elastic modulus and Poisson's ratio on sealability (i.e. contact pressure). If the elastic modulus and Poisson's ratio of elastomer seal is known at the desired temperature then, the empirical correlation developed from the modelling results can be used to predict the effect of temperature on sealability.

Typically, elastomers become stiffer with decrease in temperature and softer with increase in temperature. Specifically, elastic modulus decreases with an increase in temperature. Similar observation was made in the elastomer aging tests conducted using setup III of this project. It was observed that after aging the elastomers at a high temperature (180^{o}F) in the presence of chemicals for various days, the elastic modulus of the samples decreased. A typical temperature effect on the elastic modulus of EPDM elastomer is shown in Figure 5.19.

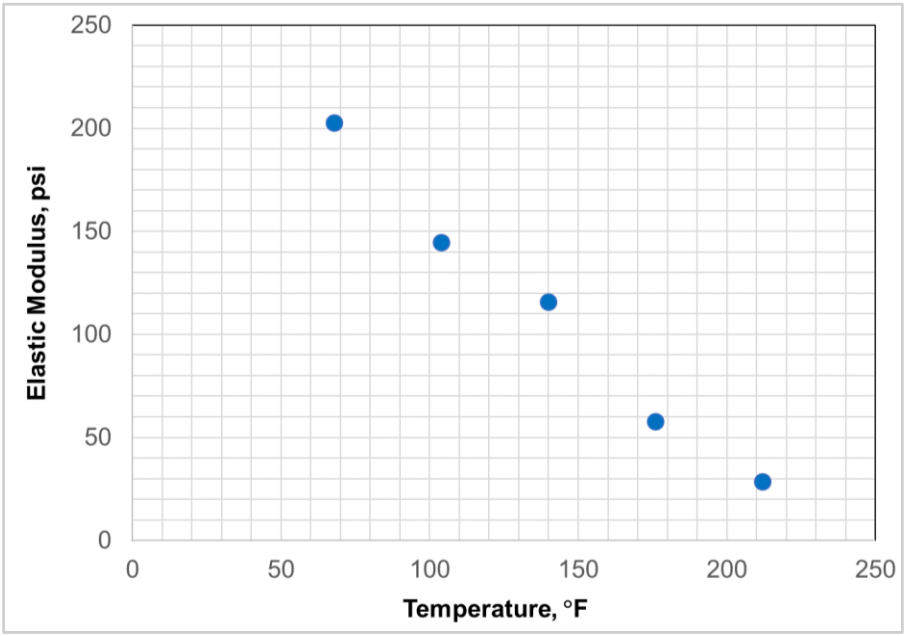

Figure 5.19: Typical temperature effect on elastic modulus of EPDM (Data source: Chanliau-Blanot et al. 1989)

As the simulation results indicates, the contact pressure is positively proportional to the elastic modulus (section ***5.4.1.1***). Therefore, any reduction in elastic modulus will result in similar percentage reduction in sealability i.e. contact pressure. For example, consider that at 70°F, the EPDM sample has an elastic modulus of about 200 psi. Increasing the temperature to 140°F, reduces the elastic modulus to about 110 psi. For a given amount of compression, reduction of 45% in elastic modulus will result in 45% loss of contact pressure. Similarly, if there is a change in Poisson's ratio because of temperature, then a corresponding change in contact stress can be estimated according to Figure 5.11.

To develop a correlation for contact pressure that is a direct function of temperature, a separate study would be required which is entirely focused on measuring several material properties of various elastomers at different temperatures and then developing correlations for predicting material properties as a function of temperature. The primary focus of this project has been on shallow depth offshore wells; hence, the operating temperatures are near to the room temperature. Therefore, the effect on thermal stresses developed in surface liner and casing strings will not be significant. If the focus of project were on ultra-deep HPHT wells, then expansions of casing strings because of thermal stresses may have been impactful in elastomer sealability.

5.4.1.10 Summary of Parametric Analysis

The results from the simulation study are summarized as follows:

- Contact pressure is linearly dependent on the elastic modulus and compression ratio.
- Contact pressure increases gradually with an increase in Poisson's ratio up to 0.425, beyond which it increases exponentially and even faster. Considering a contact pressure at $\nu = 0.35$ as reference value, the incremental contact pressure or contact pressure multiplier remains approximately the same for all the elastomers and compression ratios.
- Contact pressure reduces only by 2-3% even with an increase in seal length that is approximately 5 times (0.75 in. to 5 in.). For all practical purposes, it can be considered insignificant.
- A change in contact pressure was not significant (< 2%) even for large changes (±40%) in seal thickness.
- Contact pressure is highly sensitive to the annular fit of seal. For a fixed annular space, each ± x% change in seal thickness would require ∓ x% compression ratio to compensate for that change and achieve the same contact pressure as 100% fit seal. In other words, if the radial gap between the seal and casing is x% higher than anticipated, then it can effectively reduce compression by x% and vice versa. A radial gap of 1% that is higher than the designed value can reduce the effective contact pressure by an amount that is approximately equal to 16 times the elastic modulus of the seal.
- The average % reduction in contact pressures because of gas exposure is practically equal to the % reduction in the elastic modulus.
- The loss in sealability because of faulty support can range from 13% to 68% in a long seal (5 in.) and 51% to 95% in a short seal (2.5 in.) depending on the severity. In the case of non-uniform compression, the loss can range from 13% to 80% in a longer seal (5 in.) and 53% to 95% in a shorter seal (2.5 in.) depending on the severity. Overall, the loss is more pronounced and detrimental for a shorter seal.

All these results can be combined into the following comprehensive correlation for estimating contact pressure.

$$\text{Contact Pressure } (P_c) = 15.78\ E\ (\delta - \lambda) \left[\frac{P_c \text{ multiplier at desired } \nu}{P_c \text{ multiplier at } \nu = 0.49}\right] \ldots\ldots\ldots\ldots\ldots\ldots\ldots (11)$$

where, E is the elastic modulus, δ is the compression ratio in fraction, λ is the annular gap between seal and pipe in fraction, and Pc multiplier is a constant which can be obtained from the Figure 5.11. P_c and E are in consistent units. The effects of seal length and seal thickness can be ignored with ±2% error in the estimate. Material failure can be incorporated simply in form of change in elastic modulus and Poison's ratio.

5.4.1.11 Sensitivity Analysis

To compare the sensitivity of contact pressure to all the parameters discussed so far, a normalized plot was prepared. As shown in Table 5.6 below, a base case was selected and then each of the 8 parameters were varied, while the rest were kept constant. The values of each parameter were normalized by dividing them with a base value. 38 cases were simulated and an average contact pressure from each simulation was obtained. The normalized plot is shown in Figure 5.20.

Table 5.6: List of parameters and corresponding values used in sensitivity analysis of contact pressure

Parameter	Different Values Used in Simulations									
Elastic Modulus, psi				268 *(0.83)*	277 *(0.86)*	321 *(1.00)*	797 *(2.48)*			
Poisson's Ratio	0.35 *(0.71)*	0.400 *(0.82)*	0.425 *(0.87)*	0.450 *(0.92)*	0.475 *(0.97)*	0.49 *(1.00)*				
Seal Length, inch				0.75 *(0.15)*	2.5 *(0.5)*	5.0 *(1.00)*				
Seal Width, inch				0.25 *(0.36)*	0.50 *(0.73)*	0.6875 *(1.00)*	0.75 *(1.09)*	1.00 *(1.45)*		
Annular Fit, fraction				0.98 *(0.98)*	0.99 *(0.99)*	1.00 *(1.00)*	1.01 *(1.01)*	1.02 *(1.02)*		
Compression Ratio, fraction				0.0025 *(0.25)*	0.005 *(0.50)*	0.01 *(1.00)*	0.02 *(2.00)*	0.05 *(5.00)*	0.10 *(10.00)*	0.15 *(15.00)*
Compression area, fraction			0.25 *(0.25)*	0.50 *(0.5)*	0.75 *(0.75)*	1.00 *(1.00)*				
Support Area, fraction			0.25 *(0.25)*	0.50 *(0.5)*	0.75 *(0.75)*	1.00 *(1.00)*				

Note: In Table 5.6, each value represents a complete simulation case with rest of the parameters being equal to the base values. Values in parentheses are corresponding normalized values

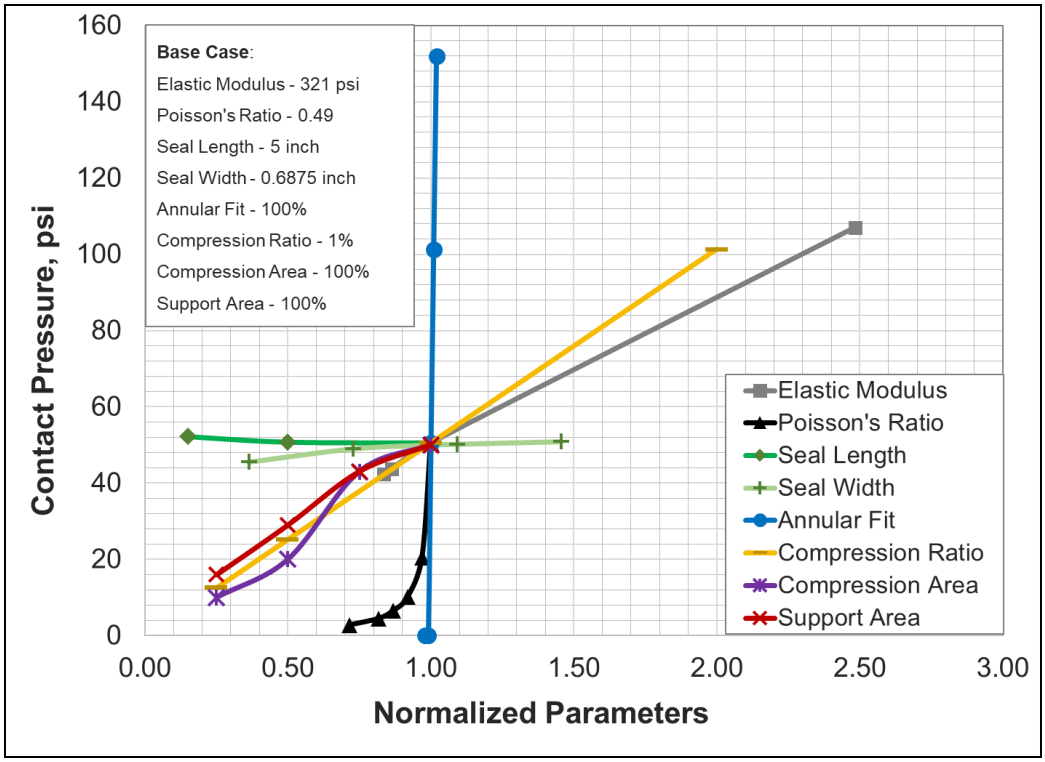

Figure 5.20: Sensitivity of contact pressure to various parameters

As shown in Figure 5.20, contact pressure (sealability) has the highest sensitivity to annular fit. This suggests that the tolerance of radial dimension of an elastomer seal is critical in liner hanger design. Sealability is also highly sensitive to Poisson's ratio (ν), specifically between 0.4 and the theoretical limit of 0.5. The sensitivity of contact pressure to elastic modulus, compression ratio, compression area, and support area are practically similar. For the range of values examined, in comparison to other parameters, seal length and seal radial width were observed to have no significant effect on sealability.

5.4.1.12 Risk Assessment

As observed from the sensitivity analysis, annular fit can be the most detrimental factor affecting sealability. Although, having the radial width more than the annular space is desirable, in reality, the seal element is always designed to be smaller than the annular space for the sake of easy conveyance while running in the hanger. However, because of improper centralization or any other operational reason, if the clearance between seal and casing is higher than the one anticipated during the design, then it can potentially result in significantly lower sealability than planned. The annular fit can also be compromised because of wearing/tearing of the seal element during storage, transportation, or running in. This necessitates tight dimensional tolerance and visual inspection before running in.

Deterioration in sealability because of change in material properties is one of the most likely mode of failure in field application. It is imperative that elastomer element is designed to

account for potential changes in material properties caused by exposure to various gases, chemical, and temperature changes. Poisson's ratio is the second most critical parameter affecting contact stress. Elastomer materials are typically assumed to exhibit a Poisson's ratio of 0.49. Nonetheless, it is important that the true value is measured and used while designing the seal component, otherwise it could result in over-estimation of sealability. The elastic modulus is linearly dependent on contact pressure and it is important that the elastic modulus of elastomer be adjusted to account for potential degradation from chemical, gas, and temperature exposure.

Compression ratio (i.e. amount of load applied to the seal assembly for energization) is an important and controllable operational parameter. Failure to apply manufacturer recommended or designed load for energization because of any reason can reduce the sealing capacity of hanger seal assembly. Compression area which represents the uniformity of an applied energization load, is a likely parameter to be affected during field installation. Lack of circumferential uniform compression because of decentralization, well deviation, or any other reason can notably compromise sealability. Support area is a manufacturer or design parameter and can represent the failure of a compression plate or slips during the energization process.

5.4.1.13 Analytical Validation

The simulated contact pressure values are the most important items that require validation. The contact pressure values were validated using two different analytical equations: (i) use of analytical equation for bulk modulus, and (ii) modified analytical equation based on the model developed by Al-Hiddabi et al. (2015) for predicting contact pressure in expandable liner hanger seals. Both equations are discussed in section **4.1.10** of the leakage modelling and risk assessment report.

Contact pressures calculated from both analytical equations were compared with the values simulated by the FEA model. Both analytical equations yielded similar values. The comparison between analytical and FEA contact pressure values for different elastomers, at various compression ratio is provided in Figure 5.21**.**

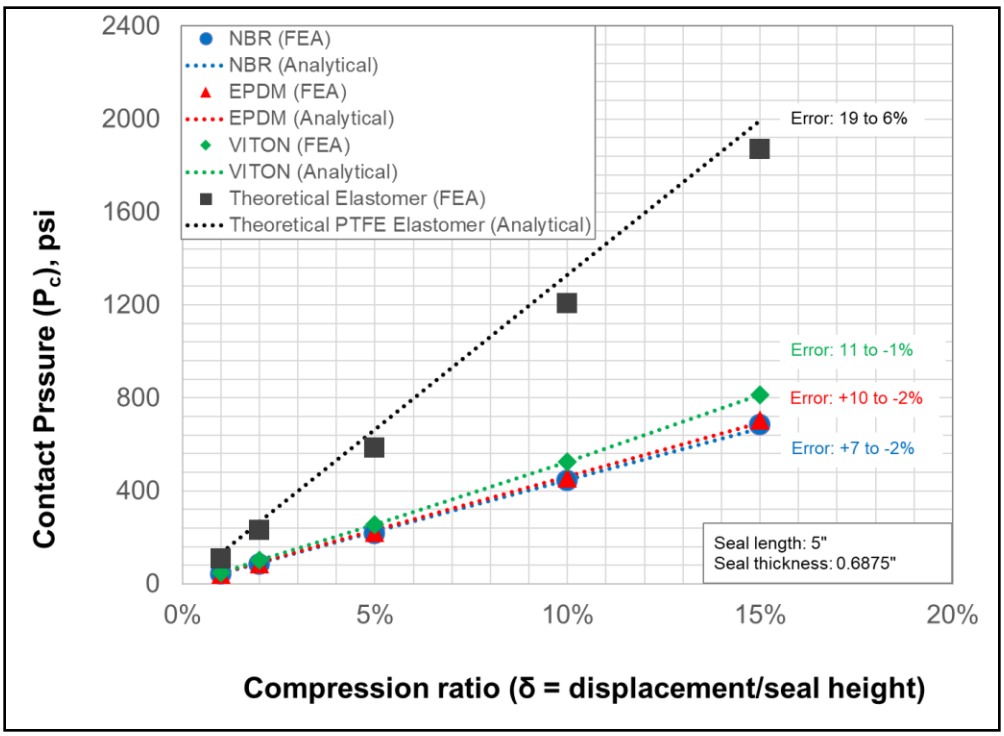

Figure 5.21: Comparison between FEA simulated and analytical contact pressure values for different elastomers at various compression ratios

FEA results matched reasonably well with the analytical solution. The error ranged from 7-22% at the lowest contact pressure values (low compression and Poisson's ratio) to 1-6% at high contact pressure values (high compression and Poisson's ratio). It should be noted that the analytical equations used are approximate and do not represent the exact compression mechanism and boundary conditions. Nonetheless, these results combined with the analytical validation of stresses in casing and liner certainly establish confidence in the FEA results.

5.4.1.14 FEA Model of Setup - 2

A special FEA model was prepared to confirm the experimental results obtained from setup II of the project. The schematic of the model with dimensions and boundary conditions are provided in the leakage modelling and risk assessment report (section **4.1.11**).

Contact pressure molded EPDM elastomer rings used in setup II were identified to have diameter approximately 1 mm greater than the annulus gap. Hence, the effect of seal interference or seal annular fit on contact pressure was examined. The summary of maximum contact pressure generated as a function of seal interference and externally applied displacement/compression is graphically presented in Figure 5.22. As expected, contact pressure is linearly correlated to displacement amount. The presence of interference leads to pre-stress condition and results in an intercept value at zero displacement. The molded EPDM seal used in conducting the tests on setup II had a diameter of 1 mm greater than the annular space. Inserting the seal into the setup led to a pre-stress condition and the system was observed to be gas tight when a 40 psig pressure injection

test was performed in the absence of an external displacement application via bolts. This is confirmed by the FEA model which predicts contact pressure of 48 psi for the EPDM seal with 1 mm interference and 0 mm displacement application (See Figure 5.22).

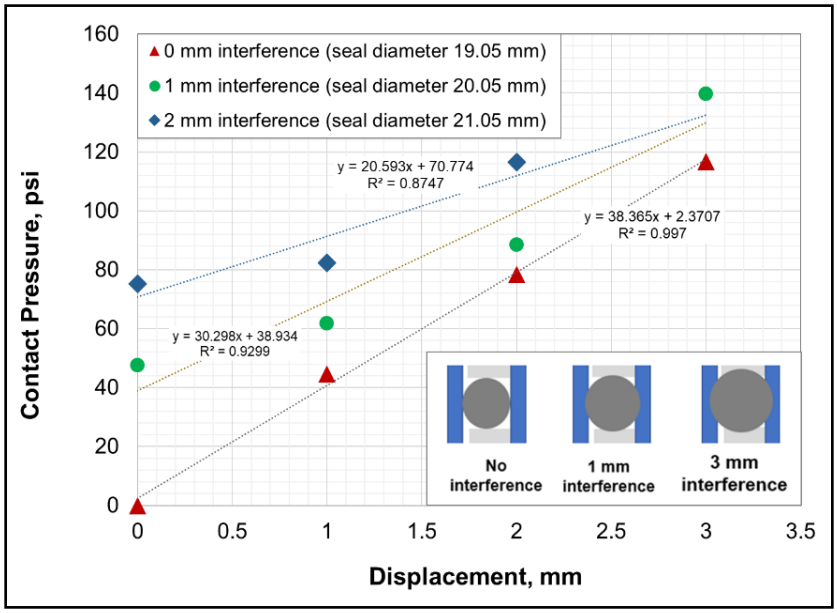

Figure 5.22: Effect of compression and interference on contact pressure at the seal – pipe interface for EPDM seal

5.4.2 Cement Model

To assess "fitness for service" of cement sheath, it is important to evaluate the likelihood of radial debonding, radial crack, and shear failure. This was accomplished by performing a parametric analysis and examining the effect of various operational and design parameters on radial stress, hoop stress, and maximum shear stress at cement-liner interface.

Based on the analytical model discussed in **Appendix A** of the leakage modelling and risk assessment report, it is expected that in the presence of only internal pressure, the stresses generated at the cement-inner pipe interface are typically higher in magnitude than at cement-outer pipe interface. In our case, this means that the cement sheath is likely to fail at the cement-liner interface before the cement-casing interface. This trend was also observed in all the simulation runs in this study. Therefore, all the results discussed in the subsequent sections are based on the stresses generated at cement-liner interface. Moreover, to avoid end effects and maintain consistency, each value of radial, hoop, and maximum shear stresses reported henceforth were observed at the middle of cement column at the cement-liner interface. Negative and positive sign represents compressive and tensile stresses respectively.

5.4.2.1 Wellbore Pressure

Wellbore pressure or internal pipe pressure is the dominant load for a set cement in a shallow depth well. Once the cement sets, any change in wellbore pressure can induce stresses in the cement

sheath. There are several possible reasons for a change in wellbore pressure. For example, events such as a casing pressure test, formation integrity test, increased mud weight for subsequent drilling, perforation or stimulation operation can lead to an increase in wellbore pressure. On the other hand, fluid loss, gas kick while drilling, or production can reduce the wellbore pressure. The effect of a change in wellbore pressure on radial, hoop, and maximum shear stresses for three different types of cement samples is presented in Figure 5.23**,** Figure 5.24**,** and Figure 5.25 respectively.

Radial Stress

As shown in Figure 5.23, change in wellbore pressure is linearly correlated to radial stress. Any increase in wellbore pressure after the cement sets, causes development of compressive (negative) radial stress at the liner-cement interface. The magnitude increases linearly with further increase in pressure. This eliminates the risk of debonding but introduces the risk of failure by compressive or stress crushing with a likelihood that depends on the compressive strength of the cement. Any decrease in pressure however, introduces tensile radial stress at the interface. If the pressure reduction is large enough to cause a radial stress that is higher than the tensile strength of the cement, then it can lead to radial debonding.

Upon closer inspection, the effect of wellbore pressure on radial stress is slightly higher in the case of brittle cement (Sample C) and lower for more ductile cement (Sample A). The difference among the three samples is however not huge.

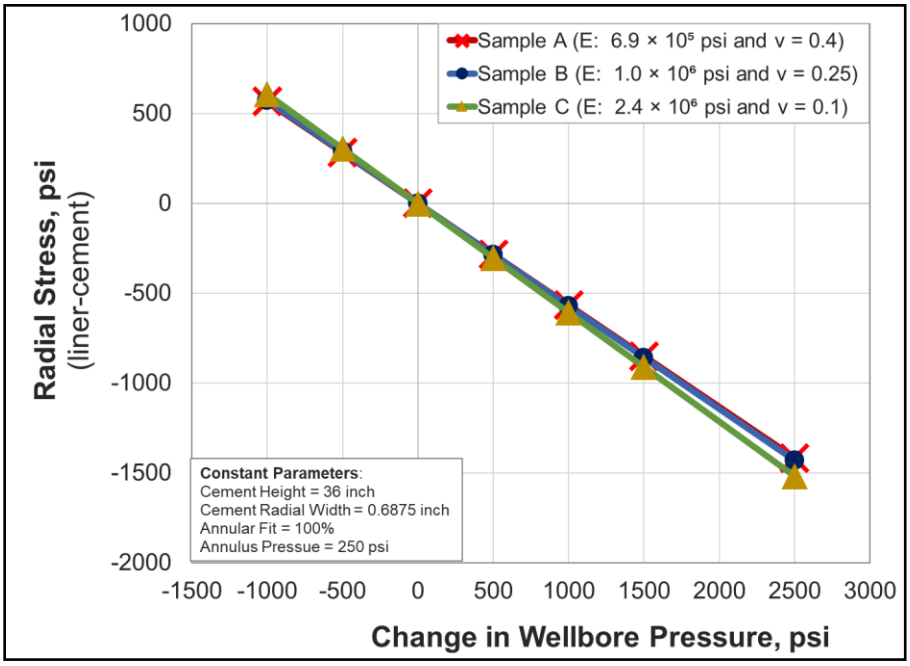

Figure 5.23: Effect of change in wellbore pressure on radial stress in cement at liner-cement interface

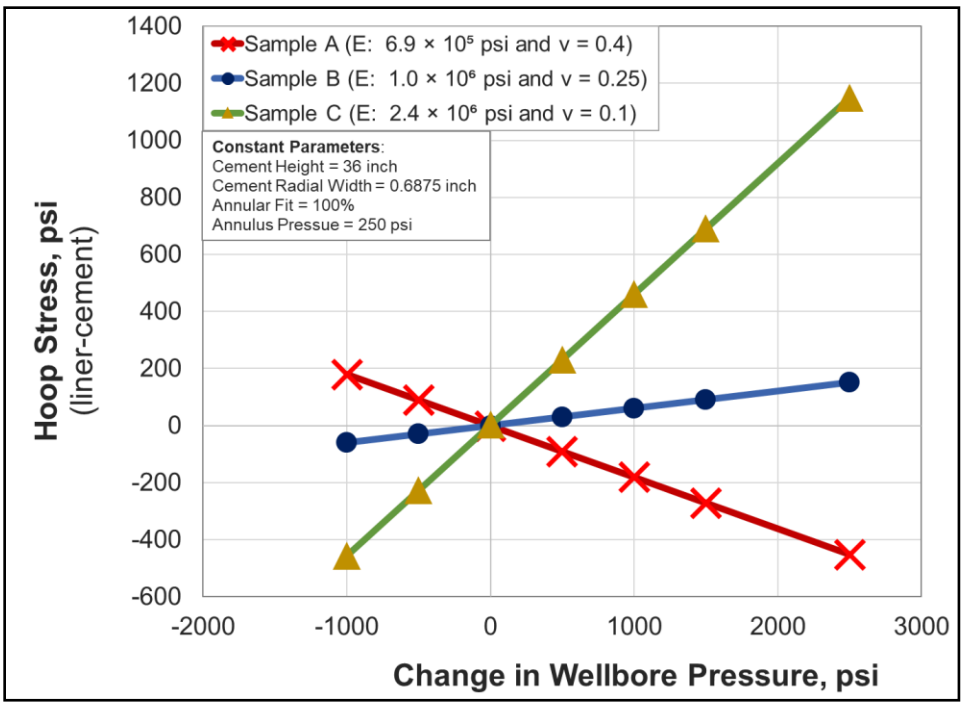

Figure 5.24: Effect of change in wellbore pressure on hoop stress in cement at liner-cement interface

Hoop Stress

Similar to radial stress, hoop stress is linearly correlated with changes in wellbore pressure. Sample C has the highest sensitivity to wellbore pressure followed by sample B and then Sample A. Interestingly, the direction of resultant hoop stress is dependent on cement material properties. Under the condition of increasing wellbore pressure, only samples B and C are susceptible to radial cracking if hoop stress exceeds their tensile strength limit. The ductile cement (sample A) is prone to radial cracking only under the condition of decreasing wellbore pressure.

This opposite effect can be attributed to Poisson's ratio. Sample A has a high Poisson's ratio of 0.4 and the applied radial pressure results in high axial deformation which dominates hoop stress and is compressive in nature because of zero displacement boundary conditions applied to the ends of the cement and pipes. For the same wellbore pressure and a low Poisson's ratio of 0.1 (Sample C), the axial deformation is very low and tensile hoop stress is still dominant. Sample B has near optimum material properties and it shows the least sensitivity to wellbore pressure compared to the other two samples.

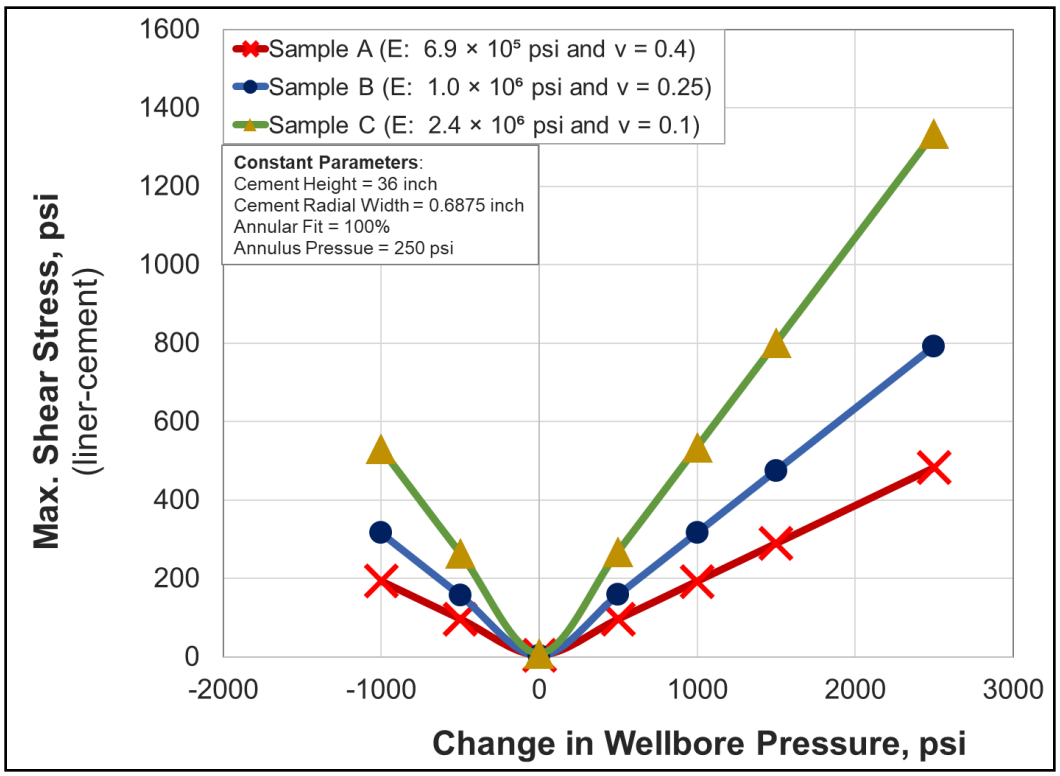

Figure 5.25: Effect of change in wellbore pressure on maximum shear stress in cement at liner-cement interface

Maximum Shear Stress

Shear failure occurs when the maximum shear stress exceeds the critical value or shear strength of cement sheath. As shown in Figure 5.25, the maximum shear stress is also linearly correlated with a change in wellbore pressure. It should be noted that its value does not depend on the direction of the pressure change. It is clearly indicated in the figure that as cement becomes more brittle (Sample A to Sample C), the sensitivity of maximum shear stress to wellbore pressure increases. This is because the shear modulus decreases from Sample A towards Sample C. In other words, the sample with low Poisson's ratio, has a higher difference between maximum principle and minimum principle stresses compared to a sample with higher Poisson's ratio.

The effect of change in wellbore pressure on radial, hoop, and maximum shear stresses can be quantified in terms of change in stress value per unit change in pressure. The summary of all the three stresses discussed above is provided in Table 5.7

Table 5.7: Effect of change in wellbore pressure on radial, hoop, and maximum shear stresses at liner-cement interface

Cement Sample	$\Delta\sigma_r/\Delta P_{wellbore}$	$\Delta\sigma_\theta/\Delta P_{wellbore}$	$\Delta\tau_{max}/\lvert\Delta P_{wellbore}\rvert$
Sample A (E: 6.9 × 10⁵ psi and ν = 0.40)	-0.5667	-0.1805	0.1918
Sample B (E: 1.0 × 10⁶ psi and ν = 0.25)	-0.5727	0.0608	0.3158
Sample C (E: 2.4 × 10⁶ psi and ν = 0.10)	- 0.6075	0.4586	0.5310

This table provides valuable information. The ductile cement has the least sensitivity to wellbore pressure in radial and shear stresses. This means that hypothetically, if all the three cement samples had the same tensile, compressive, and shear strengths, then the ductile cement (Sample A) would have the least likelihood of radial (debonding/stress crushing) and shear failure. Sample B (cement with low Young's modulus and low Poisson's ratio) exhibits the least sensitivity to pressure change when it comes to hoop stress and might be preferred.

Even though it seems like ductile cement should be the preferred choice, it should be noted that, in reality, uniaxial strengths usually tend to be smaller for ductile cement and higher for brittle cement. Hence, selection should be based on specific situations.

5.4.2.2 Annulus Pressure

Annulus pressure in the liner overlap (between the liner and casing) is exerted by the completion fluid or pre-flush fluid circulated before cementing and lying on top of the set cement column. The annulus pressure is usually less than the wellbore pressure and should not change unless under some special circumstances such as significant gravity segregation of solid particles in the fluid column or fluid influx from the top through the seal assembly.

The results indicate that there is practically no effect of changes in annulus pressure on radial, hoop, and maximum shear stresses. The simulation results and plots are provided in the leakage modelling and risk assessment report (section **4.2.2**). This is not surprising because the cement sheath is modelled to be bonded with both liner and casing, which does not permit sliding or separation and there is restriction on axial displacement. Moreover, the annulus pressure is not high enough to cause a ballooning of the annulus, push liner and casing apart, and develop radial stress at contact surfaces. These results were also confirmed by modelling contacts as the 'rough' type which allows them to separate.

5.4.2.3 Cement Sheath Height

Often, the liner overlap is not cemented all the way to the top of liner. It is logical that having more of a cement column in the annulus is beneficial as it increases the length of permeable path within the cement and help resist or delay fluid flow. Nonetheless, the purpose of varying the height of cement column was to examine whether it affects mechanical stresses and structural failure within the cement. Similar to annulus pressure, it was observed that there is no effect of changing the cement height on the stresses developed at the liner-cement interface. A change in cement height can affect the end stresses near the top and bottom of the cement column. However, the stresses at the middle of cement should be free of end effects and independent of cement length. An additional explanation for this result is the presence of bonded type contact between the cement and the liner/casing. This type of contact (similar to adhesion) does not permit any displacement. Modelling contact pairs as 'rough' and permitting separation did not change the results. The simulation results and plots are provided in the leakage modelling and risk assessment report (section **4.2.3**).

5.4.2.4 Cement Radial Width

Cement sheath radial width (i.e. thickness) was varied to account for various casing programs and investigate its effect on potential failures. The outer radius of cement was kept constant while the inner radius was varied. The thickness of the liner and the casing were kept constant. The effects of changes in the cement width on radial, hoop, and maximum shear stresses for three different types of cement samples is presented in Figure 5.26, Figure 5.27, and Figure 5.28 respectively.

As expected, an increase in cement width resulted to a decrease in the magnitude of all the three stresses. This means that the tensile stress became less tensile and compressive stress became less compressive. However, each consecutive change was approximately less than 5%, meaning there is no practical advantage of having a thicker sheath in terms of reducing the likelihood of failure.

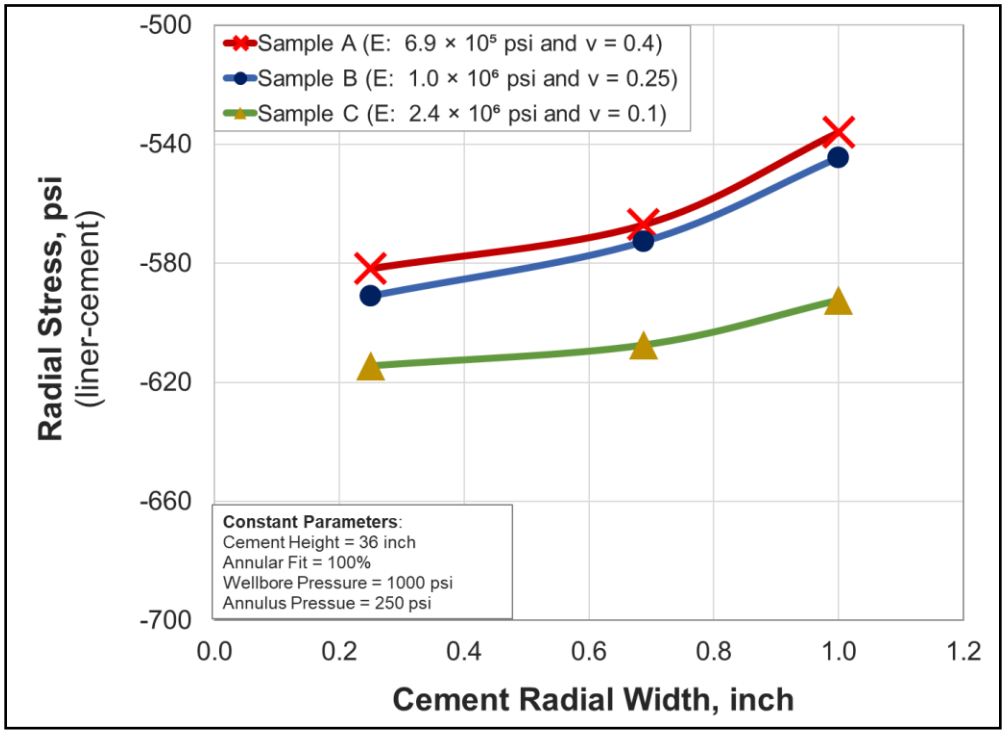

Figure 5.26: Effect of cement radial width on radial stress in cement at liner-cement interface

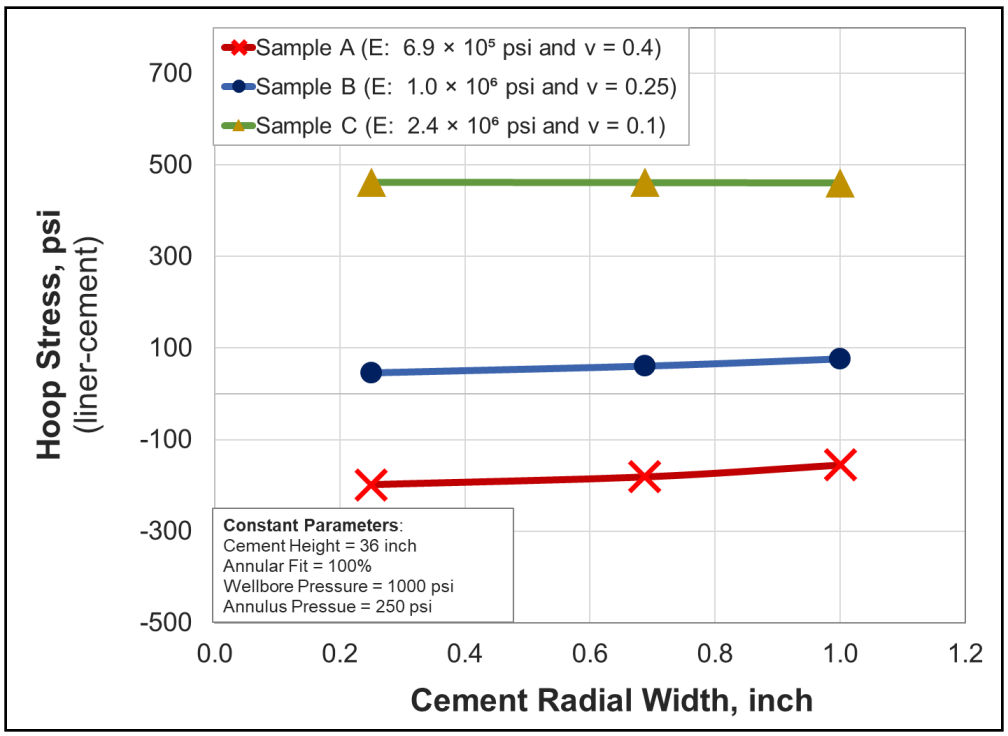

Figure 5.27: Effect of cement radial width on hoop stress in cement at liner-cement interface

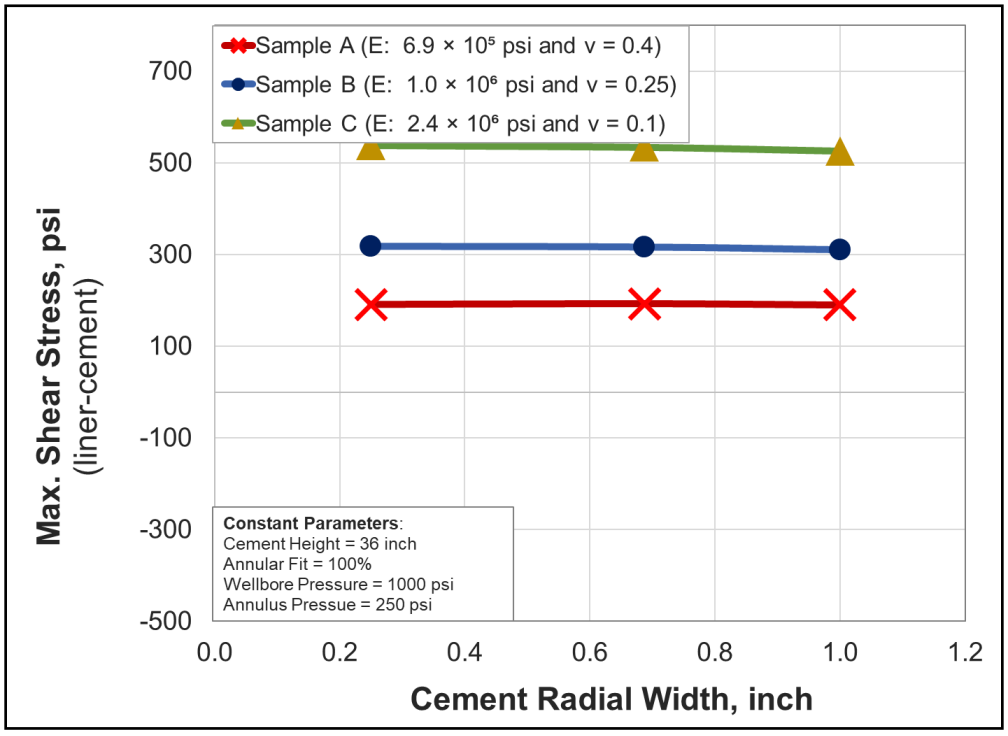

Figure 5.28: Effect of cement radial width on maximum shear stress in cement at liner-cement interface

5.4.2.5 Cement Annular Fit

Cement annular fit is defined as its radial width relative to the annular gap between the liner and the cement. As shown in Figure 5.29, an annular fit that is less than 1 (or 100%) means that the cement sheath is thinner than the annular gap between the pipes. An annular fit that is more than 1 (or 100%) corresponds to a pre-stress condition within the cement. This parameter will help analyze two distinct conditions: (i) presence of uniform micro-annulus along the liner because of volume shrinkage in set cement, insufficient mud removal, or trapped fluid pressure during setting process and (ii) expansive cement (or pre-stressed cement) versus conventional cement.

In all the simulations, wellbore and annulus pressure of 1000 psi and 250 psi were applied after setting of the cement. The annular fit was varied from 99% to 101%. The width of gap or channel along the liner corresponding to 99% and 99.5% annular fit is 175 μm and 87 μm respectively. An annular fit of 100.5% and 101% corresponds to contact stresses that are approximately 350 psi and 700 psi respectively at the liner-cement interface. For these four different annular fit cases, the simulated radial, hoop, and maximum shear stresses are graphically presented in Figure 5.30, Figure 5.31, and Figure 5.32 respectively.

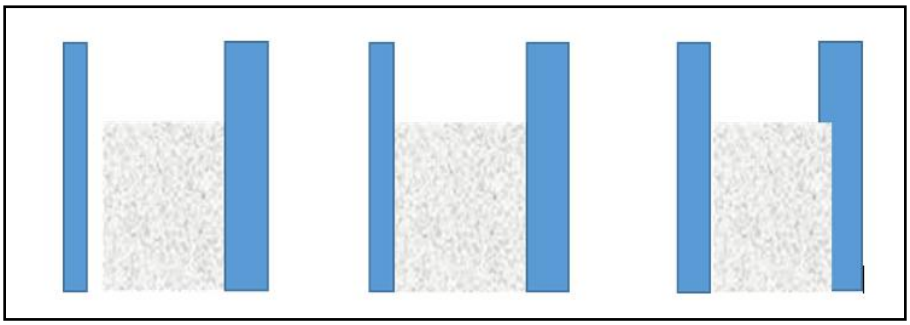

Figure 5.29: Graphical representation of models with different annular fit of cement

As shown in Figure 5.30, all the three stresses are zero at annular fit of 99%; indicating that there is no contact established between the liner and the cement. This means that the application of 1000 psi wellbore pressure does not cause sufficient ballooning of the liner to close the gap of 175 μm. Interestingly, in the case of 99.5% annular fit, the 1000 psi wellbore pressure was able to cause sufficient ballooning of the liner to close the gap of 87 μm and achieve contact. Once contact is established, the values of the stresses are in accordance with the results obtained in section **5.4.2.1.** An interesting outcome from this simulation was the observation that it is theoretically not impossible to have small micro-annuli in set cement that is masked during a 30-minute pressure test.

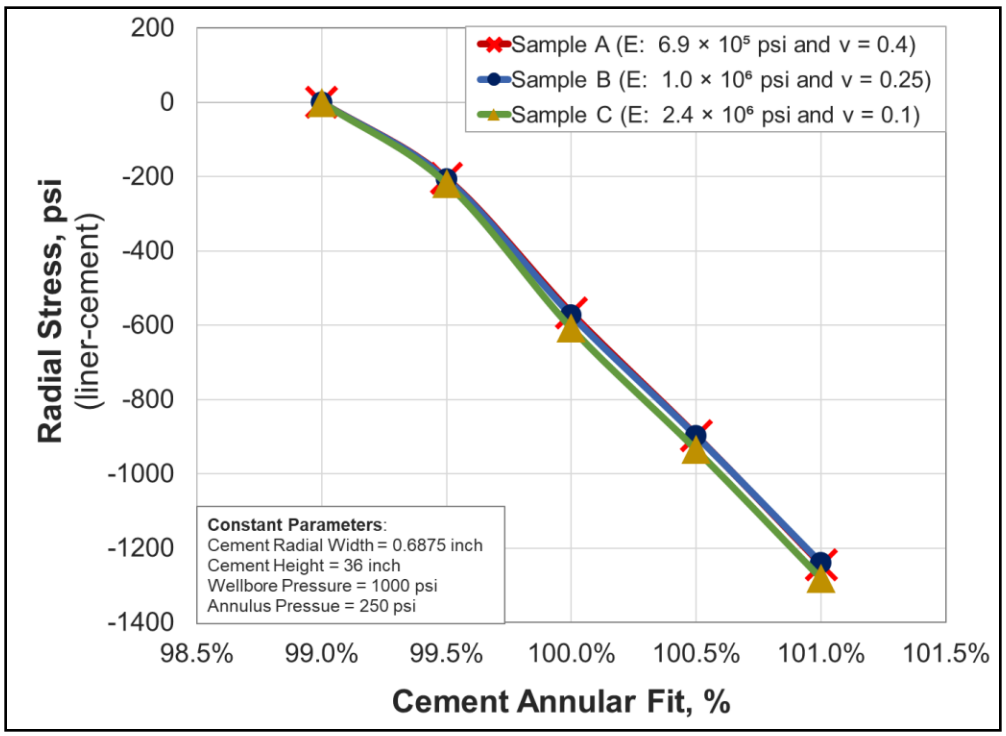

Figure 5.30: Effect of cement annular fit on radial stress in cement at liner-cement interface

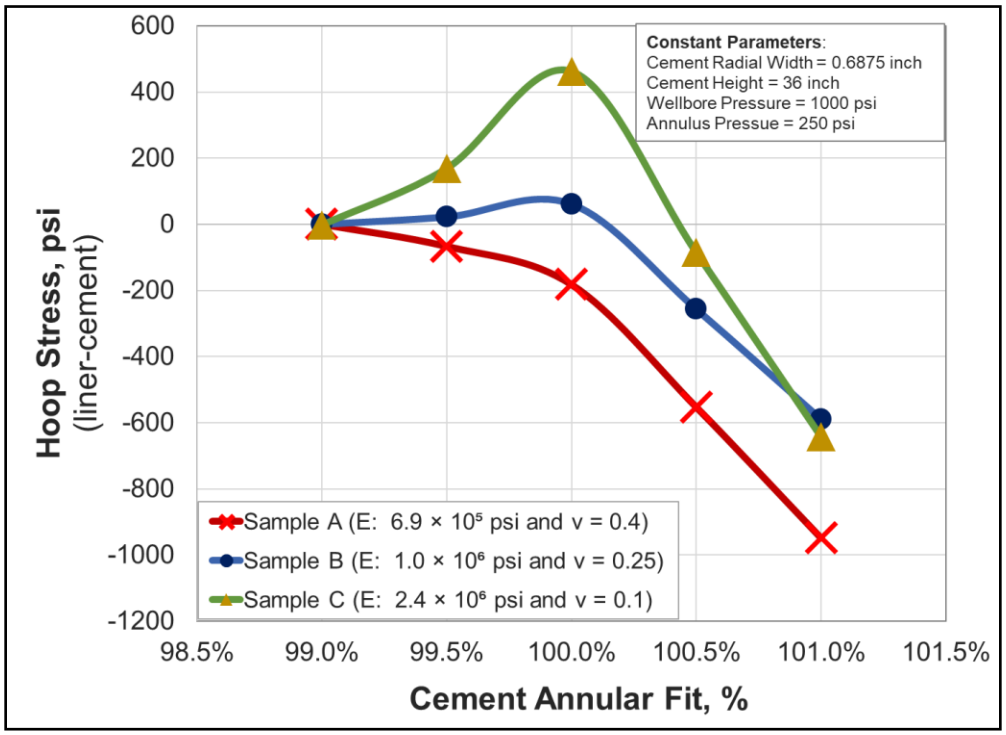

Figure 5.31: Effect of cement annular fit on hoop stress in cement at liner-cement interface

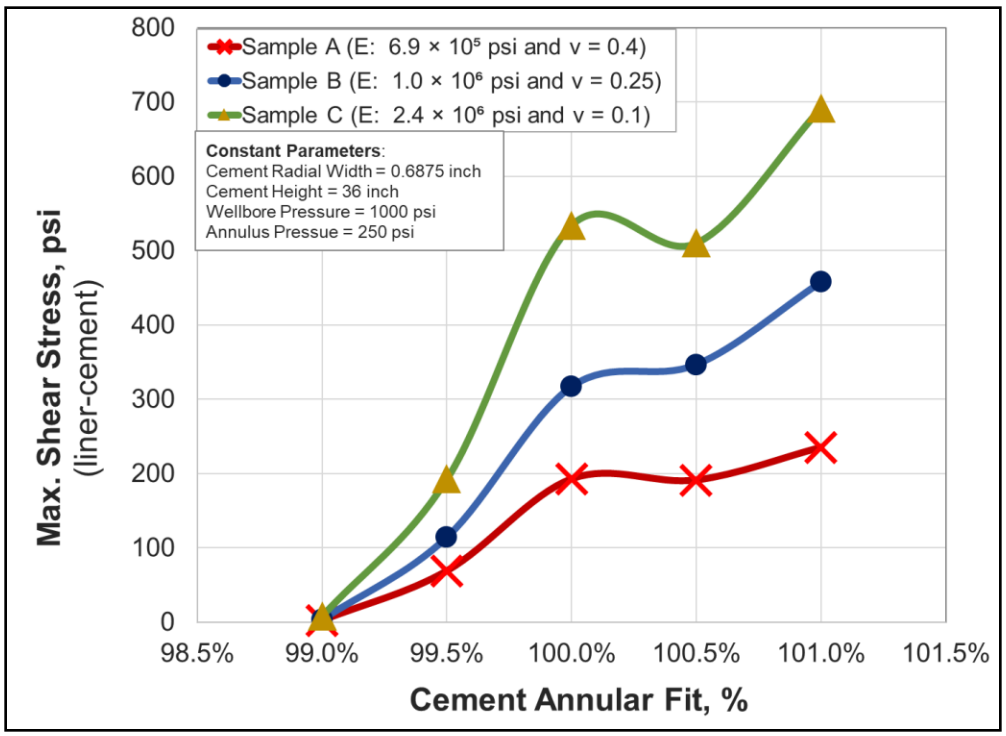

Figure 5.32: Effect of cement annular fit on maximum shear stress in cement at liner-cement interface

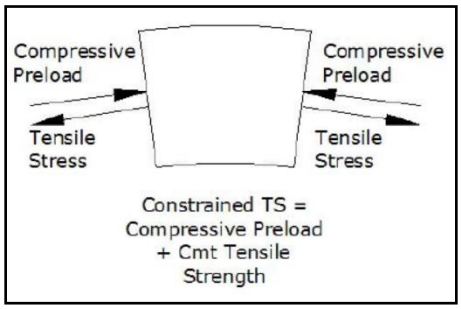

Figure 5.33: Pre-stressed expansive cement system (Teodoriu et al. 2008)

Annular fit of 100.5% and 101% mimic pre-stress conditions found in special type of cements known as expansive cement (Teodoriu et al. 2008). As shown in Figure 5.33, this type of cement develops internal compressive stress when set. When a wellbore pressure is applied, the tensile hoop stress generated by the pressure first needs to compensate for the compressive pre-load before a net tensile stress is generated. This leads to a reduction in the effective magnitude of stresses that is generated by external loads, provides more margin of safety from failure, and minimizes tensile or compressive strength requirement. This effect can be visualized in the simulation results. For the same constant wellbore pressure of 1000 psi, the hoop stress decreases as pre-load (or annular fit) increases. This can significantly minimize the risk of radial crack failure. On the contrary, the maximum shear stress increases because of pre-load. This can make things worse by reducing the

safety margin on shear failure. Thus, the selection of expansive cement should be made after carefully weighing potential benefits against the risks.

5.4.2.6 Young's Modulus

Young's modulus is a critical material property that defines the stiffness of cement sheath. As discussed in section **5.4.2.1**, a cement sheath with low Young's modulus and high tensile strength would have a low possibility of failure. When a neat cement sets, it becomes a brittle material. But researchers and manufacturers have tried various recipes to improve flexibility by adding elastomeric material or creating a foam. The objective of this simulation task was to isolate and observe the effect of Young's modulus on various stresses in set cement. For this purpose, the modulus was varied from 6.9×10^5 psi to 2.4×10^6 psi at a constant Poisson's ratio of 0.1, 0.25, and 0.4. The wellbore and annulus pressures were kept constant at 1000 psi and 250 psi respectively. The effect of Young's modulus on radial, hoop, and maximum shear stresses developed in the cement at the liner-cement interface is presented in Figure 5.34, Figure 5.36, and Figure 5.36.

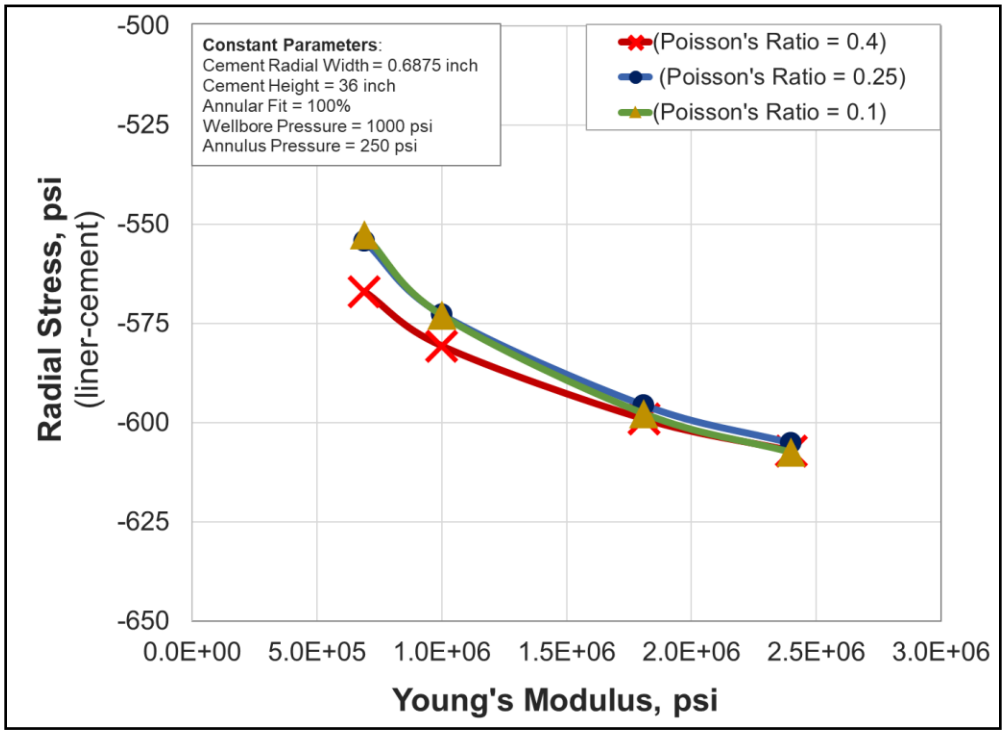

Figure 5.34: Effect of Young's modulus on radial stress in cement at liner-cement interface

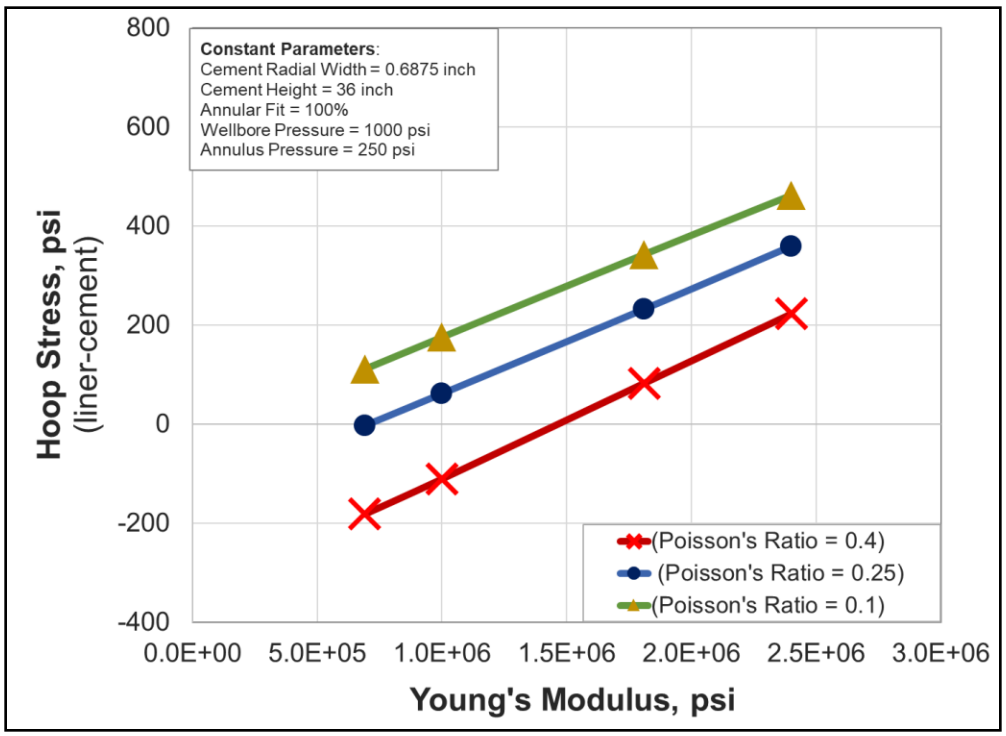

Figure 5.35: Effect of Young's modulus on hoop stress in cement at liner-cement interface

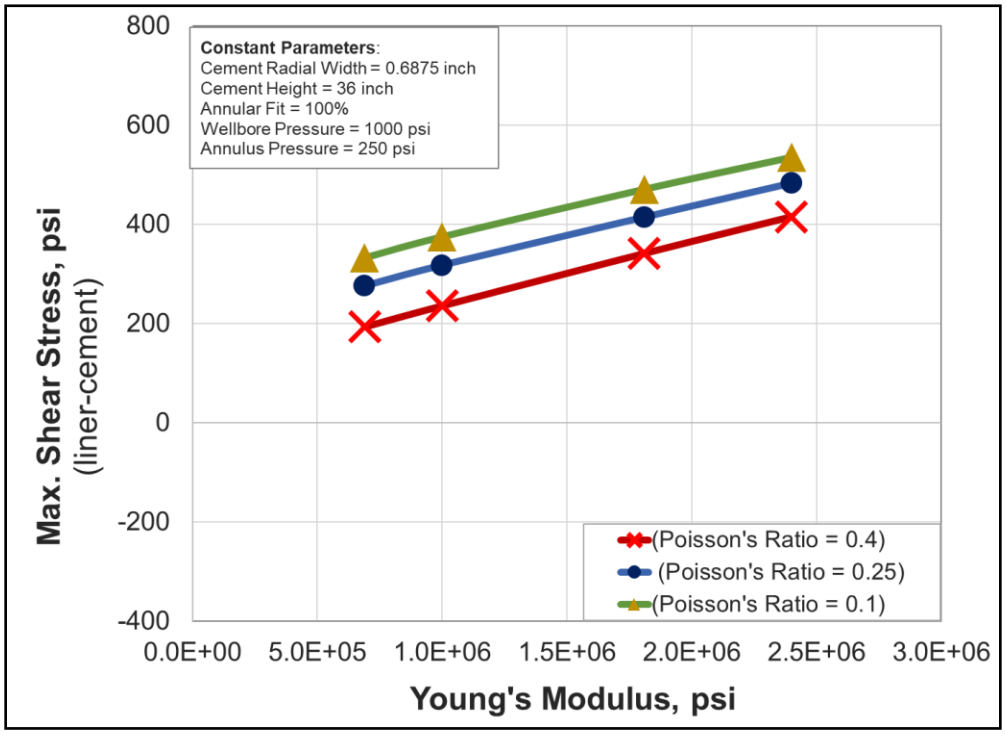

Figure 5.36: Effect of Young's modulus on maximum shear stress in cement at liner-cement interface

As shown in Figure 5.34, radial stress increases in magnitude (i.e. becomes more compressive) as Young's modulus increases. This is an expected trend and was also observed in section **5.4.2.1.** The relationship is quadratic and practically independent of Poisson's ratio. The reduction in the magnitude of radial stress is only about 7% after increasing the Young's modulus approximately 43 times. Therefore, the overall effect on radial stress is practically not important.

Unlike radial stress, the hoop and maximum shear stresses exhibit linear correlation with Young's modulus. An increase in Young's modulus resulted to an increase in both stresses. The increase is independent of Poisson's ratio. If each of the curves in Figure 5.35 and Figure 5.36 are shifted to coincide, then it can be calculated that each 100,000 psi increase in Young's modulus results in 20 psi to 24 psi and 11 psi to 14 psi increase in hoop and maximum shear stresses respectively. The amount may seem low, but it is relatively important when compared with typical tensile strengths of cement sheath such as a neat Class H that has a tensile strength of about 400 psi (Iverson et al. 2008). Another important effect can be seen in the case of hoop stress in cement with a high Poisson's ratio of 0.4 (Figure 5.35). Any further increase in Young's modulus beyond 1.5×10^6 psi changes hoop stress from compressive to tensile, making tensile strength the limiting strength and significantly reducing the safety factor.

Overall, all other factors being equal, as cement sheath becomes more brittle (i.e. Young's modulus increases), the likelihood of radial cracking and shear failure increases. Radial bonding on the other hand, has no important sensitivity to the flexibility of cement sheath.

5.4.2.7 Poisson's Ratio

Similar to Young's modulus, Poisson's ratio is a critical material property that governs material behavior (deformations/stresses) in directions perpendicular to the applied load. It is difficult to control or design Poisson's ratio independent of Young's modulus. Nevertheless, it is important to isolate and understand its effect on the risk of cement failure. In this simulation task, Poisson's ratio was varied from 0.1 to 0.45 at three different Young's moduli (6.9×10^5 psi, 1.0×10^6 psi, and 2.4×10^6 psi). The wellbore and annulus pressure were kept constant at 1000 and 250 psi respectively. Simulated radial, hoop, and maximum shear stresses are shown in Figure 5.37, Figure 5.38, and Figure 5.39 respectively.

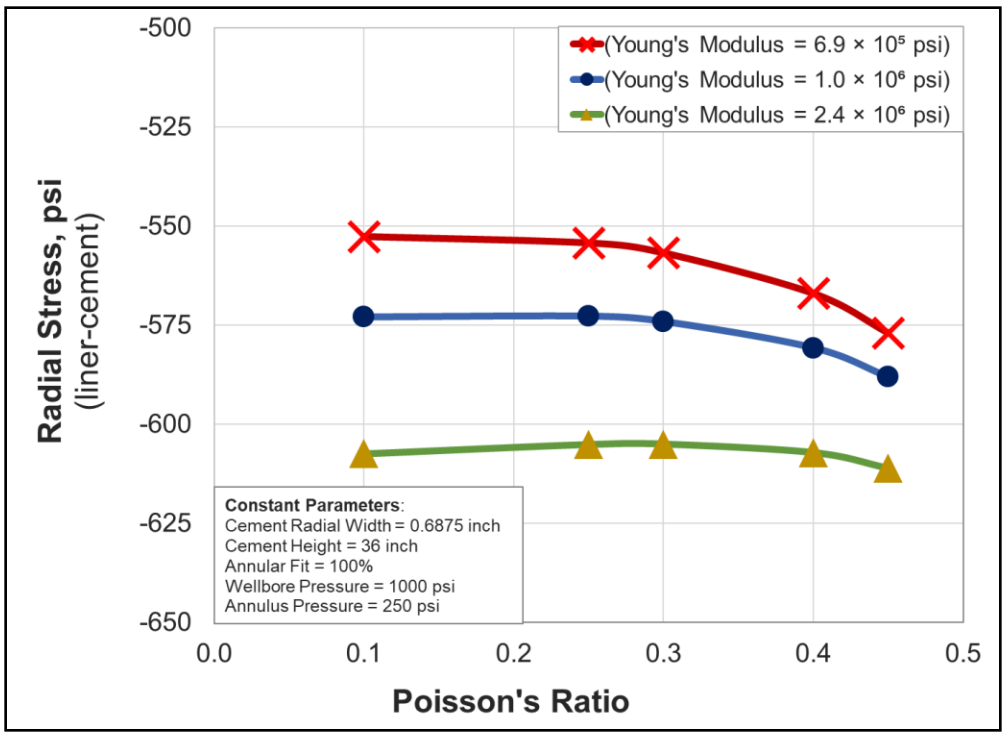

Figure 5.37: Effect of Poisson's ratio on radial stress in cement at liner-cement interface

As shown in Figure 5.37, Poisson's ratio (up to 0.3) has no effect on radial stress. Further increase resulted in an increased magnitude of radial stress. The trend is similar for all the three cases of Young's modulus. The increment however, is not significant and can be ignored for practical purposes.

Unlike radial stress, Figure 5.38 and Figure 5.39 shows that , Poisson's ratio has a clear and well defined correlation with both hoop and shear stresses. An increase in Poisson's ratio reduces the stresses (i.e. tensile stress become less tensile and compressive stress become more compressive). The effect is notable and the difference in hoop stress (between Poisson's ratio of 0.1 and 0.4) is more than 300 psi. In the case of maximum shear stress, the difference is more than 150 psi. Thus, for wellbore pressure increment of 1000 psi, a higher Poisson's ratio is preferable as it has a lower likelihood of failure. It should be noted that the change in wellbore pressure may affect the trend. This is discussed in the next section.

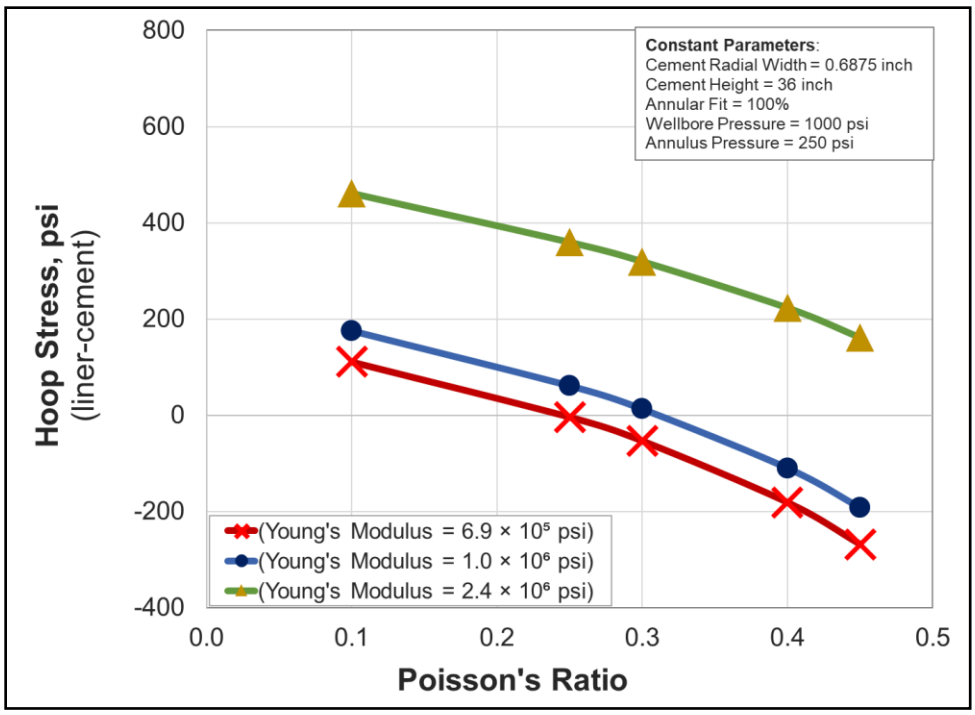

Figure 5.38: Effect of Poisson's ratio on hoop stress in cement at liner-cement interface

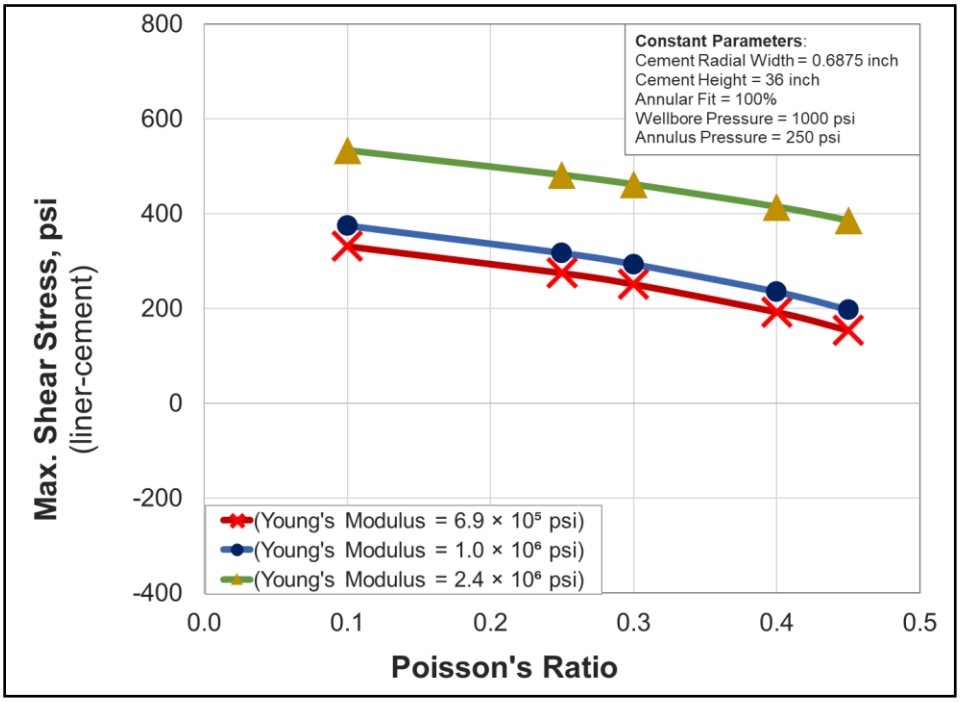

Figure 5.39: Effect of Poisson's ratio on maximum shear stress in cement at liner-cement interface

5.4.2.8 Interdependency of Wellbore Pressure and Material Properties

It was observed that wellbore pressure and material properties are inter-dependent. Hence, for the sake of easier comparison and understanding, the results are discussed based on the type of cement system –

- LYLP: Low Young's modulus & low Poisson's ratio (6.9×10^5 psi and 0.1)
- LYHP: Ductile cement i.e. low Young's modulus & high Poisson's ratio (6.9×10^5 psi and 0.4)
- HYLP: Brittle cement i.e. high Young's modulus & low Poisson's ratio (2.4×10^6 psi and 0.1)
- HYHP: High Young's modulus & high Poisson's ratio (2.4×10^6 psi and 0.4)

The fourth type of cement system is highly unlikely to exist, but it has been included as a theoretical comparison.

Radial Stress

The effect of Young's modulus, Poisson's ratio, and wellbore pressure on radial stress is graphically summarized in Figure 5.40. Important observations are as follows:

- An increase in wellbore pressure leads to a slight increase in the magnitude of radial stress. The effect is slightly more pronounced in the case of high Young's modulus cement systems.
- The nature of radial stress is compressive for decreasing wellbore pressure and tensile for increasing the wellbore pressure. Hence, for the same amount of pressure change, decreasing wellbore pressure is more detrimental than increasing pressure as the cement systems typically have higher compressive strength than tensile strength.
- In terms of magnitude of radial stress, there is no significant difference among the four types of cement systems and there is no conclusive evidence to indicate if one system is more robust to debonding or stress crushing type of failure than the other.

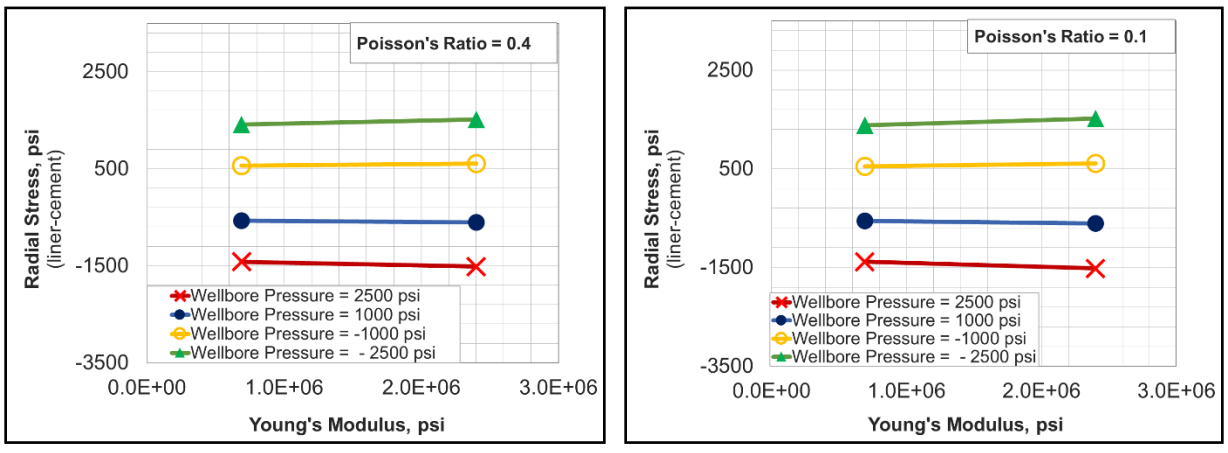

(a) **(b)**

Figure 5.40: Effect of Young's modulus and wellbore pressure on radial stress in cement at liner-cement interface – comparison between Poisson's ratio of 0.4 (a) and 0.1 (b)

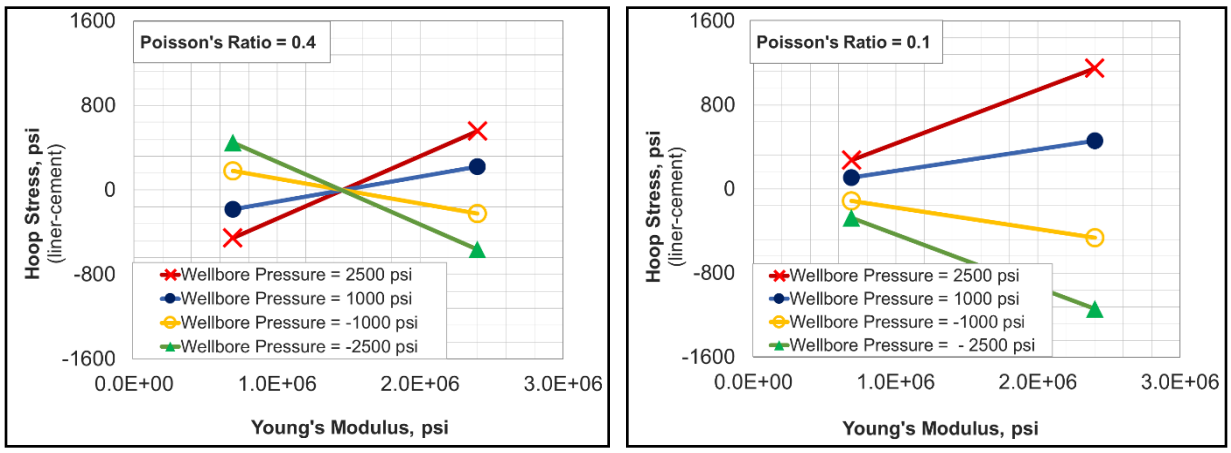

(a) **(b)**

Figure 5.41: Effect of Young's modulus and wellbore pressure on hoop stress in cement at liner-cement interface – comparison between Poisson's ratio of 0.4 (a) and 0.1 (b)

Hoop Stress

The effect of Young's modulus, Poisson's ratio, and wellbore pressure on hoop stress is graphically summarized in Figure 5.41. The following are useful observations:

- An increase in the wellbore pressure increases the magnitude of hoop stress in all cement systems. In terms of (i) magnitude of hoop stress at a constant wellbore pressure and (ii) sensitivity to change in wellbore pressure, the decreasing order of cement system is HYLP > HYHP > LYHP > LYLP. This implies that LYLP system has the least sensitivity to wellbore pressure and develops the smallest hoop stress in terms of magnitude than any other system at a constant wellbore pressure. Thus, LYLP followed by LYHP should be the preferred cement system to minimize risk of radial cracks.
- Unlike LYHP, all other cement systems developed a tensile hoop stress under increasing wellbore pressure load and developed a compressive hoop stress under decreasing pressure load. This trend is reversed for LYHP cement.
- For each Poisson's ratio, there is a critical Young's modulus at which the hoop stress becomes zero and changes direction. This optimum point does not appear to be changing significantly with change in pressure loads. This point moves towards higher Young's modulus as Poisson's ratio increases.
- Hoop stress and Young's modulus are linearly correlated. The magnitude of the slope (i.e. sensitivity of hoop stress to change in modulus) increases with increasing magnitudes of wellbore pressure. The sensitivity does not depend greatly on Poisson's ratio. At wellbore pressures of 1000 psi and 2500 psi, hoop stress changes by approximately 20 psi and 60 psi respectively per 100,000 psi change in Young's modulus.
- The sensitivity of hoop stress to change in Poisson's ratio depends on Youngs modulus as well as wellbore pressure. At wellbore pressures of 1000 psi and 2500 psi and a Young's modulus

of 2.4×10^6 psi, hoop stress changes by approximately 80 psi and 200 psi respectively per 0.1 change in Poisson's ratio.

Maximum Shear Stress

The effect of Young's modulus, Poisson's ratio, and wellbore pressure on hoop stress is graphically summarized in Figure 5.42. Unlike hoop stress, the trends are straight forward.

- An increase in the magnitude of wellbore pressure load linearly increases the maximum shear stress. At a given pressure load, in terms of magnitude of maximum shear stress, the decreasing order of cement systems is – HYLP > HYHP > LYLP > LYHP. This indicates that the cement system LYHP has the lowest risk of shear failure followed by LYLP. Overall, low Young's modulus cement systems are more robust to shear failures.
- Maximum shear stress is linearly correlated to Young's modulus. The sensitivity of stress magnitude to change in the modulus (i.e. the slope of the lines in Figure 5.42) increases with an increase in wellbore pressure. The sensitivity does not change with Poisson's ratio. At wellbore pressures of 1000 and 2500 psi, maximum shear stress changes by approximately 10 psi and 30 psi respectively per 100,000 psi change in Young's modulus.

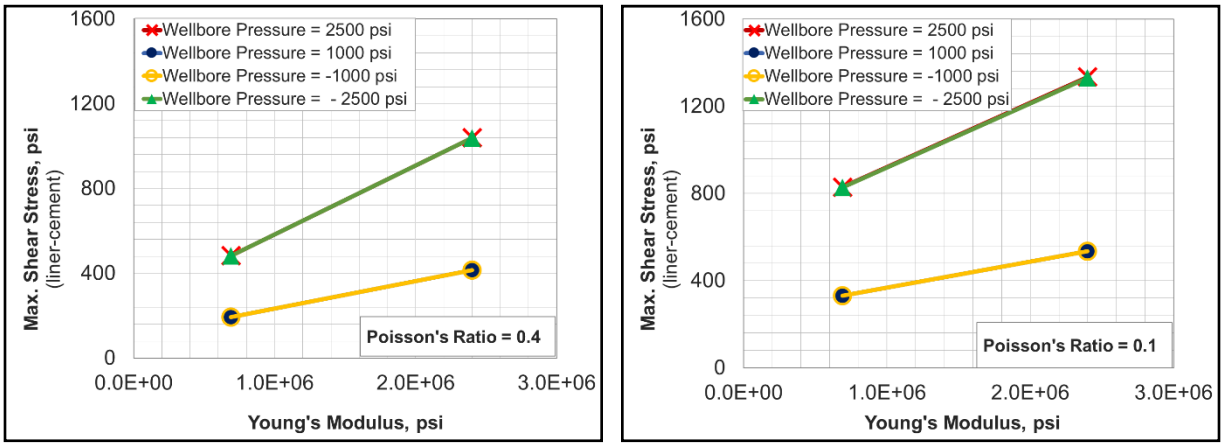

Figure 5.42: Effect of Young's modulus and wellbore pressure on maximum shear stress in cement at liner-cement interface – comparison between Poisson's ratio of 0.4 (a) and 0.1 (b)

5.4.2.9 Effect of Temperature

As stated in the scope of this project, the effect of temperature has been included in form of change in material properties. The temperature effect on cement performance can be indirectly predicted by observing and understanding the effect of change in Young's modulus and Poisson's ratio on cement integrity. If the Young's modulus and Poisson's ratio of cement is known at the desired temperature then, the performance curves developed in the present simulation study can be used to estimate the temperature effect.

For example, let's predict the effect of increasing the curing temperature from 75°F to 167°F on a Class G cement. As shown in Table 5.8, at a higher temperature, the cement exhibits

higher Young's modulus, and lower Poisson's ratio. Essentially, the cement becomes more brittle and shows a characteristic that is similar to HYLP in comparison to HYHP cement system (discussed in the previous section). This transition will not have a notable effect on radial stress as shown in Figure 5.39. However, for the same pressure loading, the hoop stress will be notably higher for this HYLP characteristic at the higher temperature (Figure 5.40). Similarly, the maximum shear stress also increases notably at a higher temperature (Figure 5.41). For example, at wellbore pressure increment of 2500 psi, the tensile hoop stress and maximum shear stress generated at 167°F will be 1120 psi and 1320 psi respectively in comparison to 560 psi and 1040 psi respectively at 75°F. The cement would fail by radial cracking as its tensile strength after 7 days of curing at 167°F is about 536 psi (Teodoriu et al. 2012).

Table 5.8: Mechanical properties of class G cement at two different temperatures (Teodoriu et al. 2012)

Temperature, °F	Young's Modulus, psi	Poisson's Ratio
75	2.32×10^6	0.3
167	2.55×10^6	0.2

Similar risk analysis can be performed for any type of cement system, using the performance curves generated in this work, as long as the material properties are known at the desired temperature. It is challenging to generalize the temperature effect and include temperature explicitly as an independent variable because different cements with various additives will exhibit distinct behavior in temperature effects on mechanical properties. It is more practical to examine cement performance as a function of material properties.

5.4.2.10 Sensitivity Analysis

To compare the sensitivity of radial, hoop, and maximum shear stresses to all the parameters discussed so far, normalized plots were prepared. As shown in Table 5.9, a base case with material properties of cement Sample B was selected and each of the 7 parameters were varied, keeping the rest constant. Values of each parameter were normalized by dividing it with the base value. 33 cases were simulated and radial, hoop, and maximum shear stresses generated at liner-cement interface were obtained. The normalized plots are provided in Figure 5.43, Figure 5.44, and Figure 5.45.

Table 5.9: List of parameters and corresponding values used in normalized plots of radial, hoop, and maximum shear stresses

Parameter	Different Values Used in Simulations							
Wellbore Pressure, psi	-1000.0 (-1.0)	-500.0 (-0.5)	0.0 (0.0)	500.0 (0.5)	1000.0 (1.0)	1500.0 (1.5)	2500.0 (2.5)	
Annulus Pressure, psi				0.0 (0.0)	250.0 (1.0)	500.0 (2.0)	1000.0 (4.0)	1500.0 (6.0)
Cement Height, inch				18.0 (0.50)	36.0 (1.00)	64.0 (1.78)	100.0 (2.78)	
Cement Width, inch				0.3 (0.36)	0.6875 (1.00)	1.0 (1.45)		
Annular Fit, fraction			0.990 (0.990)	0.995 (0.995)	1.000 (1.000)	1.005 (1.005)	1.010 (1.010)	
Young's Modulus, psi				6.9E+05 (0.69)	1.0E+06 (1.00)	1.8E+06 (1.81)	2.4E+06 (2.40)	
Poisson's Ratio				0.10 (0.4)	0.25 (1.0)	0.30 (1.2)	0.40 (1.6)	0.450 (1.8)

Note: In Table 5.9, each value represents a complete simulation case with rest of the parameters being equal to the base values. Values in parentheses are corresponding normalized values.

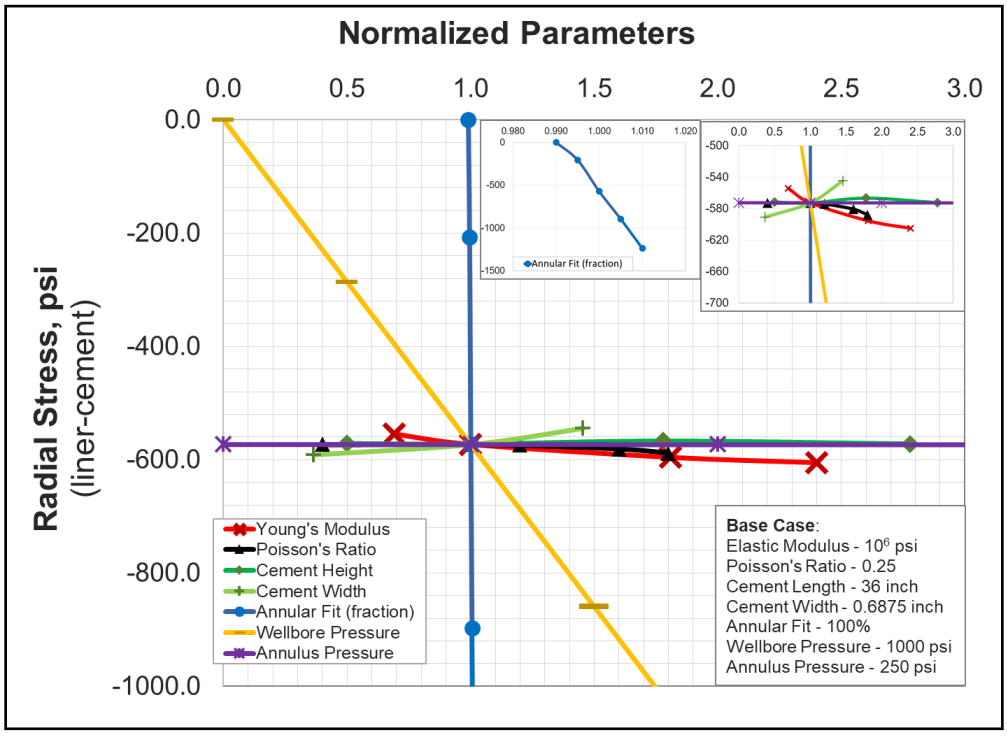

Figure 5.43: Sensitivity of radial stress to various parameters with cement Sample B as base case

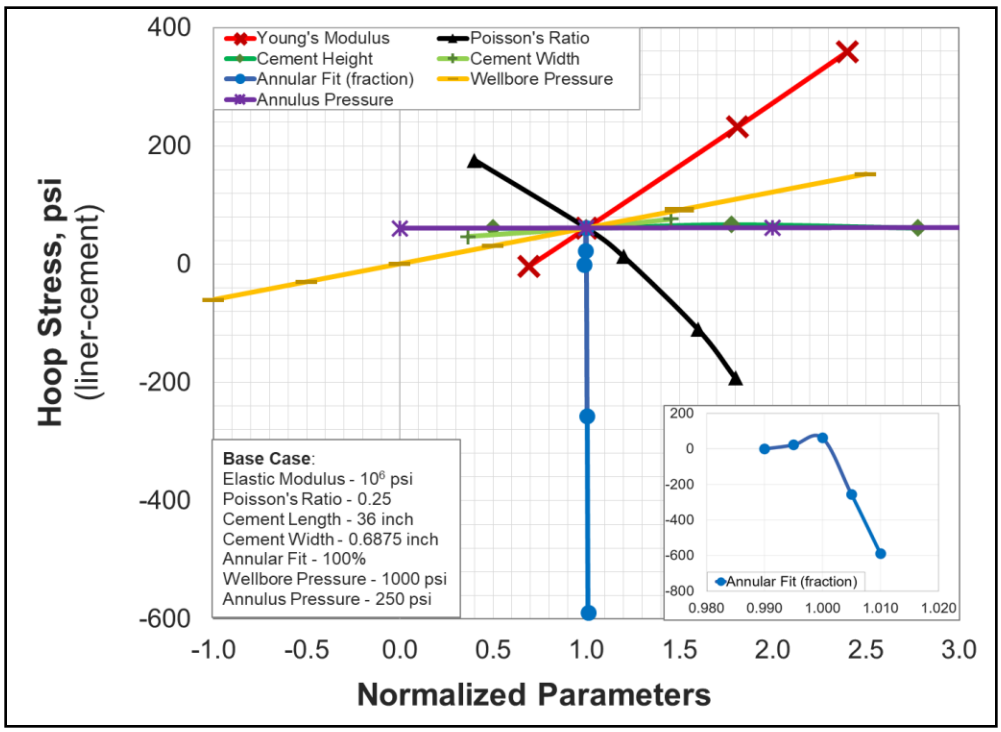

Figure 5.44: Sensitivity of hoop stress to various parameters with cement Sample B as base case

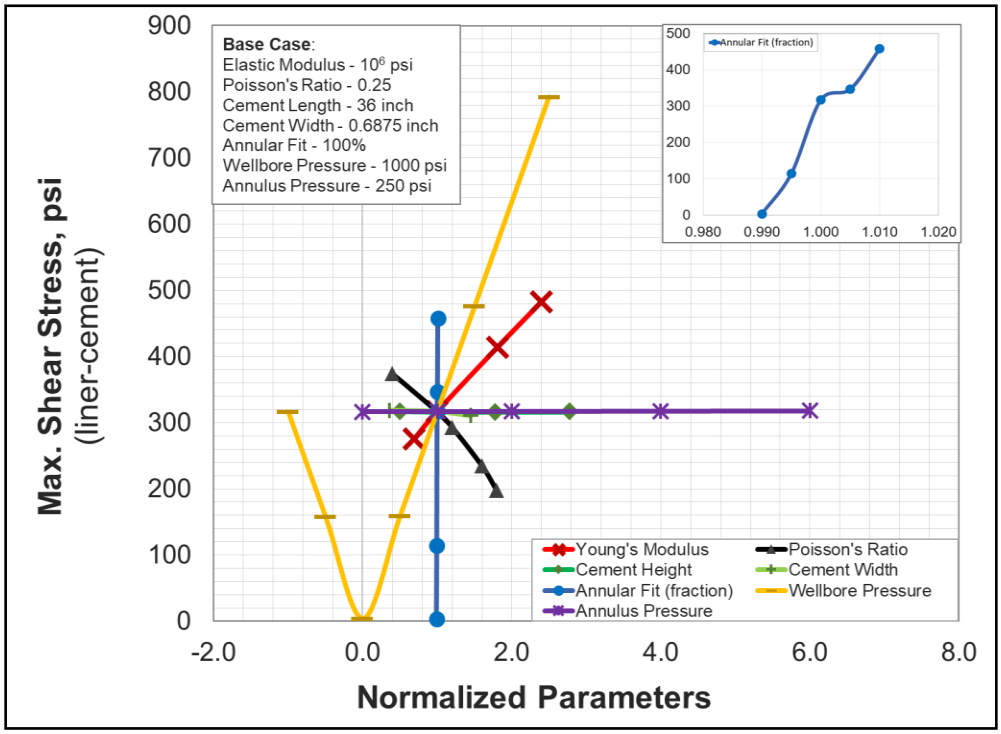

Figure 5.45: Sensitivity of maximum shear stress to various parameters with cement Sample B as base case

Radial Stress:

- Radial stress has the highest sensitivity to annular fit. This implies that the presence of micro-annuli (because of volume shrinkage or improper centralization) has a huge impact on contact stress (i.e. radial stress), compared to any other factor. Thus, preventing it should be the first priority in designing an effective cementing job.
- High sensitivity to annular fit also means that pre-stressed expansive cement can provide significant benefits in achieving higher compressive radial stresses and better sealability.
- The second most critical parameter is change in wellbore pressure. Decreasing pressure is more detrimental than increasing pressure because tensile strength governs the risk of failure and it's typically less than compressive strength for common cement systems.
- The effect of Young's modulus, Poisson's ratio, and cement width are approximately the same in terms of magnitude but notably less than wellbore pressure and annular fit. Other parameters – annulus pressure and cement height are of no importance.

Hoop Stress:

- Similar to radial stress, hoop stress also has the highest sensitivity to annular fit. It's slightly less in the case of radial stress, but still highly significant.
- Unlike in the case of radial stress, Poisson's ratio and Young's modulus have notable impacts on hoop stress.
- For this cement system B, the effect of wellbore pressure is not as significant for hoop stress as in the case of radial stress.
- Other parameters - annulus pressure and cement height - are of no importance.

Maximum Shear Stress:

- Annular fit is still the most important factor. Annular fit more than 100% tends to increase the maximum shear stress. Hence, the effect of having a pre-stressed system is not beneficial like in the case of radial and hoop stress.
- Wellbore pressure is the second most dominant factor. Followed closely by Poisson's ratio and Young's modulus. Other factors - cement width, cement height, and annulus pressure - are not important.

To examine if the sensitivity of various parameters discussed above changes with material properties, 66 additional simulation cases were run using ductile cement (Sample A) and brittle cement (Sample C) as base cases. The sensitivity plots are provided in Figure 5.46 to Figure 5.51. The summary of sensitivity for all three cement samples is provide in Table 5.10.

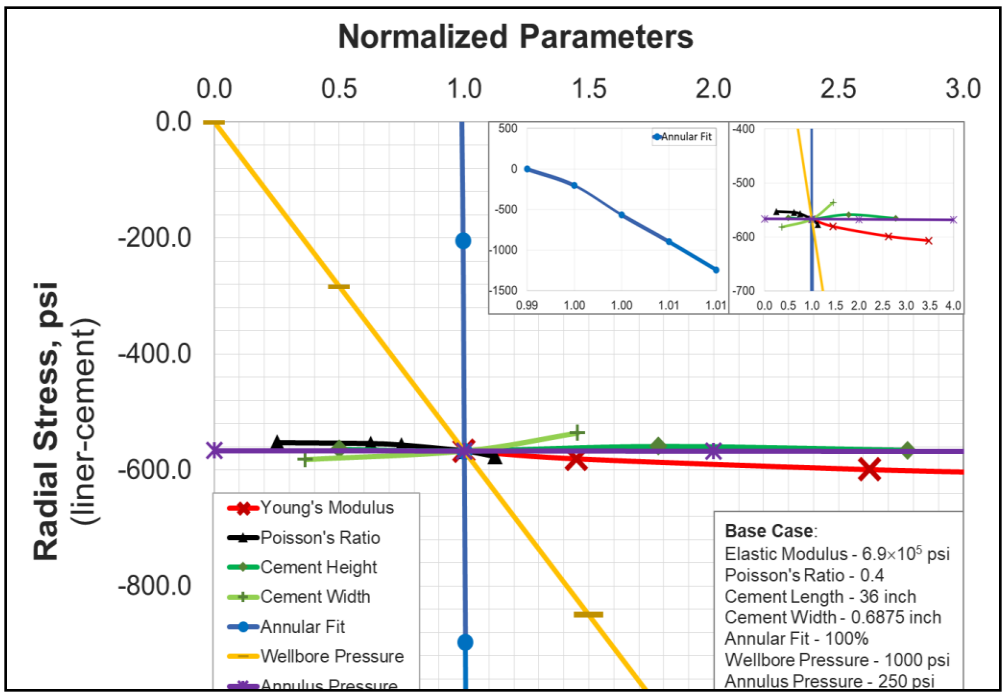

Figure 5.46: Sensitivity of radial stress to various parameters with cement Sample A as base case

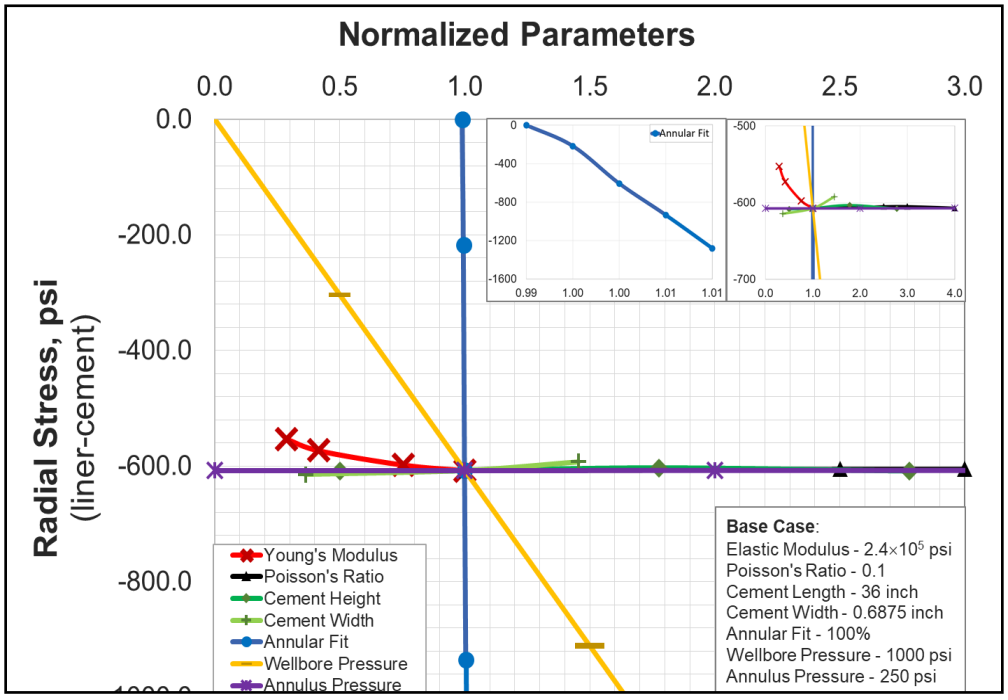

Figure 5.47: Sensitivity of radial stress to various parameters with cement Sample C as base case

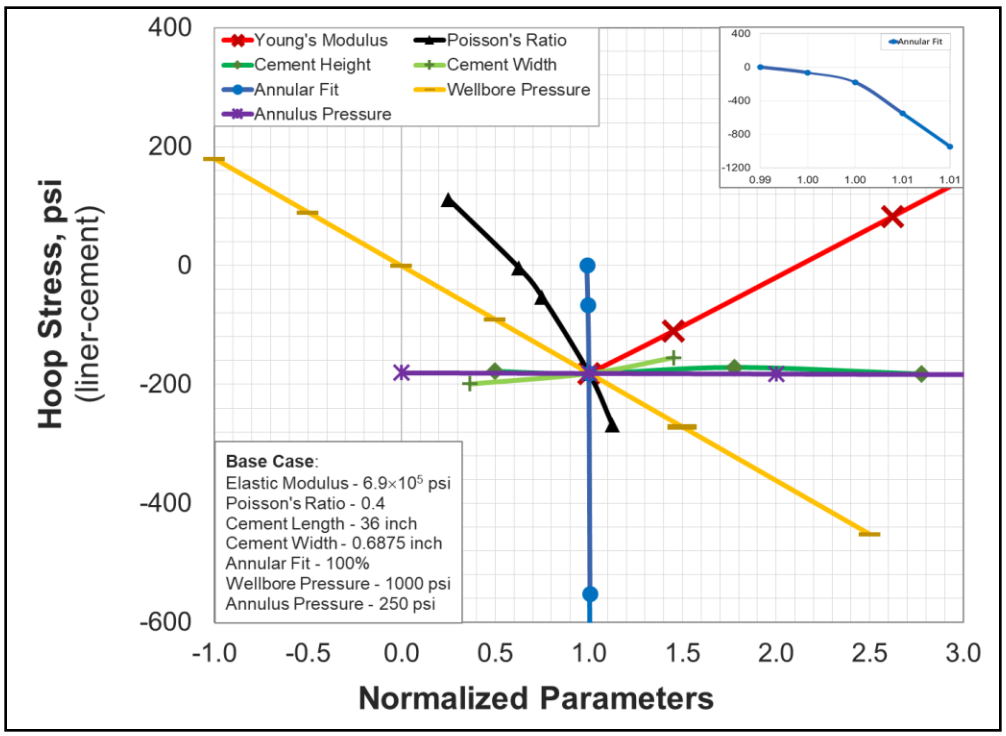

Figure 5.48: Sensitivity of hoop stress to various parameters with cement Sample A as base case

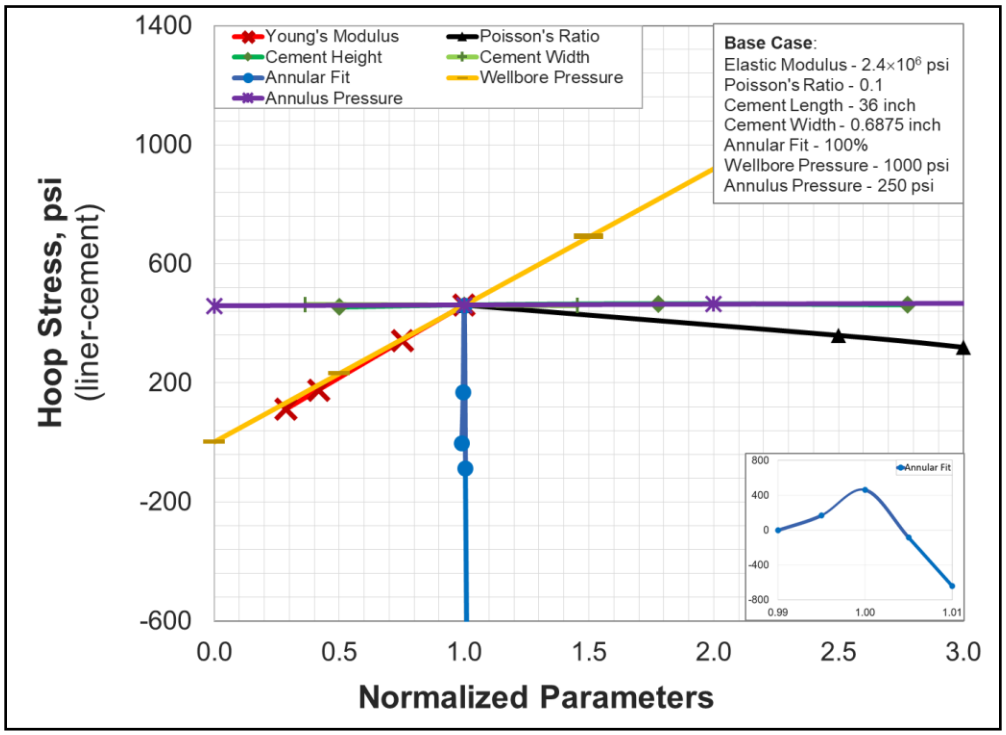

Figure 5.49: Sensitivity of hoop stress to various parameters with cement Sample C as base case

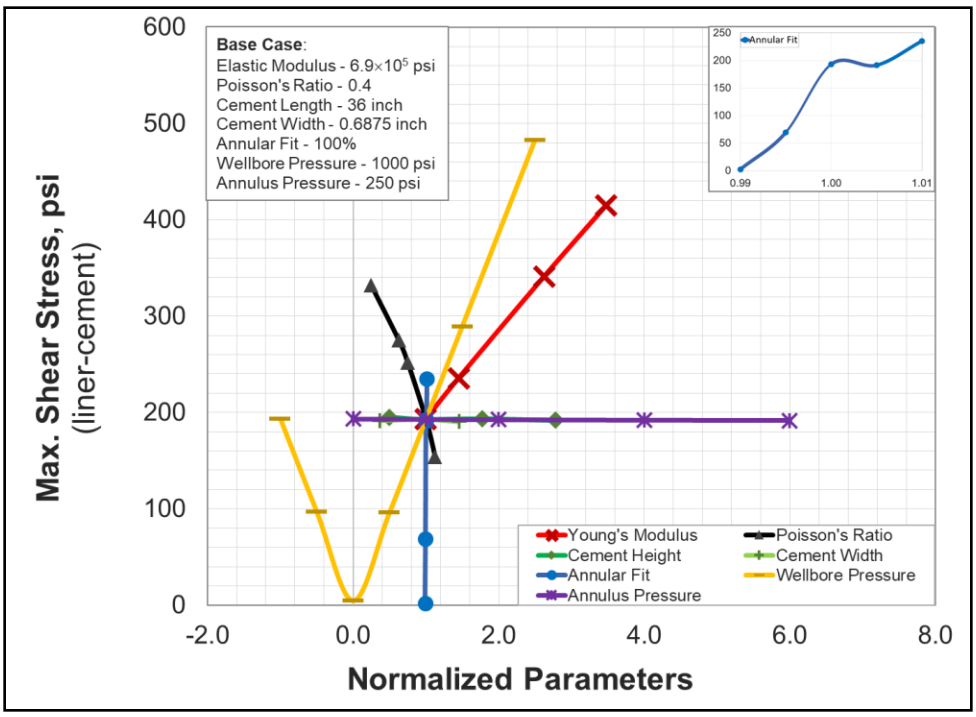

Figure 5.50: Sensitivity of maximum shear stress to various parameters with cement Sample A as base case

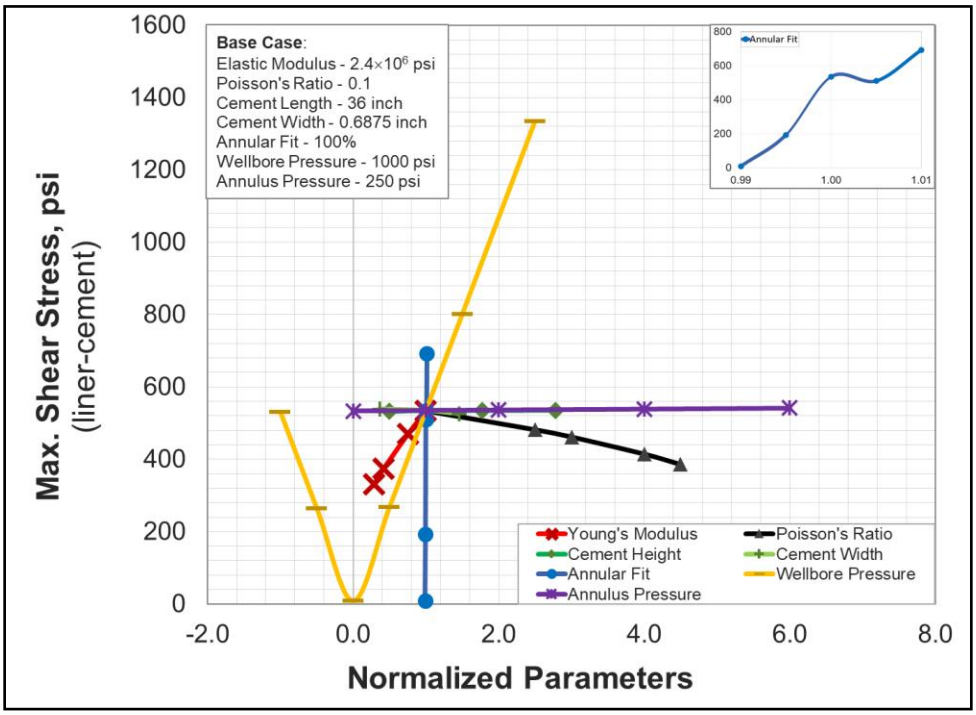

Figure 5.51: Sensitivity of maximum shear stress to various parameters with cement Sample C as base case

Table 5.10: Summary of sensitivity analysis for all three cement systems examined
(Decreasing order of importance)

Cement Sample	Radial Stress	Hoop Stress	Max. Shear Stress
Sample A (E: 6.9×10^5 psi and $\nu = 0.4$)	$\delta >> \Delta P > \nu \approx E \approx t$	$\delta >> \nu > \Delta P \approx E >> t$	$\delta >> \Delta P > \nu \approx E > t$
Sample B (E: 1.0×10^6 psi and $\nu = 0.25$)	$\delta >> \Delta P > E \approx \nu \approx t$	$\delta >> \nu \approx E > \Delta P >> t$	$\delta >> \Delta P > \nu \approx E > t$
Sample C (E: 2.4×10^6 psi and $\nu = 0.1$)	$\delta >> \Delta P > E > \nu \approx t$	$\delta >> \Delta P \approx E >> \nu > t$	$\delta >> \Delta P > E > \nu > t$
δ: Annular fit; ΔP = Change in wellbore pressure; ν = Poison's ratio; E = Young's Modulus; t = Cement radial width			

5.4.2.11 Risk Assessment

As shown in the sensitivity analysis (Table 5.10), annular fit is the most important factor affecting cement performance, regardless of the cement type or operating pressure/temperature conditions. An annular fit that is less than 100% (i.e. lack of cement bonding) would pose an instant sealability failure and also increase the risk of mechanical failure.

For shallow depth wells, radial mechanical failure (debonding and stress crushing) is highly unlikely. Radial debonding can only occur in the event of decreasing wellbore pressure when radial stresses become tensile. Stress crushing is highly unlikely because the cement would fail by radial cracking when the hoop stress exceeds tensile strength, before it fails by compressive radial stress exceeding compressive strength. Let's consider two scenarios to support the above conclusion. For typical depths of conductor and surface casings in shallow offshore wells, the changes in wellbore pressure after the cement has set would not typically range beyond ±1500 psi. Let's compare the risk of failure in different cement samples by calculating the safety factor. The tensile and compressive strength of the cement samples used are provided in Table 5.11. The failure criteria are discussed in **section 5.2.2**. As shown in Table 5.11, none of the samples exhibited failure i.e. safety factor of less than 1.0. Even for wellbore pressure increase of 2500 psi, the safety factor remains above 1.0 (Table 5.12). For wellbore pressure reduction of 2500 psi, which is highly unlikely at the shallow depths, only sample A exhibited a safety factor of 0.7 (Table 5.12). In shallow depth wells, thermal stresses are not expected to be significant. Consequently, material properties i.e. Young's modulus and Poisson's ratio are also not expected to change notably.

Table 5.11: Comparison of likelihood of cement failure for wellbore pressure change of 1500 psi

Cement	$\Delta P_{wellbore}$ = 1500 psi			$\Delta P_{wellbore}$ = - 1500 psi		
	$SF_{debonding}$	$SF_{radial\ cracking}$	SF_{shear}	$SF_{debonding}$	$SF_{radial\ cracking}$	SF_{shear}
Sample A	3.5	10.6	5.2	1.2	3.7	5.2
Sample B	5.2	16.5	4.7	1.7	49.4	4.7
Sample C	10.5	4.3	6.0	3.3	13.3	6.0

Table 5.12: Comparison of likelihood of cement failure for wellbore pressure change of 2500 psi

Cement	$\Delta P_{wellbore}$ = 2500 psi			$\Delta P_{wellbore}$ = - 2500 psi		
	$SF_{debonding}$	$SF_{radial\ cracking}$	SF_{shear}	$SF_{debonding}$	$SF_{radial\ cracking}$	SF_{shear}
Sample A	2.1	6.6	3.1	0.7	2.2	3.1
Sample B	3.1	9.9	2.8	1.0	29.6	2.8
Sample C	6.3	2.6	3.6	2.0	8.3	3.6

Based on the above discussion, it can be summarized that for shallow depth wells, mechanical failure and material properties changes are highly unlikely. Thus, from the mechanical point of view, the most important factor controlling cement performance as a barrier is annular fit i.e. bonding. In addition (as concluded from setup – I and setup – II experiments), gas migration during cement setting process and inherent permeability of cement are other critical factors that affect the cement sheath's performance as a hydraulic barrier.

5.4.2.12 Analytical Validation

The FEA model of cement was validated by comparing the analytically derived radial and hoop stresses at the liner-cement interface with the ones predicted by the FEA model. The analytical model is based on plane strain equations for composite thick cylinders. The derivation of contact stress at liner-cement and cement-casing interface is provided in the **Appendix A** of the leakage modelling and risk assessment report. As shown in Figure 5.52 and Figure 5.53**,** the accuracy of the FEA model is good. The error in radial stress prediction was between 0 to 0.4% while in the case of hoop stress, it ranged from 0 to about 4.4%.

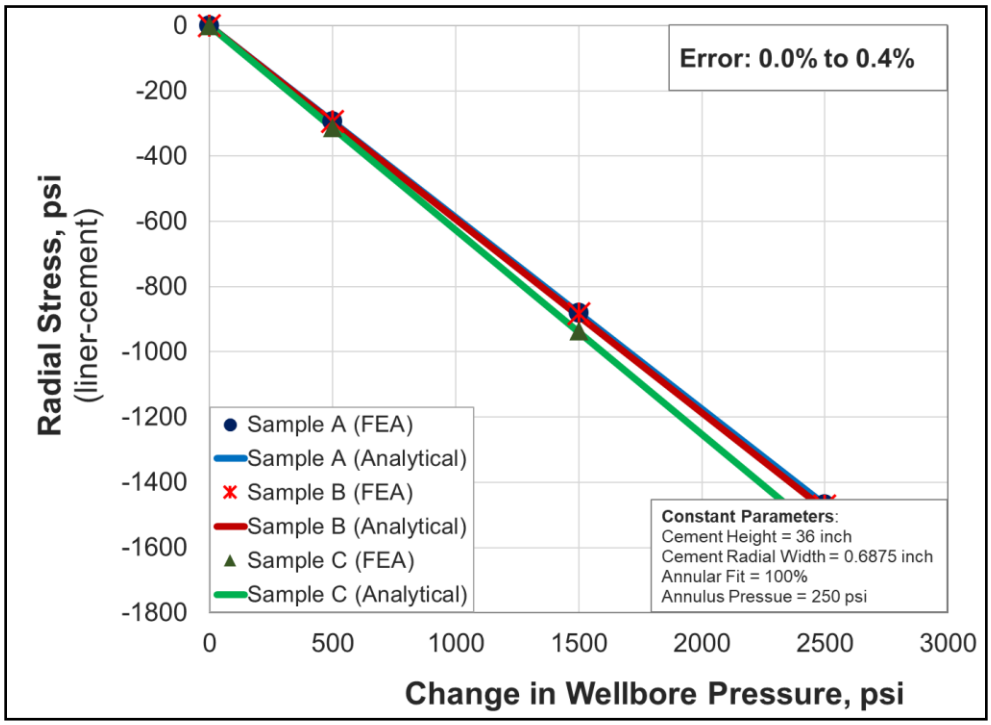

Figure 5.52: Comparison between FEA simulated and analytically calculated radial stress

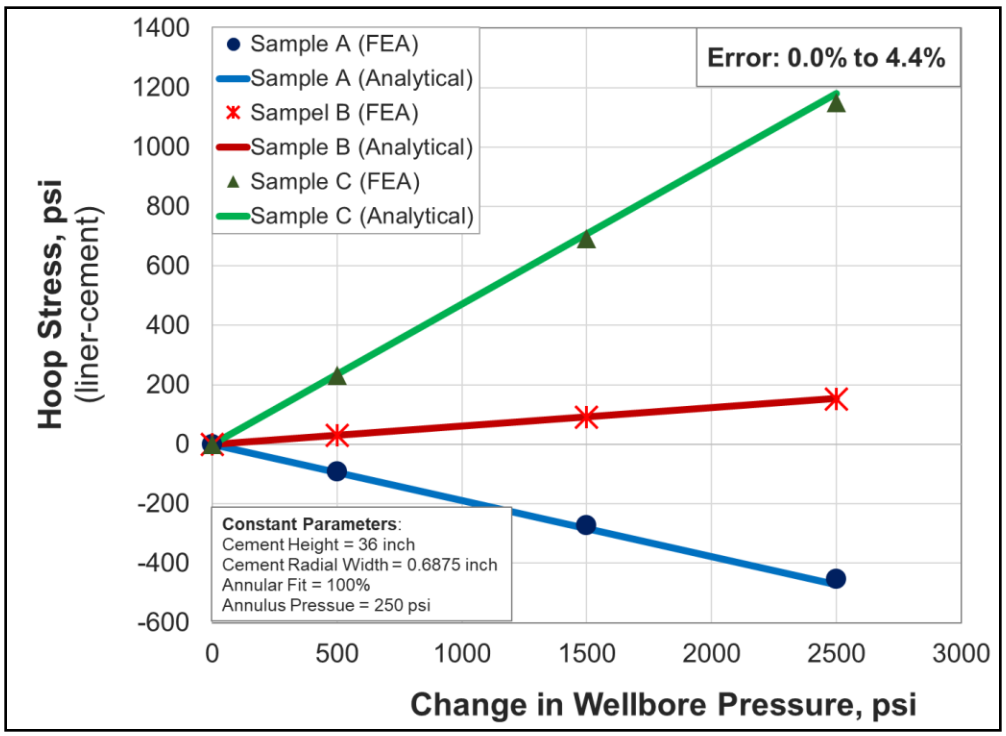

Figure 5.53: Comparison between FEA simulated and analytically calculated hoop stress

5.5 SUMMARY AND CONCLUSIONS

Three-dimensional FEA models were used to evaluate "fitness-for-service" of wellbore barrier components. Risk assessment was performed by investigating the sensitivity of contact stresses to various operational, design, and failure parameters. The FEA-generated results matched the analytical calculations with reasonable accuracy. The following conclusion are drawn from the simulation results:

5.5.1 Seal Assembly Model

- Sealability exhibited the highest sensitivity to annular fit (i.e. radial width of seal relative to annular space). If the radial gap between seal and casing is x% higher than anticipated, then it can effectively reduce compression by x% and vice versa. A radial gap of 1% more than the designed value can reduce the effective contact pressure by an amount approximately equal to 16 times the elastic modulus of the seal.
- After annular fit, the second and third most critical parameters that significantly affects sealability are Poisson's ratio and elastic modulus respectively. Contact pressure increases gradually with an increase in Poisson's ratio up to 0.425 beyond which it increases exponentially and even faster. Elastic modulus on the other hand is directly proportional to contact pressure.
- The next critical parameter is the compression ratio which is % change in axial seal length. Contact pressure exhibits a positive liner correlation with the compression ratio. The force

required to achieve certain compression ratios depends on the elastic modulus and seal axial length.

- Sealability has practically no significant sensitivity to axial seal length and radial thickness for a given annular fit. Contact pressure shows an insignificant reduction (up to 2-3%) with approximately 5 times increase in seal length. Significant changes (±40%) in seal thickness resulted in a minor change (< 2%) in contact pressure.
- Material failure can have significant impact on sealability. The average % reduction in contact pressures because of gas exposure was found to be equal to the % reduction in elastic modulus of the material. The worst case in the aging tests was observed to be 7 days exposure to pure CO_2 at 180°F. It resulted in a sealability reduction of 40% (NBR), 29% (EPDM),9% (VITON), and 2% (PTFE).
- Operational failure such as non-uniform seal energization or faulty support during energization can result in 13% to 95% less contact pressure than the designed value, depending on the severity. Overall, the loss is more pronounced and determinantal in the case of an axially shorter seal.
- All the major predictors namely elastic modulus, Poisson's ratio, compression ratio, and annular fit were incorporated into an empirical correlation that can be used to estimate contact pressure with ±2% error.
- The effect of temperature on sealability can be easily estimated using the developed empirical correlation by adjusting elastic modulus and Poisson's ratio, depending on the temperature change. Typically, elastic modulus decreases at higher temperature; i.e. elastomer becomes softer. The corresponding loss in contact pressure will be equal to percentage change in elastic modulus.

5.5.2 Cement Model

- For cement in offshore shallow depth wells, annular fit, changes in wellbore pressure, and material properties (Young's modulus and Poisson's ratio) are the four most important parameters affecting cement sealability or failure.
- All three stresses (radial, hoop, and maximum shear) at the liner-cement interface have the highest sensitivity to annular fit. Smaller than 100% annular fit (e.g. presence of micro-annuli or lack of bonding between cement and pipe) is the most likely first mode of sealability failure for cement. This could be caused by volume shrinkage, improper centralization, shallow gas channeling, etc.
- Radial mode of failure (debonding and stress crushing) is highly unlikely for shallow wells. Radial debonding can only occur in the event of decreasing wellbore pressure when radial stresses become tensile. Stress crushing is highly unlikely because the cement would fail by radial cracking when the hoop stress exceeds tensile strength, before it fails by compressive radial stress exceeding compressive strength.

- Radial cracking and shear failure are the most likely modes of failures in set cement with 100% annular fit. The likelihood and order of these failure modes depends on the cement's Young's modulus, Poisson's ratio, and limiting strength.
- Cement with low Young's modulus and low Poisson's ratio (LYLP) develops smaller hoop stress in terms of magnitude and exhibits the least sensitivity to change in wellbore pressure than any other cement system. Thus, LYLP followed by LYHP should be the preferred cement systems to minimize the risk of failure by radial cracks.
- Overall, cement systems with low Young's modulus are more robust to shear failures. LYHP cement system has the lowest risk of shear failure followed by LYLP cement system.
- Variations in material properties can have a notable impact on the designed values of hoop and maximum shear stresses. For example, at wellbore pressures of 2500 psi, hoop stress changes by approximately 60 psi per 100,000 psi change in Young's modulus and by approximately 200 psi per 0.1 unit change in Poisson's ratio.
- Pre-stressed cement system can significantly minimize the risk of radial crack failure by providing compensatory compressive stress. However, this pre-stressed system is more likely to fail by shear because the pre-load condition leads to higher values of maximum shear stress than a conventional cement system.
- For all the three cement samples, a wellbore pressure increase of 1000 psi was able to close 87 μm wide channel (99.5% annular fit). This indicates that if pressure increase is sufficiently high to balloon the liner, then it may mask the presence of a small micro-annuli in set cement.
- For shallow depth wells, the height of cement column and annular pressure (on top of the cement sheath) are not important factors contributing to the structural failure of cement.
- Temperature effect on mechanical integrity of cement was studied in form of material properties. The effect of temperature can be easily estimated using the generated performance curves if the temperature-induced change in material properties is known.

Overall, this study provided useful information on seal assembly and cement sheath as barriers. This work filled-in some of the existing knowledge gaps to help regulators and operators in improving the design, selection, and qualification of these barrier elements.

6 RECOMMENDATIONS AND FUTURE WORK

All the recommendations from this project and future works have been detailed in the draft recommendation document.

ACKNOWLEDGMENT

We thank BSEE for funding this work and providing research team with valuable feedback.

NOMENCLATURE

Acronyms

ACN	Acrylonitrile
API	American Petroleum Institute
ASTME	American Society of Tool and Manufacturing Engineers
BOP	Blow out preventer
BSEE	Bureau of Safety and Environmental Enforcement
EDS	Energy dispersive spectroscopy
EPDM	Neoprene ethylene propylene diene monomer
FEPM	Fluorocarbon/ Tetrafluoro ethylene/ Propylene rubber
FFKM	Perfluoroelastomer
FKM	Fluoroelastomer (VITON)
HNBR	Hydrogenated Nitrile Butadiene Rubber
HYHP	High Young's Modulus High Poisson's Ratio
HYLP	High Young's Modulus Low Poisson's Ratio
LYHP	Low Young's Modulus High Poisson's Ratio
LYLP	Low Young's Modulus Low Poisson's Ratio
NBR	Nitrile Butadiene Rubber
NCS	Norwegian Continental Shelf
PTFE	Polytetrafluoroethylene
RGD	Rapid gas decompression
SEM	Scanning electron microscope
W/C	Water to cement ratio
WOC	Wait on cement

Symbols

a	Inner radius of liner
b	Outer radius of liner / inner radius of cement sheath
c	Outer radius of cement sheath / inner radius of casing
d	Outer radius of casing
r	Radius of cylinder
C_0	Uni-axial compressive strength of material
E	Elastic modulus
P_c	Contact pressure
P_{c1}	Contact stress at liner-cement interface
P_{c2}	Contact stress at cement-casing interface
P_i	Pressure acting internally on liner
P_o	Pressure acting externally on casing

T_0	Uni-axial tensile strength of material

GREEK SYMBOLS

δ	Seal compression ratio
λ	Annular gap between seal and pipe
ν	Poisson's ratio
σ_1	Maximum principle stress
σ_3	Minimum principle stress
σ_r	Radial stress
σ_θ	Hoop stress
σ_z	Axial stress
ς	Cohesion or intrinsic shear strength of cement
τ_{max}	Maximum shear stress

REFERENCES

1. Adams, N. J. and Kuhlman, L. G. 1990. Case History Analyses of Shallow Gas Blowouts. Presented at the IADC/SPE Drilling Conference, Houston, Texas, 27 February - 2 March. IADC/SPE 19917. SPE-19917-MS. http://dx.doi.org/10.2118/19917-MS
2. Aggelen, A. 2016. Functional Barrier Model-A Structural Approach to Barrier Analysis. Presented at the SPE Annual Technical Conference and Exhibition on Heath, Safety, Security, Environment, and Responsibility, Stavanger, Norway, 11-13 April. SPE-179214-MS. https://doi.org/10.2118/179214-MS
3. Ahmed, R. M., Takach, N. E., Khan, U. M. et al. 2009. Rheology of Foamed Cement. *Cement and Concrete Research*: **39**(4), 353-361. http://dx.doi.org/10.1016/j.cemconres.2008.12.004
4. Al-Buraik, K., Al-Abdulqader, K., and Bsaibes, R. 1998. Prevention of Shallow Gas Migration Through Cement. Presented at IADC/SPE Asia Pacific Drilling Technology, Jakarta, Indonesia, 7-9 September. SPE-47775-MS. https://doi.org/10.2118/47775-MS
5. Al-Hiddabi, S. A., Pervez, T., Qamar, S. Z. et al. 2015. Analytical model of elastomer seal performance in oil wells. *Applied Mathematical Modelling*: **39**(10-11), 2836–2848. http://dx.doi.org/10.1016/j.apm.2014.10.028
6. Ansys®, 2017. Workbench 17.2 User Manual
7. *API RP 19 LH, Recommended Practice for Liner Hangers*, First Draft.
8. *API RP 10B-4, Preparation and Testing of Foamed Cement Formulations at Atmospheric Pressure*, Second Edition. 2015. Washington, DC: API
9. *API 11 D1, Packers and Bridge Plugs*, Third Edition. 2015. Washington, DC: API
10. *API RP 96, Recommended Practice for Deepwater Well Design and Construction*, First Edition .2013. Washington, DC: API.
11. *API RP 10B-2, Recommended Practice for Testing Well Cements*, Second Edition. 2013. Washington, DC: API

12. *API Spec 17D, Specification for Design and Operation of Subsea Production Systems—Subsea Wellhead and Tree Equipment*, Second Edition. 2011. Washington, DC: API
13. *API RP 10B-6, Recommended Practice on Determining the Static Gel Strength of Cement Formulations*, First Edition. 2010. Washington, DC: API
14. *API SPEC 10A, Specification for Cements and Materials for Well Cementing*, Twenty Fourth Edition. 2010. Washington, DC: API
15. *API TR 10TR1, Cement Sheath Evaluation*, Second Edition. 2008. Washington, DC: API
16. *API RP 65-Part 2, Standard for Isolating Potential Flow Zones During Well Construction* Second Edition .2010. Washington, DC: API.
17. *API RP 10B-5, Recommended Practice on Determination of Shrinkage and Expansion of Well Cement Formulations at Atmospheric Pressure*, First Edition. 2005. Washington, DC: API
18. *API RP 65, Standard for Cementing Shallow Water Flow Zones in Deepwater Wells*, First Edition .2002. Washington, DC: API.
19. *API BULLETIN E3, Environmental Guidance Document: Well Abandonment and Inactive Well Practices for U.S. Exploration and Production Operations*, First Edition. 1993. Washington, DC: API.
20. *ASTM D575-91, Standard Test Methods for Rubber Properties in Compression* .2012. West Conshohocken, PA: ASTM International.
21. Bellarby, J. 2009. *Well Completion Design*, volume 56, First Edition. Amsterdam, Amsterdam: Elsevier Science.
22. Bogaerts, M., De Bruijn, G. G., Khalilova, P. R. et al. 2012. Identifying and Mitigating the Risks of Shallow Flow in Deepwater Cementing Operations. Presented at SPE Deepwater Drilling and Completions Conference, Galveston, Texas, 20-21 June. SPE-155733-MS. https://doi.org/10.2118/155733-MS
23. Bosma, M. G. R., Cornelissen, E. K., and Schwing, A., 2000. Improved Experimental Characterisation of Cement/Rubber Zonal Isolation Materials. Presented at SPE Asia Pacific Oil and Gas Conference and Exhibition, 16-18 October, Brisbane, Australia. SPE-64395-MS. http://dx.doi.org/10.2118/64395-ms
24. Bureau of Safety and Environmental Enforcement (BSEE), Office of Offshore Regulatory Programs.2014. OC-FIT Evaluation of Seal Assembly & Cement Failures Interim Summary of Findings. Internal QC-FIT Report #2014-02 (December 2014). https://www.bsee.gov/sites/bsee_prod.opengov.ibmcloud.com/files/memos/public-engagement/qc-fit-bp-bolts-report-final.pdf
25. Bustgaard, M., and Nesheim, M. H. 2016. Model for Prediction of Cement Sheath Failure. MS Thesis, Norwegian University of Science and Technology, Trondheim, Norway (June 2016).
26. Carey, J. 2013. Geochemistry of Wellbore Integrity in CO_2 Sequestration: Portland Cement-Steel-Brine-CO_2 Interactions. *Reviews in Mineralogy and Geochemistry* **77** (1): 505–539. https://doi.org/10.2138/rmg.2013.77.15

27. Carroll, S., Carey, J., Dzombak, D. et al. 2016. Review: Role of Chemistry, Mechanics, And Transport on Well Integrity in CO2 Storage Environments. *International Journal of Greenhouse Gas Control* **49:** 149-160. https://doi.org/10.1016/j.ijggc.2016.01.010
28. *30 CFR 250.425, What are the Requirements for Pressure Testing Liners*? A special edition of the Federal Register, 2004. Dallas TX: Office of the Federal Register National Achieves and Records Administration.
29. Chanliau-Blanot, M. T., Nardiim, M., Donnet, J. B., et al. 1989. Temperature dependence of the mechanical properties of EPDM rubber-polyethylene blends filled with aluminium hydrate particles. *Journal of Materials Science* **24**(2): 641–648. http://dx.doi.org/10.1007/bf01107455.
30. Chen, X., Bartos, J., Salem, H. et al. 2016. Elastomers for High Pressure Low Temperature HPLT Sealing. Presented at Offshore Technology Conference held in Houston, USA, 2-5 May 2016. OTC-27227-MS. http://dx.doi.org/10.4043/27227-MS
31. Cheung, P. R. and Beirute, R. M. 1985. Gas Flow in Cements. *J Pet Technol*. SPE-11207-PA http://dx.doi.org/10.2118/11207-PA
32. Cong, C., Cui, C., Meng, X. et al. 2013. Degradation of hydrogenated nitrile-butadiene rubber in aqueous solutions of H2S or HCl. *Chemical Research in Chinese Universities*: **29**(4), 806–810. http://dx.doi.org/10.1007/s40242-013-2401-7
33. Cooke, C. E., Kluck, M. P., and Medrano, R. 1983. Field Measurements of Annular Pressure and Temperature during Primary Cementing. *J Pet Technol*. SPE-11206-PA. https://doi.org/10.2118/11206-PA
34. Dajiang, Z., Yuanhua, L., Huali, Z. et al. 2017. Experimental studies on CO2 corrosion of rubber materials for packer under compressive stress in gas wells. *Engineering Failure Analysis*: 80, 11-23. https://doi.org/10.1016/j.engfailanal.2017.01.012
35. Danenberger, E. P. 1993. Outer Continental Shelf Drilling Blowouts, 1971-1991. Presented in thte Offshore Technology Conference, Texas, Houston, 3-6 May. OTC-7248-MS. http://dx.doi.org/10.4043/7248-MS
36. Daou, F. and Piot, B. M. 2009. Cement-Slurry Performance and Set-Cement Properties vs. Microsilica Densification. *SPE Drill & Compl*. SPE-112701-PA. http://dx.doi.org/10.2118/112701-PA
37. Davies, R. J., Almond, S., Ward, R. S. et al. 2014. Oil and gas wells and their integrity: Implications for shale and unconventional resource exploitation. *Marine and Petroleum Geology*, **56**: 239-254. http://dx.doi.org/10.1016/j.marpetgeo.2014.03.001
38. Dean, G. D. and Brennen, M. A. 1992. A Unique Laboratory Gas Flow Model Reveals Insight to Predict Gas Migration in Cement. Presented in the SPE Western Regional Meeting, Bakersfield, California, 30 March-1 April. SPE-24049-MS. http://dx.doi.org/10.2118/24049-MS
39. De Andrade, J., and Sangesland, S. 2016. Cement Sheath Failure Mechanisms: Numerical Estimates to Design for Long-Term Well Integrity. *Journal of Petroleum Science and Engineering*: **147**, 682–698. https://doi.org/10.1016/j.petrol.2016.08.032

40. Dolog, R., Ventura, D., Khabashesku, V. et al. 2017. Nano-Enhanced Elastomers for Oilfield Applications. Presented at Offshore Technology Conference, Houston, Texas. 1-4 May. OTC-27609-MS. https://doi.org/10.4043/27609-MS.
41. Dusseault, M. B., Jackson. R. E., and MacDonald. D. 2014.Towards a Road Map for Mitigating the Rates and Occurrences of Long-Term Wellbore Leakage. University of Waterloo and Geofirma Engineering Ltd. (May 22, 2014). http://geofirma.com/wp-content/uploads/2015/05/lwp-final-report_compressed.pdf.
42. Federal Highway Administration. 2017. Fly Ash Facts for Highway Engineers. *U.S. Department of Transportation, Federal Highway Administration,* 06.27.2017. https://www.fhwa.dot.gov/pavement/recycling/fach01.cfm
43. Fernández, C., and Castaño, P. 2016. Compatibility Behavior of Elastomers for PCP Applications. *NACE International*: NACE-2016-7106. https://www.onepetro.org/conference-paper/NACE-2016-7106.
44. Fisher, R.A. *The Design of Experiments*. *8th edition*. Hafner Publishing Company, New York (1966).
45. Hauge, S and Øien, K. 2016. Guidance for Barrier Management in the Petroleum Industry. SINTEF Technology and Society, Safety Research. Report No. SINTEF A27623, Trondheim, Norway (September 2016).
46. Hopkins, H.A.2016. API Response to BSEE Report 2014-02, QC-FIT Evaluation of Seal Assembly and Cement Failures Interim Summary of Findings (dated December 2014). API Energy, Washington, DC (November 3, 2016). https://www.bsee.gov/sites/bsee.gov/files/seal-assembly-and-cement-failure-report-api-response-11032016.pdf.
47. Huerta, N., Hesse, M., Bryant, S. et al. 2012. Experimental Evidence for Self-Limiting Reactive Flow through a Fractured Cement Core: Implications for Time-Dependent Wellbore Leakage. *Environmental Science & Technology 47* (1): 269-275. https://dx.doi.org/10.1021/es3013003
48. Hu, G., Zhang, P., Wang, G. et al. 2017. The influence of rubber material on sealing performance of packing element in compression packer. *Journal of Natural Gas Science and Engineering*: **38**(Feb 2017), 120–138. https://doi.org/10.1016/j.jngse.2016.12.027
49. *ISO/TS 16530-2:2013, Petroleum and natural gas industries -Well Integrity-Part 2: Well integrity for the operational phase,* first edition. 2013. Geneva, Switzerland: ISO.
50. Iverson, B., Darbe, R., and McMechan, D. 2008. Evaluation of Mechanical Properties of Cements. Presented at the 42nd U.S. Rock Mechanics Symposium (USRMS), 29 June-2 July, San Francisco, California. ARMA-08-293.
51. James Walker. 2017. Elastomer Engineering Guide. https://www.jameswalker.biz/de/pdf_docs/148-elastomer-engineering-guide.
52. Jin, H., Hong, C., Cho, D. et al. 2008. Effects of Temperature on Hardness of Rubber Materials with Different Curing System. *Journal of Elastomers and Composites,* **43** (4): 213-220.
53. Khandka, R. K. 2007. Leakage Behind Casing. MS Thesis, Norwegian University of Science and Technology, Trondheim, Norway (June 2007).

54. King, G.E. and King, D.E. 2013. Environmental Risk Arising from Well-Construction Failure - Differences between Barrier and Well Failure and Estimates of Failure Frequency across Common Well Types, Locations and Well Age. Presented at the SPE Annual Technical and Exhibition Conference, New Orleans, Louisiana, 30 September –2 October. SPE 166142. https://doi.org/10.2118/166142-MS.
55. Lavrov, A. and Torsæter, M. 2016. *Physics and Mechanics of Primary Well Cementing*, First Edition. Springer. http://dx.doi.org/10.1007/978-3-319-43165-9.
56. Lécolier, E., Rivereau, A., Ferrer, N. et al. 2010. Durability of Oilwell Cement Formulations Aged in H2S-Containing Fluids. *SPE Drill & Compl*: **25**(01). SPE-99105-PA. http://dx.doi.org/10.1007/10.2118/99105-PA
57. MMS Safety Alert. U.S. Department of the Interior Minerals Management Service, Gulf of Mexico OCS Region. Safety Alert No. 216. October 22 2003. https://www.bsee.gov/sites/bsee.gov/files/safety-alerts/safety/safety-alert-no-216.pdf
58. Mohamed, A.O. and Al-Zuraigi, A. 2013. Liner Hangers Technology Advancement and challenges. Presented at the SPE Middle East Oil and Gas Show and Conference, Manama, Bahrain.10-13 March. SPE-164367-MS. https://doi.org/10.2118/164367-MS.
59. Moore, M. J., Campo, D. B., Hockaday, J.et al. 2002. Expandable Liner Hangers: Case Histories. Presented at Offshore Technology Conference, Houston, Texas. 6-9 May. OTC 14313-MS. https://doi.org/10.4043/14313-MS.
60. Moore, B., and Hamilton, T. A. P. 1993. Shallow Gas Hazard - The HSE Perspective. The Institute of Petroleum, London, UK.
61. Murray, S. J., Williamson, M. D., Gilham, S. et al. 1995. Well Design for Shallow Gas. Presented at SPE/IADC Drilling Conference, Amsterdam, Netherlands, 28 February-2 March. SPE-29343-MS. http://dx.doi.org/10.2118/29343-MS
62. Nelson B. E. and Guillot D. 2006. *Well Cementing*. Second Edition. Schlumberger, Sugar Land, Texas 77478.
63. NORSOK Standard D-010. 2014. Well integrity in drilling and well operations. (Rev. August 3, 2014) http://www.standard.no/pagefiles/1315/d-010r3.pdf
64. Omosebi, O. A. 2016. *Mechanical Degradation of Well Cement in HPHT Carbonic Acid Environment: Experimental Studies and Mathematical Modeling.* PhD dissertation, University of Oklahoma, Norman, Oklahoma (June 2016).
65. Parker Hannifin. 2002. Specialty Elastomers for Energy, Oil and Gas Industries. *Parker Hannifin Corporation Product Fact Sheet*, 1 October 2002, https://www.parker.com/literature/O-Ring%20Division%20Literature/EOGFactSheet.pdf. (Accessed July 3, 2017).
66. Parrott, L. J. 1995. Influence of cement type and curing on the drying and air permeability of cover concrete. *Magazine of Concrete Research* **47** (171): 103-111. https://doi.org/10.1680/macr.1995.47.171.103
67. Pleasants, C. W., Joseph, B. J., and Farrar, A. L. 2012. Reliable Completion System for Gas Migration Prevention. Presented at the SPE Annual Technical Conference and Exhibition, San Antonio, Texas, 8 –10 October. SPE-160217-MS. https://doi.org/10.2118/160217-MS.

68. Prince, P. K. 1990. Current Drilling Practice and the Occurrence of Shallow Gas. Presented in the Safety in Offshore Engineering: Proceedings of an international conference, London, UK, 25-26 April. SUT-AUTOE-v25-003. https://www.onepetro.org/conference-paper/SUT-AUTOE-v25-003
69. PSA. Norwegian Petroleum Safety Authority.2013. Principles for Barrier Management in the Petroleum Industry. http://www.ptil.no/getfile.php/1319891/PDF/Barrierenotatet%202013%20engelsk%20april.pdf.
70. Rahimi, R. 2014. The effect of using different rock failure criteria in wellbore stability analysis. MS Thesis, Missouri University of Science and Technology, Rolla, Missouri, USA (May 2014).
71. Rupak K. K. 2007. Leakage behind Casing. Norwegian University of Science and Technology, Trondheim, Norway
72. Sabins, F. L., Tinsley, J. M., and Sutton, D. L. 1982. Transition Time of Cement Slurries between the Fluid and Set States. *SPE J.* SPE-9285-PA. http://dx.doi.org/10.2118/9285-PA
73. Schweitzer P. A. 2000. *Mechanical and Corrosion-Resistant properties of Plastics and Elastomers*, First Edition, Boca Raton, Florida, USA: CRC Press.
74. Smith, P., and Williford, J. 2006. Case Histories: Liner-Completion Difficulties Resolved with Expandable Liner-Top Technology. Presented at Canadian International Petroleum Conference, 13-15 June, Calgary, Alberta. PETSOC-2006-103. https://doi.org/10.2118/2006-103
75. Speer, M. 2006. Introduction to Wellhead Systems. In: *Petroleum Engineering Handbook*, Vol. 2, ed. Lake, L.W. Chap. 8, 344-369. Richardson, Texas: Society of Petroleum Engineers.
76. Stormont, J. C., Fernandez, S. G. Taha, M. R. et al. 2017. Gas flow through cement-casing microannuli under varying stress conditions. *Geomechanics for Energy and the Environment* **13**: 1-13. https://doi.org/10.1016/j.gete.2017.12.001
77. Strand, G., 2017. *Well Safety: Risk Control in the Drilling Phase of Offshore Wells.* PhD Thesis. Norwegian University of Science and Technology (NTNU), Trondheim, Norway (June 2017).
78. Talabani, S., Hareland, G., and Islam, M. R. 1997. Gas Migration Eliminated Through Correct Cement Design Including Elastomers. Presented in the SPE/IADC Middle East Drilling Technology Conference, Bahrain, 23-25 November. SPE-39279-MS. http://dx.doi.org/10.2118/39279-MS
79. Tarco, J. C. and Asghari, K. 2010. Experimental Study of Stability and Integrity of Cement in Wellbores Used for CO_2 Storage. *Journal of Canadian Petroleum Technology* **49** (10): 37-44. SPE-142004-PA. https://doi.org/10.2118/142004-PA
80. Teodoriu, C., Yuan, Z., Schubert, J., et al. 2012. Experimental Measurements of mechanical parameters of Class G cement. Presented at SPE/EAGE European Unconventional Resources Conference and Exhibition, 20-22 March, Vienna, Austria. http://dx.doi.org/10.2118/153007-ms
81. Teodoriu, C., Schubert, J., and Ugwu, I. 2008. Cement Fatigue and HPHT Well Integrity with Application to Life of Well Prediction. Final Report, Contract No. MMS/OTRC CRA 1435-01-04-CA-35515. Minerals Management Service, Herndon, VA. (December 2008).

82. Thorogood, J. L. 2017. Systems Approach to Well Control Barrier Management During Drilling Operations. Presented at the IADC/SPE Drilling Conference and Exhibition, Hague, The Netherland. 14-16 March. SPE/IADC-184668-MS. https://doi.org/10.2118/184668-MS.
83. Tynan, C. 2016. Successful selection of oil and gas seals, World Pumps, Volume 2016, Issue 9, September 2016, Pages 28-30, ISSN 0262-1762, http://dx.doi.org/10.1016/S0262-1762(16)30235-8
84. Van Dinh, C., and Kubouchi, M. 2012. An Approach for the Prediction of Blistering on Polymer- Steel Lining Systems Exposed to an Aqueous Environment. *Industrial & Engineering Chemistry Research*: **51**(36), 11681-11687. http://dx.doi.org/10.1021/ie202975s
85. Walvekar, S. and Jackson, T. 2006. Expandable Technology Improves Reliability of Conventional Liner Hanger Systems. Presented at the IADC/SPE Drilling Conference, Miami, Florida. 21-23 February. SPE-99186-MS. https://doi.org/10.2118/99186-MS.
86. Wang, Z., Chen, C., Liu, Q. et al. 2017. Extrusion, slide, and rupture of an elastomeric seal. *Journal of the Mechanics and Physics of Solids:* **99**, 289–303. https://doi.org/10.1016/j.jmps.2016.12.007
87. Wardak, A., Williford, J., Walker, A. et al. 2010. Ensuring Success on an Extended-Reach Well with Expandable Liner Hangers and Advanced Software Modeling. Presented at the IADC/SPE Asia Pacific Drilling Technology Conference and Exhibition, Ho Chi Minh City, Vietnam 1-3 November. IADC/SPE-136300. https://doi.org/10.2118/136300-MS.
88. Watters, L. T. and Sabins, F. L. 1980. Field Evaluation of Method to Control Gas Flow Following Cementing. Presented in the SPE Annual Technical Conference and Exhibition, Dallas, Texas, 21-24 September. SPE-9287-MS. http://dx.doi.org/10.2118/9287-MS
89. Williford, J and Smith, P. 2007. Expandable Liner Hanger Resolves Sealing Problems and Improves Integrity in Liner Completion Scenarios. Presented at the SPE 2007 Production and Operations Symposium, Oklahoma City, Oklahoma, 31 March-3 April. SPE-106757-MS. https://doi.org/10.2118/106757-MS.
90. Wu, B., Doble, R., Turnadge, C. et al. 2016. Well Failure Mechanism and Conceptualisation of Reservoir-Aquifer Failure Pathways. Presented at the SPE Asia Pacific Oil & Gas Conference and Exhibition, Perth, Australia, 25-27 October. SPE-182460-MS. https://doi.org/10.2118/182460-MS.